

Towards Clinical Testing of Intraspinial Microstimulation for Restoration of Walking after Spinal  
Cord Injury

by

Amirali Toossi

A thesis submitted in partial fulfillment of the requirements for the degree of

Doctor of Philosophy

Neuroscience  
University of Alberta

© Amirali Toossi, 2018

# Abstract

The overall goal of this thesis was to advance intraspinal microstimulation (ISMS) towards clinical testing for the purpose of restoring walking after spinal cord injury. ISMS implants focus on restoring mobility after spinal cord injury by activating the intact spinal motor networks below the injury. This is done by delivering electrical stimulation to the ventral horns of the lumbosacral enlargement through implanted microelectrodes, and activating the motoneuronal pools controlling the leg muscles. Preclinical studies have shown that by tapping into the spinal cord motor networks, ISMS can activate synergistic leg muscles across single or multiple joints. This is shown to be the case even after a complete spinal cord injury. Combining the functional synergies using physiologically-based control algorithms has allowed ISMS to produce balanced weight-bearing standing and over-ground walking. Standing and walking produced by ISMS are significantly more fatigue-resistant than those produced with intramuscular electrical stimulation. Collectively, these results suggest that ISMS has potential to become an effective intervention for restoring leg mobility after a complete spinal cord injury.

This thesis aimed to move ISMS closer to clinical testing by addressing two main questions: 1) What are the design specifications for chronic ISMS implants in humans? 2) Where should the ISMS implants be placed in the human spinal cord for functional success? The first question was addressed with a focus on the requirements for mechanical stability of ISMS implants in the spinal cord. The biomechanics of the spine and spinal cord near the implant region was studied in domestic pigs as a model for the human spinal anatomy. The critical forces for dislodging implanted electrodes were also measured. Based on this information, design specifications for mechanically stable implants were provided.

While the second question is best answered by direct investigation of the functional organization of the motoneuronal pools (functional map) in the lumbosacral enlargement of humans, this thesis took an intermediate step. The functional map of the lumbosacral enlargement was obtained in non-human primates for the first time. Results showed that ISMS can produce functional leg movements in monkeys, similar to those studied in smaller animals. They also suggest that the relative organization of the motoneuronal pools in the functional maps of monkeys is similar to those known for cats. The findings demonstrated that the functional maps are preserved across species. Therefore, the maps from the monkeys and cats will guide the first clinical tests of ISMS.

In preparation for the first clinical testing of ISMS, a spinal-stereotactic-system was also developed for accurate placement of ISMS implants in the human spinal cord. This system is mounted onto the subject's spine to minimize relative movement between the implanted electrode and the stereotactic system. It also utilizes intraoperative ultrasound imaging for target selection and guidance of the implantation trajectory. The targeting accuracy of this stereotactic system for implants into the ventral horns was found to be  $<0.32$  mm. This system will be used for the first clinical tests of ISMS for walking.

Finally, the effect of a common clinical neurosurgical anesthetic protocol on the motor responses to ISMS was investigated. Understanding the effect of anesthesia on the evoked responses to ISMS is critical for optimal placement of its microelectrodes. It is also important for the correct interpretation of the intraoperative responses to ISMS, especially in human studies. Therefore, a comparison was made between the effect of a common clinical neurosurgical anesthetic protocol and those of two anesthetic protocols commonly used in preclinical studies. Results demonstrated that a clinical total intravenous anesthesia (TIVA) protocol with propofol

allows ISMS to produce strong movements with large ranges of motion. The responses produced under this clinical protocol were also not different from those produced under the most common preclinical anesthesia (pentobarbital) used in ISMS studies. Taken together, these results suggest that clinical TIVA protocol with propofol is a suitable anesthetic protocol for use in humans. It also suggests that clinical intraoperative observations would be comparable with those in the preclinical literature.

Collectively, this thesis proposed mechanical design specifications for chronic ISMS implants in large animals and addressed the requirements for the first clinical testing of ISMS.

# Preface

This thesis is an original work by Amirali Toossi. A version of chapter 2 has been published as A. Toossi, D. G. Everaert, P. Seres, J. L. Jaremko, K. Robinson, C. C. Kao, P. E. Konrad, V. K. Mushahwar, “Ultrasound-guided spinal stereotactic system for intraspinal implants”, *Journal of Neurosurgery: Spine*, 2018, vol. 29, issue 3, 292-305. My contributions included: Experimental design, joint-design of the stereotactic system, data collection and analyses, writing the manuscript draft, incorporating co-authors inputs and revisions during the peer-review process.

A version of chapter 3 has been submitted to a peer-review journal as: A. Toossi, D. G. Everaert, R. Uwiera, D. Hu, F. Gragasin, V. K. Mushahwar, “Effect of anesthesia on motor responses evoked by spinal neural prostheses during intraoperative procedures”. My contributions to this project included: Joint-design of experiments, data collection and analyses, writing the manuscript draft, and incorporating co-authors inputs.

A version of chapter 4 has been submitted to a peer review journal as: A. Toossi, D. G. Everaert, S. I. Perlmutter, V. K. Mushahwar, “Functional organization of motor networks in the lumbosacral spinal cord of non-human primates”. My contributions to this project included: Joint-design of experiments, data collection and analyses, writing the manuscript draft, and incorporating co-authors inputs.

A version of chapter 5 has been published as: A. Toossi, D. G. Everaert, A. Azar, C. R. Dennison, V. K. Mushahwar, “Mechanically stable intraspinal microstimulation implants for human translation”, *Annals of Biomedical Engineering*, 2017, vol. 45, issue 3, 681-694. My contributions to this project included: Experimental design, data collection and analyses, writing the manuscript draft, and incorporating co-authors inputs.

The research projects, of which this thesis is a part, received research ethics approval from the Institutional Animal Care and Welfare Committees at the University of Alberta and the University of Washington. Details are listed below:

-Project Name: “Effect of anesthesia on Intraspinal Microstimulation”, No. AUP00002424, Date: November 6, 2017. University of Alberta.

-Project Name: “Mechanical Stability of Intraspinal Implants in Large Animal Models”, No. AUP00000799, Date: February 3, 2014. University of Alberta.

-Project Name: “Intraspinal Stimulation”, Protocol No. 4187-04, Date: September 22, 2014. University of Washington.

# Acknowledgements

First, I would like to thank Dr. Vivian Mushahwar, my supervisor, for the encouragements, support and the mentorship she provided me with throughout this program. I am also grateful to her for all the opportunities she tirelessly made possible during these years that allowed me to benefit from a wide range of scientific and professional experiences. I want to thank Dr. Dirk Everaert for his friendship and support during the moments of success and failure in my PhD journey and his assistance to my projects. I thank my PhD supervisory committee, Dr. Dave Collins, Dr. Simon Gosgnach, and Dr. Peter Konrad, for their invaluable mentorship for my scientific and professional development. I also want to thank the entire Mushahwar lab.

I thank the Canadian Institutes of Health Research, Alberta Innovates: Health Solutions (AIHS), Government of Alberta, and the University of Alberta for their support through Vanier Canada Graduate Scholarship, AIHS Graduate Studentship, Queen Elizabeth II Graduate Scholarship, University of Alberta President's Doctoral Prize of Distinction, University of Alberta Faculty of Medicine and Dentistry 75<sup>th</sup> Anniversary Graduate Student Award, and University of Alberta Doctoral Recruitment Scholarship.

For the project presented in chapter 2, I would like to thank Rod Gramlich for modification of the surgical table for pigs to allow the suspension of the animal's hind limbs. I also thank Bethany Kondiles for her contribution to the design of the marker insertion tool and her assistance with the pilot experiments, Ashley Dalrymple and Dr. Leandro Solis for their assistance with the data collection process during pilot experiments.

For the project presented in chapter 3, I thank Dr. Francois Roy and Dr. Aleksandra King for providing access to a TES stimulator for this study. I also thank Neil Tyreman, Deb Dixon, and Ryan Edgar for their assistance with animal care during the surgeries.

For the project presented in chapter 4, I thank Dr. Christoph P. Hofstetter for implantation of the pedicle screws, Robert Robinson, Dr. Stephanie Seeman, Tyler Libey, Brian Mogen, Rebekah Schaefer and the Washington National Primate Research Centre staff for their assistance with the surgeries. I also thank Rod Gramlich for building a signal amplifier for force transducers, Neil Tyreman for histological tissue processing of the spinal cords and Dr. Douglas Weber for providing the MotionTracker2D software.

For the project presented in chapter 5, I thank Robert Butz for assistance with early measurement of electrode dislodgement forces, and Theodore Ng and Dr. Anastasia Elias for assistance in preparing surrogate spinal cords.

Finally, I would like to especially thank Maedeh, Reza, and my parents for their unwavering support and encouragement throughout these years, without whom none of this would have been possible. I dedicate this thesis to them.

# Table of Contents

Abstract .....	ii
Preface.....	v
Acknowledgements.....	vii
Table of Contents .....	ix
List of Tables .....	xiii
List of Figures.....	xiv
List of Abbreviations .....	xviii
Chapter 1. Introduction .....	1
1.1 Spinal Cord Injury .....	2
1.1.1. Improving Quality of Life for People with SCI.....	4
1.2 Interventions for Restoration or Improvement of Standing and Walking after SCI.....	5
1.2.1 Rehabilitation strategies .....	6
1.2.2 Orthoses for the restoration of standing and walking .....	8
1.2.3 Neuroprostheses for restoration of standing and walking.....	11
1.3 Intraspinal Microstimulation for Restoration of Standing and Walking .....	31
1.3.1 Mechanism of Action.....	31
1.3.2 Design, safety and stability of the implants .....	34
1.3.3 Functional Benefits of ISMS implants.....	39
1.4 Clinical translation of ISMS implants and thesis outline .....	42

Chapter 2. Ultrasound-Guided Spinal Stereotactic System for Intraspinal Implants .....	46
2.1 Introduction.....	47
2.2 Materials and Methods .....	50
2.2.1 The spinal stereotactic system.....	50
2.2.2 Surgery and device placement .....	53
2.2.3 Assessment of the accuracy of ultrasound-guided electrode implantation in the pig .....	54
2.2.4 <i>Bench-top</i> assessment of the ultrasound-guided electrode implantation technique.....	58
2.2.5 Functional testing of the ultrasound-guided stereotactic system in a live pig .....	60
2.3 Results.....	61
2.3.1 Findings related to ultrasound imaging of the spinal cord .....	61
2.3.2 Assessment of electrode alignment in pigs .....	61
2.3.3 Benchtop assessments .....	64
2.3.4 Intraoperative ISMS using the spinal stereotactic system.....	65
2.4 Discussion.....	65
2.5 Conclusions.....	69
2.6 Figures .....	71
Chapter 3. Effect of anesthesia on the intraoperative responses to intraspinal microstimulation and its implications for clinical translation.....	84
3.1 Introduction.....	85
3.2 Methods.....	87

3.3	Results .....	95
3.4	Discussion .....	101
3.5	Conclusions .....	106
3.6	Tables .....	108
3.7	Figures .....	109
	Chapter 4. Functional organization of motor networks in the lumbosacral spinal cord of non-human primates .....	122
4.1	Introduction .....	123
4.2	Methods .....	125
4.3	Results .....	130
4.4	Discussion .....	135
4.5	Conclusions .....	140
4.6	Figures .....	142
	Chapter 5. Mechanically Stable Intraspinal Microstimulation Implants for Human Translation	162
5.1	Introduction .....	163
5.2	Methods .....	166
5.2.1.	Biomechanics of the Implant Region .....	166
5.2.2.	Measurement of Dislodgement Forces .....	168
5.2.3.	Coil Fabrication and Testing .....	170
5.3	Results .....	171

5.3.1. Biomechanics of the Implant Region .....	171
5.3.2. Measurement of Dislodgement Forces.....	173
5.3.3. Coil Fabrication and Testing.....	174
5.4 Discussion .....	175
5.4.1. Overview .....	175
5.4.2. Similarity between the biomechanics of the spine in humans and pigs .....	176
5.4.3. Design implications for human implants .....	177
5.5 Conclusions.....	180
5.6 Tables .....	181
5.7 Figures.....	182
Chapter 6. General Discussions.....	194
6.1 Summary and Significance .....	195
6.2 Future Directions.....	199
Bibliography .....	202

# List of Tables

Table 3. 1. Summary of arterial blood gas measurements.....	108
Table 5. 1. Specifications of the fabricated coil types and results of bench characterization and in-situ testing in fresh pig cadavers. ....	181

# List of Figures

Figure 2. 1. The spinal stereotactic setup and its elements with special application to intraspinal microstimulation (ISMS). .....	71
Figure 2. 2. The spinal stereotactic setup.....	72
Figure 2. 3. The spinal stereotactic system used in a domestic pig. ....	73
Figure 2. 4. Spinal cord in the transverse (left) and sagittal (right) planes and the landmarks (dotted-lines) that can be used to determine its orientation. ....	74
Figure 2. 5. Ultrasound images obtained from the lumbar enlargement of the pig spinal cord. ..	75
Figure 2. 6. Magnetic resonance (MR) and ultrasound images of similar segments of the spinal cord. ....	76
Figure 2. 7. Bench testing setup and methods. ....	77
Figure 2. 8. Suspension setup used for visualization of hind limb movements produced by ISMS in the pig spinal cord.....	79
Figure 2. 9. Detection accuracy of electrode insertion angle for intraoperative ultrasound imaging. ....	80
Figure 2. 10. Alignment accuracy of implant in the <i>transverse plane</i> of the spinal cord measured in pigs.....	81
Figure 2. 11. Alignment accuracy of implant in the spinal cord measured <i>on the bench</i> .....	82
Figure 2. 12. Suspension setup used for intraoperative testing of ISMS in the pig spinal cord and an example of the results produced.....	83
Figure 3. 1. Experimental design. Shown is the sequence of anesthesia protocols and outcome measurements throughout each experiment.....	109
Figure 3. 2. Setup for measurements of muscle activity and kinematics.....	110

Figure 3. 3. Location of microelectrode tips in the spinal cord. A total of 76 microelectrodes were used for intraspinal microstimulation (ISMS) across all animals. ....	111
Figure 3. 4. Plasma concentration of propofol after cessation of infusion. ....	112
Figure 3. 5. Vital signs during electrophysiological and functional measurements. ....	113
Figure 3. 6. Comparison of responses to intraspinal microstimulation (ISMS) under various anesthesia protocols. ....	114
Figure 3. 7. Comparison of responses to intraspinal microstimulation (ISMS) under various anesthesia protocols. ....	116
Figure 3. 8. Comparison of EMG responses evoked by intraspinal microstimulation (ISMS) under various anesthesia protocols. ....	118
Figure 3. 9. Comparison of EMG responses evoked by intraspinal microstimulation (ISMS) under various anesthesia protocols. ....	120
Figure 3. 10. Comparison of motor evoked potentials (MEP) in the tibialis anterior muscle under various anesthesia protocols. ....	121
Figure 4. 1. Experimental setup for functional mapping of the lumbosacral spinal cord in non-human primates. ....	142
Figure 4. 2. Microelectrode alignment using bubble levels. ....	143
Figure 4. 3. MR imaging and histological analyses results. ....	144
Figure 4. 4. Spatial distribution (in the rostrocaudal direction) of the maps of the lumbar enlargement in cats and rhesus monkeys. ....	145
Figure 4. 5. Functional map of the lumbosacral enlargement of the spinal cord of 4 rhesus monkeys (A-D). ....	146
Figure 4. 6. All stimulated locations within the spinal cord across all animals. ....	148

Figure 4. 7. Characterization of the movements evoked by ISMS.....	149
Figure 4. 8. Distribution of the stimulation thresholds for producing leg movements in the gray (GM) and white (WM) matters ( $n_{GM}=221$ and $n_{WM}=100$ ) of the spinal cord ( $n=4$ animals).....	151
Figure 4. 9. Distribution of changes in joint angle (i.e., range of motion) for the movements evoked by microstimulation at sites in the gray and white matter (GM and WM) in all animals. .....	152
Figure 4. 10. Joint range of motion (ROM) of hip, knee and ankle produced by ISMS in the gray matter of the spinal cord (in Red). ....	153
Figure 4. 11. Isometric torque measurements for knee extension movements evoked at 17 select locations across 4 animals.....	154
Figure 4. 12. Example of evoked electromyographic (EMG) activity during a knee extension movement produced by ISMS in the lumbar enlargement. ....	155
Figure 4. 13. Cluster analysis of the EMG responses evoked by stimulation in the gray matter of the spinal cord. ....	156
Figure 4. 14. Rostrocaudal organization of the lumbar enlargement of the spinal cords of rhesus monkeys, cats and humans.....	158
Figure 4. 15. The distribution of stimulation thresholds in cats and monkeys. ....	161
Figure 5. 1. Conceptual representation of an ISMS implant.....	182
Figure 5. 2. Reflective markers on the spinal cord and spinal canal. ....	183
Figure 5. 3. Changes in marker position during movements within the physiological range of motion. ....	185
Figure 5. 4. Bench and in-situ setups for measurement of electrode dislodgement forces.....	186
Figure 5. 5. Biomechanics of the lumbar spinal cord and canal in fresh pig cadavers. ....	188

Figure 5. 6. Summary of electrode dislodgment forces obtained without coils in the lead wires.  
..... 190

Figure 5. 7. Force vs. strain and displacement profiles of different coils obtained from bench and  
in-situ tests. .... 192

Figure 5. 8. Summary of coil design specifications and average *in-situ* test dislodgment  
outcomes. .... 193

# List of Abbreviations

3D	Three dimensional
AD-ISMS	Activity dependent intraspinal microstimulation
AE	Ankle extension
AF	Ankle flexion
AIS	ASIA impairment scale
AnGap	Anion Gap
ARGO	Advanced reciprocating gait orthosis
BE	Base excess
BF	Biceps femoris
BWSTT	Body weight supported treadmill training
CSF	Cerebrospinal fluid
EMG	Electromyography
ETO	Ethylene oxide
FBR	Foreign body response
FES	Functional electrical stimulation
GM	Gray matter
H-reflex	Hoffmann's reflex
HE	Hip extension

HF	Hip flexion
HGO	Hip guidance orthosis
IQR	Interquartile range
Ir	Iridium
ISI	Inter-stimulus interval
ISMS	Intraspinal microstimulation
KE	Knee extension
KF	Knee flexion
LG	Lateral gastrocnemius
LIFE	Longitudinal intrafascicular electrodes
MAC	Minimum alveolar concentration
MEP	Motor evoked potential
MRI	Magnetic resonance imaging
MTP	Metatarsophalangeal
OL-ISMS	Open loop intraspinal microstimulation
PAD	Post activation depression
PB	Pentobarbital
PCI	Physiological cost index
Pt	Platinum
PWBT	Partial weight bearing therapy

Q1	First quartile
Q3	Third quartile
RGO	Reciprocating gait orthosis
ROM	Range of motion
Sart	Sartorius
SCI	Spinal cord Injury
SMA	Semimembranosus
SSEP	Somatosensory evoked potential
TA	Tibialis anterior
TE	Toe extension
TES	Transcranial electrical stimulation
TF	Toe flexion
tHb	Total hemoglobin
TIME	Transverse intrafascicular multichannel electrodes
TIVA	Total intravenous anesthesia
TM	Transmembrane
UPLC	Ultra-performance liquid chromatography
VHP	Vaporized hydrogen peroxide
VL	Vastus lateralis
VM	Vastus medialis

WM

White matter

# **Chapter 1. Introduction**

The overall goal of this thesis project was to advance the development of an implantable spinal-cord-neuroprosthesis towards clinical implementation for restoring lower limb mobility after spinal cord injury. This chapter provides an overview of spinal cord injury and the existing and emerging interventions for improving standing and walking after injury. It also describes the scope and specific aims of this thesis project.

## **1.1 Spinal Cord Injury**

A spinal cord injury (SCI) can be defined as any temporary or permanent injury to the spinal cord parenchyma or the nerves in the spinal canal (NSCISC National Spinal Cord Injury Statistical Center 2018a; “WHO | Spinal Cord Injury” 2013). SCI is a serious and complex injury which may lead to a range of physical and mental health complications for the individual.

Depending on the severity and location of injury, the affected individuals may have physical complications such as the loss of sensation and motor control in the limbs, difficulty or inability to breathe (Berlowitz, Wadsworth, and Ross 2016), bowel and bladder control issues (Hicken, Putzke, and Richards 2001; Glickman and Kamm 1996), and autonomic dysfunction (Karlsson 2006; Benevento and Sipski 2002). People with SCI may also be affected by mental health conditions such as depression, anxiety disorder, post-traumatic disorder, and grief (Migliorini, Tonge, and Taleporos 2008; Fann et al. 2011; Turner et al. 2002; Klyce et al. 2015; Arango-Lasprilla et al. 2011; Charlifue and Gerhart 1991).

SCIs can be classified into complete or incomplete injuries depending on the absence or presence of sensorimotor function below the level of the injury. The cervical region of the cord is the most common region for SCIs in the United States, (~54%) followed by the thoracic (~35%), lumbar (~10%), and sacral (0.4%) levels (National Spinal Cord Injury Statistical Center 2017).

One of the most commonly used clinical assessment scales for the classification of SCIs is the ASIA impairment scale (AIS). This scale classifies injuries into 5 groups depending on the type (sensory or motor) and strength of the remaining functions (Kirshblum et al. 2011). In 2015-2017, approximately 30% of the people with SCI had a complete injury at the time of discharge from the hospital in the United States (National Spinal Cord Injury Statistical Center 2017).

SCIs can occur as a result of traumatic incidents such as vehicular accidents, falls, acts of violence (NSCISC National Spinal Cord Injury Statistical Center 2018b), or non-traumatic pathologies such as cancer, spinal stenosis, and ischemia (McKinley, Seel, and Hardman 1999). In Canada, it is estimated that the traumatic etiology of SCI constitutes 51% of the total prevalence (Noonan et al. 2012). In 2012, it was estimated that ~85,000 people live with SCI in Canada, with an annual incidence rate of ~4000 people (Noonan et al. 2012).

With the advances in medicine and the care pathways for people with SCI in the developed countries over the past few decades, the survival rates and the life expectancy of people with SCI have improved (McCaughey et al. 2015; Savic et al. 2017; Shavelle et al. 2015). Similarly over the past few decades, the age at the time of injury has also been increasing in the developed world (NSCISC National Spinal Cord Injury Statistical Center 2018b; Montoto-Marqués et al. 2017; Kriz et al. 2017). For instance, in the United States, the mean age of injury has increased from 29 to 42 years since the 1970s (NSCISC National Spinal Cord Injury Statistical Center 2018b). This is an important trend to consider, since the age at the time of injury has been suggested to be an important factor for the prognosis of the SCI, with older population having comparatively worse outcomes (M. J. DeVivo et al. 1990; Ahn et al. 2015; Gwak et al. 2004).

The global trends of SCI, however, may be heading in a different direction. The world health organization estimates that road traffic accidents will become the third or fourth cause of disability in the world by 2030 (from 9<sup>th</sup> place in 2004) due to an increasing number of vehicles in developing countries (McCaughey et al. 2015; Mathers and Loncar 2006; World Health Organization 2004; “WHO | Metrics: Disability-Adjusted Life Year (DALY)” n.d.). This may lead to an increased prevalence of individuals with SCI worldwide and a different makeup of the population with SCI in the developed and developing countries.

SCI also has a significant economic burden for the health care system and the people affected by it. A survey in Alberta, Canada, found that healthcare cost for treatment of SCI ranges from \$40,000-\$120,000 in the first year post-injury followed by an annual cost of \$2,800-\$5,400, in the next five years (expenses estimated based on the 2002 Canadian dollar value). The life-time economic burden for a person living with traumatic SCI in Canada is estimated to be ~1.5-3.0 million dollars depending on the type of SCI (2013 Canadian dollar value) (Krueger et al. 2013).

### **1.1.1. Improving Quality of Life for People with SCI**

Living with a complex and multi-faceted condition such as SCI requires adaptations to social, economical and health-related challenges (Kunj 2016). Examples include unemployment (Krause and Anson 1996; Lidal, Huynh, and Biering-Sørensen 2007; Krause and Anson 1997), changes to the relationships with family and friends (Kreuter 2000; Scelza et al. 2007; Michael J. DeVivo et al. 1995; Westgren and Levi 1994; Chan, Lee, and Lieh-Mak 2000), loss of autonomy and necessity for a caregiver (Kunj 2016), persistent risk for secondary health-complications (e.g., pressure ulcers (Byrne and Salzberg 1996; Regan et al. 2009), deep vein thrombosis

(Mackiewicz-Milewska et al. 2016), etc.), and the health-risks posed onto the caregivers (Weitzenkamp et al. 1997; Ünalán et al. 2001; Arango-Lasprilla et al. 2010; Schulz et al. 2009). Given the complexity of the impact of this condition on the life of people with SCI, it is important to include their point of view in planning research endeavours that aim to improve their quality of life.

Multiple studies have surveyed the priorities of people with SCI for recovery. In these surveys, people with quadriplegia considered upper limb function, sexual function, bladder, bowel and autonomic function, walking function, and trunk stability as their top priorities for recovery (Anderson 2004; Collinger et al. 2013; Simpson et al. 2012; Mattu 2017). Top priorities of people for paraplegia for recovery were walking function, bowel and bladder function, sexual function, and trunk stability (Anderson 2004; Collinger et al. 2013; Simpson et al. 2012; Mattu 2017).

The focus of this thesis project was on the recovery of standing and walking after SCI, one of the most frequently expressed priorities of people with paraplegia (Anderson 2004; Collinger et al. 2013).

## **1.2 Interventions for Restoration or Improvement of Standing and Walking after SCI**

This section describes the interventions for restoring standing and walking for people with SCI, in three categories: rehabilitation paradigms, orthoses, and neuroprostheses. In this section, standing and walking is limited to functional leg movements for standing and stepping and does not include balance. Balance requirements are fulfilled by the use of assistive devices such as crutches or walkers.

### 1.2.1 Rehabilitation strategies

Conventional rehabilitation paradigms for improvements of standing and walking after SCI have traditionally focused on the prevention of secondary complications such as contractures (Nas et al. 2015) and training standing and walking using compensatory strategies (Behrman and Harkema 2007). Examples of these compensatory strategies are strengthening muscles with spared neural control, learning compensatory movement strategies, and use of assistive devices. For people with motor incomplete SCI, these paradigms also include over-ground gait training (Lucareli et al. 2011). Conventional over-ground gait training involves standing and walking exercises with the help of assistive devices/setup (e.g., walker or parallel bars) and therapists as needed (Behrman and Harkema 2007).

More recent rehabilitation strategies involve repetitive task-dependent training of the nervous system with sensory input, aiming to induce functional neuroplastic changes across the injury site in the spinal cord (Lam et al. 2007; Dietz and Müller 2004; Behrman and Harkema 2007). An example of such training strategy for improvements of walking is *locomotor training*, also known as body weight supported treadmill training (BWSTT), or Laufband therapy. In the BWSTT paradigm, the individual is trained to step on a treadmill belt with their body weight supported (Smith and Knikou 2016). BWSTT paradigms were motivated by preclinical studies that had demonstrated improvements in walking, in animals with SCI that had undergone step training on treadmill (Leon et al. 1998; Lovely et al. 1986; Barbeau and Rossignol 1987). Specific methods and parameters for implementation of BWSTTs vary in the literature in treadmill speed, intensity of the training, length of training, type of assistance (e.g. manual and robotic), and amount of assistance (partial, complete, resistance) (Yang and Musselman 2012).

An advantage of robot-assisted BWSTT over manual-assisted BWSTT is that it does not require multiple therapists to help each individual perform the training (Hesse et al. 2003).

Both the conventional over-ground walking exercises (Dobkin et al. 2006; Field-Fote and Roach 2011; Nooijen, Ter Hoeve, and Field-Fote 2009) and BWSTT (Lam et al. 2007; Dobkin et al. 2006; Field-Fote and Roach 2011; Nooijen, Ter Hoeve, and Field-Fote 2009) can significantly improve walking after SCI, and their improvements are similar in terms of walking speed, distance, and functional independence. Both training paradigms have shown effectiveness in improving walking measures in sub-acute and chronic stages of SCI (Dobkin et al. 2006; Alexeeva et al. 2011; Schwartz et al. 2011). The limitation of these interventions however, is that their effectiveness for improving over-ground walking is limited to individuals with motor incomplete injuries (AIS-C and AIS D) (Yang and Musselman 2012).

Effectiveness of BWSTT can vary depending on the level of assistance provided for stepping. A randomized clinical trial in people with chronic motor incomplete SCI showed that, unlike manual BWSTT, complete robotic-assistance for BWSTT did not result in a significant improvement in walking (Field-Fote and Roach 2011). One difference between these two protocols is that the metabolic cost of training is lower for stepping with complete assistance compared to manual assistance (Israel et al. 2006). It is also important to note that under conditions of complete assistance, individuals' movements may lack mindfulness and voluntary drive, which has been suggested to be an important factor for reorganization of the sensorimotor cortex (Lotze et al., n.d.; McDonnell et al. 2015; L. Jaeger et al. 2014).

More recently, another rehabilitation training paradigm for improvements of walking after an SCI was examined by Zhou et al (Zhou et al. 2018), in which individuals were trained by cycling as opposed to walking. Zhou et al (Zhou et al. 2018), demonstrated that leg cycling with

the assistance of functional electrical stimulation may lead to improvements in walking that are similar to those obtained with rehabilitation paradigms focusing on walking exercises. Moreover, they showed that simultaneous training of the arms and legs in cycling exercises with the assistance of functional electrical stimulation, increased the improvements in walking further. The contribution of training the arms to the improvements in walking performance is thought to occur as a result of training the propriospinal networks controlling the upper and lower limbs (Kawashima et al. 2008) and strengthening the corticospinal connections to the networks controlling the lower limbs (Zhou et al. 2017). Similar to the above-mentioned paradigms this study also focused on individuals with motor incomplete injuries.

It is also important to consider that improvements in walking performance are not the only beneficial aspect of the rehabilitation trainings for walking (Audrey L. Hicks and Ginis 2008). Improvements in cardiovascular health (S. M. Phillips et al. 2004; Ditor et al. 2005), psychological health, and life satisfaction (Semerjian et al. 2005; A. L. Hicks et al. 2005) have also been reported for people participating in these training paradigms.

### 1.2.2 Orthoses for the restoration of standing and walking

The application of modern orthoses for standing and walking after paralysis dates back to 1970s and 1980s, with hip-knee-ankle-foot orthoses such as the hip guidance orthosis (HGO) (Major, Stallard, and Rose 1981), reciprocating gait orthosis (RGO) (Douglas et al. 1983), and Steeper's orthosis (also known as advanced reciprocating orthosis or ARGO) (Jefferson and Whittle 1990). All three examples have braces that extend from the middle of the trunk down to the feet and allow flexion and extension movements of the hips, while the knees and ankles are locked (Jefferson and Whittle 1990). These orthoses were used in conjunction with assistive devices

such as crutches (Major, Stallard, and Rose 1981; Butler, Major, and Patrick 1984). Movement of the hips (right and left) are independent in HGO, while in RGO and ARGO, their movements are reciprocal: when one is in extension, the other moves into flexion and vice versa. The reciprocal hip function is implemented in these orthosis using one or two cables connecting the right and left hip braces (Jefferson and Whittle 1990). Unlike HGO and RGO, ARGO allows for a transition from sitting with the knees flexed, to standing (Jefferson and Whittle 1990). Since utilization of these orthoses is only possible in conjunction with assistive devices, their application is limited to people with paraplegia.

Despite the functional benefits provided by gait orthoses, their usage did not become widespread among people with SCI. This has been attributed to the high energy cost of their use (Bernardi et al. 1995) and their weakness in cosmetic appearance (Mokhtar Arazpour, Bani, and Hutchins 2013). Merati et al (Merati et al. 2000) compared the energy expenditure for the use of wheelchairs with RGO orthotics and found a significantly *lower energy cost/locomotion speed* ratio for wheelchairs.

Recent technological advances have led to the development of a new wave of orthoses, known as exoskeletons, that are electrically powered and have more complex electromechanical designs (Herr 2009; Food and Drug Administration, HHS 2015). Similar to the passive orthoses, all but one exoskeleton (REX, Rex Bionics Co., Auckland, New Zealand), require the individual to use assistive devices for balance. Most of the studies on exoskeletons have been conducted in people with thoracic SCI (Contreras-Vidal et al. 2016). The most studied exoskeleton so far is the ReWalk (Rewalk Robotics Inc, Marlborough, MA, USA) (Contreras-Vidal et al. 2016) which was the first model receiving an FDA approval for home use (“ReWalk™ Personal Exoskeleton System Cleared by FDA for Home Use” 2014). ReWalk has two motors on each side, one at the

hip and one at the knee, and initiates stepping by detecting trunk tilt. Stepping parameters are controlled in a closed loop algorithm using sensor data from the foot plate and joint motors (joint angle and angular velocity) (Contreras-Vidal et al. 2016). Rewalk is also programmed for sit-to-stand and sitting motions, and can accommodate a walking speed of up to 2.6 km/h (Contreras-Vidal et al. 2016).

Zeilig et al reported that individuals with SCI required an average of 13 training sessions for using the ReWalk exoskeleton, to have sufficient proficiency to complete the walking assessment tests independently (Zeilig et al. 2012). Arazpour et al measured the physiological cost index (PCI) of using exoskeletons in people with motor complete SCIs (n=5), and showed that they were lower than the PCI for passive RGO orthoses by ~50% (Arazpour et al. 2013). They also showed that the distance covered in the 6 minute walk test with an exoskeleton was significantly longer (~25%) than that with the RGO (Arazpour et al. 2013). Walking speed was also ~30% higher with exoskeletons reaching ~20 m/min (Arazpour et al. 2013). Besides the direct benefits of ambulation, anecdotal evidence also exists for possible improvements in neuropathic pain (Kressler et al. 2014; Esquenazi et al. 2012) for users of exoskeletons with SCI.

Despite the rapid growth of the field of exoskeletons in recent years, seamless and more intuitive control of their operation by the user has been cited as one of their ongoing challenges (Young and Ferris 2017). In this context, research into the application of brain computer interfaces for the control of exoskeletons is also emerging. Lopez-Larraz et al, used EEG recordings from exoskeleton users with SCI for detection of intent and controlling the exoskeleton (López-Larraz et al. 2016).

### 1.2.3 Neuroprostheses for restoration of standing and walking

Neuroprosthetic approaches for restoring standing and walking after SCI primarily focus on utilizing the uninjured and intact parts of the neuro-musculo-skeletal system to produce functional movements. One of the most widely investigated types of neuroprostheses for restoring motor function is functional electrical stimulation (FES). FES uses electrical stimulation to activate excitable tissues such as the nervous system or the muscles to produce a functional motor output. For individuals with SCI, achieving this goal is possible through the application of electrical stimulation to the peripheral nerves (FES in the peripheral nervous system), or applying the electrical stimulation to spinal cord networks below the injury level (FES in the central nervous system). This section reviews important examples in both categories of FES.

#### FES in the Peripheral Nervous System.

Extracellular electrical stimulation activates excitable tissue (e.g., axons) by sufficiently reducing the extracellular potential, leading to depolarization of their membrane potential. If the depolarization of the membrane potential goes beyond threshold, an action potential is produced. Electrical stimulation may reduce the extracellular potential by injecting negative ions or by removing positive ions from the targeted extracellular space (Grimnes and Martinsen 2015).

Peripheral FES can target sensorimotor axons and/or muscles for activation depending on its electrical current path and the stimulation waveform. The current path is affected by the location of the stimulating and return electrodes, electrode design, impedance of the electrode-tissue interface, and the stimulation waveform.

The relationship between the stimulation waveform parameters (amplitude and pulse-width) and the requirements for activation of an excitable tissue is described by the strength-duration curves based on the rheobase hyperbolic model (Grimnes and Martinsen 2015). Based on this model, for each excitable tissue, the larger the stimulation intensity, the smaller the required pulse width for its activation and vice versa. In the context of peripheral FES, it is also important to note that the excitability of muscle tissue is significantly less than that of the nerves; therefore, nerves are activated at lower stimulus intensities than muscles (Mogyoros, Kiernan, and Burke 1996).

Stimulating electrodes for peripheral FES may be placed on the surface of the skin, over excitable nerve or muscle tissue, implanted in the muscle tissue (intramuscular), or implanted around or into nerves (nerve-cuff or penetrating nerve electrodes). Surface electrodes are the least invasive option, but are furthest from their target muscles, and therefore lack targeting specificity. These electrodes are only suitable for activating superficial muscles. Another disadvantage of these electrodes is that due to their distance from the target, they require higher current amplitudes to produce functional outcomes. Therefore, as part of a neuroprosthetic device, they impose higher requirements of power and battery capacity. Placement of electrodes under skin and in the muscle tissue (intramuscular electrodes) increases the stimulation selectivity and reduces the current amplitude requirements for stimulation.

Various types of electrodes have also been developed for stimulation and recording from the peripheral nerves. The most common type is a *nerve cuff* electrode (Rutten 2002) which wraps around a nerve, placing the stimulating and recording sites in contact with the nerve's perineurium. Being closer to target, cuff electrodes require less stimulation amplitude than surface electrodes for activation of their targets (Aoyagi et al. 2004). Cuff electrodes can

accommodate multiple stimulation sites on their non-conductive substrate and therefore allow for multipolar stimulation. Having multiple stimulation sites around and/or along the nerve provides a more uniform access to the fascicles within, and can allow for spatially selective targeting of the fascicles (Goodall, de Breij, and Holsheimer 1996; Grill and Mortimer 1996). In some cases, targeting selectivity can be further enhanced by the use of *current steering* stimulation paradigms (Tarler and Mortimer 2004).

Penetrating peripheral nerve electrodes (e.g., transverse and longitudinal intrafascicular electrodes, also referred to as TIMEs (Boretius et al. 2010) and LIFEs (Badia et al. 2011)), have also been developed to access the deeper fascicles of the nerve. The stimulation thresholds with LIFEs and TIMEs are even lower than cuff electrodes (Badia et al. 2011). TIMEs have access to more fascicles than LIFEs due to their orientation (transverse vs. longitudinal) (Badia et al. 2011). These electrodes are however more invasive and may be more damaging to the targeted nerve.

Choice of stimulation waveform (e.g., pulse width and frequency parameters) can influence the preferential activation of sensory vs. motor axons. This is due to the difference in the excitability of the sensory and motor axons which is reflected in their strength-duration curves. Sensory axons have a lower rheobase and longer chronaxie than motor axons and therefore can be selectively activated with longer pulse-widths and lower amplitudes (Veale, Mark, and Rees 1973; Barss et al. 2018). The difference in the excitability of the sensory and motor axons is due to the presence of a larger number of persistent Na<sup>+</sup> channels (Kuwabara et al. 2006; Bostock and Rothwell 1997) and larger inward rectification currents in the sensory axons (Kiernan, Lin, and Burke 2004). Physical characteristics of axons are also a factor in their excitability. Under the same conditions, axons with larger diameters are more excitable than the

smaller ones and have lower chronaxie and rheobase values (Horch and Kipke 2017). Therefore, larger axons can be selectively activated with lower stimulation amplitudes and shorter pulse-widths.

Over the past few decades, various peripheral FES systems have been developed and extensively studied for the restoration of functional lower limb movements, such as standing (Braz et al. 2009), walking (Brissot et al. 2000) and sit-to-stand transitions (Jovic et al. 2015) for people with paraplegia. Non-invasive implementations of peripheral FES using surface electrodes, have not become widely accepted for functional use in applications of daily living. This may be due to limitations such as: need for electrode placement each time before use, skin sensitivity resulting from chronic regular use, and the low number of muscles accessible by electrical stimulation over the skin (Jaeger 1992). Research is ongoing for the development of clothing embedded with stimulating surface electrodes and addressing some of these challenges (Zhou et al. 2015). Semi-implantable peripheral FES systems with percutaneous electrodes have also been utilized (Handa et al. 1989; Shimada et al. 1996). However these systems also lack mechanical stability and are at risk of electrode breakage, dislodgment, or infection over time (R. J. Jaeger 1992; Shimada et al. 1996). The most commonly implemented and accepted form of peripheral FES for functional daily use is the implantable systems.

Examples of implantable FES systems include the Praxis FES system developed by Neopraxis Pty. Ltd. (Lane Cove, Australia) (Davis, Patrick, and Barriskill 2001) and the Freestand system developed by Case Western Reserve University (Cleveland, USA) (Triolo et al. 2012). Praxis is an implantable system for restoring function in the lower extremities and bladder. This system is comprised of 22 stimulating channels, 18 of which are dedicated to the lower extremities, targeting the femoral, gluteal, peroneal, tibial, and sciatic nerve branches

bilaterally (Davis, Patrick, and Barriskill 2001). Different stimulation algorithms are used for transferring from sitting to standing, standing, and stepping, and each algorithm is selected by a button pressed by the user (Johnston et al. 2005). Johnston et al reported on the use of the system by three people with motor complete thoracic SCI (Johnston et al. 2005). Since after SCI, paralyzed muscles undergo changes such as atrophy (Gorgey and Dudley 2007), increase in intramuscular fat (Gorgey and Dudley 2007), and muscle fiber type changes (Burnham et al. 1997), all participants underwent muscle conditioning exercises and intense training (5 days a week, minimum of 13 weeks) (Johnston et al. 2005).

Muscle atrophy resulting from muscle inactivity after SCI has been shown to be reversible. Mahoney et al showed that 12 weeks (2 days/week) of resistance exercise training with peripheral FES can lead to muscle hypertrophy after chronic complete SCI (Mahoney et al. 2005). Muscle fiber type changes after SCI have also been shown to be reversible with BWSTT (Stewart et al. 2004). Overtime after SCI, type I and type II muscle fiber compositions change to mostly type IIb, fast-twitch, glycolytic muscle fibers (Burnham et al. 1997). Stewart et al, observed significant increases in the distribution of muscle fiber type IIa and a significant reduction in IIb fiber type in people with incomplete SCI (AIS-C) after 6 months of BWSTT training (3 times/week) (Stewart et al. 2004). BWSTT training, however, was not part of the muscle conditioning trainings of the participants of the Praxis system study.

After completing muscle conditioning training, all participants were able to complete tasks independently with the system while using assistive devices. The longevity of standing with this system ranged from ~2 to 35 minutes (Johnston et al. 2005). In the 6 minute walk test, the distance covered by the individuals ranged from ~39 to 215 m (Johnston et al. 2005).

The Freestand system was designed for the purpose of restoring standing function and the ability to transfer from sitting-to-standing. This system had 8 stimulation channels connected to epimysial and intramuscular electrodes targeting the following muscles: vastus lateralis, gluteus maximus, semimembranosus, and erector spinae at the level of T12-L2 (Uhlir et al. 2004). Uhlir et al reported on the use of the system in 10 people with complete thoracic SCI (AIS-A) and 3 people with incomplete low cervical injuries (AIS-B) (Uhlir et al. 2004). One of the 13 participants in this study had an infection that resulted in the implant removal. Approximately 5% of the electrodes experienced mechanical failure throughout this study and required a revision surgery (Uhlir et al. 2004). Similar to the Praxis system, recipients of these implants underwent muscle conditioning and rehabilitation training for functional use of the system (Triolo et al. 2012). Maximal standing time using this system was on average 27 minutes at the time of discharge. However, this value had dropped by approximately 40% at the one-year follow up (Triolo et al. 2012).

Taken together, the examples provided here demonstrate that FES neuroprostheses aiming to restore functions of the lower limbs have been successfully implemented in people. However, the scope of their application and success have been limited mainly due to the rate of fatigue experienced by the individuals. The early onset of fatigue is partly due to other physiological recruitment order of motor units by peripheral FES. This recruitment order depends on the distance of the targeted nerves from the stimulation site and their excitability (Barss et al. 2018). For instance, axons closer to the stimulation site and those with larger diameters are recruited first (Barss et al. 2018). Fast fatigable muscles are innervated by larger axons than slow muscles (Rhoades and Bell 2009). Unlike voluntary motor unit recruitment that typically recruits slow-twitch, fatigue resistant muscles first, the recruitment order of peripheral

FES is not organized based on muscle fiber type, leading to an earlier onset of fatigue. Additionally, FES, unlike voluntary contractions, activates the targeted group of motor units in a time-locked fashion to the stimulus, and at high discharge rates, thus contributing to faster development of fatigue (Gregory and Bickel 2005). Multiple FES strategies have attempted to reduce the motor unit discharge rates in order to reduce the rate of fatigue. Pournizam et al, demonstrated that “sequential” stimulation of different muscles of the quadriceps, reduces the rate of fatigue for each (Pournizam et al. 1988). In this paradigm each muscle was stimulated for 5-10 s at 20 Hz, before moving to the next (Pournizam et al. 1988). Malesevic et al, replicated these results in individuals with SCI, and demonstrated that sequential stimulation of four sites on the quadriceps muscle at a lower frequency (15 Hz), reduces the rate of fatigue compared to single-site stimulation (30 Hz) (Malesević et al. 2010). However, they demonstrated that daily, 30 minutes long sessions of stimulation with the single-site stimulation method resulted in larger improvements of muscle strength and endurance than the sequential stimulation (Malesević et al. 2010). Lou et al, employed an interleaved stimulation paradigm alternating between stimulation of the muscle belly (40 Hz) and the nerve (40 Hz) (Lou et al. 2017). This approach reduces the overlap between the motor units activated (Wiest et al. 2017). Application of interleaved stimulation in able-bodied individuals reduced the tibialis anterior muscle fatigue compared with stimulation at either the muscle belly or the nerve (Lou et al. 2017). However, when applied to individuals with SCI, Bergquist et al did not find a difference in the fatigue produced by interleaved or nerve stimulation in the triceps surae muscle (Bergquist et al. 2017). Muscle fatigue produced by stimulation at the muscle belly was larger than both interleaved and nerve stimulation (Bergquist et al. 2017). Similar results have also been reported using interleaved stimulation with two implanted intrafascicular electrodes in cats (Yoshida and Horch

1993). Yoshida et al demonstrated that the gastrocnemius muscle fatigue was significantly reduced using interleaved stimulation compared with continuous stimulation of each electrode individually (Yoshida and Horch 1993). These developments of physiologically-based stimulation paradigms show promise for mitigation of the fatigue induced by peripheral FES (Barss et al. 2018).

Another component of fatigue experienced by neuroprosthetic users that limits prolonged use of a device is that of the arms, which are involved in partial bodyweight support and balance for standing and walking (Bijak et al. 2005). Recent studies developing control strategies for restoring standing-balance using FES systems, have shown promising results in models of neurological injuries (Vette et al. 2009; A. H. Vette et al. 2005; Rouhani et al. 2017; Tan et al. 2014).. Future inclusion of such strategies in the FES systems may reduce the fatigue experienced by the arms during standing. Arms-free standing would also provide more freedom for functional interactions with the surroundings in tasks of daily living (Nataraj, Audu, and Triolo 2017). As with any other implantation procedure, implantation of FES electrodes also poses the risk of infection. The implants are also at risk of mechanical failure as they are implanted in or near mobile tissue (muscles).

Peripheral FES paradigms have also been used in conjunction with other strategies such as rehabilitation training (Zhou et al. 2018; Donaldson et al. 2000; Baldi et al. 1998) and exoskeletons (Ama et al. 2013; Tu et al. 2017; Zhang et al. 2017) to restore lower limb function for people with SCI. Multiple studies have shown that rehabilitation of walking with the assistance of peripheral FES systems can improve voluntary walking performance in people with chronic incomplete SCI (Granat et al. 1993; Kapadia et al. 2014; Thrasher, Flett, and Popovic 2006; Wieler et al. 1999). Wieler et al showed that walking with FES in the community setting

(for >3 month), can result in significant improvements in voluntary walking speed for people with chronic incomplete SCI (Wieler et al. 1999). Kapadia et al compared BWSTT with FES assistance with resistance and aerobic training (walking or cycling exercises) in people with chronic incomplete SCI (Kapadia et al. 2014). They showed that both rehabilitation paradigms resulted in improvements in voluntary walking (walking speed, endurance and balance). The improvements, however, were not different between training groups except for the spinal cord independence measure (mobility sub-score). Individuals who received FES assisted BWSTT had a larger improvement in their spinal cord independence measure (Kapadia et al. 2014). FES systems have also been used in conjunction with rehabilitation paradigms involving cycling (example provided in section 1.2.1).

Exoskeletons incorporating FES (hybrid exoskeletons) are recently being investigated with the goal of combining the benefits of both strategies. Ha et al reported the use of a hybrid Indego exoskeleton (Parker company, Cleveland, OH, USA) by an individual with complete low thoracic SCI (Ha et al. 2012). In these exoskeletons, FES was applied to the hamstring muscles. The FES-evoked-torques produced around the hip joints contributed to the movement and reduced the power consumption of the joint motor by ~30%. They also showed that as the muscles fatigue, exoskeleton contribution increases and walking function can continue. While research and development of hybrid exoskeletons is still in its early stages, results obtained so far suggest that they may hold potential for becoming an ambulation device for people with SCI with the additional rehabilitative and health benefits of peripheral FES.

## FES in the Central Nervous System.

This section focuses on two spinal-cord-neuroprosthetic techniques that aim to restore or improve standing and walking after SCI, namely epidural stimulation and intraspinal microstimulation.

**Epidural Stimulation.** Epidural spinal cord stimulation is a technique that applies electrical pulses to the exterior surface of the dura mater, on the dorsal side of the spinal cord. Similar to the other electrically active implants, the epidural stimulation system (also referred to as spinal cord stimulator) is comprised of an implanted stimulator, connecting wires and stimulation electrodes (also referred to as ‘lead’). Clinical stimulators can be programmed wirelessly. Stimulation leads consist of a carrier with multiple contacts for stimulation (Jeon 2012; Shils and Arle 2012). Two types of lead carriers are clinically available: percutaneous and paddle leads. Implantation of the percutaneous leads is minimally invasive and can be done through Tuohy epidural needles (“Tuohy Epidural Needle, Pain Management | Smiths Medical.” n.d.). Paddle leads however, require a more invasive surgical procedure for implantation in which a partial or full laminectomy is required (Jeon 2012).

As a treatment, this technique was first used to alleviate chronic pain (Shealy, Mortimer, and Reswick 1967) and has since been utilized for other applications including management of spasticity (G. Barolat, Myklebust, and Wenninger 1988; Pinter, Gerstenbrand, and Dimitrijevic 2000), rehabilitation training for functional recovery after paralysis (Rejc, Angeli, and Harkema 2015), and promoting regeneration after spinal cord injury (SCI) (Shapiro 2014; Shapiro et al. 2005).

Understanding the mechanism of action of epidural stimulation requires an understanding of the pathways the stimulation current takes, as well as the anatomy of the stimulated region. As

with any electrical stimulation system, detailed knowledge about the electrical properties of the environment surrounding the electrodes is essential for determining the resulting stimulation current pathway. In this system, the environment surrounding the electrodes is comprised of various materials such as meninges, cerebrospinal fluid (CSF), spinal cord white and gray matter, dorsal rootlets, epidural fat, vertebral bone, muscles, and electrode lead insulation. Among these materials, CSF has the highest electrical conductivity ( $\sim 3x$  the longitudinal conductivity of white matter,  $\sim 7x$  the conductivity of the gray matter and  $\sim 21x$  the transverse conductivity of white matter) (Giancarlo Barolat et al. 1993; Sin and Coburn 1983; Struijk et al. 1991). Detailed information about the electrical conductivity of these materials can be found in the following references (Holsheimer 1998; Oakley and Prager 2002). The implication of these significant conductivity differences is that most of the electrical current will flow through the path of highest conductivity, in this case the CSF. Analysis of the exact current pathway, however, is a complex problem considering variables such as geometry and volume of the anatomical elements around the electrode, position, spacing between electrodes, the number of cathodes/anodes, and the frequency dependence of the electrical properties of biological tissue. Computer modeling has been used to address this problem further.

Coburn et al (Coburn 1980; Coburn 1985; Coburn and Sin 1985) and Struijk et al (Struijk et al. 1993, 1991) were among the first to develop two- and three-dimensional models of the human thoracic spine and spinal cord and conduct simulations using finite element analysis for epidural stimulation. They also incorporated mathematical nerve fiber models into their simulations. Using these models, they demonstrated the generated patterns of current and voltage distribution and estimated the activation thresholds of different neural structures. For instance, Coburn (Barry Coburn 1985) incorporated nerve fiber models of the dorsal columns and dorsal roots into his

simulation model and verified the simulation results for activation thresholds of dorsal column fibers with experimental values in literature. He then used the model to calculate the activation threshold of dorsal root fibers in the transverse plane, and found that their activation threshold can be lower than the dorsal column fibers, depending on their curvature. Struijk et al (Struijk, Holsheimer, and Boom 1993) modelled dorsal root fibers in the case where the cathode is centered on the midline. They demonstrated that the smallest activation thresholds belong to dorsal root fibers bending and entering the spinal cord perpendicularly. Based on the computer modelling literature, the following elements can be activated using epidural stimulation with clinical therapeutic stimulation amplitudes (Holsheimer 1998; Holsheimer, Struijk, and Rijkhoff 1991): : Dorsal root fibers, 0.2 – 0.3 mm depth of the dorsal and dorsolateral spinal cord, and posterior spinocerebellar tracts.

Epidural stimulation for the improvement of standing and walking after SCI is commonly applied to the lumbosacral region of the spinal cord which houses the locomotor networks. Given the estimated current spread, epidural stimulation does not directly activate the neurons in the ventral horns of the spinal cord. However, it can target them trans-synaptically (mono- and polysynaptic pathways) through activation of indirect pathways, such as afferent projections entering the spinal cord's dorsal surface (Sharpe and Jackson 2014; Capogrosso et al. 2013). This is supported by the analyses of the latencies of the evoked EMG responses as well as the interaction of the epidural stimulation with peripheral nerve stimulation on the evoked EMGs (Hunter and Ashby 1994).

Rehabilitation training and functional recovery after paralysis: This application was first motivated by the evidence that epidural stimulation can produce stepping-like movements in the

lower/hind limbs, both in animal models (cats (Gerasimenko et al. 2003) and rats (Ichiyama et al. 2005)) and in humans with complete SCI (Dimitrijevic, Gerasimenko, and Pinter 1998). Dimitrijevic et al (Dimitrijevic, Gerasimenko, and Pinter 1998) were the first to demonstrate that non-rhythmic epidural stimulation over the lumbar enlargement of the spinal cord in human subjects with complete SCI (in supine position) can produce rhythmic leg movements (alternating between flexion and extension phases). They also demonstrated its ability to produce tonic leg movements in supine position, using different stimulation parameters. The optimal location of the stimulation lead was suggested to be over the lumbar enlargement and in the case of rhythmic locomotor-like movements segment L2 was suggested.

Later in 2002, Herman et al combined epidural stimulation with partial weight bearing therapy (PWBT) on a participant with incomplete SCI (AIS-C) (Herman et al. 2002). They reported that the addition of epidural stimulation to the protocol led to an increase in walking speed and reduced the energy cost of walking (Herman et al. 2002). In 2011, Harkema et al (Harkema et al. 2011) conducted a similar study on a participant with an incomplete spinal cord injury (AIS-B; clinically motor complete). Before introducing epidural stimulation to the rehabilitation protocol, the participant had received locomotor training using body weight supported treadmill (BWSTT) for over 2 years without improvement in leg muscle EMG activity. After receiving the epidural stimulation implant, the participant was trained for standing combined with epidural stimulation for 7 months. During this period, improvements in body weight support during standing was demonstrated. At the end of the training protocol, the participant was able to stand with minimal assistance for up to ~4 minutes. During standing, assistance was provided for hip extension and balance (Rejc, Angeli, and Harkema 2015). After obtaining these promising results, the group recruited three more participants (Angeli et al. 2014; Rejc, Angeli, and Harkema 2015),

two with AIS-A and one with AIS-B SCI. Similar to the case study, all the participants underwent BWSTT before the epidural stimulation implant and were trained for standing with epidural stimulation post-implant. At the end of these studies, the AIS-B participant was able to stand with epidural stimulation with minimal assistance, similar to the participant in the case study. The unexpected finding was that both AIS-A participants performed better than the individuals with AIS-B injuries, and were able to stand with stimulation and assistance only for balance (none for hip extension). The stimulation paradigm used for standing in these individuals was customized and optimized for each person and cross-testing of the settings between participants was not successful (Rejc, Angeli, and Harkema 2015). The observation that epidural stimulation paradigms optimized for standing produced no/small EMG activity in the sitting position but was significantly amplified after the weight transfer on the legs, suggested that sensory input is essential for standing with epidural stimulation (Rejc, Angeli, and Harkema 2015).

Another important observation in these studies was that in the presence of epidural stimulation, all of the participants were able to gain voluntary control for producing selective leg movements (e.g., ankle dorsiflexion) (Angeli et al. 2014; Harkema et al. 2011). A possible explanation for restoration of voluntary control could be that epidural stimulation partially depolarizes the membrane of neurons with spared descending projections, bringing them closer to firing threshold. The enhanced excitability of the spinal networks would then allow for cortical control using the limited spared projections. This is consistent with the observation of this study that participants with higher spasticity and clonus required less stimulation threshold to establish voluntary control of the movements (Angeli et al. 2014).

Interestingly, the epidural stimulation parameters that facilitate voluntary control of leg movements were different from those producing weight-bearing knee extension for standing and

these conditions could not be combined (Rejc, Angeli, and Harkema 2015). Combination of the two modes of stimulation in future using higher density electrode arrays and more complex pulse generators may increase the functionality of the voluntarily controlled movements.

In addition to the above-mentioned observations, other benefits were also reported as a result of training with epidural stimulation (Edgerton and Harkema 2011). These included improvements in voluntary bladder control, body temperature control, regulation of blood pressure, and sexual function. Voluntary bladder control continued to exist even in the absence of stimulation. The exact timeline for the onset of these benefits were not reported in the early studies (Edgerton and Harkema 2011). A subsequent clinical study investigated the effect of locomotor training with epidural stimulation on the bladder and bowel function of 8 individuals with SCI (AIS A-D) (Hubscher et al. 2018). In this study, the stimulation was applied over the lumbosacral enlargement of the spinal cord. After 80 daily training sessions, significant improvements were demonstrated in bladder capacity, voiding efficiency and reduction of the duration of defecation, compared to the control group (Hubscher et al. 2018). More recently, another clinical study also demonstrated the ability of epidural stimulation of the lumbosacral enlargement in modulating blood pressure, for treatment of orthostatic hypotension after chronic SCI (Phillips et al. 2018).

Collectively, the clinical case studies presented here suggest that application of epidural stimulation to the lumbosacral enlargement of the spinal cord, combined with intense rehabilitation training of walking, may result in limited functional improvements of standing for individuals with SCI. Further conclusions about the efficacy and effect size of epidural stimulation in improving standing function after SCI would require larger controlled clinical trials. Future studies should also compare the quality and longevity of standing achieved using this technique with alternative established methods such as peripheral FES.

Recent clinical results from the application of epidural stimulation for improvements in blood pressure modulation and bowel and bladder function are promising (Phillips et al. 2018; Hubscher et al. 2018). Further investigations into their mechanisms of action are needed to optimize their implementation and resulting benefits.

**Intraspinal Microstimulation.** Intraspinal microstimulation (ISMS) is an FES technique that applies electrical stimulation to targets within the gray matter of the spinal cord. Historical utilizations of ISMS date back to the year 1940, with experiments conducted by Birdsey Renshaw for the study of synaptic delays of spinal reflex pathways in cats (Renshaw 1940). Renshaw compared the onset delays for responses recorded from the ventral L7 (or S1) root that were evoked either by dorsal root stimulation at the same level and/or ISMS (Renshaw 1940). To implement ISMS and evoke motoneuronal activity, Renshaw implanted bipolar needle electrodes into the intermediate and ventral parts of the gray matter of the spinal cord (Renshaw 1940).

In 1976, Gustafsson and Jankowska (Gustafsson and Jankowska 1976) used ISMS for investigating the effect of extracellular stimulation on the evoked motoneuronal activity in the lumbar spinal cord of cats. They quantified the changes in extracellular stimulation threshold based on the distance of the electrode from targeted motoneurons. The lowest thresholds for direct activation of the motoneurons were produced by electrodes located closest to the initial segment of the axons (Gustafsson and Jankowska 1976). Lowest thresholds for transynaptic activation of the motoneurons were produced by electrodes located closer to the motoneuronal dendrites as opposed to the axon (Gustafsson and Jankowska 1976). Jankowska et al also used ISMS to investigate various interneuronal populations in the gray matter of the spinal cord of

cats (Jankowska 1992), such as those involved in reciprocal inhibition (Jankowska and Roberts 1972).

The first application of ISMS as a neuroprosthesis for restoring lost functions after SCI was in the sacral region of the spinal cord with the aim of improving bladder function. Friedman et al (Friedman, Nashold, and Senechal 1972; Blaine S. Nashold, Friedman, and Boyarsky 1971) demonstrated that voiding of bladder can be triggered, in 36 female cats and dogs, by ISMS in the intermediate depths of the gray matter at the S1-S2 levels. This was achieved in 55% of animals with intact spinal cords and 62.5% of those with a lumbar spinal cord transection (Friedman, Nashold, and Senechal 1972). Nashold et al later implemented this technique in 27 people with SCI in north America and Europe over a period of ten years (Nashold et al. 1972, 1977; Nashold, Friedman, and Grimes 1982). The clinical implant design was comprised of two electrodes (one in each side of the spinal cord) that were placed at the level of S1-S2 of the spinal cord (Nashold et al. 1972). In total, 55% of the recipients of these implants were able to regain control of bladder emptying with this neuroprosthesis (Nashold et al. 1977). The majority (66%) of the functionally successful implants were in female patients (Nashold, Friedman, and Grimes 1982). Besides bladder emptying, a few other effects were also reported which are interesting to note. In few patients, continuous stimulation for up to a minute resulted in autonomic responses such as sweating, piloerection, temperature increase below the level of the injury, and erythema (Nashold et al. 1972). In one patient with a high thoracic injury, episodes of autonomic dysreflexia were also reported as a result of stimulation (Nashold et al. 1972). Nashold et al reported that the unintended triggering of autonomic responses were minimized by adjusting the stimulation parameters (amplitude and frequency) for each patient (Nashold et al. 1972).

The second neuroprosthetic application of ISMS was for restoration of standing and walking after SCI. In 2000, Mushahwar and Horch used ISMS electrodes to obtain an electrophysiological map of the lumbosacral spinal cord of cats, and assess the evoked motor responses (Mushahwar and Horch 2000b). They demonstrated that ISMS can selectively evoke coordinated and strong movements in the hindlimbs (Mushahwar and Horch 1997; Mushahwar and Horch 2000b) with relatively low stimulation intensities. In the past two decades, research related to ISMS for walking has continued and shown important promising outcomes such as its ability to produce stepping movements in the hindlimbs of cats after an SCI (Saigal, Renzi, and Mushahwar 2004), and produce prolonged standing (Lau, Guevremont, and Mushahwar 2007) and over-ground walking (Holinski et al. 2016). This neuroprosthesis is the main focus of the present thesis. Previous work and background related to ISMS are described in more detail in section 1.3.

ISMS has also been used to restore movements of the upper limbs after SCI (Zimmermann, Seki, and Jackson 2011). One of the earliest studies was conducted by Moritz et al where they investigated the organization of the neural networks using ISMS in the ventral horns of the cervical enlargement (C6-T1) in non-human primates (Moritz et al. 2007). They demonstrated that depending on the location of the electrode, stimulation through a single electrode can produce various functional movements in the shoulder, elbow, wrist, and fingers (Moritz et al. 2007). Most of the ISMS evoked movements involved synergistic activity among multiple muscles, in some cases even up to 12 muscles (Moritz et al. 2007). By stimulation through one electrode, synergies were also observed across different joints. The most commonly produced multi-joint movement was synergistic flexion of the thumb and fingers (Moritz et al. 2007). The ability of ISMS in producing synergistic movements is beneficial from a

neuroprosthesis design perspective because fewer implanted electrodes are required to produce a functional synergistic movement involving multiple muscles. Later studies by Zimmermann et al (Zimmermann and Jackson 2014) and Nishimura et al (Nishimura, Perlmutter, and Fetz 2013) utilized ISMS implants in the cervical spinal cord of monkeys to control forelimb muscles that were temporarily or permanently paralyzed. Both groups used brain computer interfaces to detect the animals' intent to perform a movement and activated the forelimb muscles with the ISMS neuroprosthesis (Zimmermann and Jackson 2014; Nishimura, Perlmutter, and Fetz 2013). Most recently, ISMS has been investigated for activating paralyzed muscles for breathing such as the diaphragm and the intercostal muscles. This work focuses on activating the networks in the mid-cervical to high-thoracic regions of the spinal cord (Sunshine et al. 2018; Mercier et al. 2017).

ISMS has also been used to improve the recovery of motor function after an SCI. Kasten et al applied daily ISMS to the ventral horns below the level of injury, in the cervical enlargement of the spinal cord of rats with SCI (contusion injury, C4-C5) (Kasten et al. 2013). ISMS was implemented using implants with 3 microelectrodes in each side of spinal cord levels C6-T1. Starting 4 weeks post injury, the stimulation was applied 7 hours a day, 5 days a week for 12 weeks. All animals also received daily reaching training without stimulation for 5 days a week. Functional outcomes in this study were measured by the precision forelimb reaching test (Schrimsher and Reier 1992; McKenna and Whishaw 1999). This test involved scoring the number of times an animal successfully reached with its forelimb and grabbed a food pellet, 2 cm away from its cage. In this task the food pellet was on a freestanding pillar 1 cm away from the cage, preventing the animal from successfully sliding the pellet towards itself, instead of grabbing. Rats receiving regular ISMS stimulation recovered their upper limb function

significantly better those that did not. Improvements became significantly different from the control group starting 2 weeks after the start of *therapeutic ISMS* until the end of the treatment.

McPherson et al (McPherson, Miller, and Perlmutter 2015) took a step further and investigated the effect of activity-dependent ISMS on the recovery of forelimb function in rats with SCI (incomplete contusion injury at C4-C5). In this study, ISMS was applied below the level of injury in spinal cord levels C6-C8, 5 days a week, for 13 weeks. They used online EMG recordings to trigger activity dependent single-pulse-ISMS at amplitudes 10% smaller than the resting motor threshold (McPherson, Miller, and Perlmutter 2015). Precision forelimb reaching was used as a measure of forelimb function in this study. A comparison was conducted between the recovery of forelimb function for animals that were subject to rehabilitation in conjunction with activity dependent ISMS (AD-ISMS), those only undergoing rehabilitation, and those undergoing rehabilitation in conjunction with open-loop ISMS (OL-ISMS) (McPherson, Miller, and Perlmutter 2015). After 13 weeks of treatment, animals in the AD-ISMS group recovered significantly better than those in the rehabilitation only group or the OL-ISMS group (McPherson, Miller, and Perlmutter 2015). These trends were shown to persist up to at least three months after discontinuation of ISMS and with reduced rehabilitation training (reduced from 2 sessions/day to 1 session/day) (McPherson, Miller, and Perlmutter 2015). These promising results suggest that activity dependent ISMS may be a promising approach for enhancing recovery after SCI.

## **1.3 Intraspinal Microstimulation for Restoration of Standing and Walking**

ISMS for the purpose of restoring standing and walking after SCI is implemented in the lumbosacral enlargement. ISMS implants are comprised of microelectrode arrays that penetrate the spinal cord parenchyma from the dorsal surface and target the neural networks in the ventral horns of the gray matter. This section describes the technological design, mechanism of action and the functional outcomes of the ISMS technique for restoring walking.

### **1.3.1 Mechanism of Action**

The neural elements targeted by spinal cord stimulation depend on the location of the stimulation site. Placement of electrodes in the dorsal and intermediate parts of the gray matter of the lumbosacral enlargement (from lamina I to VII) results in flexion only movements (Mushahwar et al. 2007). Moving the electrodes more ventromedial (lamina VIII), produces bilateral contractions and stimulation in the ventral and ventrolateral regions (lamina IX) produces synergistic movements (in one joint or across multiple joints) in the ipsilateral hindlimb (Mushahwar et al. 2007). EMG responses evoked by ISMS in different laminae of the spinal cord in the cervical enlargement (in rhesus monkey) have highest to lowest stimulation thresholds in the following locations, respectively: dorsal subdural space, dorsal and intermediate gray matter, ventral gray matter, ventral subdural space (Sharpe and Jackson 2014). Stimulation thresholds reduce moving from dorsal to ventral side of the spinal cord. Responses to ISMS in the ventral part of the gray matter have the largest gradation range, compared to all the above-mentioned stimulation sites (Sharpe and Jackson 2014). Gradation range is defined as the range

of stimulation intensity over which increasing (or decreasing) stimulation intensity results in an increase (or decrease) in the magnitude of the response (Sharpe and Jackson 2014). Large gradation ranges are desirable because they provide flexibility for control of the evoked responses. Collectively, the ventral horns of the gray matter are the most suitable stimulation sites for ISMS neuroprostheses aiming to restore mobility. This is because ISMS in this region has the largest gradation range, a low stimulation threshold for producing movements, and can produce functional synergistic movements in the ipsilateral limb.

The ventral horns of the spinal cord house cell bodies of motoneurons and interneurons along with the axonal projections associated with them such as propriospinal, afferent and descending projections. ISMS in the ventral horns can activate these neurons directly and trans-synaptically, depending on the location of the electrodes relative to the neurons and the stimulation intensity (Gustafsson and Jankowska 1976). For instance, ISMS in the ventral horns commonly activates afferent axons at a lower stimulation threshold than the motoneurons (Gaunt et al. 2006). Stimulation through a single ISMS electrode, can activate afferents that are up to 17 mm away (rostrocaudally) from the stimulation site and trans-synaptically activate their post-synaptic motoneurons and interneurons (Gaunt et al. 2006). ISMS may also activate propriospinal fibers in passage which are known to have excitatory monosynaptic and excitatory or inhibitory disynaptic projections to motoneurons (Jankowska et al. 1974; Yakovenko, Kowalczewski, and Prochazka 2007). Propriospinal projections can span multiple spinal cord segments and commonly terminate in lamina VII and VIII in the intermediate and ventromedial parts of the gray matter of the spinal cord (Barilari and Kuypers 1969; Ruder, Takeoka, and Arber 2016).

Bamford et al (Bamford, Putman, and Mushahwar 2005), showed that ISMS in the ventral horns of the lumbosacral enlargement of rats recruits fatigue resistant muscle fibers more often than peripheral FES and has graded force recruitment curves. This suggests that ISMS has a motor unit recruitment order similar to that of voluntary recruitment. Voluntary recruitment of motor units is thought to follow Henneman's size principle (Henneman and Olson 1965), in which more fatigue resistant motor units are recruited first. Then, faster and more fatigable motor units are recruited, increasing the size of the muscle contraction and the resulting torque (Barss et al. 2018). This characteristic of ISMS is likely mediated by the trans-synaptic activation of the motor neuronal networks. This is also consistent with observations made with peripheral FES (tibial nerve) where, motor units recruited trans-synaptically by H-reflex are shown to be more fatigue resistant than those recruited by M-waves, in people with complete SCI (Bergquist et al. 2014).

The locations of various motoneurons in the lumbosacral enlargement of the spinal cord has been extensively studied in cats using retrograde labeling (Vanderhorst and Holstege 1997). Mushahwar et al (Mushahwar and Horch 2000b; Saigal, Renzi, and Mushahwar 2004; Mushahwar et al. 2002) also investigated the functional organization of the motoneurons in the lumbosacral enlargement of the spinal cord using ISMS. The functional organization of the motoneuronal pools is defined as the organization of the motor responses (e.g. movements or muscle activity) to electrical stimulation in various parts of the ventral horns of the spinal cord. Mushahwar et al (Mushahwar and Horch 2000b; Saigal, Renzi, and Mushahwar 2004; Mushahwar et al. 2002), demonstrated that stimulation through a single electrode in the ventral horns of the spinal cord can evoke coordinated activity in the hindlimb muscles acting on the same joint as well as those across multiple joints (Saigal, Renzi, and Mushahwar 2004;

Mushahwar and Horch 2000a; Mushahwar et al. 2002). ISMS with a single electrode has also been shown to produce isometric joint forces up to ~73% of the maximal twitch force (evoked by supramaximal stimulation of the nerve) in the cats' hindlimbs (Mushahwar and Horch 2000a). These results are consistent with the mechanism of action of ISMS in trans-synaptic activation of homonymous and/or heteronymous motoneurons that are farther than its stimulation current spread.

The relative functional organization of the motoneuronal pools in the lumbosacral spinal of cats is consistent from animal to animal (within species) (Mushahwar and Horch 2000b; Saigal, Renzi, and Mushahwar 2004; Mushahwar et al. 2002). Importantly, Saigal et al demonstrated that the organization of the motor networks targeted by ISMS in cats are unchanged when tested two to four weeks post SCI (complete transection at T10-T12) (Saigal, Renzi, and Mushahwar 2004). Clinical evidence from the implementation of ISMS for controlling bladder function in people with chronic SCI also suggests that networks targeted by ISMS are still present and excitable even chronically after complete SCI (Nashold et al. 1972).

### 1.3.2 Design, safety and stability of the implants

Design of the ISMS implants for restoration of walking in cats consists of an array of 16-24 microelectrodes implanted bilaterally in the ventral horns of the lumbosacral enlargement (Bamford et al. 2016). The microelectrodes are made out of 30  $\mu\text{m}$  platinum iridium (80%/20%) microwires, insulated with a 4  $\mu\text{m}$  thick layer of polyimide, except for 70-200  $\mu\text{m}$  at the tip. The de-insulated tips of the microelectrodes are bevelled to 15° in order to reduce the mechanical resistance of the tissue to their insertion (Sean Snow et al. 2006). The microelectrodes are advanced through the dorsal surface of the spinal cord, with tips targeting the ventral horns.

Since the subdural space in cats is relatively small (~0.25 mm), the ISMS microelectrodes are implanted trans-durally through small holes in this membrane. The spacing between consecutive microelectrodes in the array is 3 mm for cats (Bamford et al. 2016). The microelectrodes are connected to a pulse generator through lead-wires of the same material and size (Bamford et al. 2016). The lead-wire bundle is typically oriented rostrally and fixed to the first spinous process rostral to the implant region (L3 in cats), before connecting to the pulse generator (Holinski et al. 2013).

Most of the preclinical literature on the use of ISMS implants for walking were conducted using microelectrodes with a single stimulation site. In 2006, Snow et al developed multi-site microelectrodes for ISMS applications (Snow et al. 2006; Snow, Horch, and Mushahwar 2006). These electrodes had 4 stimulation sites along their shafts and were made on a cylindrical fiber optic substrate (85  $\mu\text{m}$  in diameter) (Snow et al. 2006). Multisite electrodes improved the chance of successful targeting of the motoneuronal pools in the ventral horns of the spinal cord (Snow, Horch, and Mushahwar 2006).

Implantation trajectory of the ISMS microelectrodes is most commonly chosen to be perpendicular to the coronal plane of the spinal cord. Given that microelectrode alignment is subject to visual error caused by the curvature of the surface of the spinal cord, an alignment method has been developed to assist in this process. This method involves the use of a mechanical microelectrode insertion guide for implants in cats and has been shown to reduce alignment error in bench tests (Bamford et al. 2016). The implantation of the ISMS arrays in small animals is typically done manually by the surgeon, by inserting the microelectrodes individually.

One of the critical design aspects for chronic success of ISMS implants is their mechanical design including their points of fixation and strategies for relieving mechanical stresses. From a mechanical perspective, the spinal cord is a viscoelastic tissue that can move in the spinal canal and experience length changes as a result of normal, physiological movements of the body (White and Panjabi 1990). In order to accommodate for these movements without dislodging the microelectrodes, ISMS implants incorporate extra lead-wire length (slack) in their design in an effort to mechanically dissociate the implanted electrodes from the fixation of the lead-wires on the bone. In the studies of ISMS in small animal models, sustained functionality overtime and unchanged/reduced stimulation thresholds are used as functional signs of mechanical stability of the ISMS implants (Bamford et al. 2016). In this context, spinalized rats (complete transection at T8) with chronic ISMS implants were studied for 30 days. The majority of the implanted electrodes (8/12) showed a reduction in their stimulation threshold over the course of 30 days, 1 electrode did not experience change in its threshold, 2 had an increase in their threshold, and 1 electrode failed on day 14 (Bamford, Todd, and Mushahwar 2010). The reason behind the threshold increase seen in 2 out of 12 electrodes is likely due to relative dislodgment of the electrode from its initial position and therefore moving away from its target (Bamford, Todd, and Mushahwar 2010). The reason behind the failure of the electrode that stopped working in the second week of experimentation was not reported in this study (Bamford, Todd, and Mushahwar 2010). However, most of the implanted electrodes were stable and functional and experienced a drop in their stimulation threshold (Bamford, Todd, and Mushahwar 2010).

Mushahwar et al (Mushahwar, Collins, and Prochazka 2000) also studied cats (intact spinal cord) with chronic ISMS implants in which 6-12 electrodes were implanted in each

animal. These experiments showed that in each animal at least 67% of the electrodes remained functional for the whole duration of the study ranging from 2 to 24 weeks. Similar to experiments in rats, these experiments also showed that the majority of the implanted electrodes remained functional for the duration of the testing (Mushahwar, Collins, and Prochazka 2000). The reason behind the failure of the rest of the electrodes were not reported. In these experiments, unlike the experiments in the rats, the stimulation thresholds increased over time for all electrodes (Mushahwar, Collins, and Prochazka 2000). One of the differences between this study and the study conducted in rats is that, spinal cords of rats were stimulated daily (continuously for 4 hours) for the duration of the study (30 days) (Bamford, Todd, and Mushahwar 2010). Stimulation of the spinal cords of cats however was more limited and involved short stimulation pulse trains, twice a week for the duration of the study (Mushahwar, Collins, and Prochazka 2000). A possible reason for the reduction of stimulation thresholds in rats maybe neuroplasticity resulting from chronic electrical stimulation in the spinal cord. This may be mediated by migration of the neuronal targets closer to the stimulating electrodes (Bamford et al. 2016; Jeong et al. 2009).

Safety of electrical stimulation in the spinal cord using the ISMS microelectrodes has also been investigated. In a study in rats, Bamford et al (Bamford, Todd, and Mushahwar 2010) compared the effect of daily stimulation (4 hours/day) over a period of 30 days on the spinal cord tissue with unstimulated implanted electrodes as a control. The daily stimulation protocol in this study included trains of pulses with a frequency of 0.5 Hz and 50% duty cycle (i.e. 1 s 'on' and 1 s 'off'). Each train included stimulation pulses with a frequency of 25 Hz, pulse width of 200  $\mu$ s, and intensities ranging between 140 – 260  $\mu$ A (on average 2.5x the stimulation threshold), that produced functional movements (Bamford, Todd, and Mushahwar 2010). These stimulation

amplitudes are substantially larger than amplitudes typically used for production of functional walking in studies in cats ( $<100 \mu\text{A}$ ) (Holinski et al. 2016); however, the electrochemical processes ongoing at the electrode-tissue interface are dependent on the specifications of the electrode (Cogan 2008). Electrodes tested in this study had the same diameter ( $30 \mu\text{m}$ ) as the implants in cats (Bamford et al. 2016; Bamford, Todd, and Mushahwar 2010), but may have had substantially different tip exposure sizes and impedances. Bamford et al found no change in the neuronal density in the ventral horns in animals with stimulated ISMS electrodes compared with those with non-stimulated implants or controls (no implants) (Bamford, Todd, and Mushahwar 2010). No difference was also found between the glial response to the stimulated and non-stimulated electrodes (Bamford, Todd, and Mushahwar 2010). Collectively, these results suggest that chronic stimulation of spinal cord tissue with the mentioned microelectrode specifications and stimulation parameters does not cause damage in the form of cell death. Implantation of the electrodes themselves does result in limited mechanical damage to the spinal cord tissue. The presence of electrodes, as a foreign body, in the spinal cord results in a limited glial response. However, Bamford et al, demonstrated that the electrodes remain functional despite this glial encapsulation (Bamford, Todd, and Mushahwar 2010).

Chronic ISMS implants (2-24 weeks) in cats with intact spinal cords also resulted in no functional sensorimotor deficits throughout the study (Mushahwar, Collins, and Prochazka 2000). Moreover, ISMS evoked movements were produced in these animals without any sign of pain or discomfort (Mushahwar, Collins, and Prochazka 2000), despite their intact sensory pathways.

### 1.3.3 Functional Benefits of ISMS implants

ISMS neuroprosthesis can produce various functional coordinated movements in the hindlimbs of paralyzed animals, that when activated through a control algorithm, can form into standing and walking (Stein and Mushahwar 2005). The ability of the ISMS technique in producing coordinated single- and multi-joint synergistic movements through single-electrode stimulation, makes these implants compact and efficient. Using ISMS implants with as few as 4 electrodes on each side of the lumbosacral enlargement of the spinal cord (spanning 3 cm long in cats and 5 cm in humans), bilateral stepping movements can be produced in the hindlimbs. The ability to produce multi-joint synergistic movements also simplifies the control of ISMS implants for production of more complex repertoire of functional movements.

One of the important benefits of ISMS for producing hindlimb movements is its ability to produce significantly more fatigue-resistant movements compared with those produced by peripheral FES. This is attributed to the motor unit recruitment order of ISMS which is more similar to that of voluntary contractions than peripheral FES (Mushahwar and Horch 2000a; Bamford, Putman, and Mushahwar 2005). The motor unit recruitment order of the voluntary contractions referenced here, is that of voluntary contractions gradually increasing in size. More details were discussed in sections 1.3.1 and 1.2.3.

Mushahwar et al measured force recruitment curves for ISMS-evoked activation of the quadriceps, triceps surae and tibialis anterior motoneuronal pools in cats (Mushahwar and Horch 2000a). Force recruitment curves with ISMS were graded with average slopes of 7.9%, 8.5%, and 2.9% (plateau force/nC), for quadriceps, triceps surae and tibialis anterior muscles, respectively (Mushahwar and Horch 2000a). Bamford et al, compared the force recruitment curves of the quadriceps muscle in rats, measured through ISMS and nerve cuff stimulation of

the femoral nerve (Bamford, Putman, and Mushahwar 2005). The force recruitment slope was found to be 4.9 times larger for nerve cuff stimulation than ISMS. They also demonstrated that ISMS depleted a larger proportion of fatigue resistant muscle fibers from glycogen than nerve cuff stimulation, at stimulation intensities 3x the threshold (Bamford, Putman, and Mushahwar 2005). Similar results were also obtained in cats by Snow et al (Snow, Horch, and Mushahwar 2006), showing the force recruitment slope to be 2.9 times larger for nerve cuff stimulation (femoral nerve) compared with ISMS.

Mushahwar and Horch, investigated the effect of interleaved ISMS stimulation, on the fatigue rate of the quadriceps muscles in cats (Mushahwar and Horch 1997). They compared the typical stimulation paradigm of ISMS (50 Hz frequency, 300  $\mu$ m pulse width) with an interleaved stimulation paradigm. The interleaved paradigm involved stimulation through two ISMS electrodes activating the same motoneuronal pool, in an interleaved manner, at half the stimulation frequency (25 Hz) (Mushahwar and Horch 1997). They demonstrated that interleaved stimulation significantly reduces the rate of fatigue compared with the typical stimulation paradigm of ISMS (Mushahwar and Horch 1997).

Influence of the motor unit recruitment order of ISMS has also been observed in studies that utilized these implants for producing functional standing and walking. For instance, Lau et al (Lau, Guevremont, and Mushahwar 2007) investigated the rate of fatigue during ISMS-evoked standing in anesthetized cats. They developed a closed-loop control algorithm for ISMS implants to produce stable balanced standing posture. The closed-loop controller used ground reaction force along with joint angle information (from accelerometers) as sensory feedback to modulate ISMS intensity (Lau, Guevremont, and Mushahwar 2007). For comparison, a similar controller was also implemented for standing produced by peripheral FES using intramuscular electrodes.

They demonstrated that ISMS was able to produce substantially longer durations of stable standing (on average 20.89 minutes) compared with peripheral FES (on average 4.24 minutes) (Lau, Guevremont, and Mushahwar 2007). The rate of ground reaction force decay was also significantly smaller (on average 4.7 times smaller) with ISMS compared to peripheral FES (Lau, Guevremont, and Mushahwar 2007).

Holinski et al implemented ISMS in anesthetized cats to evaluate its performance in producing over-ground walking (Holinski et al. 2016). They demonstrated that animals with ISMS implants can walk for ~870 m over-ground while still producing weight-bearing ground reaction forces (Holinski et al. 2016). Similar to the control strategies for prolonged standing, long walking distances were achieved by implementing a closed-loop control algorithm using ground reaction forces and limb position as sensory input (Holinski et al. 2016). The walking distances achieved by ISMS can be put in context when compared with walking performance of cats with peripheral FES (using intramuscular electrodes). Mazurek et al used a similar closed loop algorithm to control peripheral FES implants for walking in cats and demonstrated that these animals could only walk up to an average of ~52 m before losing weight-bearing force levels (Mazurek et al. 2012).

Importantly, ISMS implants have also been able to produce functional stepping movements in the hindlimbs of spinalized cats (complete low thoracic SCI) in decerebrate conditions without the effect of anesthesia (Saigal, Renzi, and Mushahwar 2004). Saigal et al demonstrated that functional weight-bearing stepping movements can be produced in cats with complete SCI (2-4 weeks post injury) using ISMS implants (Saigal, Renzi, and Mushahwar 2004).

ISMS implants are compact and require low levels of electrical current (<100-150  $\mu$ A). Low power requirements are an attractive feature for an implantable system since it reduces the requirements for battery size.

Collectively, ISMS implants present a promising strategy for restoring standing and walking, even after complete SCIs. In contrast with peripheral FES, the ability of ISMS implants in producing fatigue resistant movements is an important advantage for its application as a neuroprosthesis for daily activities. Since ISMS implants benefit from activation of the innate circuitry of the spinal cord for synergistic activation of muscles, planning and controlling the evoked movements is less complex compared with peripheral FES. In comparison with epidural stimulation, ISMS also provides an important functional advantage in its degree of selectivity in targeting specific motor neuronal pools and therefore motor outputs.

In addition to the neuroprosthesis application of ISMS for restoring mobility, its recent implementations as a promoter of neuroplasticity in conjunction with rehabilitation ('therapeutic ISMS') has also shown promise for enhancing functional recovery of rehabilitation interventions.

## **1.4 Clinical translation of ISMS implants and thesis outline**

As discussed in this chapter, multiple interventions exist that aim to restore or improve standing and walking for people with paraplegia. Each or a combination of these intervention strategies provide recovery opportunities for a sub-population of people with SCI; a universal cure for all SCIs has not been achieved yet. For instance, rehabilitation interventions for improvements of walking have been most effective for people with motor incomplete injuries (Yang and Musselman 2012). With the recent technological advances, a new wave of powered orthoses and exoskeleton are emerging and may hold promise as a mode of ambulation and rehabilitation for

people with SCI. Despite the functional success of peripheral FES neuroprostheses for restoring standing and stepping in people with paraplegia, their implementation has not become widespread. This may be due to their limitations such as fatigue or implant failure. Peripheral FES (especially non-invasive approaches) is becoming more accepted as a rehabilitation tool for SCI (“Functional Electrical Stimulation Exercise - The Steadward Centre for Personal & Physical Achievement” n.d.; “First Steps Wellness Centre” n.d.). Epidural stimulation in conjunction with rehabilitation training, has also shown promising results in improvement of standing function for people with incomplete SCI. Among all of these interventions however, a gap still exists for interventions for people with complete injuries. The results from preclinical studies of ISMS, show potential for this technique to become a viable option for restoration of walking, especially in people with complete SCIs.

The overall goal of this thesis project was to take steps in the path of clinical translation of ISMS and prepare this approach for testing in people for the first time. The first step in this path is to prepare ISMS for testing in an intraoperative setting. Intraoperative testing would allow us to identify the functional organization of the motor networks in the lumbosacral spinal cord of humans and assess their excitability. This step would assess the feasibility of producing functional movements in the legs of humans with SCI using ISMS. The acquired information is also paramount for finalizing the technological design of a clinical implant. In preparation for intraoperative testing, the following aspects needed to be addressed: 1) Development of a stereotactic system for precise placement of ISMS microelectrodes in the spinal cord of humans, 2) Investigating the effect of clinical anesthesia on the responses to ISMS 3) Intraoperative testing of ISMS in non-human primates as the closest available neurophysiological animal model to humans. After addressing these aspects, this thesis took a step further and focused on the

requirements of chronic ISMS implants in humans. These requirements were investigated from the perspective of mechanical stability. The outline of the remainder of this thesis is provided below.

Chapter 2 - Ultrasound-Guided Spinal Stereotactic System for Intraspinal Implants: This chapter discusses an image guided, spine-mounted, stereotactic setup that was developed for precise (sub-millimeter accuracy) placement of ISMS implants into the gray matter of the spinal cord. The setup was developed in a swine model and has since been tested in non-human primates and human cadavers. In this chapter, I also discuss the experiments that evaluated the performance of this system for effective targeting of the gray matter of the spinal cord. This system has direct application in the upcoming intraoperative experiments in humans.

Chapter 3- Effect of Anesthesia on the Responses to Intraspinal Microstimulation and its Implications for Clinical Translation: In preparation for intraoperative testing of ISMS in humans under anesthesia, the effect of a common neurosurgical anesthesia protocol on ISMS responses was investigated. This effect was compared with the effects of two of the most commonly used anesthetic protocols for preclinical studies of ISMS. This is especially important, since understanding the relative influence of anesthetic protocols on the ISMS evoked responses is critical for correct interpretation of the clinical intraoperative testing results and comparison with the literature.

Chapter 4- Functional organization of motor networks in the lumbosacral spinal cord of non-human primates: In this project, in preparation for intraoperative testing of ISMS in the human

spinal cord, an intermediate step was taken and similar intraoperative testing was conducted in the spinal cord of non-human primates. These experiments obtained the functional organization of the motoneuronal pools in the lumbosacral enlargement of the spinal cord of monkeys for the first time. Monkeys were chosen, as the closest available neurophysiological animal model to humans. These results were then compared with the available functional maps of the lumbosacral spinal cord in cats and its implications for the human functional map were discussed.

Chapter 5- Mechanically stable intraspinal microstimulation implants for human translation: This study was conducted in a swine model, and quantified the biomechanics of the spine and spinal cord in proximity of the ISMS implant region (lumbosacral enlargement) using a motion capture system. This was done when the animal's spine was taken into extreme flexion and extension ranges of motion. The critical forces that would dislodge implanted ISMS microelectrodes from the spinal cord were also characterized *in-situ*. Taken collectively, these design constraints can be used for the design of any mechanically stable spinal cord implant. A proof of concept design for a mechanically stable ISMS implant was provided and also acutely tested *in-situ*.

Chapter 6- General Discussions summarizes the key findings of the thesis and discusses the possible future directions in the path to clinical translation of ISMS.

## Chapter 2. Ultrasound-Guided Spinal

# Stereotactic System for Intraspinal Implants<sup>1</sup>

Amirali Toossi<sup>1,7</sup>, Dirk G. Everaert<sup>2,7</sup>, Peter Seres<sup>3</sup>, Jacob L. Jaremko<sup>4</sup>, Kevin Robinson<sup>5</sup>, C. Chris Kao<sup>6</sup>, Peter E. Konrad<sup>6,7</sup>, Vivian K. Mushahwar<sup>1,2,7</sup>

<sup>1</sup>Neuroscience and Mental Health Institute, University of Alberta, Edmonton, Canada. <sup>2</sup>Division of Physical Medicine and Rehabilitation, Department of Medicine, University of Alberta, Edmonton, Canada. <sup>3</sup>Department of Biomedical Engineering, University of Alberta, Edmonton, Canada. <sup>4</sup>Department of Radiology and Diagnostic Imaging, University of Alberta, Edmonton, Canada. <sup>5</sup>School of Physical Therapy, Belmont University, Nashville, TN, USA. <sup>6</sup>Department of Neurosurgery, Vanderbilt University Medical Center, Nashville, TN, USA. <sup>7</sup>Sensory Motor Adaptive Rehabilitation Technology (SMART) Network, University of Alberta, Edmonton, Canada

---

<sup>1</sup> A version of this chapter has been published. Toossi et al., 2018. “Ultrasound-guided spinal stereotactic system for intraspinal implants,” *Journal of Neurosurgery: Spine*. 29(3): 292–305.

## 2.1 Introduction

Intraspinal microstimulation (ISMS) is a form of functional electrical stimulation (Peckham and Knutson 2005) in which arrays of fine microelectrodes are implanted within the spinal cord, targeting the ventral horns. Low amplitudes of electrical pulses ( $<100 \mu\text{A}$ ) are delivered through the electrodes, activating neuronal networks and motor neuronal pools resulting in behaviorally measured outcomes (Bamford and Mushahwar 2011; Mushahwar, Collins, and Prochazka 2000; Mushahwar and Horch 2000a). To date, applications of ISMS have been mainly focused on restoring functions lost after a spinal cord injury (SCI). Early clinical studies in humans utilized ISMS implants in the sacral segments of the spinal cord (S1-S2) and showed successful bladder voiding in more than 75% of female patients (total of 13 patients) with bladder paralysis (Nashold, Friedman, and Grimes 1982). Since then, preclinical studies have investigated the use of ISMS for restoration of standing and walking (Holinski et al. 2016; Lau, Guevremont, and Mushahwar 2007; Mushahwar, Collins, and Prochazka 2000; Saigal, Renzi, and Mushahwar 2004), hand movements (Sunshine et al. 2013; Zimmermann and Jackson 2014) and respiration (Mercier et al. 2017) in animal models. ISMS for standing and walking is one of the more widely studied types of ISMS in which the electrodes are implanted in the lumbosacral region of the spinal cord. Previous studies have shown promising functional outcomes for these implants and have motivated their translation towards clinical testing (Bamford and Mushahwar 2011; Holinski et al. 2016; Mushahwar, Collins, and Prochazka 2000; Saigal, Renzi, and Mushahwar 2004; Toossi, Everaert, Azar, et al. 2016).

An important requirement for clinical testing of ISMS is the development of a safe and precise implantation system. Precise manipulation and placement of ISMS microelectrodes into the spinal cord requires a stereotactic setup and an accurate targeting method. For restoring

walking with ISMS, the cross-sectional area of the smallest target in the ventral horn of the feline spinal cord is  $\sim 0.2\text{-}0.3\text{ mm}^2$ , corresponding to the tibialis anterior motor neuronal pool (Mushahwar and Horch 1997, 1998, 2000b). This size is not directly known for humans; however, assuming that the functional activation size of the motor pools is proportional to the overall size of the spinal cord, homologous targets in the human spinal cord are likely only  $\sim 30\%$  larger (Mushahwar and Horch 1998, 2000b; Sengul et al. 2012).

Existing stereotactic systems for intraspinal procedures can be categorized into two groups based on how they are mounted (Medani et al. 2016): 1) on the surgical table (Lima et al. 2010; Saberi et al. 2008), or 2) on the spine of the patient (Riley et al. 2014). Systems mounted on the surgical table for positioning implants in the spinal cord have the risk of causing spinal cord trauma because of relative displacements of the surgical table and the spinal cord. Systems mounted on the spine of the patient alleviate this drawback.

Two spine-mounted stereotactic systems exist in the literature. The first, called the *spinal derrick* (Federici et al. 2012; Riley et al. 2011), was developed for intraspinal stem cell delivery and has been tested clinically. The system involves the fixation of a micromanipulator platform onto the patient's spine using four percutaneous laminar screws (Riley et al. 2011). In most of the preclinical and clinical studies using this system, estimation of the implant trajectory within the spinal cord was based on dorsal anatomical landmarks, micromanipulator coordinates and magnetic resonance imaging (MRI) acquired prior to the surgery (Riley et al. 2014; Riley et al. 2011). The targeting accuracy of this implant delivery system was not systematically reported; however, the reported injection targets in human spinal cords are in the ventral horns of the gray matter. These targets are at depths ranging from 3-5 mm from the dorsal surface (Riley et al. 2012) and unlike ISMS, may not require sub-millimeter targeting accuracies. More recently, a

prototype of an MR-compatible *spinal derrick* was used for MRI guided insertion of injection needles through the interlaminar space (Lamanna et al. 2017).

The second patient-mounted stereotactic system was developed at the Mayo clinic (Grahn et al. 2016) for ISMS in pigs. The system anchors to the spine through eight MR-compatible pedicle screws spanning four vertebral levels. MRIs are obtained following the laminectomy and pedicle screw placement, using a custom MR coil and MRI markers. The coil and markers are then removed and a micromanipulator setup is mounted on the pedicle screws. The acquired MR images guide the coordinates on the micromanipulator system for targeting within the spinal cord. The reported targeting accuracy of this system in a bench setup was  $1.09 \pm 0.2$  mm (mean  $\pm$  standard deviation).

The required targeting accuracy for trajectory alignment of ISMS implants can be estimated based on the size of the electrical current spread around the electrode tip. The functional stimulation amplitudes required for ISMS in cats range from 60 to 100  $\mu$ A (Holinski et al. 2016). For these stimulation amplitudes, the estimated radius of current spread is 0.4 and 0.5 mm, respectively (Bagshaw and Evans 1976; Mushahwar and Horch 1997). Therefore, to ensure overlap between the intended electrode target and the electrically activated area, the spatial targeting error should be  $<0.5$  mm. A higher targeting accuracy minimizes the number of required electrode passes for successful stimulation and is critical for the safety and functional success of the implant. To date, the targeting accuracy goal of 0.5 mm has not been met with the existing spine-mounted systems (Grahn et al. 2016; Riley et al. 2011). This is due to the inherent visual illusions when eyeballing the trajectory of the electrode as well as the limitations in spatial resolution of MR images obtained from real-time MR-guided systems. Additionally, methods

that only use MR images collected prior to the insertion of the electrodes lack the ability to provide guidance and feedback during or after insertion.

We propose a novel spinal stereotactic system for ISMS that is mounted on the spine and for the first time relies on intraoperative ultrasound imaging for guiding the electrode trajectory into the spinal cord. Ultrasound is a desirable imaging modality for this task since it provides dynamic real-time imaging, and is capable of providing very high spatial resolution. As a first application, we used the system for intraoperative ISMS implants. The specific aims of this study were to: 1) develop a modular spinal stereotactic system with a minimal number of components that would allow precise 3D targeting within the spinal cord gray matter, 2) develop an intraoperative ultrasound imaging method that allows the visualization of the gray and white matter of the spinal cord as well as measurement of the electrode insertion angle, and 3) quantify electrode alignment accuracy using the spinal stereotactic system and ultrasound guidance in pigs and a benchtop setup using a surrogate spinal cord.

## **2.2 Materials and Methods**

A spinal stereotactic system using ultrasound image guidance was developed and optimized through experiments on the bench and in pigs.

### **2.2.1 The spinal stereotactic system**

This system provides a stereotactic framework that allows precise measurements in 3 dimensions and consists of 3 main components: a set of two metal frames (further referred to as loops), a platform, and a micromanipulator (figure 4.1). The loops form an elevated base for attachment of the platform onto the spine and the platform provides an adjustable base for the

micromanipulator. Intraoperative ultrasound imaging is also used as part of this system to improve target selection and provide feedback during implantation procedures.

**Loops.** The loops are made of surgical spine rods (in this case, 5.5 mm diameter, Medtronic, Dublin, Ireland), that were shaped, under high heat, in a trapezoid-like shape and spot welded on one side. The loops can be closed (figure 2.1) or open (figure 2.2) and are mounted on the vertebrae with four pedicle screws. The trapezoid-like loops can have a range of dimensions: for ISMS implants, the bottom edge is shorter (11 cm) than the top (17 cm), and the height is 7 cm. This construction reduces the exposure of bone in the craniocaudal direction, while providing a sufficiently large working window at the top. The left and right loops can be stabilized laterally with length-adjustable cross links that connect the loops across the top (in this case, 5.5 cm maximal range). The open space between the L-shaped handle and the top bars of the open loops (figure 4.2) provides a wide working area in the transverse direction for ultrasound probe maneuvers.

**Platform.** The platform (in this case, 8.5 cm long x 8 cm wide) serves as a mounting base for the micromanipulator system (figure 2.2b). The micromanipulator system attaches simply with an adaptor plate with a cross shaped slit that slides over 2 screws in the platform (figure 2.2b and 4.2c). Once the micromanipulator is in the desired position, the 2 screws are tightened. The platform is designed to provide flexibility in the placement of the micromanipulator system in the lateral and craniocaudal directions. In this case, this is implemented by placing 6 rows of 10 screw holes in the platform. The cross-shaped slit in the adaptor plate further increases the lateral

and craniocaudal placement options and allows the manipulator to be rotated in the coronal plane (figure 2.2b).

The platform is mounted on the loops with 2 “sliders.” The 5-cm long sliders have a longitudinal slit along the underside that fits over the loops (figure 2.2c). Two transverse screws with cone tips are tightened to clamp the sliders onto the loops.

**Micromanipulator system.** The micromanipulator system in this paper contains four commercially available components that we combined in order to obtain a sufficient range of motion in three directions of translation and two planes of rotation. The top stage, for the purposes of this paper, is a Narishige MMN-33 micromanipulator (Narishige Company, Tokyo, Japan) with 35 mm range craniocaudally, 20 mm mediolaterally, and 37 mm dorsoventrally. The MMN-33 allows rotation in the transverse plane (figure 2.2d). The Narishige micromanipulator is mounted on a 2D translation middle stage which adds 60 mm in both the craniocaudal and mediolateral directions (Edmund Optics Inc, Barrington, NJ, USA). The bottom stage is a goniometer (B54-40U2NR, Suruga Seiki Company, Tokyo, Japan) which provides  $\pm 20$  degrees of rotation in the sagittal plane (figure 2.2e).

**Mounting procedure.** Pedicle screws are placed bilaterally in the pedicles of two neighboring vertebrae, or two vertebrae skipping one level. The loops are placed in the swivel heads and loosely secured with the caps. A transverse cross link is loosely attached to connect the two top bars, providing some lateral stability. The platform is loosely positioned on the loops, and the loops are adjusted so that the midline of the platform aligns with the spinal cord, and the platform is parallel with the frontal plane of the body. The pedicle screw caps, crosslink and

platform screws are then securely tightened, locking all angles of the platform framework. The micromanipulator is then placed on the platform by sliding the adaptor plate under the top screws of the platform (figure 2.2b). The micromanipulator is rotated on the platform so that the main translation axis is aligned with the spinal cord (in the craniocaudal direction). The top screws of the platform are fastened, locking the micromanipulator in place.

**Intraoperative ultrasound imaging.** The ultrasound probe used in this study was an intraoperative Philips L15-7io linear array probe with a footprint of 23 mm. The operating frequency of the probe was set to 15 MHz. Pixel size was 0.067 mm x 0.067 mm. The size of the probe allowed it to fit in the space above the spinal cord and scan it in the transverse plane during electrode insertion. The probe was not in contact with the cord, and therefore had to be submerged in saline filling the spinal canal above the cord.

### **2.2.2 Surgery and device placement**

Animal experiments were conducted in 7 domestic pigs (6 freshly euthanized pigs and one live pig) with an average weight of  $43.7 \pm 9.1$ kg. Pigs were the main animal model for this study due to the anatomical similarity of their spinal column and spinal cord to that of humans (Busscher et al. 2010; Sheng et al. 2010; Toossi, Everaert, Azar, et al. 2016). All animal experiments were conducted in accordance to protocols approved by the Institutional Animal Care and Welfare Committee at the University of Alberta.

The fresh pig cadavers were obtained after the animals were euthanized using an IV euthanyl injection. In the experiment using the live animal, the pig was deeply anesthetized and maintained in surgical plane throughout the duration of the experiment. In all animals, a

laminectomy was performed to expose the lumbosacral enlargement of the spinal cord (lumbar vertebrae L4 to L6). Four multiaxial Medtronic pedicle screws (4.5 mm diameter x 25 mm length) were placed bilaterally in the pedicles. The dura mater and the arachnoid layers were then opened. The spinal stereotactic system was mounted onto the pedicle screws as described in section 2.1.

### **2.2.3 Assessment of the accuracy of ultrasound-guided electrode implantation in the pig**

Intraoperative ultrasound imaging was used to guide the trajectory of glass-tube markers into the spinal cord prior to insertion. Markers were then implanted into the spinal cord using a custom-built insertion tool attached to the stereotactic system. After each experiment, the spinal cords were extracted and imaged using MRI. MR images were used as the reference for measurement of the insertion angles of the implanted markers with respect to the major axis of the spinal cord. Targeting error of the ultrasound-guided implantation with the stereotactic system was assessed by comparing the insertion angles measured using ultrasound imaging and MRI.

**Ultrasound visualization of electrode and spinal cord.** In order to find the suitable tilt angle range of the ultrasound probe for viewing the gray and white matter of the spinal cord, a custom-made apparatus was used. As shown in figure 2.3a, the orientation of the probe was varied in the transverse oblique scanning plane to obtain the best gray and white matter contrast in cross-sectional images of the spinal cord.

The suitable range in probe tilt angle for visualizing the gray and white matter was 25° to 45° from the short-axis view of the spinal cord. Tilt angles less than 25° did not provide

sufficient contrast between gray and white matter to distinguish between them. While tilting the probe in the transverse oblique plane improves gray-white discrimination, it distorts the shape of the spinal cord in the dorsoventral direction. Therefore, the smallest tilt angle providing the appropriate contrast is preferred (Ihnatsenka and Boezaart 2010). When visualizing the electrode and the spinal cord in one image, the ultrasound probe was positioned caudal to the electrode in the transverse oblique plane.

**Marker implantation system.** Instead of implanting metal microelectrodes which produce large artifacts in the MR images, small glass tubes were implanted in the spinal cord as markers that were visible in both the ultrasound and MR images. The glass-tube markers were approximately 5 mm long and had an outer diameter of 170  $\mu\text{m}$  (Wale Apparatus Company, Hellertown, USA). The markers were inserted using a custom-built insertion tool that replaces the electrode stylus in the micromanipulator as shown in figure 2.3b. The tool contains a holder for a 25 gauge needle. Prior to each insertion, a glass tube is back-loaded into a needle which is then placed in the holder. The needle was lowered by the micromanipulator and inserted 2 mm deep into the spinal cord. The glass tube was then inserted through the needle in the spinal cord using a tungsten wire acting as a plunger. The needle was then carefully retracted with the micromanipulator, leaving the tube implanted in the cord.

**Electrode alignment in the transverse plane.** Traditionally for ISMS, surface landmarks such as dorsal root entry zone are used as reference points to determine the laterality of the entry point of the electrode. Since ultrasound imaging can visualize the gray and white matter, it can also be used to guide and provide feedback on the laterality of the entry point of the electrodes.

Successful projections from the entry point to the target in the ventral horn require that the

electrode is inserted “straight” into the spinal cord. For this purpose, “straight” is defined as perpendicular to the major axis of the cord’s elliptical shape. In the case of a perfectly symmetrical cord, this would mean the electrode is also perpendicular to the line connecting the tips of the ventral or dorsal horns, and parallel with the anterior fissure (figure 2.4). Therefore, the goal in the experiments was to align the marker insertion needle perpendicularly to cord’s major axis, prior to insertion of the markers.

The angle of the insertion needle in the micromanipulator system was aligned using three methods: 1) eyeballing, 2) ultrasound-guidance while holding the probe by hand (figure 2.3c), and 3) ultrasound-guidance with the probe attached to the stereotactic setup (figure 2.3d). The probe was attached to the loops using a multi-jointed arm. These methods were investigated under two conditions: 1) no time limitation for insertion of each marker and in case of eyeballing no limitation on the points of view used by the surgeon (referred to as ‘unlimited time condition’); 2) time limit of 90 seconds for each insertion and for the eyeballing method, the surgeon was asked to remain on their side of the patient, thus limiting the viewpoints to a more realistic condition (referred to as ‘time constrained condition’). In each experiment, at least 9 markers were implanted using each of the three alignment methods. Conditions 1 and 2 were each tested in 3 pigs.

The ultrasound-guided alignment of the insertion needle involved three steps: 1) Tilting the probe to visualize the electrode and the spinal cord in one image. 2) Identifying the orientation of the spinal cord (figures 2.5a and 2.5b) by drawing a line over the anterior fissure, drawing a line across the boundaries of the ventral or dorsal horns, and/or drawing a tangent line over the dorsal surface of the spinal cord at the midline. 3) Adjusting the orientation of the electrode by rotating the micromanipulator in the transverse plane until the alignment becomes

acceptable. The micromanipulator rotation stage was then locked and an ultrasound picture was taken of the needle in its final position prior to implantation to document the insertion angle (figures 2.5a and 2.5b). The marker was then implanted in the cord as described above. Tilting the ultrasound probe in the transverse oblique plane did not affect the viewed orientation of the cross-section of the spinal cord (Ihnatsenka and Boezaart 2010).

**Electrode alignment in the sagittal plane.** The space was not sufficient for ultrasound imaging of the insertion in the sagittal plane due to the design of the glass marker insertion tool (figure 2.3d). Therefore, an assisted eyeballing alignment method was used in the sagittal plane for all of the tested conditions. This method involved attaching a stylus to the micromanipulator and lowering it to the dorsal surface of the spinal cord. The stylus was then translated in the craniocaudal direction while adjusting the sagittal rotation angle until its translation path became parallel with the surface of the spinal cord.

In two experiments, after the markers were implanted into the spinal cord, the marker insertion tool was removed and an ultrasound image of the marker in the sagittal plane of the spinal cord was recorded and the insertion angle was documented.

**Verification of marker placement using magnetic resonance imaging.** After all of the markers were inserted into the spinal cord, the animal was euthanized (in case of the live pig experiment) and the lumbar spine (including the spinal cord) was extracted and fixed in formalin solution. The extracted spine was then scanned while submerged in saline using a 3T Siemens Prisma MRI scanner at the Peter S. Allen MR Research Centre, University of Alberta. MRI scans were acquired using a 1Tx/15Rx knee coil and a 3D MEDIC sequence with a resolution of 0.25

mm x 0.25 mm x 1 mm in the transverse plane and 0.31 mm x 0.31 mm x 1 mm in the sagittal plane. The implanted markers in the spinal cord were identified in the MR images and angle measurements were obtained using ImageJ software (U.S. National Institute of Health, Bethesda, MD, USA) (figure 2.6a).

**Statistical analysis.** A two-way ANOVA was performed to analyze the effect of testing conditions (time constrained and unlimited time) and the alignment methods (eyeballing, ultrasound-guidance using a handheld probe and ultrasound-guidance using a mounted probe) on the alignment error of the electrode trajectory. A subsequent one-way ANOVA and Tukey HSD post-hoc analysis were performed for each testing condition to compare the 3 alignment techniques. T-tests were performed to compare the two testing conditions for each alignment method. Differences were considered significant for  $p \leq 0.05$ . All analyses were performed using IBM SPSS software (version 22, IBM Co., Armonk, USA).

#### **2.2.4 *Bench-top* assessment of the ultrasound-guided electrode implantation technique**

Testing the ultrasound-guided electrode implantation technique on the bench aimed to assess its capabilities and limitations in a more controlled setting with a higher spatial resolution. The bench setup and the testing protocol not only directly measured the electrode insertion angle, but also allowed for reliable measurement of targeting depth in the transparent surrogate cords (figure 2.7a). This is in contrast with the pig experiments where the MR images were used to measure electrode insertion angles only.

Four gelatin hydrogel surrogate spinal cords were prepared as previously described (Cheng et al. 2013), and a cut was made at their midline to simulate the anterior fissure (figure 2.7b). Hydrogel cords were selected due to their transparency and near physiological mechanical properties. The anterior side of the spinal cords was fixed onto a plastic plate (figure 2.7a) and the dorsal surface of the spinal cords was painted black to prevent the operator from using visual feedback for alignment. The plastic plate was then placed in a transparent container filled with saline for implantation.

A 125  $\mu\text{m}$  diameter Pt/Ir electrode (FHC Company, Bowdoin, ME, USA) was used for insertion into the spinal cord. Alignment of the electrode prior to insertion was performed under ultrasound guidance (with the probe held by hand) in both the transverse and sagittal planes (figures 2.7e and 2.7f). Landmarks used for identifying the alignment of the surrogate spinal cords in the ultrasound images were the orientation of the dorsal surface and the orientation of the simulated anterior fissure. Similar to the pig experiments, before each trial the initial orientation of the electrode was randomly set.

After the electrode was aligned perpendicularly with respect to the spinal cord, the electrode was inserted to a depth of 4 mm using the micromanipulator. Electrical stimulation was used to mark the electrode track in the spinal cord for further analysis. Direct current (DC) stimulation at 20 V was delivered across the implanted electrode and a needle electrode placed in the saline bath. After the stimulation was turned on the electrode was slowly retracted from the spinal cord to mark the full length of the track (figures 2.7c, 2.7d).

A camera was positioned parallel to the sagittal plane of the cord to measure the insertion angle in this plane. In each surrogate spinal cord three to five tracks were made from electrode insertions. After all insertions were completed and tracks marked, the surrogate spinal cords

were detached from their underlying plate and thin transverse sections were cut, each containing one electrode track. Microscopic images were taken from these sections to measure the insertion angle and the track length in the transverse plane (figure 2.7b). All angle measurements in the images were obtained using the ImageJ software.

Tests were conducted to compare the alignment errors of the experiments conducted on the bench and in pigs in both sagittal and transverse planes using IBM SPSS software.

## **2.2.5 Functional testing of the ultrasound-guided stereotactic system in a live pig**

In order to demonstrate the application of the ultrasound-guided spinal stereotactic system for intraoperative ISMS, an experiment was conducted in a domestic pig (weight: 51 kg). The surgical procedure was identical to the description provided in section 2.2. A 100  $\mu\text{m}$  Pt/Ir electrode was used (FHC Co., Bowdoin, ME, USA) and the stimulation trains consisted of: frequency of 50 Hz, pulse width of 200  $\mu\text{s}$ , biphasic charge-balanced pulses with amplitudes up to 150  $\mu\text{A}$ . A needle return electrode was placed in the paraspinal muscles. In order to visualize the movements generated by ISMS, the animal's legs were suspended as shown in figure 2.8. For kinematic analysis of the generated movements, black marks were painted on the hip, knee, ankle and metatarsophalangeal (MTP) joints as well as on the iliac crest, and videos of the generated movements were recorded. Electromyographic (EMG) signals were also recorded using a Noraxon digital telemetry system and ambu blue sensor electrodes (Noraxon Co., Scottsdale, AZ, USA). Pairs of EMG electrodes were placed on the following muscles: rectus femoris, biceps femoris, lateral gastrocnemius and tibialis anterior. The kinematics data was assessed using the MR3 (Noraxon Co.) and imageJ software packages. The EMG data were

analyzed using custom-written programs in Matlab (version 2015a, MathWorks Co., Natick, USA).

## **2.3 Results**

### **2.3.1 Findings related to ultrasound imaging of the spinal cord**

An ultrasound probe tilted to an angle of 25° to 45° in the transverse oblique scanning plane provided an acceptable contrast for viewing the gray and white matter of the spinal cord. Careful cleaning of the surgical site was found to be important for achieving an acceptable image quality. Layers of blood clots forming on the dorsal surface of the cord or in the lateral recesses of the spinal canal are hyperechoic and can result in a distorted image.

The electrode and the glass markers were visualized in the ultrasound images of the spinal cord before and after implantation (figures 2.5a, 2.6b). There was no evident difference in the quality of the ultrasound images of the gray and white matter between experiments conducted in the cadavers and live animals. However, an additional way of visualizing the anterior fissure of the spinal cord was using Doppler imaging (figure 2.5c) which was only possible in the live animals.

### **2.3.2 Assessment of electrode alignment in pigs**

*Detection accuracy* of the electrode insertion angle was expressed as an error score defined by the difference between the marker insertion angle, measured from the MR image, and the needle insertion angle, measured from the ultrasound image. In calculating this error score, it was assumed that the marker insertion and careful tissue extraction (after the completion of the experiment) did not cause changes in the alignment of the marker. The detection accuracy was

measured for 137 insertions in 6 animals in the transverse plane and for 36 insertions in two animals in the sagittal plane. The detection accuracy was  $2.15^\circ \pm 0.38^\circ$  and  $2.09^\circ \pm 0.35^\circ$  (mean  $\pm$  95% confidence interval) in the transverse and sagittal planes, respectively (figure 2.9).

**Alignment accuracy** of electrode insertion was expressed as an error score defined by the difference between the measured insertion angle on the MRI scans and the target electrode orientation, which was perpendicular to the major axis of the spinal cord (figure 2.4). The spatial targeting error for a stereotactic system with degrees of freedom in the spherical coordinate system depends on the targeted depth. Therefore, for implementing the  $<0.5$  mm limit of acceptable spatial targeting error for ISMS (Bagshaw and Evans 1976; Mushahwar and Horch 1997) in the spherical coordinate system, the following equation was used:

$$0.5 > \sqrt{r'^2 + (r)^2 - 2(r)r'[\sin(90^\circ) \sin\theta' \cos(90^\circ - \varphi') + \cos(90^\circ) \cos\theta']}$$
 (1)

where  $r$  is the depth of the target from the dorsal surface of the spinal cord,  $r'$  is the implanted length of the electrode, and  $\varphi'$  and  $\theta'$  are the electrode trajectory angles in the sagittal and transverse planes, respectively. The maximal depth of the ventral horns of the gray matter in the lumbar enlargement of the human spinal cord ( $r$ ) is approximately 6 mm (Sengul et al. 2012) from the dorsal surface.

In 6 pig experiments, a total of 225 markers were implanted into the spinal cords. Alignment in the sagittal plane alignment was based on eyeballing and resulted in an overall alignment error of  $1.4^\circ \pm 0.27^\circ$  (mean  $\pm$  95% confidence interval). Considering equation 1, the

~1.5° error measured for the alignment technique used in the sagittal plane results in a limit of ~4.5° in alignment error in the transverse plane for ISMS targets.

Electrode alignment in the transverse plane was conducted under two conditions (time constrained and unlimited time) three different alignment techniques (eyeballing, ultrasound guidance using a handheld probe, and ultrasound guidance using a mounted probe). The alignment errors in the transverse plane are shown in figure 2.10. For both conditions, alignment error using ultrasound-guidance was significantly smaller than eyeballing ( $p < 0.01$  for unlimited time, and  $p < 0.001$  for time constrained). However, alignment errors were not significantly different between the two ultrasound-guidance methods ( $p = 0.99$  for unlimited time,  $p = 0.84$  for time constrained). The upper bound for the confidence interval (95%) of the mean alignment error for ultrasound-guidance with handheld probe and ultrasound-guidance with mounted probe were 2.45° and 2.63°, respectively for the unlimited time condition, and 3.07° and 3.57°, respectively for the time constrained condition. Overall, for targets 6 mm deep into the cord, the Cartesian equivalent of the maximal alignment errors under ultrasound guidance (time-constrained, mounted probe for the transverse plane and eyeballing for the sagittal plane) were: 0.37 mm in the mediolateral, 0.01 mm in the anterior-posterior, and 0.17 mm in the craniocaudal axes.

Limiting the insertion time and the view point for eyeballing and ultrasound-guidance (only when the probe was fixed to the stereotactic setup) alignment methods resulted in significantly larger alignment errors ( $p = 0.02$  and  $p = 0.02$ , respectively). No significant interaction was found between the condition (unlimited time, time constrained) and the alignment method ( $p = 0.21$ ).

### 2.3.3 Benchtop assessments

**Detection accuracy** of the electrode insertion angle in the benchtop experiments was expressed by the difference between the measured insertion angle based on the ultrasound image and the measured angle from the microscopy image of the surrogate spinal cord section. The detection accuracies were  $1.98^\circ \pm 0.84^\circ$  and  $0.91^\circ \pm 0.31^\circ$  (mean  $\pm$  95% confidence interval), in the transverse and sagittal planes, respectively (figure 2.9).

The bench setup not only allowed the measurement of **alignment accuracy** (deviation angles in transverse and sagittal planes as measured in pigs), but also allowed direct measurement of the spatial targeting error (3D distance from target which in addition to the alignment error also includes the error associated with the implantation depth). Alignment accuracy of the inserted electrodes in the sagittal and transverse planes were  $0.95^\circ \pm 0.50^\circ$  and  $2.29^\circ \pm 0.81^\circ$  (mean  $\pm$  95% confidence interval), respectively (figure 2.11). Depth of the electrode tips in the transverse plane was  $3.95 \pm 0.11$  mm. Based on these results, the spatial targeting error of ultrasound-guided implantation was calculated using equation 1 (in this case,  $r = 4$  mm), and was  $0.22 \pm 0.02$  mm (mean  $\pm$  standard deviation). These results were obtained for a surrogate cat spinal cord and target depth of 4 mm for the electrode tip. Based on the measured deviation angles, if the targeting depth for the lumbar enlargement of a human spinal cord were to be considered (maximal gray matter depth of 6 mm), and assuming perfect depth targeting ( $r = r' = 6$  mm), the calculated spatial targeting error (equation 1) remains below the 0.5 mm limit. The upper boundary of the spatial targeting error in this case is calculated to be 0.36 mm, using the upper boundaries of the 95% confidence intervals of the measured deviation angles for the electrode trajectory. The Cartesian equivalent of the maximal alignment errors in this case is:

0.32 mm in the mediolateral, 0.01 mm in the anterior-posterior, and 0.15 mm in the craniocaudal axes.

The alignment error in the benchtop experiments (ultrasound guidance) in the sagittal plane was significantly smaller than that in the experiments in pigs (assisted eyeballing method) ( $p=0.01$ ). The alignment errors in the transverse plane (using ultrasound guidance), however, were not significantly different from each other ( $p=0.83$ ).

### **2.3.4 Intraoperative ISMS using the spinal stereotactic system**

The lumbar enlargement of the spinal cord of a live pig was intraoperatively mapped using the ultrasound-guided spinal stereotactic system. In this experiment, 21 locations were electrically stimulated in the spinal cord resulting in functional movements in the leg. The generated movements included both single joint movements such as knee extension and ankle extension as well as multi-joint synergistic movements such as extensor synergy involving the hip, knee and ankle. An example of the movements and EMG signals produced by ISMS in one locations is shown in figure 2.12. The observed functional organization of the mapped region of the spinal cord in this animal was consistent with functional maps for the lumbar spinal cords of pigs (Hachmann et al. 2013), cats (Mushahwar and Horch 1998, 2000b) and rhesus monkeys (Toossi, Everaert, Perlmutter, et al. 2016).

## **2.4 Discussion**

In this study, we proposed and evaluated a new spinal stereotactic system that relies on real-time (i.e., instantaneous) ultrasound guidance for accurate targeting inside the gray matter of the

spinal cord. Comparisons conducted with traditional visual targeting methods demonstrated superior performance of ultrasound-guided targeting.

Emerging intraspinal interventions for spinal cord repair and restoration of lost functions require appropriate neurosurgical setups and tools that ensure their safe and successful clinical implementation. Despite the advances in this area (Blanquer et al. 2010; Féron et al. 2005; Mazzini et al. 2010; Medani et al. 2016) important challenges remain for reaching sub-millimeter sized targets within the spinal cord. The ability of intraoperative ultrasound imaging to visualize gray and white matter of the spinal cord not only can guide the electrode alignment and target selection prior to implantation, but also provide feedback during and after insertion. This is not possible for the existing MR guided stereotactic systems due to the inherent restrictions and challenges of MR imaging compared to ultrasound imaging. Examples of such challenges are imaging artifacts resulting from metallic instrumentation and implants, and safety concerns associated with possible current induction through them. This is critical for ISMS since it utilizes an electrically active implant consisting of an array of microelectrodes, lead-wires, connectors and a wireless stimulator. In the context of ISMS, another limitation of currently available MR guided systems is that the size of the laminectomy region is driven by the size of the MR coils. This is because the MR coil is placed in the exposed region over the spinal cord for best image quality. For example, the system developed by the Mayo Clinic (Grahm et al. 2016) utilizes a custom-built coil which is 7.5 cm long and therefore the length of the laminectomy has to be larger than this value. This is in contrast with the intraoperative ultrasound imaging probe used in this study which has a footprint of 2.3 cm. As image fusion software platforms become more available for ultrasound images and MRI (Lee 2014; Logan et al. 2014; Marks, Young, and

Natarajan 2013), ultrasound imaging of the spinal cord in conjunction with pre-operative MRI has the potential to provide even more information intraoperatively.

Detection error of the insertion angle using ultrasound imaging was, on average, less than 2.2° in the transverse plane, both in pigs and bench setup testing. However, as shown in figure 2.9, the detection error in the sagittal plane with respect to MRI in pigs, was higher compared to the direct benchtop measurements. This difference may be partly due to the lower MR imaging resolution obtained in the sagittal plane (0.31 x 0.31 mm in the sagittal plane vs. 0.25 x 0.25 mm in the transverse plane). The importance of detection accuracy is in its relationship to targeting accuracy. The targeting error (independent of any set target angle) is a sum of the detection error of the insertion angle, the errors involved in performing the alignment using the stereotactic hardware and the errors involved in the implantation process. Therefore, the value of the detection accuracy provides a best-case scenario for the targeting accuracy of the ultrasound-guided alignment.

Targeting resolution of ultrasound-guided electrode insertion was also assessed both in pigs and on the bench. In the pig experiments, ultrasound guidance was only used in the transverse plane due to the spatial limitations imposed by the glass marker insertion tool. Nevertheless, ultrasound-guidance (transverse plane) in conjunction with eyeballing (sagittal plane) was able to meet the targeting error limit of <0.5 mm for ISMS (figure 2.10). A comparison between the alignment methods used in the transverse plane demonstrated the superior targeting accuracy of ultrasound-guidance compared with eyeballing. The targeting accuracy through eyeballing did not meet the targeting goal for ISMS.

The two ultrasound-guided alignment methods provided similar targeting accuracies. However, when the ultrasound probe was fixed to the stereotactic setup, the surgeon could use

both hands to make the required adjustments to the micromanipulator stages for a desired alignment. Limiting the electrode alignment time and the surgeon's viewpoints resulted in larger targeting errors for both the eyeballing and ultrasound-guided alignment methods. However, the ultrasound-guided alignment methods under these conditions still met the targeting accuracy goal set for ISMS.

Comparison between the targeting accuracy results from eyeballing in the transverse and sagittal planes shows a larger error in the transverse plane than the sagittal plane. This may be explained by the transverse curvature of the spinal cord which makes visual alignment more difficult. It is also worth noting that the spatial limitation that prevented the use of ultrasound imaging in pigs in the sagittal plane (design of the glass-tube insertion tool) does not exist for ISMS where the glass-tube insertion tube is replaced with the electrode stylus (figure 2.2a). The glass-tube insertion tool was used only for purposes of placing markers in the spinal cord to allow subsequent analysis using MRI.

Benchtop experiments utilized the electrode stylus and used ultrasound guidance for alignment of the electrode in both the transverse and sagittal planes. The spatial targeting error for these experiments was  $<0.23$  mm (upper bound of its 95% confidence interval) for a target 4 mm below the surface. This targeting resolution is approximately 5 times higher than the values reported for an existing MRI-guided system ( $1.09 \pm 0.2$  mm) (Grahn et al. 2016). Ultrasound-guided alignment in the transverse plane in benchtop experiments performed similarly to the experiments in pigs. Ultrasound-guidance in the sagittal plane in the benchtop experiments provided higher alignment accuracy than eyeballing in the pigs.

Although this study only focused on the application of intraoperative ISMS, the proposed setup has the potential to be used for implantation of ISMS arrays for chronic use as well. This

may be realized by using a modified electrode holder design that can release the electrodes after implantation. The bench setup used in this study can be utilized as a training tool for users of the proposed image-guided stereotactic system. It can also provide a high throughput testing apparatus of the accuracy of targeting of various intraspinal interventions.

The proposed spinal stereotactic system is easy to assemble and remove and is compatible with existing surgical instrumentations. The system can be sterilized using gas sterilization methods such as vaporized hydrogen peroxide (VHP) and ethylene oxide sterilization (ETO), or other low temperature sterilization techniques such as STERRAD (data not shown). Also, since the stereotactic setup is fixed onto the spine through pedicle screws, its application is not limited to a specific region of the spine. Additionally, the design of the stereotactic setup provides spinal fixation at the implantation site. This is especially beneficial for applications such as intraoperative ISMS where movements produced in the leg can result in unwanted movements in the spine and spinal cord.

Nonetheless, since this system mounts onto pedicle screws, a limitation of its application may be in people with compromised bone strength. In such cases, addition of infra-laminar hooks on the levels above and below the laminectomy region may be considered (DeWald and Stanley 2006; Murakami et al. 2006). Also in such cases, the proposed stereotactic system allows for the addition of a counter weight over the loops to balance the weight of the micromanipulator system and minimize the torque transferred to the spine.

## **2.5 Conclusions**

In this study, a novel ultrasound-guided spinal stereotactic system was developed. The system is mounted onto the spine and has 6 degrees of freedom with sufficient range of motion that allows

targeting various parts of the spinal cord precisely. Guidance provided by intraoperative ultrasound imaging can assist with localizing the implant site, and accurately guide the electrode trajectory.

This system can be used to perform procedures on the spinal cord that require high precision, accurate location, and do not tolerate relative movement between the device and the spinal cord. Examples of such procedures are injections (e.g., stem cells, drugs) into the spinal cord, or insertion of electrodes into the spinal cord for electrical stimulation. This system will be used in the first clinical tests of ISMS, thus facilitating the clinical translation of this electrical stimulation modality for restoring standing and walking after spinal cord injury.

## 2.6 Figures

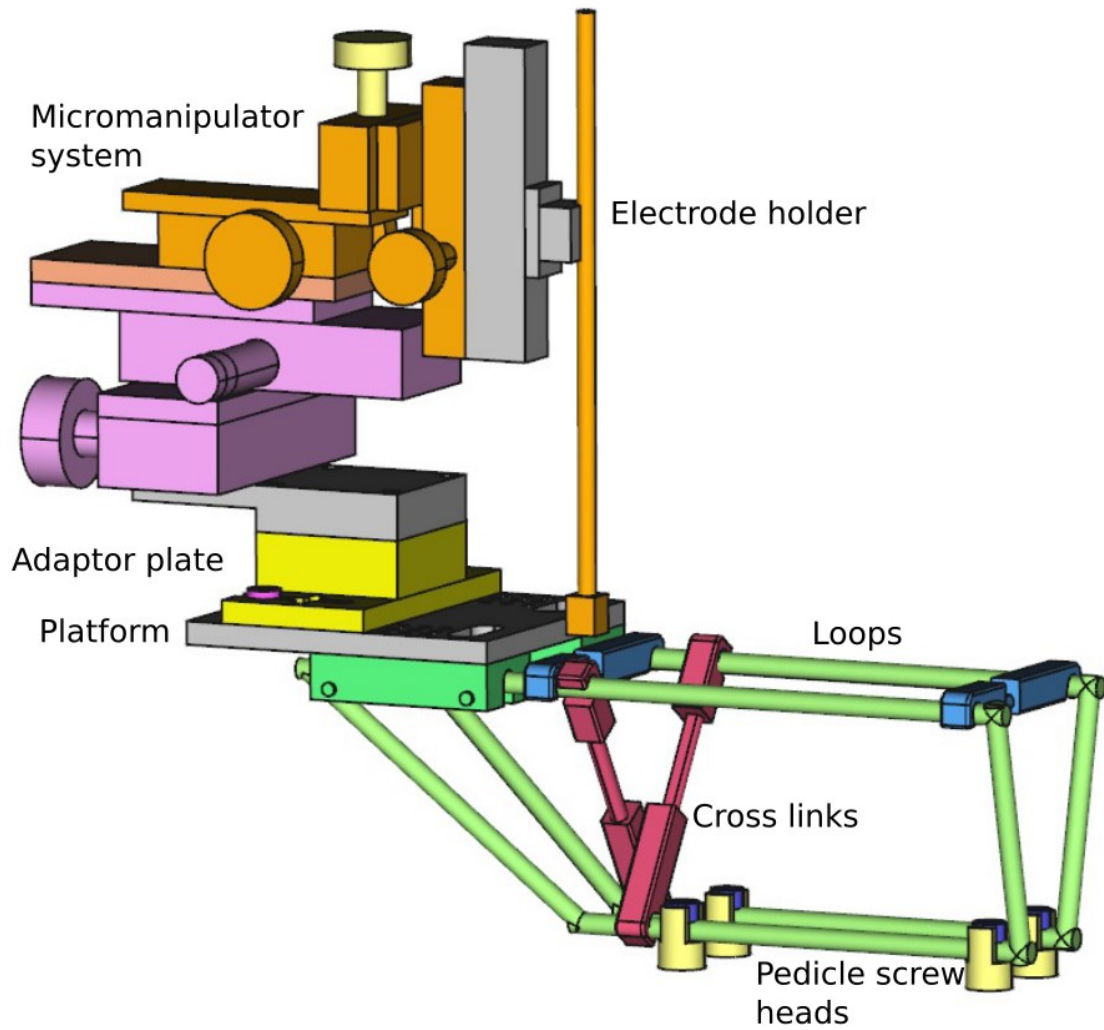


**Figure 2. 1.** The spinal stereotactic setup and its elements with special application to intraspinal microstimulation (ISMS).

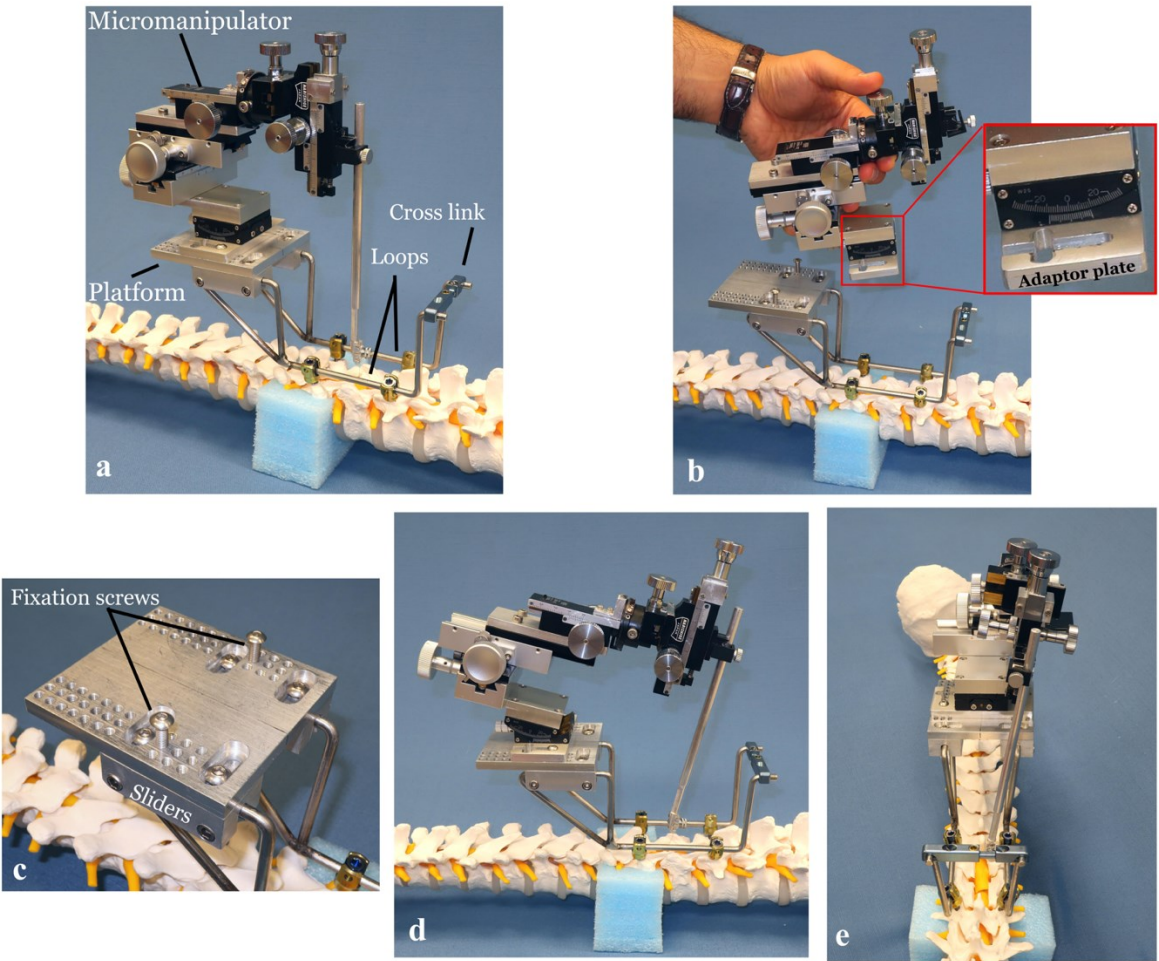


**Figure 2. 2.** The spinal stereotactic setup. (a) Elements of the spinal stereotactic system (b) Micromanipulator placement onto the platform using an adaptor plate. The attachment allows for both translation in the craniocaudal direction and adjustment of angles in the coronal plane. (c) The platform and its associated elements: fixation screws and sliders. (d) Rotation of the electrode in the transverse plane using the stereotactic system. (e) Rotation of the electrode holder and electrode in the sagittal plane using the stereotactic system.

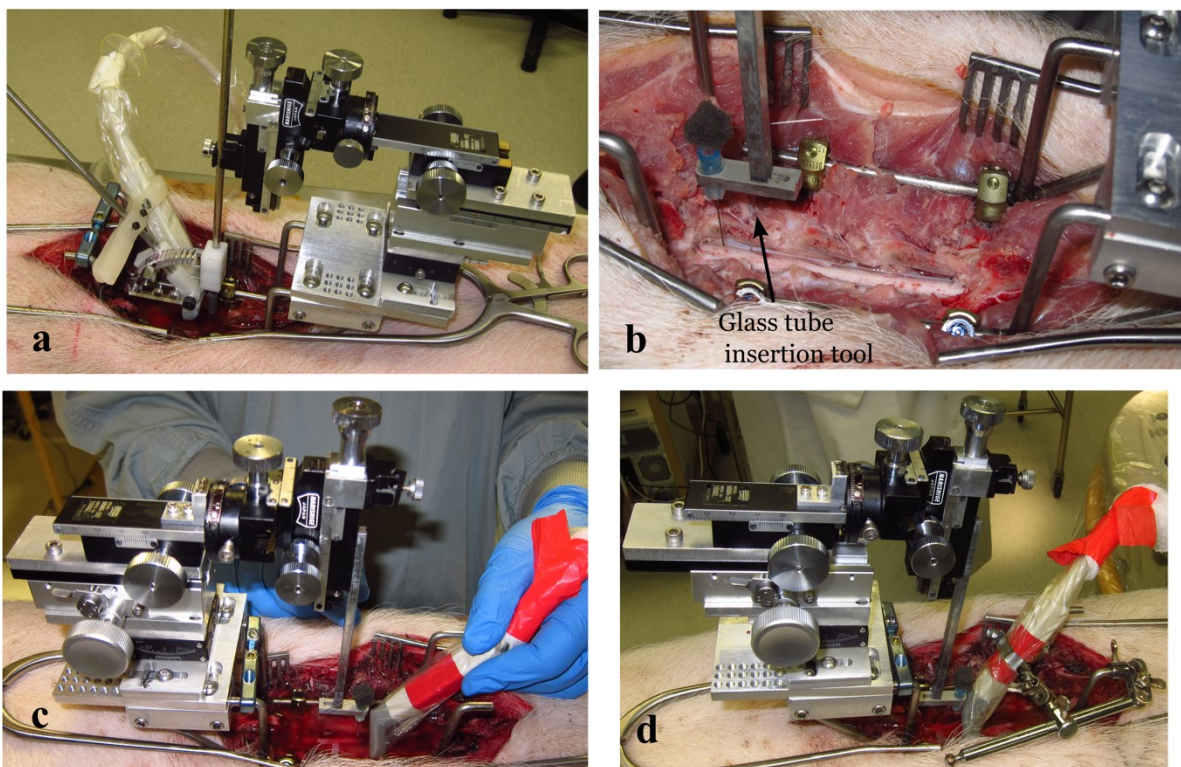


**Figure 2. 3.** The spinal stereotactic system used in a domestic pig. (a) Customized setup for accurate modification of the ultrasound probe tilt angle in the sagittal plane. (b) Glass-tube insertion tool. (c) Ultrasound-guided electrode alignment with a handheld probe. (d) Ultrasound-guided electrode alignment with the probe mounted onto stereotactic setup.

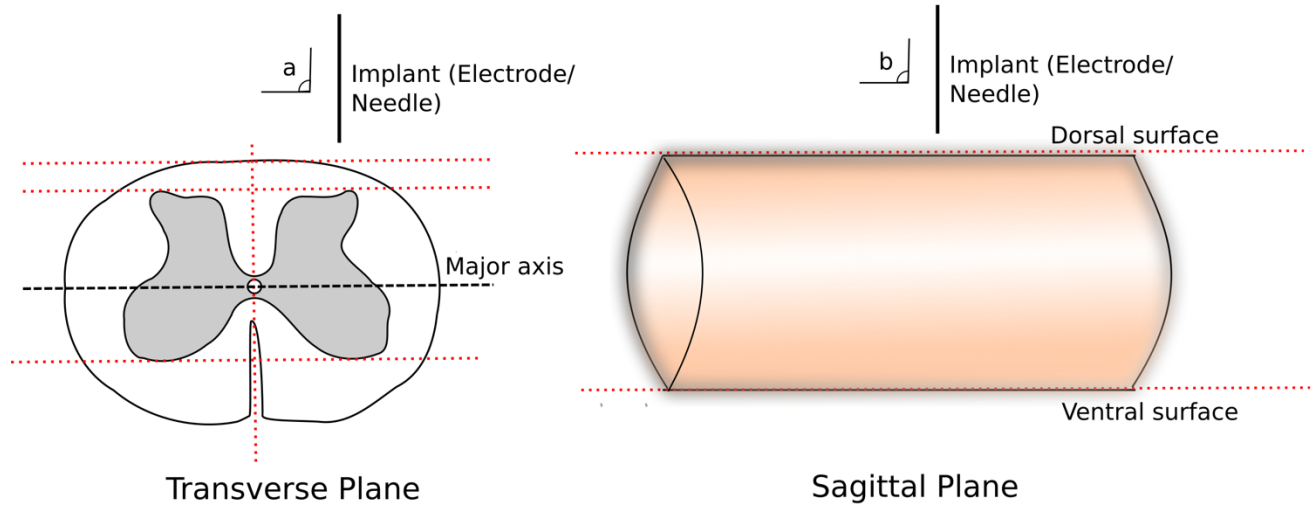


**Figure 2. 4.** Spinal cord in the transverse (left) and sagittal (right) planes and the landmarks (dotted-lines) that can be used to determine its orientation. In this study, the target for electrode insertion angle (a and b) is 90°.

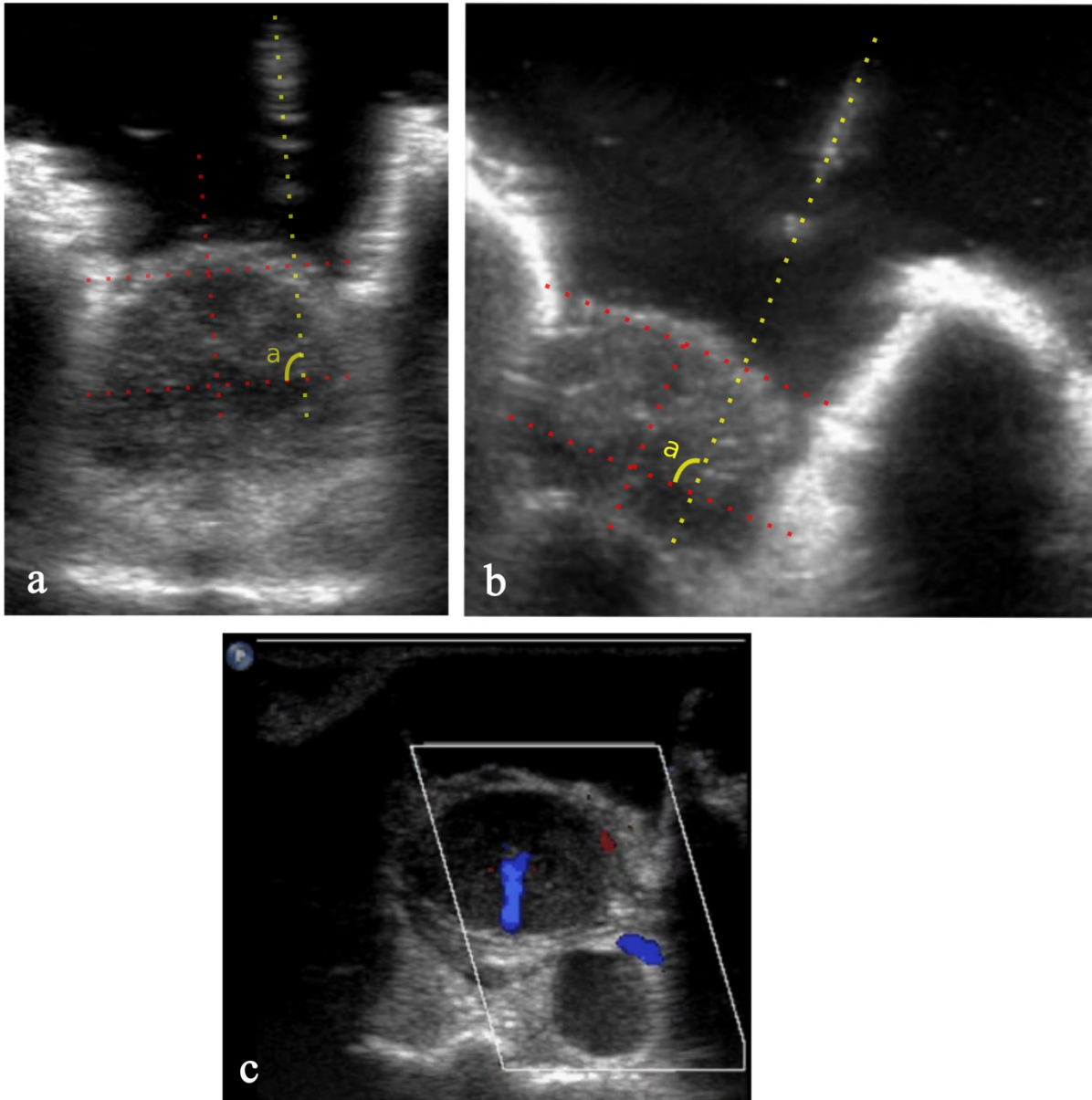


**Figure 2. 5.** Ultrasound images obtained from the lumbar enlargement of the pig spinal cord. (a-b) Ultrasound guided electrode alignment using the needle artifact and the spinal cord landmarks. (c) Doppler ultrasound image of the spinal cord showing cerebrospinal fluid (CSF) pulsations in the anterior fissure of the spinal cord. The orientation of the anterior fissure can be used to determine the orientation of the spinal cord.

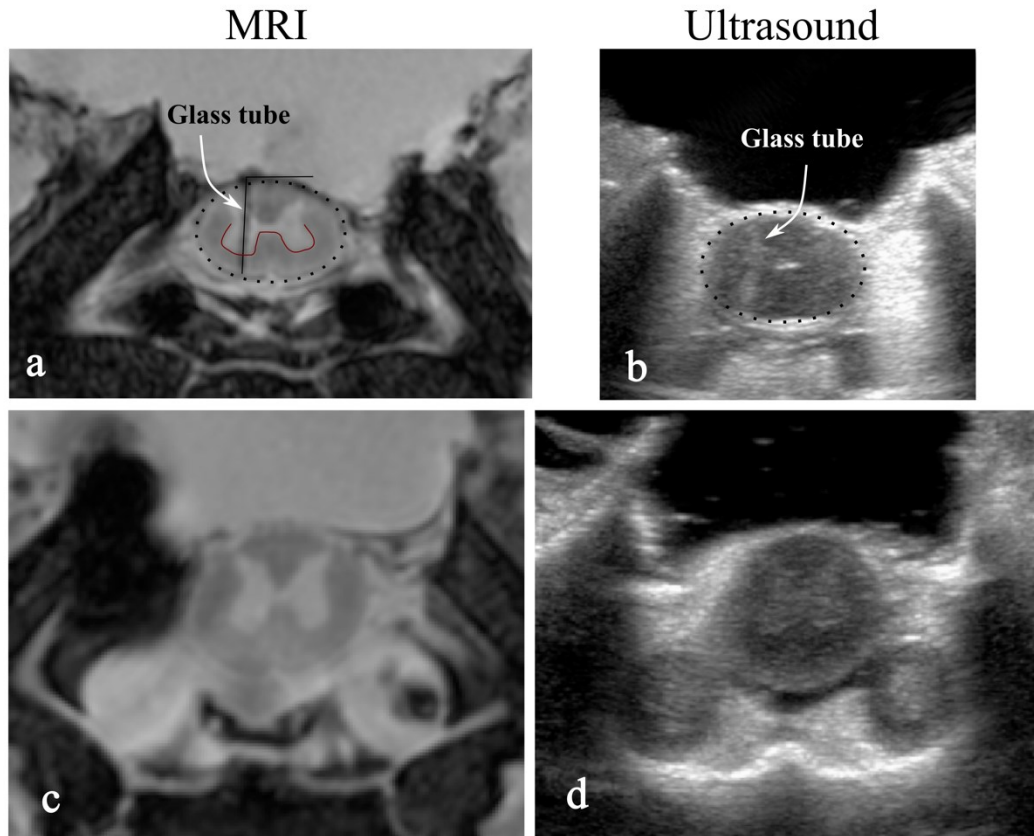


**Figure 2. 6.** Magnetic resonance (MR) and ultrasound images of similar segments of the spinal cord. Images in each row (a, b; c, d) belong to the same slice of the spinal cord (a) Measurement of insertion angle in MR images. (b) Ultrasound image showing an implanted glass-tube marker. (c) MR image of the spinal cord in the transverse plane showing the gray and white matter. (d) Ultrasound image in the transverse plane of the spinal cord for a similar section of the spinal cord as shown in (c).

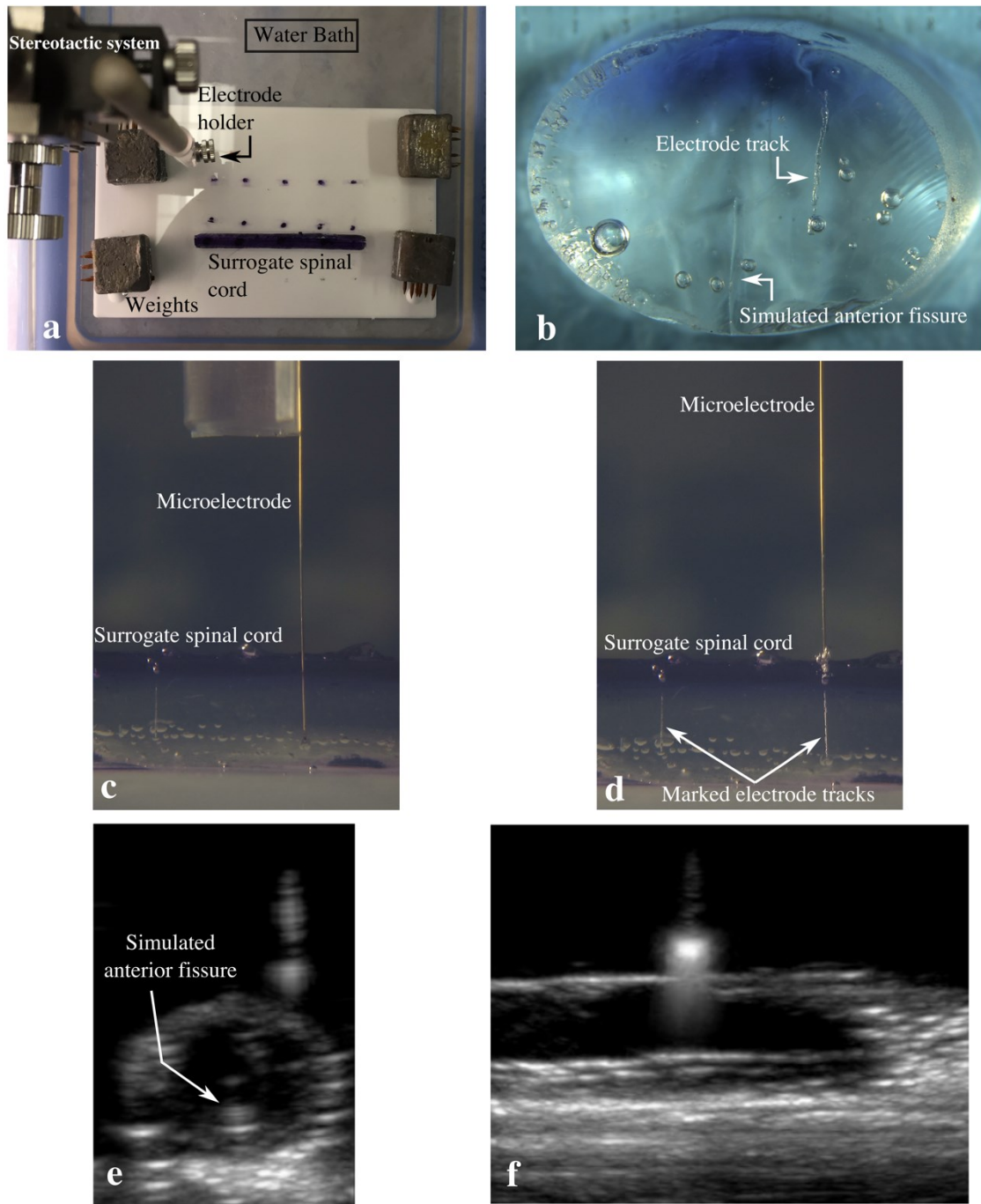


**Figure 2. 7.** Bench testing setup and methods.(a) Setup used for bench-tests: a surrogate spinal cord submerged in a saline bath with the stereotactic system positioned over it. Weights are used to prevent the plastic plate and the attached spinal cord from floating. (b) Prior to testing, a partial cut was made on one side of the surrogate spinal cords to simulate the anterior fissure.

This was performed while the surrogate cords were in their molds to ensure the cuts were properly aligned with the major axis of the surrogate cords. This figure also shows, in a slice of gelatin spinal cord, an electrode track resulting from electrical stimulation through the implanted electrode. (c) The electrode implanted in the gelatin spinal cord. (d) The electrode track and bubbles produced by stimulation through the electrode to mark the electrode's position for further analysis. (e) Ultrasound image of the gelatin spinal cord and the electrode prior to its implantation in the transverse plane. (f) Ultrasound image of the gelatin spinal cord and the electrode prior to its insertion in the sagittal plane.

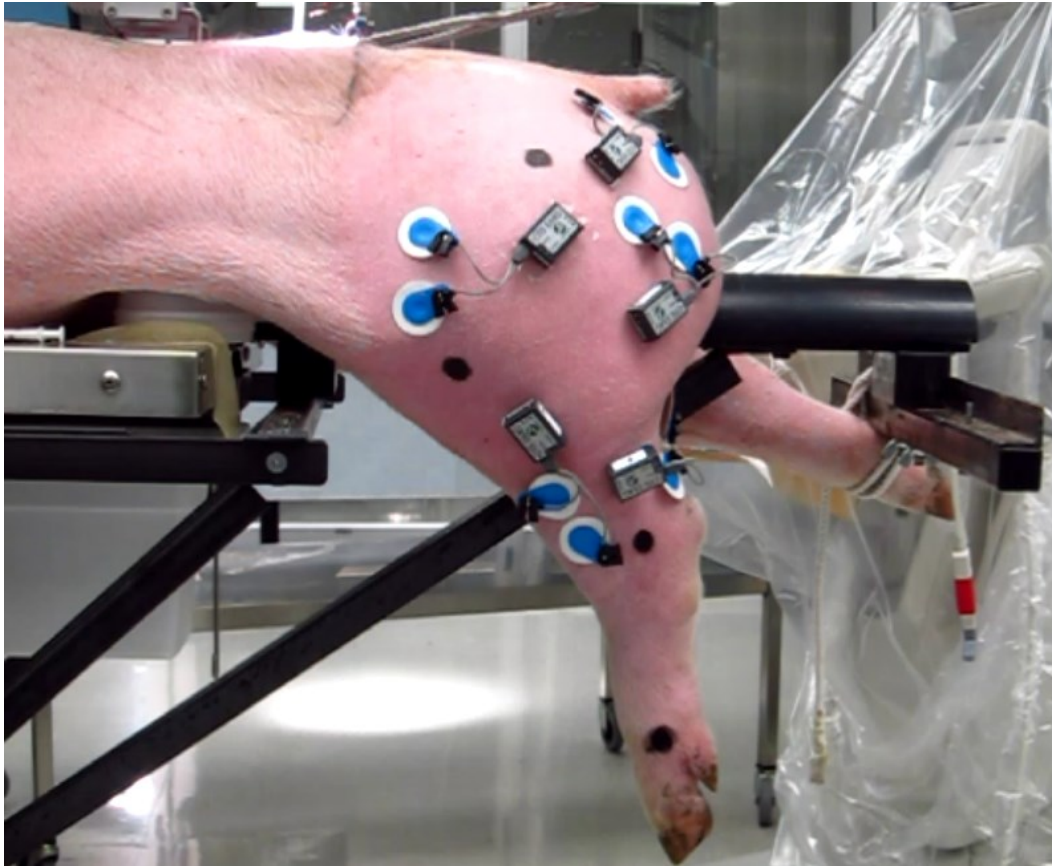


**Figure 2. 8.** Suspension setup used for visualization of hind limb movements produced by ISMS in the pig spinal cord.

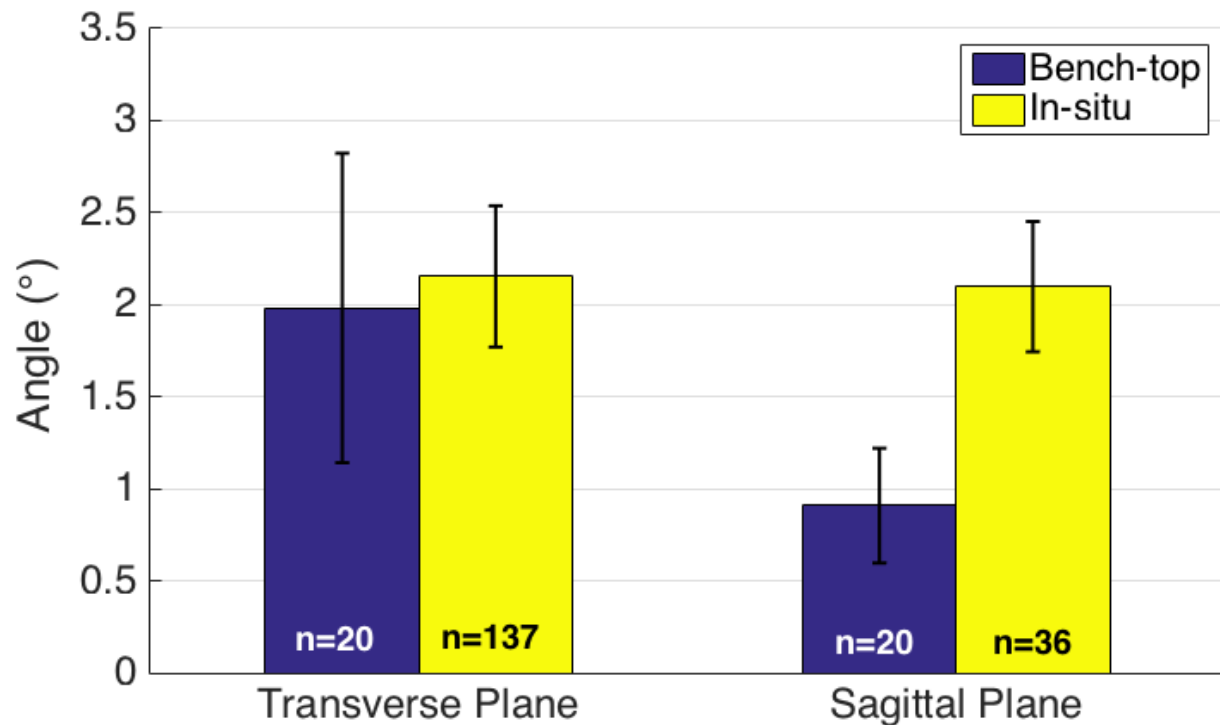


**Figure 2. 9.** Detection accuracy of electrode insertion angle for intraoperative ultrasound imaging. Bench-top results are a comparison between the ultrasound measurements and the light microscopy measurements of the sample (text section 2.3), and measurements in pigs are a comparison between ultrasound and MRI measurements (text section 2.2). The bench-top measurements were performed in 4 gelatin spinal cord samples and the measurements in pigs were performed in a total of 6 animals (transverse plane measurements performed in 6 animals and sagittal plane measurements performed in 2). Error bars represent the 95% confidence interval.

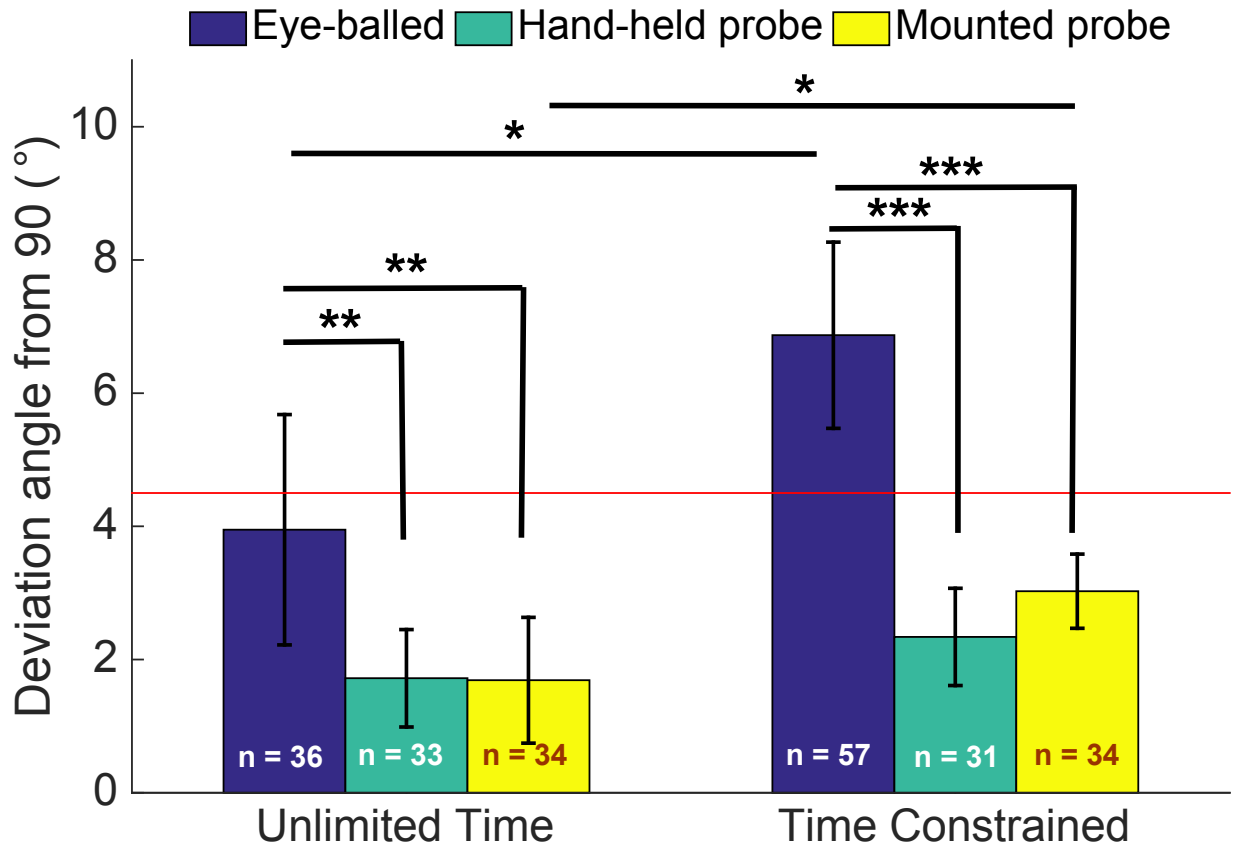


**Figure 2. 10.** Alignment accuracy of implant in the *transverse plane* of the spinal cord measured in pigs. Different bar colors represent different implantation techniques: eye-balling (blue), ultrasound imaging with a hand-held probe (green), and ultrasound imaging with a mounted probe (yellow). Implants conducted under ‘unlimited time condition’ were not limited in time and the surgeon was allowed to move around the subject freely to obtain different viewpoints of the implant site. Conversely, ‘time constrained condition’ simulated a more realistic surgical scenario in which the implantation time for each electrode was limited to 90 seconds and the surgeon was only allowed to move on one side of the subject. The red horizontal line represents the limit up to which a deviation angle from 90° is acceptable for ISMS applications in the human spinal cord. Error bars represent 95% confidence interval. \*  $p \leq 0.05$ ; \*\*  $p \leq 0.01$ ; \*\*\*  $p \leq 0.001$ .

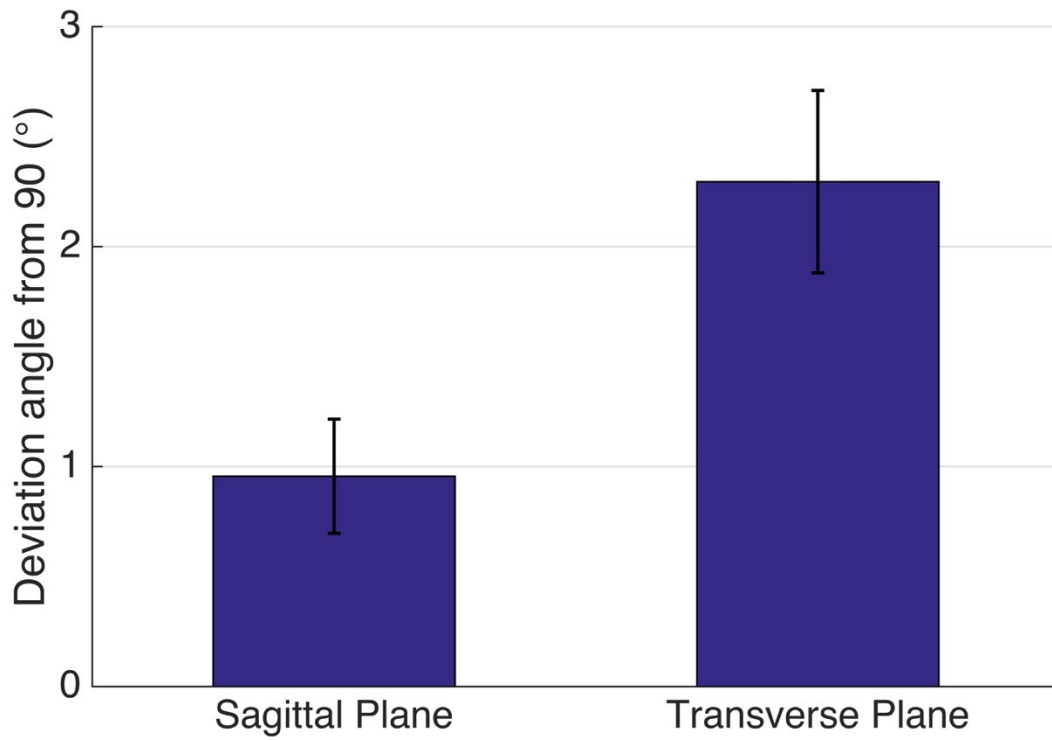


**Figure 2. 11.** Alignment accuracy of implant in the spinal cord measured *on the bench*.

Electrodes were placed using ultrasound guidance (with the probe held by hand) in both planes and consistent with time constrained condition (n=17).

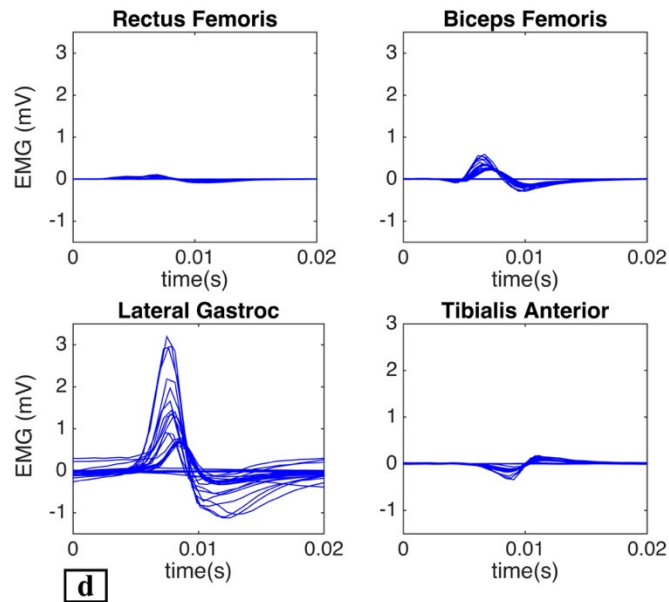
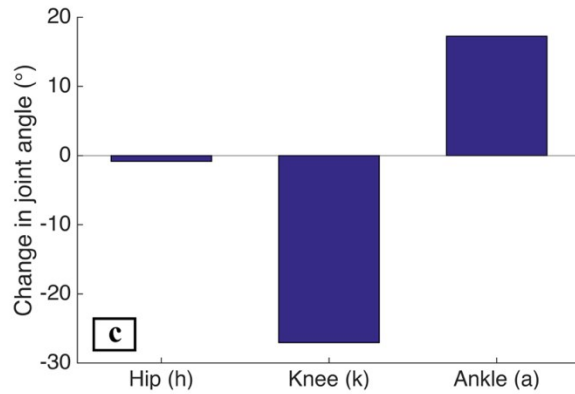
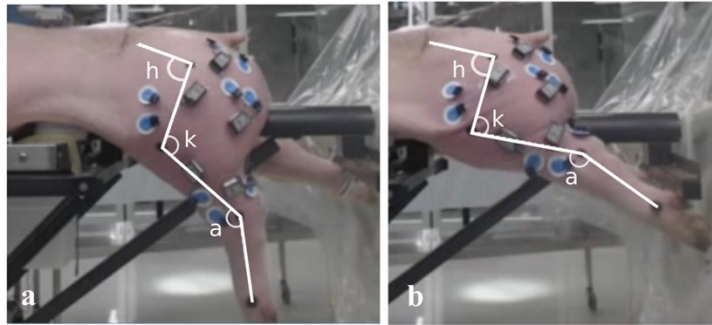


**Figure 2. 12.** Suspension setup used for intraoperative testing of ISMS in the pig spinal cord and an example of the results produced. (a) Leg position before stimulation, (b) leg position after stimulation at an amplitude of  $75 \mu\text{A}$ , (c) joint angle changes as a result of the generated movement, and (d) evoked EMG activity.

# **Chapter 3. Effect of anesthesia on the intraoperative responses to intraspinal microstimulation and its implications for clinical translation<sup>2</sup>**

Amirali Toossi<sup>1,6</sup> Dirk G. Everaert<sup>2,6</sup> Richard R. E. Uwiera<sup>3</sup> David Hu<sup>2,6</sup> Kevin Robinson<sup>4</sup>  
Ferrante S. Gragasin<sup>5</sup> Vivian K. Mushahwar<sup>1,2,6</sup>

<sup>1</sup>Neuroscience and Mental Health Institute, University of Alberta, Edmonton, AB, Canada.

<sup>2</sup>Division of Physical Medicine and Rehabilitation, Department of Medicine, University of Alberta, Edmonton, AB, Canada. <sup>3</sup>Department of Agricultural, Food and Nutritional Science,

University of Alberta, Edmonton, AB, Canada. <sup>4</sup>School of Physical Therapy, Belmont

University, Nashville, TN, USA. <sup>5</sup>Department of Anesthesiology and Pain Medicine, University

of Alberta, Edmonton, AB, Canada <sup>6</sup>Sensory Motor Adaptive Rehabilitative Technology (SMART) Network, University of Alberta, Edmonton, AB, Canada

---

<sup>2</sup> A version of this chapter has been submitted to a peer-review journal.

### **3.1 Introduction**

Intraspinal microstimulation (ISMS) is a spinal-cord-neuroprosthetic approach aiming to restore lost functions after spinal cord injury (Bamford and Mushahwar 2011; Jackson and Zimmermann 2012). ISMS activates the motor networks in the spinal cord distal to the site of injury, by delivering electrical currents through a microelectrode array implanted into the ventral horns of the cord (Bamford et al. 2016). One of the most widely studied applications of ISMS is for restoring standing and walking by placing the implants in the lumbosacral enlargement of the spinal cord (Lau, Guevremont, and Mushahwar 2007; Saigal, Renzi, and Mushahwar 2004; Mushahwar, Collins, and Prochazka 2000; Holinski et al. 2016). Preclinical studies of ISMS have demonstrated its ability in producing coordinated weight-bearing standing and walking movements that are fatigue resistant (Holinski et al. 2016; Lau, Guevremont, and Mushahwar 2007; Mushahwar, Collins, and Prochazka 2000) even following spinal cord injury (Saigal, Renzi, and Mushahwar 2004; Bamford, Putman, and Mushahwar 2005). These functional benefits have motivated recent efforts for translating this technique towards clinical implementation (Toossi et al. 2017, 2018).

One of the critical requirements for implementation of ISMS neuroprostheses in any species is knowledge about the functional organization of the targeted motor networks in the lumbosacral enlargement. This information is important for the optimal design and precise placement of the ISMS implants. A direct method for obtaining this information is through stimulation in various parts of the lumbosacral cord and creation of a map representing the evoked responses (i.e., functional map). Although functional maps exist for the lumbosacral spinal cord of animals used in ISMS research (Saigal, Renzi, and Mushahwar 2004; Mushahwar and Horch 2000b; Mushahwar et al. 2002; Toossi et al. 2016), they have not yet been

investigated in humans. Therefore, the first tests in humans will focus on this objective in an intraoperative setting under anesthesia (Toossi et al. 2018).

The most common anesthetic used for functional mapping of the lumbosacral spinal cord in animal models is sodium pentobarbital (Mushahwar and Horch 2000b; Toossi et al. 2016; Lau, Guevremont, and Mushahwar 2007; Mushahwar and Horch 2000a; Mushahwar, Collins, and Prochazka 2000). Historically, pentobarbital has been used for the implantation and intraoperative testing of ISMS microelectrode arrays (Saigal, Renzi, and Mushahwar 2004; Mushahwar, Collins, and Prochazka 2000; Holinski et al. 2016; Mushahwar et al. 2002; Holinski et al. 2013; Mazurek et al. 2012), assessment of functional outcomes of ISMS in anesthetized animals as a model for spinal cord injury (Holinski et al. 2016; Snow, Horch, and Mushahwar 2006; Lau, Guevremont, and Mushahwar 2007; Holinski et al. 2013) and for developing control algorithms for standing and walking using this approach (Lau, Guevremont, and Mushahwar 2007; Holinski et al. 2013; Mazurek et al. 2012; Guevremont, Norton, and Mushahwar 2007; Mazurek et al. 2016). Isoflurane (Rouhani and Erfanian 2018; Hachmann et al. 2013) and ketamine (Borrell et al. 2017) have also been used in a few animal studies of ISMS for standing and walking.

Propofol is one of the most commonly used anesthetic agents for functional neurosurgeries (Venkatraghavan et al. 2006; Sala et al. 2014; Ostrý et al. 2013; Sala et al. 2006) and for placement of neuroprostheses such as deep brain stimulators (Chakrabarti, Ghazanwy, and Tewari 2014) and spinal cord stimulators (Shils and Arle 2012). This is due to its rapid onset of anesthesia, rapid recovery times and easy application of dose titrations in people (Erickson and Cole 2012), along with its good capacity for sensorimotor neurophysiological monitoring (Pajewski, Arlet, and Phillips 2007; MacDonald et al. 2013). Therefore, in preparation for

intraoperative clinical testing of ISMS, understanding the effect of propofol anesthesia on ISMS responses is essential. This is especially important for the accurate interpretation of experimental results and their comparison with existing literature. While propofol has been the subject of studies investigating its influence on intraoperative neurophysiological monitoring measurements (e.g., somatosensory evoked potentials (SSEP) and motor evoked potentials (MEP)) (Sloan 2002), its influence on neuromuscular responses evoked by ISMS has not been investigated. Our goal in this study was to investigate this in a swine model through a comprehensive comparison of the effect of propofol anesthesia on the responses produced by ISMS (e.g., leg movements, joint torques and their stimulation thresholds) with those evoked under more commonly used anesthetic agents for preclinical research of ISMS, namely pentobarbital and isoflurane.

## **3.2 Methods**

Pigs were chosen for this study as they are a good model for translational biomedical research (Swindle et al. 2012) and are increasingly considered a suitable large animal model for studies of spinal cord injury (Benavides et al. 2016; Lee et al. 2013; Kwon et al. 2015) and intraspinal microstimulation (Toossi et al. 2017, 2018; Hachmann et al. 2013). All experiments were conducted in accordance with protocols approved by the Animal Care and Use Committee at the University of Alberta.

**Surgery.** Experiments were conducted in seven male domestic pigs ( $49.0 \pm 9.1$  kg) with intact spinal cords. Animals were premedicated with an intramuscular injection of ketamine (22 mg/kg), and glycopyrrolate (0.01 mg/kg), induced with isoflurane (4%, 100% O<sub>2</sub>) and intubated through direct laryngoscopy. The pigs were mechanically ventilated (18-22 breaths/min) and

anesthesia was maintained with inhalational isoflurane (2.0-3.5%, 100% O<sub>2</sub>) in combination with remifentanyl intravenous infusion for enhanced anesthesia and analgesia for the duration of the surgery. All animals were surgically implanted with an indwelling distal brachial arterial catheter for continuous direct blood pressure monitoring and collection of arterial blood for blood gas analyses. Muscles and fascia were carefully dissected and a laminectomy was performed from lumbar vertebra L3 through L5 to expose the lumbosacral enlargement of the spinal cord (Toossi et al. 2017). Spine levels L3 to L5 were then fixed by placement of four pedicle screws bilaterally (4.5 mm in diameter, Medtronic Co., Dublin, Ireland) in the pedicles of vertebrae L3 and L5, secured longitudinally with surgical rods. Spinal fixation was implemented to minimize the movement between the spinal column and the lumbosacral enlargement of the spinal cord, the implantation site for the ISMS microelectrode array. Prior to microelectrode implantation, the dura mater over the exposed region of the spinal cord was incised and secured with lateral stay sutures.

**ISMS microelectrode array and implantation procedure.** The ISMS microelectrode array was made out of 12 microwires (50 µm diameter; California Fine Wire Co., Grover Beach, CA, USA), insulated with 4 µm polyimide except for 200 µm at the sharpened tip. Each microwire had a bent portion of 4.8-5.0 mm at the distal end (tip) for insertion in the cord. The array was secured to the L2 spinous process and extended over the 5 cm long region of the lumbosacral enlargement. The return electrode consisted of a multi-stranded stainless steel wire (Cooner Wire Co., Chatsworth, CA, USA), 300 µm in diameter, insulated with Teflon except for a 5 cm-long region at the tip. Details of the design of the ISMS microelectrode arrays are described by Bamford et al (Bamford et al. 2016).

The microwire electrodes were individually implanted into the ventral horn of the spinal cord on one side. Implantation targets were chosen based on the available functional maps of the lumbosacral spinal cords of cats and monkeys (Saigal, Renzi, and Mushahwar 2004; Mushahwar and Horch 2000b; Mushahwar et al. 2002; Toossi et al. 2016). In animals #5-7, ultrasound imaging was used to acquire intraoperative feedback on the location of the implanted electrode tips within the spinal cord, and allow for adjustments if necessary (Toossi et al. 2018).

**Anesthesia protocols.** After completion of the surgery and placement of the ISMS implant, a series of measurements were conducted under three anesthetic protocols. For all measurements, the animals were maintained in surgical plane of anesthesia, as determined by the absence of responses to nose pinch and maintenance of baseline heart rate (80-120 beats/min).

Protocol 1: Inhalational isoflurane anesthesia. The average inspiratory concentrations of isoflurane used in this study ranged from 2% to 3.5%.

Protocol 2: A total intravenous anesthesia (TIVA) protocol with a combination of propofol (40-145  $\mu\text{g}/\text{kg}/\text{min}$ ), remifentanyl (0.03-0.14  $\mu\text{g}/\text{kg}/\text{min}$ ), lidocaine (fixed dosage: 1.0  $\text{mg}/\text{kg}/\text{hr}$ ), and dexmedetomidine (fixed dosage: 0.2  $\mu\text{g}/\text{kg}/\text{hr}$ ). The depth of anesthesia was controlled by adjusting the dosages for propofol and remifentanyl. The drugs were administered intravenously through catheters in ear veins using 4 syringe pumps. At the start of the protocol, loading doses of 0.8-3.5  $\text{mg}/\text{kg}$  of intravenous propofol were administered to the pig to transition from gas anesthesia to TIVA. Boluses of propofol were also occasionally administered during the procedure to assist in maintaining adequate anesthesia when required. The addition of lidocaine

and dexmedetomidine either individually or in combination to a mixture of remifentanyl and propofol reduces the amount of propofol and remifentanyl required to maintain effective levels of surgical anesthesia (Xu et al. 2017; Sloan et al. 2014) and reduces post-operative pain (Xu et al. 2017). Lidocaine (Urban et al. 2017; Sloan et al. 2014) and dexmedetomidine (Li et al. 2016) have also been shown to not affect the intraoperative MEP and SSEP recordings for neurophysiological monitoring.

Protocol 3: A TIVA protocol with pentobarbital (8-13 mg/kg/hr). At the start of the protocol, a loading dose of 25 mg/kg pentobarbital was administered over 10-20 minutes.

**Study design.** The anesthesia protocols were tested in series, with washout periods to transition from one protocol to another (figure 3.1). This study design allowed the comparison of the responses to ISMS under different anesthetic protocols for each implanted microelectrode in the same animal. The order of the anesthetic protocols was maintained for all experiments and pentobarbital anesthesia was chosen to be the last in the sequence due to its prolonged drug clearance and recovery time (Frederiksen et al. 1983).

The following outcome measures were recorded under stable conditions in each anesthetic protocol: i) MEP produced by transcranial electrical stimulation (TES); ii) Stimulation thresholds for evoking a visible movement twitch or electromyographic (EMG) activity in the recorded muscles; iii) Kinematics of the movements evoked by ISMS; iv) Joint torques evoked by ISMS; and v) EMG signals evoked by ISMS.

After completing the measurements under one anesthetic protocol, administration of the drugs was stopped, and the animal was transitioned to drugs for the next protocol. The anesthetic

protocols overlapped to ensure the pig remained in surgical plane of anesthesia throughout the procedure. After transitioning to the new anesthetic protocol and prior to initiating the measurements, a washout period was implemented to clear the drugs from the previous protocol. The criterion used for choosing the duration of the washout periods was the estimated time until awakening for each anesthetic protocol.

The first washout period between isoflurane (protocol 1) and propofol (protocol 2) anesthesia was 30-60 minutes (30 minutes for animals #1-3, and 60 minutes for animals #4-7). This duration was chosen based on an estimated context-sensitive decrement time for recovery in humans and assuming it to be the same for pigs.

Given that the inspiratory concentrations of isoflurane ranged from 2%-3.5% (0.5-0.65 L/min total flow) in this study, the maximal expiratory concentration of isoflurane can be estimated to be 3.5% or less. We utilized an open circle anesthesia circuit; therefore, it is unlikely that expiratory isoflurane approached 3.5%. Nonetheless, this concentration is equivalent to 2.3x the estimated minimum alveolar concentration (MAC) in pigs (Steffey et al., 1994).

The context-sensitive 80% decrement time for isoflurane plateaus at approximately 30 minutes, after 350 minutes of anesthesia (Bailey 1997; Eger and Shafer 2005). Therefore, after 30 minutes of washout, the maximal expiratory isoflurane concentration (2.3x MAC) reduces to an estimated concentration of 0.46x MAC. These concentrations are in the range of MAC-awake levels (50% of the patients respond to verbal directives) for isoflurane (Dwyer et al. 1992). Therefore, washout durations longer than 30 minutes meet the washout criteria for this study.

The duration of the second washout period, between propofol and pentobarbital protocols, was 60 minutes. The average reported time for recovery (awakening and

understanding verbal directives) from propofol-remifentanyl anesthesia in humans (average anesthesia time: ~193 min), is reported to be 8.5 minutes post-anesthesia (Rocha et al. 2017). The 60 minute washout period is also sufficient for an effective clearance of remifentanyl, dexmedetomidine and lidocaine as their context-sensitive decrement times are relatively short. The 90% decrement time of remifentanyl for a 3 hour infusion in humans is approximately 10 minutes (Kapila et al. 1995). The context-sensitive half time for dexmedetomidine after 2 hours of infusion is approximately 40 minutes in humans (Talke et al. 1997). Context-sensitive half-time of lidocaine for infusions up to 72 hours long is 20-40 minutes (Eipe, Gupta, and Penning 2016).

**Plasma concentration of propofol post-infusion.** After the termination of propofol infusion (end of protocol 2), arterial blood samples were collected in heparinized tubes. Plasma samples were collected at 0, 5, 10, 15, 20, 30, 40, and 60 minutes after the discontinuation of the anesthetic infusion to determine the plasma elimination kinetics for propofol and confirm the sufficiency of the washout period. Blood samples were centrifugated at 4°C and 1000 g acceleration for 10 minutes, and collected plasma samples were snap frozen by liquid nitrogen and stored in -80°C. Ultra-performance liquid chromatography (UPLC) analysis was performed on the collected samples to measure the concentration of propofol in plasma.

**Vital signs and blood gas monitoring.** Vital signs including heart rate, expiratory carbon dioxide concentration, pulse oximetry, temperature, and arterial blood pressure were monitored and recorded. Arterial blood gas analyses were also conducted intermittently throughout the experiments. These analyses were: pH, partial pressures of oxygen and carbon dioxide, oxygen

saturation, bicarbonate content, anion gap, base excess, total hemoglobin, total carbon dioxide concentration, and concentration of sodium, potassium, and chloride ions.

**Motor evoked potentials (MEP).** Two corkscrew TES electrodes were placed in the FC1 and FC2 landmarks over the animal's skull, according to the modified 10-20 international system for electroencephalography electrode placement in pigs (Benavides et al. 2016). These landmarks were 5 mm lateral to the midline and 7.5 mm rostral to the cranial vertex. The TES paradigm was 5 pulses with an inter-stimulus interval (ISI) of 1 ms at an amplitude of 600 V. The resulting MEPs were recorded using a Noraxon digital telemetry system (Noraxon Co., Scottsdale, AZ, USA). EMG recordings were digitized at a sampling frequency of 3000 Hz from 5 muscles using surface electrodes (gluteus medius, biceps femoris, vastus lateralis), or intramuscular electrodes (tibialis anterior, gastrocnemius). MEP recordings were obtained at the beginning and at the end of each anesthesia protocol. Each recording was repeated three times. Data analyses were conducted using a custom written program in Matlab (version 2015a, MathWorks Co., Natick, USA).

**Intraspinal microstimulation (ISMS) and recordings of stimulation thresholds.** The ISMS protocol consisted of 0.5 s-long trains of biphasic, symmetric, charge-balanced pulses with a frequency of 50 Hz, pulse width of 200  $\mu$ s and intensities up to 150  $\mu$ A.

In order to detect the stimulation threshold for each implanted electrode, a series of stimulation trains with gradually decreasing intensities were delivered. The smallest stimulation intensity that evoked an EMG activity in the recorded muscles or a visible muscle twitch was

defined as the stimulation threshold. Stimulation thresholds for all implanted microelectrodes were recorded at the beginning and at the end of each anesthesia protocol.

**Kinematics, joint torques, and EMG activity.** Reflective markers were placed on the iliac crest, hip, knee, ankle, and metatarsophalangeal joints (figure 3.2) in order to capture the hind limb movements produced by ISMS. A video camera (Logitech Co., Lausanne, Switzerland) was positioned perpendicularly to the recorded hindlimb, capturing the movements in the sagittal plane. Video recordings and kinematic data analyses were performed using the Noraxon MR3 software package (Noraxon Co.).

Joint torques produced by ISMS were calculated from isometric forces measured using a 150 lb-load cell (Interface Inc., Scottsdale, AZ, USA) with a sampling frequency of 3000 Hz. ISMS-evoked EMG activity was also recorded from 5 muscles as described for MEP recordings. Data analyses for torques and EMG recordings were performed using custom written Matlab programs.

**Euthanasia, post-mortem procedures and magnetic resonance imaging.** After the completion of data collection under the last anesthetic protocol, the animal was euthanized with an intravenous injection of euthanyl, followed by the extraction of the spine along with the spinal cord from vertebral levels L2-L6. The extracted specimen was then fixed in formaldehyde solution (4%). In order to identify the location of the implanted electrodes in the spinal cord, samples underwent magnetic resonance imaging (MRI) while submerged in saline. MRI scans were obtained using a 3T Siemens Prisma MRI scanner and a 1Tx/15Rx knee coil at the Peter S.

Allen MR Research Centre, University of Alberta. The images were acquired using a 2D T<sub>2</sub>-weighted turbo spin echo sequence with a resolution of 0.25 mm x 0.25 mm x 1 mm. MRIs were analyzed using ImageJ software (U.S. National Institute of Health, Bethesda, MD, USA).

**Statistical analyses.** Before conducting comparative statistics, each dataset was tested for distribution normality using a Shapiro-Wilk test. Measurements of stimulation threshold, joint torque, and joint ranges of motion (change in joint angle) did not pass the normality distribution test, while the EMG amplitudes were normally distributed. In each animal, the stimulation thresholds at the beginning and the end of each anesthetic protocol were compared using a Mann-Whitney U test. One-way ANOVA with repeated measures tests followed by Bonferroni post-hoc tests were performed to compare the stimulation thresholds, joint torques, range of motions, and EMG amplitude under different anesthetic protocols. Mauchly's test of sphericity was conducted for all groups compared using the repeated measure ANOVA test. In cases that the assumption of sphericity was not valid, Greenhouse-Geisser correction was used. Interquartile ranges (IQR) were calculated by subtracting the first quartile (Q1) from the third quartile (Q3). Differences were considered significant for  $p \leq 0.05$ . All statistical analyses were conducted using IBM SPSS software (version 22, IBM Co., Armonk, USA).

### **3.3 Results**

**Electrode locations.** Locations of the tips of the implanted microelectrodes in the spinal cords of all animals are shown in figure 3.3. In total, the tips of 57 microelectrodes were positioned in the gray matter and those of 19 microelectrodes in the white matter. Microelectrode tips located on the boundary of the gray and white matter of the spinal cord were considered to be in the white

matter. Microelectrode tips implanted in the gray matter were located in Rexed laminae VII – IX (Rexed 1952). Microelectrode tips implanted in the white matter were in the ventral and ventrolateral funiculi.

**Concentration of propofol in plasma after cessation of infusion.** Plasma concentration curves of propofol after stopping its infusion are shown in figure 3.4. These curves were recorded to validate the sufficiency of the duration of the washout period applied for propofol. Assuming a two compartment model for the pharmacokinetics of propofol (Hill 2004), a 2-term exponential equation was fit to the plasma concentration measurements. While propofol was given as continuous infusion, in 3 experiments (animals 5, 6, and 7) a bolus of propofol was also administered less than 10 minutes before the termination of infusion. Influence of the bolus injections can be seen in the higher initial plasma concentrations in these experiments. The total infusion time of propofol was  $124 \pm 27$  minutes and the plasma concentration of propofol at 60 minutes post infusion was  $0.228 \pm 0.061$   $\mu\text{g/mL}$ .

The reported range of plasma concentration of propofol ( $C_{50}$ ) for awakening in humans is 0.7-1.59  $\mu\text{g/mL}$  (Wessén et al. 1993; Schüttler et al. 1988; Kazama et al. 1998). In pigs, the average awakening concentration of propofol in whole blood is 1.1  $\mu\text{g/mL}$  (Adam, Glen, and Hoyle 1980). The ratio of whole blood and plasma concentrations of propofol has been studied in rats and humans and the ratios are 1.7 (Yeganeh and Ramzan 1997) and 1.25 (Fan et al. 1995), respectively. Assuming similar ratios apply to pigs, the awakening plasma concentration of propofol in pigs is estimated to be 0.65-0.88  $\mu\text{g/mL}$ . The measurements of plasma concentration of propofol conducted at the end of the washout period (60 minutes) ranged from 0.17 to 0.32

$\mu\text{g/mL}$ . These concentrations are on average 65% smaller than the lowest concentration reported for awakening in pigs and humans ( $0.65 \mu\text{g/mL}$ ).

The plasma concentration half-time of propofol for animals 1-4 (without an extra bolus of propofol at the end of the anesthetic protocol) and 5-7 (with an extra bolus of propofol at the end of the anesthetic protocol) were  $18.7 \pm 11.2$  and  $6.2 \pm 6.7$  minutes, respectively. The values are comparable to those in humans, where half-times for infusions for 2 hours (the average duration of the propofol protocol in this study) and for bolus injections, are approximately 15 minutes and 5 minutes, respectively (Hill 2004; Hughes, Glass, and Jacobs 1992).

**Clinical parameters.** The vital signs for all animals under the three anesthesia protocols are shown in figure 3.5. The average ( $\pm$  standard error) heart rate, mean arterial pressure, expiratory  $\text{CO}_2$  concentration, blood oxygen saturation level, and temperature, for all animals ( $n=7$ ) were  $111.9 \pm 5.8$  beats/min,  $71.7 \pm 4.8$  mmHg,  $49.1 \pm 3.3$  mmHg,  $97.5 \pm 0.3$  %,  $39.3 \pm 0.3$  °C, respectively. Measurements of arterial blood gases are also provided in table 1.

The vital signs and blood gases remained stable throughout each experiment and the values were within clinically acceptable ranges. The only exceptions were a few time points in the experiment involving animal #3, during which abnormal increases in partial pressure of carbon dioxide ( $>60$  mmHg) and potassium ion concentration ( $>10$  mmol/L) had occurred. The data collected during these time points were excluded from all analyses.

**Stimulation thresholds.** Stimulation thresholds were measured once at the beginning and once at the end of each anesthetic protocol for all implanted microelectrodes (in 6 experiments), to assess the stability of evoked responses under the plane of anesthesia in which all measurements

were conducted (figure 3.6a). The starting and ending stimulation thresholds were not significantly different from each other in any of the anesthetic protocols and animals ( $p>0.378$ ), demonstrating that the depth of anesthesia was stable and consistent for measurements of ISMS responses.

Stimulation thresholds measured at the beginning of each anesthetic protocol were used for comparisons across anesthetic protocols (figure 3.6b). The median stimulation thresholds for electrodes in the gray and white matter of the spinal cord were 16  $\mu\text{A}$  (IQR=13.5  $\mu\text{A}$ ) and 17  $\mu\text{A}$  (IQR=12.5  $\mu\text{A}$ ) under isoflurane anesthesia (protocol 1), 11  $\mu\text{A}$  (IQR=11  $\mu\text{A}$ ) and 12.5  $\mu\text{A}$  (IQR=32.25  $\mu\text{A}$ ) under propofol anesthesia (protocol 2), and 11  $\mu\text{A}$  (IQR=14  $\mu\text{A}$ ) and 12  $\mu\text{A}$  (IQR=40  $\mu\text{A}$ ) under pentobarbital anesthesia (protocol 3). A significant difference was found in the stimulation thresholds depending on the anesthetic protocol ( $p<0.001$  for microelectrodes implanted in the gray matter). For microelectrodes implanted in the gray matter, the stimulation thresholds were significantly larger under isoflurane anesthesia than those under propofol ( $p=0.003$ ) and pentobarbital ( $p=0.002$ ). However, the stimulation thresholds under propofol and pentobarbital anesthesia were not statistically different from each other ( $p=1.00$ ). The median of the stimulation thresholds under isoflurane were 45% larger than the median thresholds under pentobarbital and propofol.

**Joint torques.** The ISMS-evoked joint torques are shown in figure 3.7a. Torques were measured for knee extension (39% of all measurements), ankle extension (15.6% of all measurements), ankle flexion (12.5% of all measurements), extensor synergy movements consisting of hip, knee and ankle extension (10.9% of all measurements), and hip flexion (9.3% of all measurements), hip extension (6.25% of all measurements), hip abduction (1.5% of all measurements), hip and

knee extension synergy (4.7% of all measurements), in 7 experiments. For electrodes with tips in the gray matter, the measured joint torques ranged from 0 to 5.95 N.m (median 0.67, IQR 1.97 N.m) under isoflurane, 0.003 to 15.62 N.m (median 1.44, IQR 5.06 N.m) under propofol, and 0.0006 to 17.47 N.m (median 1.68, IQR 4.78 N.m) under pentobarbital. For electrodes with tips in the white matter, the joint torques ranged from 0 to 1.81 N.m (median 0.17, IQR 0.49 N.m), 0.01 to 7.17 N.m (median 0.51, IQR 1.14 N.m), and 0.05 to 9.19 N.m (median 0.48, IQR 0.81 N.m), under isoflurane, propofol and pentobarbital, respectively.

A comparison of the joint torques showed an anesthetic-dependent effect ( $p < 0.001$  for electrodes in the gray matter). The produced torques were significantly larger under pentobarbital ( $p < 0.001$ ) and propofol ( $p < 0.001$ ) anesthesia compared with those under isoflurane anesthesia. The torques however were not significantly different between pentobarbital and propofol anesthesia ( $p = 0.106$ ). The median normalized joint torques produced during pentobarbital anesthesia were 2.5x larger than those produced under isoflurane. Median joint torques produced during propofol anesthesia were 2.15x larger than those under isoflurane.

**Joint kinematics.** The range of motion produced by ISMS, exemplified by changes in joint angle, is shown in figure 3.7b. Half of the range of motion measures were obtained for the knee joint and the other half for the ankle joint in three experiments. All measurements were obtained for microelectrodes with tips in the gray matter of the spinal cord. The median ranges of motion were  $3^\circ$  (IQR:  $7^\circ$ ),  $20^\circ$  (IQR:  $14.5^\circ$ ), and  $19^\circ$  (IQR:  $13.25^\circ$ ), under isoflurane, propofol, and pentobarbital, respectively. The range of motion evoked by ISMS was also anesthetic dependent ( $p < 0.001$ ) and was significantly larger under pentobarbital ( $p < 0.001$ ) and propofol ( $p < 0.001$ ) anesthesia than under isoflurane. The range of movement was not different under propofol and

pentobarbital anesthesia ( $p=1.00$ ) (figure 3.7b). The median values of the ranges of motion were 6.33x and 6.67x larger under pentobarbital and propofol anesthesia than under isoflurane, respectively.

**EMG responses.** A comparison of the EMG responses produced by ISMS under different anesthetic protocols also showed an anesthetic-dependent effect ( $p<0.001$ ). An example of an EMG response in the vastus lateralis muscle to ISMS delivered through the same microelectrode under the different anesthetic agents is shown in figure 3.8a. The average amplitudes of the evoked EMG pulses across various muscles under the different anesthetic protocols are shown in figure 3.8b. Comparison of the EMG amplitudes demonstrated that they were significantly smaller under isoflurane than under propofol and pentobarbital anesthesia ( $p<0.003$ ) for vastus lateralis, gluteus medius, biceps femoris muscles. The amplitude of the EMG responses however were not significantly different from each other under propofol and pentobarbital anesthesia ( $p>0.173$  for gluteus medius, biceps femoris, gastrocnemius, tibialis anterior). An exception to this trend, was the vastus lateralis muscle, in which the EMG amplitudes were larger under pentobarbital than propofol anesthesia ( $p<0.006$ ).

As shown in figures 3.8c and 3.9, the pattern of the EMG pulse train was also influenced by the choice of anesthesia. Under isoflurane anesthesia, the amplitude of the EMG pulses gradually decreased over the first few pulses and stabilized at a lower amplitude ( $p\leq 0.012$  for vastus lateralis, gluteus medius, and gastrocnemius muscles). This was in contrast with the responses under propofol and pentobarbital anesthesia where the EMG pulse amplitudes stabilized at a similar ( $p\geq 0.054$  for gluteus medius, biceps femoris, tibialis anterior and

gastrocnemius under propofol and pentobarbital) or larger ( $p < 0.012$  for vastus lateralis under propofol and pentobarbital) amplitude.

**MEP measurements.** MEP recordings were conducted in 3 experiments at the beginning and end of each anesthetic protocol (figure 3.10). MEPs were completely suppressed under the isoflurane anesthetic protocol. However, responses were present under propofol and pentobarbital protocols and had larger amplitudes under propofol than pentobarbital anesthesia. Nonetheless, the MEP responses, when present, tended to have different amplitudes at the beginning and end of each anesthetic protocol.

### **3.4 Discussion**

The overall goal of this study was to investigate the effect of three clinical and preclinical anesthetic protocols on the intraoperative responses evoked by ISMS. Understanding the effect of anesthesia on the physiology of the nervous system is essential for optimal placement of implantable neuroprosthetic devices. Similar to deep brain stimulation for treating movement disorders, intraoperative responses to stimulation provide necessary feedback for fine-tuning the site of ISMS in the spinal cord. Therefore, an acceptable anesthetic protocol is one that does not substantively suppress the responses to ISMS during intraoperative testing, where understanding the organization, excitability, and functionality of the motor networks targeted by ISMS in the human lumbosacral spinal cord is necessary. An accurate interpretation of intraoperative results of ISMS is only possible with an understanding of the effects of different anesthetic protocols on measured outcomes in preclinical and clinical studies. To our knowledge, this is the first study

that quantifies the effects of different anesthetic agents on motor outcomes produced by spinal implants.

The results of the study demonstrated that responses to ISMS such as stimulation thresholds, evoked joint torques, movement-ranges and EMG amplitudes are substantially affected by the choice of anesthesia. In comparison with propofol and pentobarbital anesthesia, isoflurane significantly increased ISMS thresholds for evoking a movement or EMG activity in the hindlimbs, and significantly reduced the size of joint torques, ranges of motion, and EMG pulses evoked by ISMS. The responses to ISMS, however, were not significantly different between propofol and pentobarbital anesthesia.

All three anesthesia protocols tested in this study produce effective general anesthesia and have similarities in their cellular mechanisms. Isoflurane potentiates the activity of GABA<sub>A</sub> (Topf et al. 2003; Jia et al. 2008) and glycine (Harrison et al. 1993) receptors, as well as presynaptic inhibition of glutamate release (Baumgart et al. 2015). Pentobarbital acts by activation and potentiation of GABA<sub>A</sub> receptors (Ho and Harris 1981; Richter and Holtman 1982), presynaptic inhibition of glutamate release, and inhibition of AMPA and kainate receptors (Löscher and Rogawski 2012). The cellular activity of propofol is more selective and mainly involves the potentiation of the activity of GABA<sub>A</sub> receptors (Hemmings et al. 2005; Jurd et al. 2002; Sonner et al. 2003). Despite the shared effect of these anesthetics on the GABA<sub>A</sub> receptor, the specific binding sites they interact with vary. Using genetically modified GABA<sub>A</sub> receptors, it was demonstrated that specific point mutations in transmembrane segments 2 and 3 (TM2 and TM3) of the  $\alpha 1$ ,  $\alpha 2$ , or  $\alpha 3$  subunits result in the receptors becoming insensitive to isoflurane (Schofield and Harrison 2005; Nishikawa et al. 2002; Mihic et al. 1997; Jenkins et al. 2001; Hall et al. 2004; Krasowski et al. 1998). Likewise, propofol's selectivity was demonstrated by

introducing mutations in the  $\beta$  subunits, which eliminated its potentiation of GABA<sub>A</sub> receptors (Jurd et al. 2002; Krasowski et al. 1998).  $\beta$  subunit dependence has also been shown for the potentiating action of pentobarbital on these receptors (Zeller et al. 2007; Maldifassi, Baur, and Sigel 2016). Collectively, these findings suggest that preferential binding by the anesthetic agents under investigation may play a role in the varying potentiation effects of these anesthetics through the GABA<sub>A</sub> receptor.

Dexmedetomidine is an  $\alpha_2$  adrenoreceptor agonist and its action on the adrenergic receptors in the brain stem is considered to be the main source of its sedative function (Gertler et al. 2001). Intravenous lidocaine has analgesic properties through presynaptic inhibition and hyper-polarization of the nociceptive neurons in the dorsal horns of the spinal cord (Kurabe, Furue, and Kohno 2016). The addition of dexmedetomidine and lidocaine to the propofol TIVA protocol has been shown to reduce the amount of propofol and remifentanyl needed to maintain anesthesia and reduce post-operative pain (Xu et al. 2017; Sloan et al. 2014).

With respect to their action on the spinal cord, isoflurane and propofol have been shown to reduce the activity of neurons in both the dorsal and ventral horns (Kungys et al. 2009; Kim et al. 2007; Jinks et al. 1999; Antognini et al. 2000). Suppression of the activity of neurons in the dorsal horns of the spinal cord has also been shown under pentobarbital (Nagase et al. 1994). Application of picrotoxin (GABA antagonist) significantly reverses (to ~80% of control) the suppressive effect of propofol in the spinal cord, indicating its action on GABA receptors (Kungys et al. 2009). The effect of isoflurane on the spinal cord neurons is more broad and mediated through both GABA<sub>A</sub> and glycine receptors (Kungys et al. 2009; Zhang et al. 2004; Grasshoff and Antkowiak 2006). Consistent with the evidence of suppression of neurons in the ventral horns, depression of the H-reflex has also been reported for isoflurane and propofol

(Zhou, Mehta, and Leis 1997; Kerz et al. 2001; J. H. Baars et al., n.d., 2006; King and Rampil 1994). Furthermore, all three anesthetics reduce the excitability of spinal motoneurons (based on F-wave recordings for isoflurane and propofol, and ventral root recordings for pentobarbital) (Zhou, Mehta, and Leis 1997; Kerz et al. 2001; J. H. Baars et al., n.d., 2006; King and Rampil 1994; Nicoll and Wojtowicz 1980; Dueck et al. 2003). This evidence suggests that all three anesthetic agents impose a level of suppression onto the motor networks in the spinal cord, and therefore influence the responses evoked by ISMS compared to the awake state. However, without direct comparative evaluations as conducted in this study, limited knowledge may be gained about their effects relative to each other on motor output.

Measurements of the H-reflex under propofol and sevoflurane (a halogenated ether with larger surgical-MAC (Hikasa et al. 1998) and lower tissue solubility (Sloan 2002) than isoflurane) showed a significantly larger suppression of this monosynaptic reflex under sevoflurane compared with propofol (Baars et al. 2009; Matute, Rivera-Arconada, and López-García 2004). These results are consistent with the findings of the present study where larger suppression of ISMS responses were observed under isoflurane in comparison with propofol.

The EMG responses evoked by ISMS had different amplitude profiles under isoflurane compared with propofol and pentobarbital anesthesia. The EMG responses under isoflurane showed a progressive depression in amplitude after the first pulse, resembling the post activation depression (PAD) seen with repetitive activation of the H-reflex (Clair et al. 2011). One of the proposed mechanisms for PAD is presynaptic inhibition at the terminals of Ia afferents projecting onto the motoneurons (Schieppati 1987; Crone and Nielsen 1989). This is mediated by an inhibitory (last order PAD) interneuron with an axo-axonal synapse onto the Ia axon terminal (Rudomin and Schmidt 1999). The Ia axon terminal contains GABA<sub>A</sub> receptors (Rudomin and

Schmidt 1999) which are sites of action for isoflurane, facilitating presynaptic inhibition for PAD. This is supported by the evidence of increased presynaptic inhibition of Ia afferents under sevoflurane in humans (Baars et al. 2007).

Similar reasoning would also apply to the effects of propofol and pentobarbital anesthesia since these anesthetics also are GABA<sub>A</sub> receptor agonists. Baars et al. reported facilitation of presynaptic inhibition of Ia afferents under propofol anesthesia (Baars et al. 2006). Nevertheless, the relationship between the level of facilitation of presynaptic inhibition provided by isoflurane, propofol and pentobarbital is unclear and may be a mechanism for the observed differences in EMG amplitude profiles under the different anesthesia protocols. Further studies are needed to determine the mechanism behind the different EMG patterns observed.

MEP measurements had the largest amplitude under propofol anesthesia, followed by pentobarbital. In comparison, isoflurane completely abolished the MEP responses. These findings are in-line with other investigations reporting significant suppression of MEPs under isoflurane anesthesia, moderate suppression and more variable MEPs (amplitude) under pentobarbital, and consistent MEP recordings with moderate suppression under propofol (MacDonald et al. 2013; Sloan 2002; Calancie et al. 1991; Nathan et al. 2003; Kalkman et al. 1995). In contrast to the stimulation thresholds for ISMS which were stable throughout the duration of each anesthetic protocol, the amplitudes of MEP responses changed over time. This suggests that the cortical/spinal/neuromuscular pathway of the MEPs is more sensitive to the effects of anesthesia than the spinal/neuromuscular pathway associated with the ISMS responses. This is reasonable due to the presence of a larger number of synapses in the MEP pathway (MacDonald et al. 2013; Sloan 2002). Nonetheless, the observed difference emphasizes that

knowledge of the effect of various anesthetics on MEP responses only may not directly be generalized to spinal cord stimulation paradigms such as ISMS.

Based on the results presented, both propofol and pentobarbital are deemed suitable anesthetic agents for intraoperative testing of ISMS. Propofol anesthesia is a more suitable protocol due to anesthetic traits that include fast recovery and easy drug titration. Additionally, in cases where neuromonitoring has merit (e.g., incomplete spinal cord injury or intact spinal cord), propofol anesthesia is preferred over pentobarbital anesthesia, since it provides more reliable recordings of MEP and somatosensory evoked potentials (Sloan 2002).

### **3.5 Conclusions**

This study demonstrated, for the first time, that the responses evoked by ISMS are similar under propofol and pentobarbital anesthesia. Sodium pentobarbital has been the primary intraoperative anesthetic agent in preclinical studies of ISMS, and the functional outcomes obtained under this anesthetic agent are representative of those obtained in the awake state. Therefore, the propofol TIVA protocol used in clinical neurosurgical procedures, and duplicated in this study, is an appropriate protocol for intraoperative testing of ISMS. Intraoperative testing of ISMS is a critical step in the translation of this promising neural prosthetic approach to the clinic for restoring standing and walking after spinal cord injury. In this study, the ISMS-evoked responses under propofol anesthesia were clear, stable, strong and functional. Similar responses by ISMS are expected during human intraoperative testing, allowing, for the first time, an unambiguous electrophysiological assessment of the motor networks for standing and walking in people with spinal cord injury. This study also demonstrated that isoflurane is an inappropriate anesthetic agent for preclinical studies that investigate the electrophysiological properties of the spinal cord.

Isoflurane is also an inappropriate anesthetic agent for ISMS implants that require accurate placement of electrodes in the cord.

### 3.6 Tables

**Table 3. 1.** Summary of arterial blood gas measurements. Measurements are presented as mean  $\pm$  standard deviation. ‘n’ is the number of measurements obtained in each experiment. tHb: total hemoglobin; HCO<sub>3</sub>: Bicarbonate content; AnGap: Anion Gap; BE: Base excess; tCO<sub>2</sub>: total carbon dioxide content.

Measurements (unit)	Animal #1 (n=13)	Animal #2 (n=14)	Animal #3 (n=11)	Animal #4 (n=6)	Animal #5 (n=8)	Animal #6 (n=7)	Animal #7 (n=8)
<b>pH</b>	7.49 $\pm$ 0.07	7.48 $\pm$ 0.04	7.41 $\pm$ 0.09	7.45 $\pm$ 0.01	7.55 $\pm$ 0.06	7.48 $\pm$ 0.05	7.45 $\pm$ 0.04
<b>HCO<sub>3</sub></b> (mmol/L)	25.67 $\pm$ 2.37	25.5 $\pm$ 1.75	26.04 $\pm$ 2.53	23.43 $\pm$ 4.84	24.01 $\pm$ 1.95	21.27 $\pm$ 3.72	24.86 $\pm$ 2.27
<b>AnGap</b> (mmol/L)	12.02 $\pm$ 2.77	12.09 $\pm$ 2.09	12.98 $\pm$ 2.28	15 $\pm$ 3.61	12.94 $\pm$ 2.76	13.13 $\pm$ 2.96	11.75 $\pm$ 1.82
<b>tHb</b> (g/dL)	10.07 $\pm$ 0.62	10.21 $\pm$ 0.84	10.35 $\pm$ 0.64	9.85 $\pm$ 9.19	10.78 $\pm$ 0.97	7.65 $\pm$ 1.55	9.38 $\pm$ 1.21
<b>BE</b> (mmol/L)	3.05 $\pm$ 2.76	2.66 $\pm$ 1.81	1.8 $\pm$ 3.22	0.43 $\pm$ 3.63	3.34 $\pm$ 2.81	0.69 $\pm$ 3.40	1.51 $\pm$ 1.13
<b>Na<sup>+</sup></b> (mmol/L)	136.85 $\pm$ 2.64	137.64 $\pm$ 5.05	136.55 $\pm$ 4.55	140.84 $\pm$ 2.32	141.13 $\pm$ 1.89	140 $\pm$ 3	140 $\pm$ 1.51
<b>K<sup>+</sup></b> (mmol/L)	6.01 $\pm$ 0.95	5.22 $\pm$ 1.38	7.39 $\pm$ 2.14	5.4 $\pm$ 0.82	4.16 $\pm$ 0.55	4.24 $\pm$ 0.86	5.34 $\pm$ 0.87
<b>Cl<sup>-</sup></b> (mmol/L)	105.15 $\pm$ 1.72	105.29 $\pm$ 3.63	103.73 $\pm$ 3.23	108 $\pm$ 3.16	108.5 $\pm$ 1.51	109.86 $\pm$ 3.44	109 $\pm$ 1.07

### 3.7 Figures

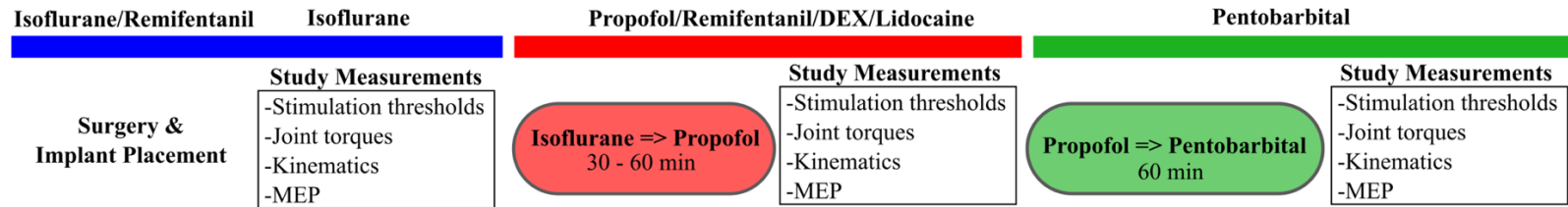


**Figure 3. 1.** Experimental design. Shown is the sequence of anesthesia protocols and outcome measurements throughout each experiment. Oval shapes represent the transition periods from one anesthetic to another. MEP: motor evoked potential; DEX: dexmedetomidine.

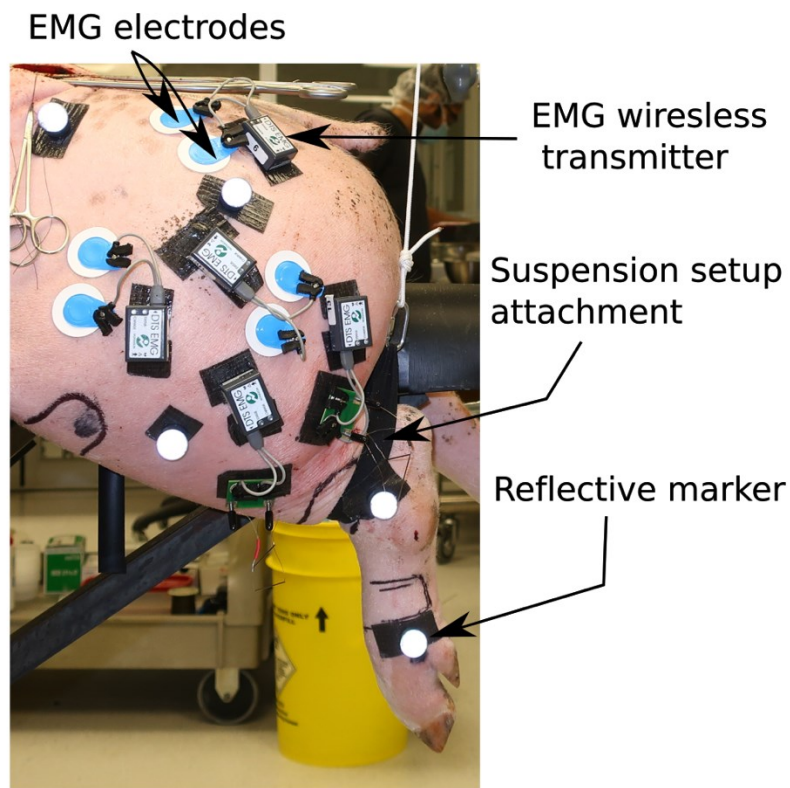


**Figure 3. 2.** Setup for measurements of muscle activity and kinematics. Reflective markers were placed on the main hindlimb joints to capture evoked movements. Wireless electromyography (EMG) electrodes and transducers were used to record the activity evoked in five muscles: gluteus medius, biceps femoris, vastus lateralis, tibialis anterior, and gastrocnemius. The hindlimb was suspended through pulleys and a counterweight mechanical system to allow for visualization and quantification of flexor and extensor movements evoked in the sagittal plane. The pulley system was attached to the hindlimb through a cord fitted around the limb proximally to the ankle joint.

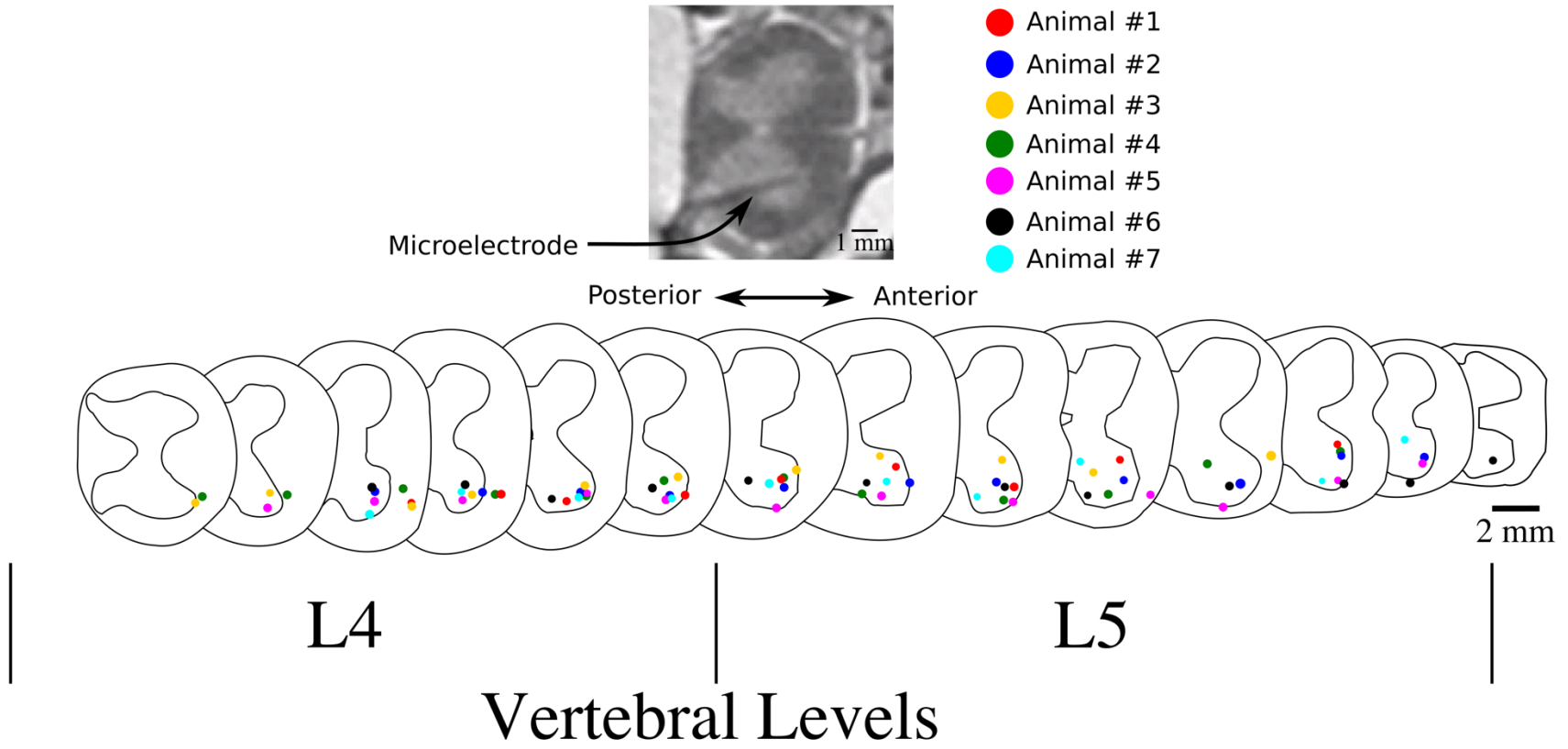


**Figure 3. 3.** Location of microelectrode tips in the spinal cord. A total of 76 microelectrodes were used for intraspinal microstimulation (ISMS) across all animals. Magnetic resonance imaging (MRI) of the post-mortem excised cord was used to identify the location of the microelectrode tips in the ventral region of the lumbosacral enlargement. The majority of the microelectrode tips (57) were located in the gray matter and the remainder (19) were located in the white matter just outside the ventral horn. Different colors represent different animals. The MRI image shows a microelectrode implanted in the spinal cord of animal #1.

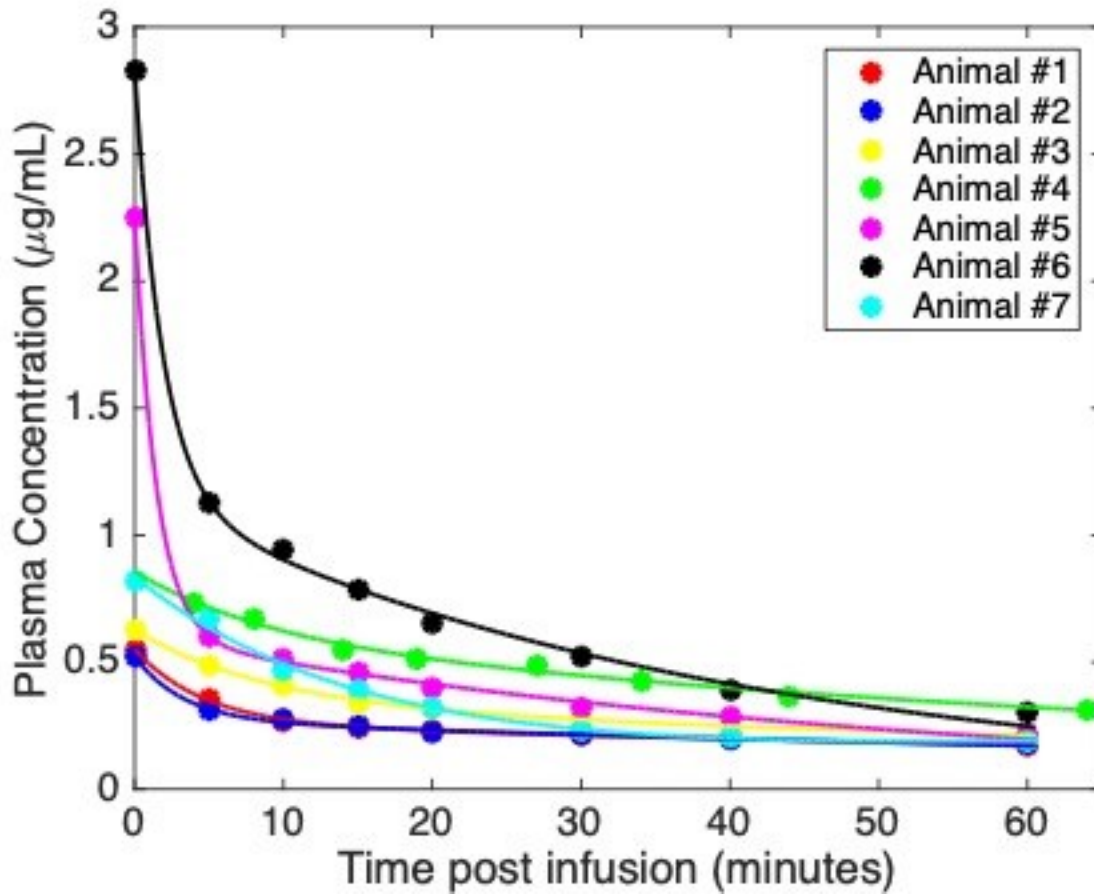


**Figure 3. 4.** Plasma concentration of propofol after cessation of infusion. Shown are ultra-performance liquid chromatography (UPLC) measurements for concentration of propofol over 60 minutes following the cessation of infusion. Lines represent fit curves based on a 2 compartment model of pharmacokinetics. Different colors indicate the different animals in the study.

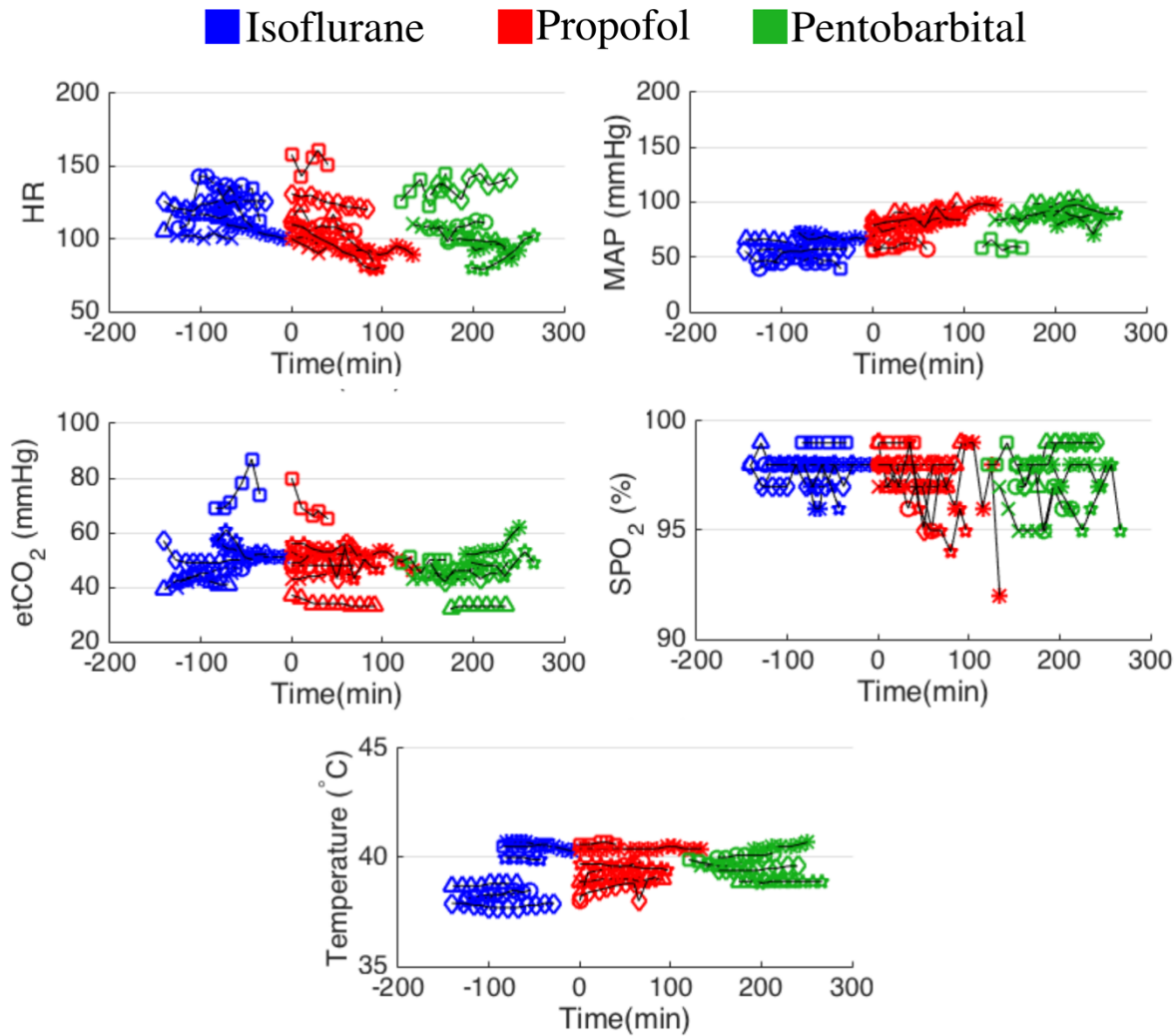


**Figure 3. 5.** Vital signs during electrophysiological and functional measurements. Stable vital signs were maintained throughout the experimental protocol across all animals. Different symbols represent different animals (n=7): Animal #1 (☆), animal #2 (◇), animal #3 (□), animal #4 (o), animal #5 (Δ), animal #6 (x), animal #7 (\*). Time = 0 on the x-axis represents the time when the anesthesia was switched from isoflurane to propofol. HR: heart rate; MAP: mean arterial pressure; etCO<sub>2</sub>: end-tidal CO<sub>2</sub>; SPO<sub>2</sub>: blood oxygen saturation level as measured by pulse oximetry.

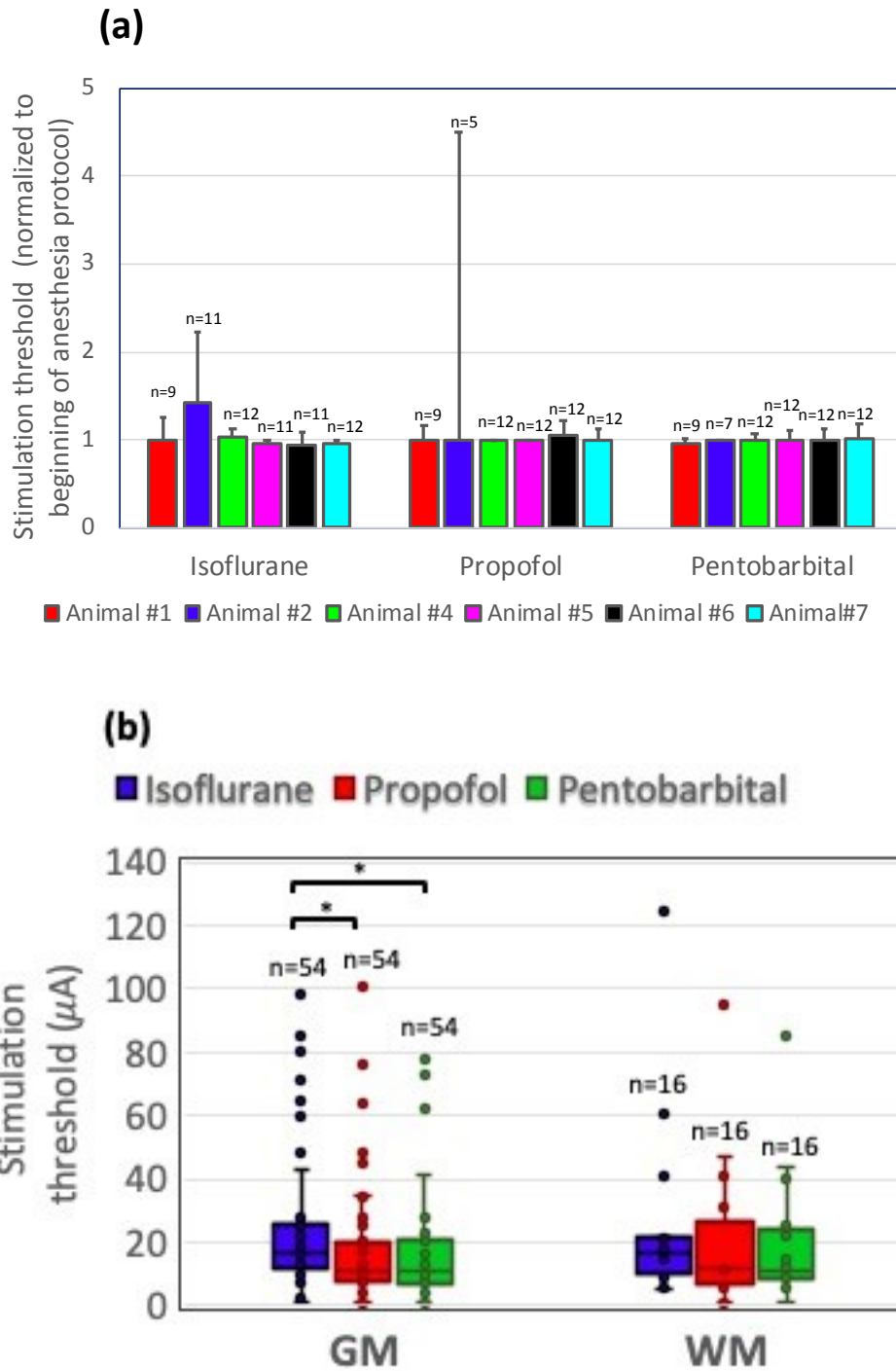


**Figure 3. 6.** Comparison of responses to intraspinal microstimulation (ISMS) under various anesthesia protocols. (a) Comparison of the stimulation thresholds at the beginning and end of each anesthetic protocol in all animals, with the stimulation thresholds at the end of each anesthetic protocol normalized to their value at the beginning of the protocol. Bars represents median and error bars represent third quartile (Q3) - median. Data acquired from experiments in

6 pigs. (b) ISMS thresholds for activating hindlimb muscles as determined by evoked EMG activity or observed movement. Boxes represent the interquartile range; horizontal line shows the median for each group; whiskers represent the minimum and maximum. Data obtained from experiments in 7 pigs. PB: pentobarbital, GM: electrode tips in the gray matter of the spinal cord, WM: electrode tips in the white matter of the spinal cord. n: number of implanted electrodes used for measurements in each group. \*:  $p < 0.05$ .

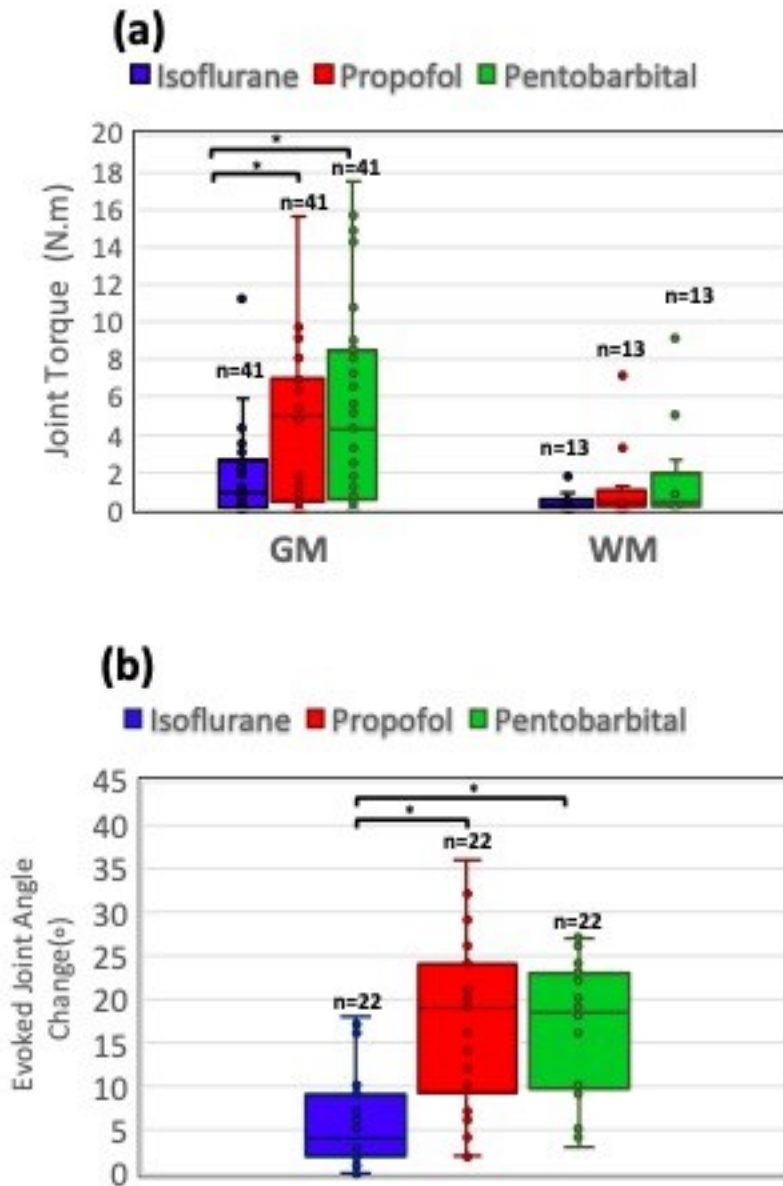


**Figure 3. 7.** Comparison of responses to intraspinal microstimulation (ISMS) under various anesthesia protocols. (a) Joint torques evoked by ISMS with stimulation intensity of 150  $\mu$ A in 7 pigs. (b) Range of motion (changes in joint angle) evoked by ISMS with stimulation intensity of 150  $\mu$ A in 3 pigs. Only microelectrodes with tips in the gray matter are represented in this figure. Boxes represent interquartile range; horizontal line shows the median; whiskers represent the

minimum and maximum. n: number of implanted microelectrodes used for measurements in each group. \*:  $p < 0.05$ .

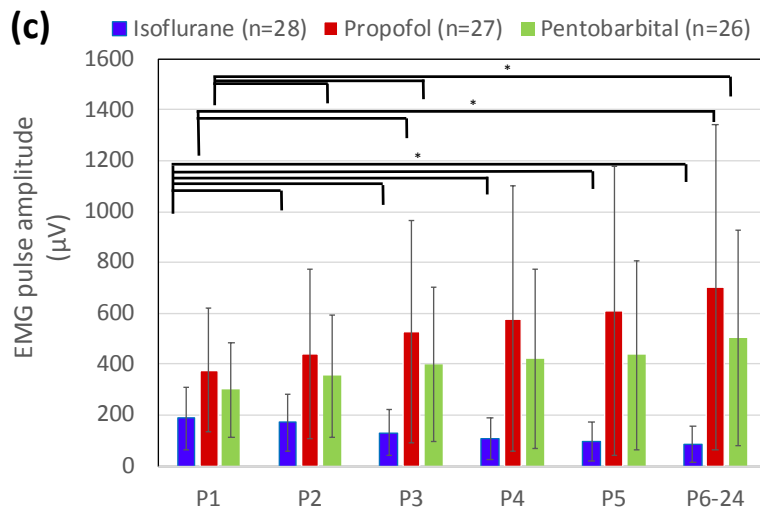
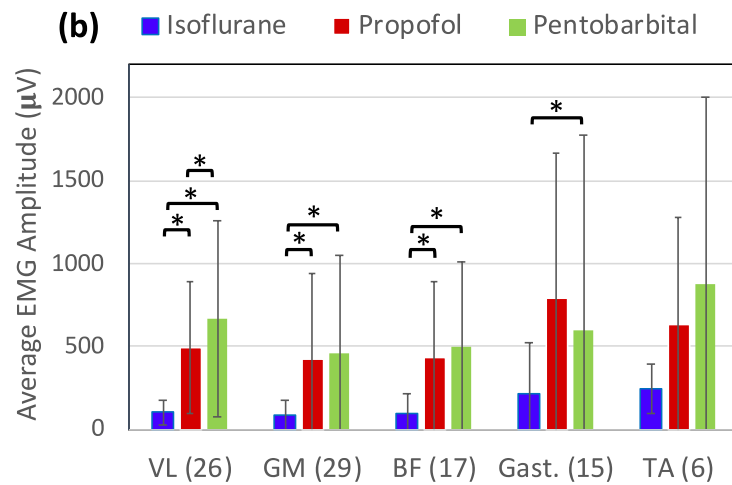
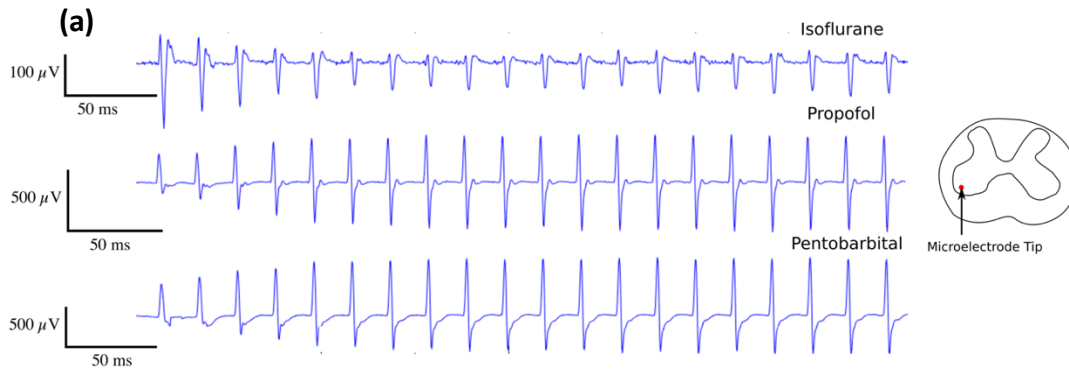


**Figure 3. 8.** Comparison of EMG responses evoked by intraspinal microstimulation (ISMS) under various anesthesia protocols. (a) An example of EMG activity evoked in vastus lateralis by

a 0.5 s train of ISMS under the three anesthetic protocols. The location of the ISMS site in the gray matter is illustrated. Under isoflurane, EMG pulse amplitudes progressively reduced in size and plateaued on a lower amplitude than the first pulse. Under pentobarbital and propofol, the EMG pulses retained the same amplitude or progressively increased in amplitude relative to the first pulse. (b) Mean  $\pm$  standard deviation of EMG amplitudes evoked in various hindlimb muscles under the different anesthetic protocols. Sample sizes are provided in parenthesis for each muscle. VL: vastus lateralis, GM: gluteus medias, BF: biceps femoris, Gast: gastrocnemius, TA: tibialis anterior. \*:  $p < 0.05$ . (c) EMG amplitude (mean  $\pm$  standard deviation) for the vastus lateralis muscle. P1, P2, P3, P4 and P5 are the 1<sup>st</sup>, 2<sup>nd</sup>, 3<sup>rd</sup>, 4<sup>th</sup> and 5<sup>th</sup> pulses in the EMG response train. P6-24 represents the normalized mean amplitude of the EMG pulses from the 6<sup>th</sup> to the 24<sup>th</sup> pulse. All measurements were obtained with stimulation intensity of 150  $\mu$ A in 7 pigs, and through microelectrodes with tips in the gray matter. \*:  $p < 0.05$ .

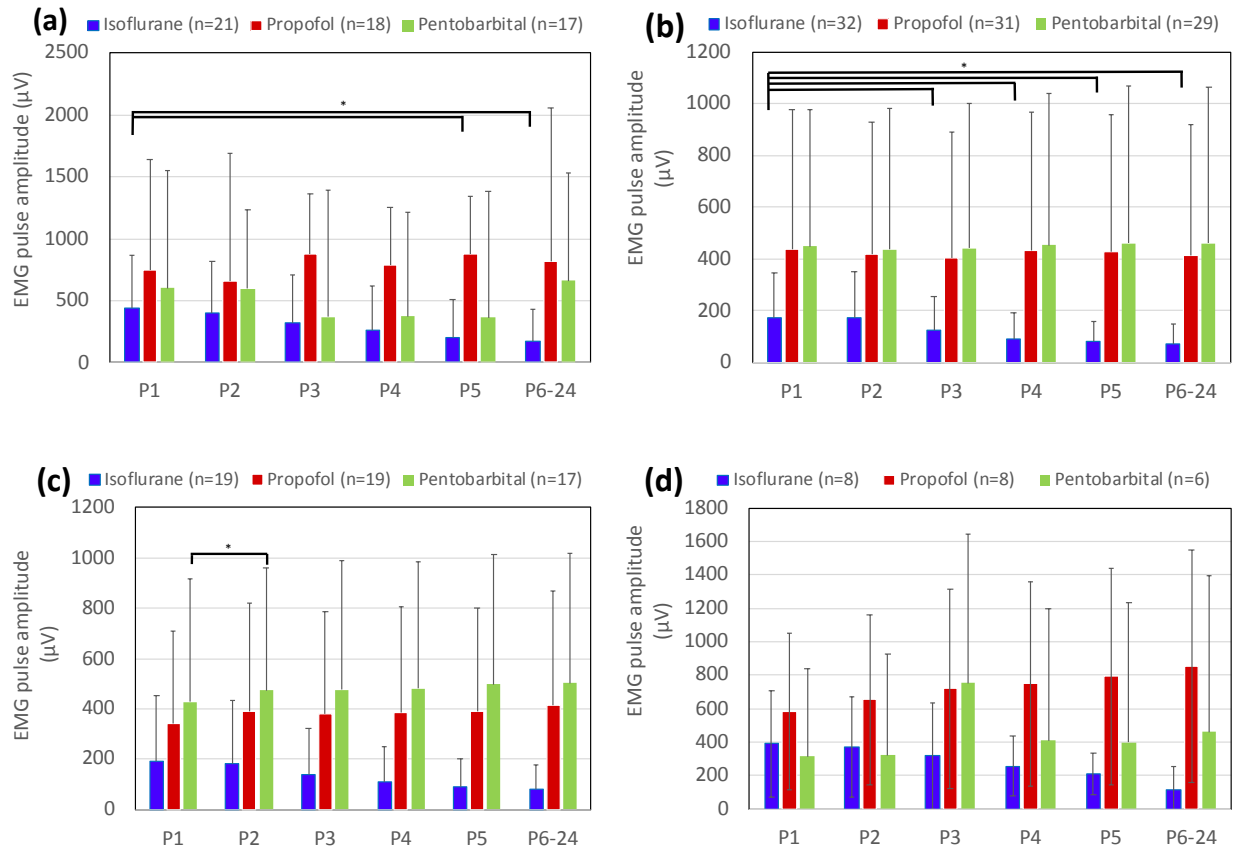


**Figure 3. 9.** Comparison of EMG responses evoked by intraspinal microstimulation (ISMS) under various anesthesia protocols. (a) EMG amplitude (mean  $\pm$  standard deviation) for the gastrocnemius muscle. P1, P2, P3, P4 and P5 are the 1<sup>st</sup>, 2<sup>nd</sup>, 3<sup>rd</sup>, 4<sup>th</sup> and 5<sup>th</sup> pulses in the EMG response train. P6-24 represents the mean amplitude of the EMG pulses from the 6<sup>th</sup> to the 24<sup>th</sup> pulse. (b) EMG amplitude (mean  $\pm$  standard deviation) for the gluteus medius muscle. (c) EMG amplitude (mean  $\pm$  standard deviation) for the biceps femoris muscle. (d) EMG amplitude (mean  $\pm$  standard deviation) for the tibialis anterior muscle. All Measurements were obtained with stimulation intensity of 150  $\mu$ A and through microelectrodes with tips in the gray matter. “n” is the number of electrodes used for measurements in each group. \*:  $p < 0.05$ .

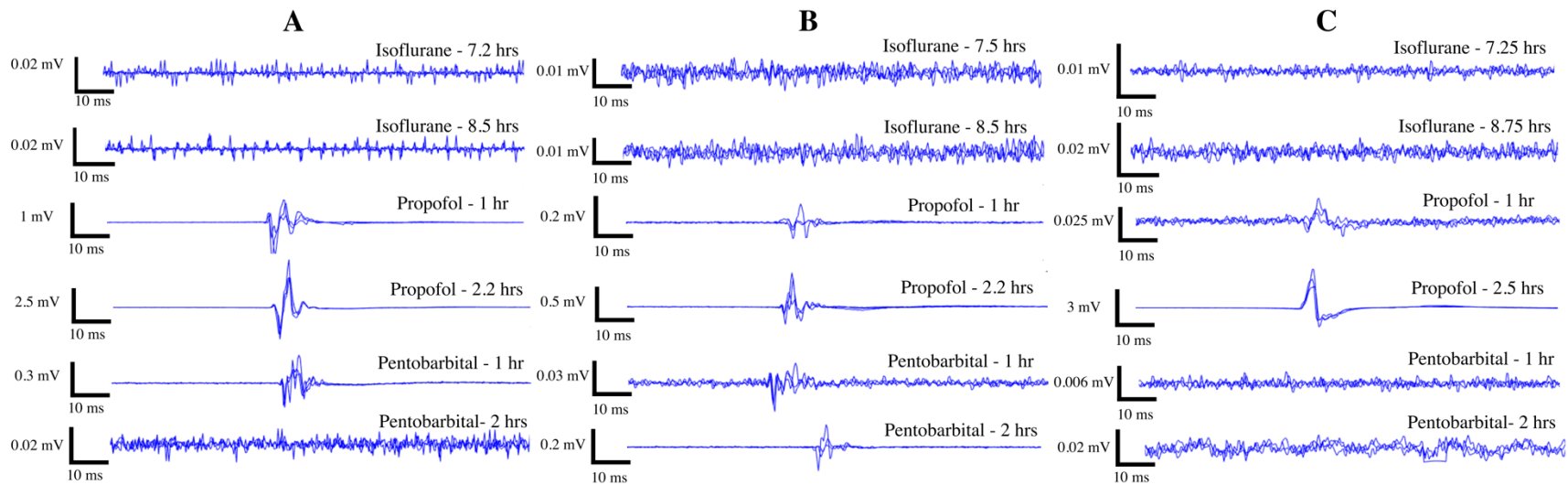


**Figure 3. 10.** Comparison of motor evoked potentials (MEP) in the tibialis anterior muscle under various anesthesia protocols. MEP measurements were obtained in three animals. The MEPs were evoked through transcutaneous electrical stimulation (TES) of the motor cortex. The duration of anesthesia is indicated for each MEP trace and represents the total time spent under the specific anesthesia protocol at the time of MEP measurement. A: animal #7, B: animal #6, and C: animal #5.

# **Chapter 4. Functional organization of motor networks in the lumbosacral spinal cord of non-human primates<sup>1</sup>**

Amirali Toossi<sup>1,5</sup>, Dirk G. Everaert<sup>2,5</sup>, Steve I. Perlmuter<sup>3,4,5,6</sup>, Vivian K. Mushahwar<sup>1,2,5</sup>

<sup>1</sup> Neuroscience and Mental Health Institute, University of Alberta, Edmonton, Alberta, Canada.

<sup>2</sup> Division of Physical Medicine and Rehabilitation, Department of Medicine, Faculty of Medicine and Dentistry, University of Alberta, Edmonton, AB, Canada. <sup>3</sup> Department of Physiology and Biophysics, University of Washington, Seattle, Washington, USA. <sup>4</sup> Washington National Primate Research Centre, Seattle, Washington, USA. <sup>5</sup> Sensory Motor Adaptive Rehabilitation Technology (SMART) Network, University of Alberta, Edmonton, Alberta, Canada. <sup>6</sup> Center for Sensorimotor Neural Engineering, Seattle, Washington, USA

---

<sup>1</sup>A version of this chapter has submitted to a peer review journal.

## 4.1 Introduction

Recent advances in neuroprostheses have motivated a new wave of technologies aiming to augment the human body or restore its lost functions (Mushahwar et al. 2007; Stein and Mushahwar 2005; Tator, Minassian, and Mushahwar 2012). Neural networks of the spinal cord are one of the targets of these neuroprostheses for applications such as reanimating paralyzed limbs (Holinski et al. 2016; Saigal, Renzi, and Mushahwar 2004; Mushahwar, Collins, and Prochazka 2000; Zimmermann, Seki, and Jackson 2011; Zimmermann and Jackson 2014; Sunshine et al. 2013), reducing mobility deficits (Capogrosso et al. 2016), and promoting targeted plasticity and recovery (McPherson, Miller, and Perlmutter 2015) after neural injury and disease.

An example of these neuroprostheses is the intraspinal microstimulation (ISMS) implant which is comprised of an array of ultra-fine electrodes that deliver electrical pulses to the ventral horns of the spinal cord (Bamford et al. 2016). ISMS can produce functional movements of the lower and upper limbs (lumbosacral and cervical implants) (Saigal, Renzi, and Mushahwar 2004; Sunshine et al. 2013), breathing (cervical implant) (Mercier et al. 2017) or bladder function (sacral implant) (Nashold et al. 1972) depending on the targeted region within the spinal cord. Stimulation through an individual intraspinal electrode can activate motor networks including motoneurons, afferent (Gaunt et al. 2006) and propriospinal (Jankowska et al. 1974) projections, and associated axons that span multiple spinal cord segments (Gaunt et al. 2006). A small number of implanted electrodes can evoke synergistic muscle contractions and produce coordinated movements involving a single or multiple joints that can perform functional tasks (Holinski et al. 2016; Jeremy A. Bamford and Mushahwar 2011; Lau, Guevremont, and Mushahwar 2007; Moritz et al. 2007).

ISMS in the lumbosacral spinal cord has been widely studied and has shown promising results in animals for the restoration of hindlimb movements after paralysis. Notably, hindlimb movements evoked by ISMS in cats were significantly more fatigue resistant compared to those obtained by intramuscular electrical stimulation (Lau, Guevremont, and Mushahwar 2007; Holinski et al. 2016). With ISMS implants, animals could stand for ~5x longer durations (Lau, Guevremont, and Mushahwar 2007) and walk over-ground for ~10x longer distances (Holinski et al. 2016) than animals with intramuscular implants.

The cat has been the classical model for ISMS research in the lumbosacral spinal cord. Placement of ISMS electrode arrays in this species is guided by knowledge of the functional organization of the motor networks in the spinal cord (Mushahwar and Horch 2000b; Saigal, Renzi, and Mushahwar 2004; Mushahwar et al. 2002). This knowledge was derived from investigations of the movements evoked by ISMS in various parts of the ventral horn along the length of the lumbosacral enlargement, which led to the formation of a functional map (Mushahwar and Horch 2000b). Numerous studies of ISMS in cats have shown that the functional map is consistent between animals (Holinski et al. 2016; Saigal, Renzi, and Mushahwar 2004; Mushahwar, Collins, and Prochazka 2000; Lau, Guevremont, and Mushahwar 2007; Mushahwar and Horch 2000b; Mushahwar et al. 2002; Mushahwar and Horch 1998; Mazurek et al. 2012).

One requirement for translating ISMS to clinical implementation is gaining knowledge about the functional organization of the motor networks to be targeted in the lumbar spinal cord of humans. Evidence exists about the anatomical organization of the motoneuronal cell bodies in the human lumbar spinal cord that innervate the leg muscles (Sharrard 1964; Sharrard 1955). However, unlike in cats, the functional organization and connectivity of various motoneuronal

pools, and the required stimulation amplitudes for their activation, are not known. In this study, we took a critical step towards answering these questions and investigated the functional map of the lumbar spinal cord in another primate, the macaque monkey. Based on the evidence from functional mapping experiments in various mammals (cats, rats (Bamford, Putman, and Mushahwar 2005; Bamford, Todd, and Mushahwar 2010; Borrell et al. 2017; Shen et al. 2016) and pigs (Hachmann et al. 2013)), we hypothesized that a similar functional organization of motor networks is preserved in non-human primates. This study allowed us to identify, for the first time, the functional connectivity of motor networks in the primate lumbosacral spinal cord.

## 4.2 Methods

All experiments were conducted in accordance to protocols approved by the Institutional Animal Care and Welfare Committee at the University of Alberta and the University of Washington.

**Surgery and the experimental setup.** All surgical procedures and data collection were conducted under a continuous intravenous infusion of sodium pentobarbital anesthesia combined with fentanyl analgesia. The lumbar enlargement was exposed by laminectomy of the T12 to L2, L3, or L4 vertebrae in animals with 6, 7, or 8 lumbar vertebrae, respectively.

Prior to electrode implantation, the dura mater and arachnoid were opened and retracted with sutures placed in the paraspinal muscles. Four pedicle screws (3.5 mm diameter x 25 mm length, Medtronic Inc., Dublin, Ireland) were placed bilaterally in L1 and L3 pedicles, over which a spine-mounted stereotactic setup (Toossi et al. 2017) was assembled. The setup consisted of 2 frames and a platform with a micromanipulator that was used to place the microelectrode into the spinal cord (Toossi et al. 2017). The frames, which were secured to the

pedicle screws, provided mechanical fixation over vertebral levels L1 to L3. The use of a spine-mounted setup was intended to reduce the relative movements between the spinal cord and the implanted microelectrode caused by breathing and limb movements, which reduced the risk of damage to the cord. To stabilize the spinal column further while allowing free movements in the hindlimbs, the animals were positioned in a custom built suspension frame (figure 4.1). The pelvis was suspended with 2 pins at the iliac crest, while the spine was fixed with spinous process clamps at T12, L7 and S1.

In order to visualize the movements evoked by ISMS, the ankle was fitted with a string that was run over two pulleys and attached to a counter weight that balanced the weight of the leg (figure 4.1). Reflective markers were placed on the hip, knee, ankle, and metatarsophalangeal (MTP) joints, and on the distal phalanx of the 5<sup>th</sup> digit. A video camera (120 fps, JVC, Yokohama, Japan) was used to capture movements of the leg in the sagittal plane. EMG activity was recorded using a Ripple Grapevine neural interface system (sampling frequency: 2000 Hz; Ripple, Salt Lake City, UT, USA) through bipolar intramuscular electrodes placed in 8 hindlimb muscles. Force measurements were obtained isometrically using a 150 lb-load cell (Interface Inc., Scottsdale, AZ, USA) at a sampling frequency of 1000 Hz. A custom-built adjustable stand was used to position the load cell perpendicularly to the axis of a given limb segment while blocking the movement.

At the end of experiments, custom-made bipolar nerve cuffs were placed around the femoral nerve (in the femoral triangle) and the tibial nerve to measure isometric forces produced by supra-maximal nerve stimulation.

**Microelectrode insertion in the spinal cord.** Platinum/iridium (Pt/Ir 90%/10%)

microelectrodes of 75  $\mu\text{m}$  diameter (Microprobes, Gaithersburg, MD, USA), were used for ISMS. Care was taken to advance the microelectrode tip to the ventral horn of the spinal cord while inserting the shaft of the electrode parallel to the minor axis of the spinal cord and without dimpling (compressing) its dorsal surface. Alignment of the insertion trajectory of the microelectrode was performed using an end-to-end alignment approach at the beginning of each experiment. This approach involved the use of two 2D bubble levels (5 mm in diameter, Level Developments Ltd., Chicago, IL, USA) over the dorsal surface of the spinal cord and over an L-shaped stylus held by the micromanipulator. The bubble levels were used to align the electrode holder perpendicularly to the surface of the spinal cord (figure 4.2).

In order to puncture the pia matter and avoid dimpling of the dorsal surface of the spinal cord during microelectrode insertion, a custom-made needle guide was used. The needle guide consisted of a 30-gauge needle, which could be lowered independently of the stimulating microelectrode. The microelectrode was fed through the lumen of the needle, and advanced into the cord after the needle punctured the pia.

The mapping protocol involved the insertion of the microelectrode into the spinal cord in steps of 2 mm x 0.5 mm in the rostrocaudal and mediolateral directions, respectively. This pre-planned mapping resolution was subject to change in cases where a dorsal vessel was in the way of the microelectrode. In each track, stimuli were delivered at sites 0.5 mm apart dorsoventrally.

**Electrical stimulation protocol.** a) Spinal cord stimulation: The ISMS protocol consisted of 0.5 s-train of biphasic, charge-balanced pulses, 200  $\mu\text{s}$ -long and delivered at 50 Hz frequency. The stimulation amplitude ranged from 10  $\mu\text{A}$  to a maximum of 300  $\mu\text{A}$ . b) Femoral nerve

stimulation: 0.5 s-train of biphasic, charge-balanced pulses, 200  $\mu$ s in width and 50 Hz frequency, with amplitudes ranging from 0.5 to 10 mA.

**Post-mortem spinal cord extraction.** At the end of each experiment, animals were deeply anesthetized and perfused transcardially with 4% formaldehyde solution for tissue fixation. The spine was then carefully dissected and the vertebral levels were identified based on the articulation with the last rib and lumbosacral transition. The laminectomy was expanded to visualize all nerve roots from the last thoracic level to S2 or S3. The fixed lumbosacral spinal cord with identified roots was then extracted and preserved in the formaldehyde solution for further processing. To reconstruct the mapped region of the spinal cord, cord segments were identified based on the entry zones of the dorsal rootlets. The boundaries of segment levels were marked by inserting 5 mm long glass tubes (175  $\mu$ m in diameter, Wale Apparatus, Hellertown, USA) into the cord for identification in MRI images and histological sections (figure 4.3).

**Magnetic resonance imaging.** The spinal cord samples were inserted in glass tubes filled with Fluorinert fluid (FC-770, Milipore Sigma, Darmstadt, Germany). The cords were imaged using a 3D gradient echo sequence with a resolution of 0.125 x 0.125 x 1 mm (figure 4.3). Imaging was performed on a 4.7 T Varian MR imaging system (Varian Inc., Palo Alto, CA, USA) using a 38 mm diameter volume coil employing the Litz design (Doty Scientific, Columbia, SC, USA) (Doty, Entzminger, and Hauck 1999).

**Tissue histological processing.** The extracted spinal cord samples were cut in 50  $\mu$ m cross-sections and stained using Mallory's trichrome and neutral red Nissl stains for gross

morphological analysis. Spinal cord sections were also analyzed to find electrode tracks from the mapping procedure (figure 4.3).

**Force, EMG and kinematic data analyses.** EMG signals were filtered using a high-pass second order Butterworth filter with a corner frequency of 20 Hz to reduce motion artifacts. Kinematics, Force and EMG recordings were analyzed using custom written programs in Matlab (version 2015a, MathWorks, Natick, MA, USA), including the cluster analysis of EMG activity patterns.

**Map creation.** The functional map of the lumbosacral spinal cord was constructed primarily based on the movements that were evoked by ISMS. Three-dimensional coordinates of each of the mapped locations within the spinal cord were recorded using the coordinate system of the micromanipulator of the spinal stereotactic system. In order to link this external coordinate system with MR images and histological sections, a superficial suture was placed in the spinal cord at known rostrocaudal coordinates at the end of each experiment. For each of the animals, map creation involved the following steps: *(i)* The outlines of the gray and white matter were traced and digitized from MR images of the extracted spinal cords. *(ii)* Histological processing of the spinal cord tissue. Suture tracks were used to link the mapped coordinates in the external coordinate system (stereotactic setup) to true spinal cord geometries. Electrode insertion trajectories were initially assumed to be in parallel with the minor axis of the spinal cord after the trajectory alignment step (Fig. 4.14). These insertion trajectories were confirmed or corrected in the reconstructed map based on the electrode tracks found in histological sections. *(iii)* Illustration of the responses for various movements with their corrected coordinates were superimposed on the digitized traces of the spinal cord gray and white matter.

**Spatial distribution of the functional and anatomical maps in cats.** Functional (Mushahwar et al. 2002; Saigal, Renzi, and Mushahwar 2004; Mushahwar and Horch 2000b) and anatomical (Yakovenko et al. 2002; Vanderhorst and Holstege 1997) maps of the lumbosacral spinal cords of cats in the literature are presented only based on spinal cord segments and do not include a size estimate for each segment. In order to compare the spatial distribution of these maps, knowledge of the sizes of the segments in the cat spinal cord was necessary. As part of this study, 4 cat spinal cords (cord segments L1-S1) were extracted post-mortem after perfusion with 4% paraformaldehyde solution. Spinal cord segments were identified and marked with glass tubes as described earlier in ‘Post-mortem spinal cord extraction.’ For all spinal cords, the sizes of the marked cord segments were then measured with a ruler and used to create the spatial distribution maps shown in figure 4.4.

### 4.3 Results

**Functional map of the lumbosacral spinal cord.** Experiments were conducted on 4 skeletally-mature rhesus macaque monkeys (three females and one male,  $9.3 \pm 1.8$  kg) under pentobarbital anesthesia. The lumbosacral enlargement of the spinal cord was surgically exposed and a stereotactic setup with a micromanipulator was assembled onto the spine (Toossi et al. 2017). The micromanipulator was used to guide a microelectrode to various locations in the ventral horn of the gray matter. Each of the locations was stimulated with current amplitudes up to  $120 \mu\text{A}$ . If no movement was evoked with currents up to this amplitude, the micromanipulator was advanced to a new location. For all locations where movements were produced, movement type and stimulation threshold were recorded. At select locations, kinematics, joint torque, and electromyographic (EMG) activity were also recorded. In order to visualize and quantify the

evoked movements, the hindlimb ipsilateral to the stimulated side of the spinal cord was suspended through a pulley system as shown in figure 4.1.

The lumbosacral enlargement of the spinal cord spanned an approximately 4 cm-long region. Two animals (B and C in figure 4.5) had 7 lumbar vertebrae and spinal cord segments, one animal (A) had 6 lumbar vertebrae and spinal segments and one (D) had 8. The lumbosacral enlargement contained spinal segments L3-S1, L2-L6, and L3-L8 for animals with 7 (most common anatomy (Sherrington 1892)), 6 and 8 lumbar vertebrae, respectively. This region was located within vertebral levels L1-L2 for animals with 6 lumbar vertebrae, and L1-L3 for animals with 7 and 8 lumbar vertebrae.

The functional maps constructed from all animals are shown in figure 4.5. Because of the differences in the number of lumbar vertebrae and lumbosacral spinal cord segments between animals, the cross-sections of the lumbosacral enlargement for the 4 animals (A-D) were aligned by matching the morphology of the ventral horns. Dots in the figure show sites where movements were evoked by ISMS. The color of each dot represents the joint or limb movement evoked by the microstimulation. The size of the dots reflects the estimated current spread based on the amplitude of the stimulation threshold at that location (Bagshaw and Evans 1976). Therefore, smaller dots represent locations that required smaller stimulation amplitude to produce a movement. Spinal cord sections that do not show any colored dots were not mapped. In all animals, stimulation in segments rostral to the lumbosacral enlargement evoked paraspinal muscle contractions while stimulation in segments caudal to the enlargement evoked tail movements.

In total, 697 locations were stimulated in the spinal cords of all animals, of which 56% (390) evoked a movement. All mapped locations, including those that did not produce

movements with current amplitudes up to 120  $\mu\text{A}$ , are shown in figure 4.6. Stimulation in the most rostral quarter of the enlargement ( $\sim 1$  cm long) predominantly evoked hip flexion. Caudal to this region, a region  $\sim 1.6$  cm-long, produced knee extension, hip adduction and ankle flexion (dorsiflexion). Locations evoking ankle flexion were found laterally to locations that evoked knee extension. The remaining caudal third of the enlargement ( $\sim 1.4$  cm long) evoked more diversified movements including single joint movements such as: ankle extension (plantar flexion), knee flexion, toe flexion and extension, and multi-joint synergistic movements such as extensor and backward synergies.

Distribution of the main evoked movements is shown in figure 4.7a. Knee extension was the most common movement (99/390), followed by hip flexion (62/390). Almost a quarter of the evoked movements (89/390) involved more than one joint (figure 4.7b). Most of these movements were evoked by ISMS in the caudal third of the enlargement. Multi-joint movements were more commonly combinations of joint extension than flexion movements (figure 4.7c). The most common multi-joint movement was hip and ankle extension (15/390), followed by knee and ankle extension (12/390).

**Stimulation thresholds.** Stimulation threshold was defined as the lowest ISMS amplitude required to evoke a visible twitch or movement in the targeted muscles. The stimulator used for this study provided stimulation amplitudes as low as 10  $\mu\text{A}$ , but not lower. The largest proportion of the stimulation thresholds were  $\leq 10$   $\mu\text{A}$  (figure 4.8). This was the case for locations stimulated in both the gray matter (45.7%) and white matter (40%) of the spinal cord.

**Kinematics.** Hindlimb movements were recorded in the sagittal plane with a single camera. The pelvis was fixed in a frame at the iliac crests. Free movement of hip, knee and ankle joints was achieved by suspending the leg with a counter weight attached through a pulley system to a strap fitted above the ankle joint (figure 4.1). In total, 40% of all evoked movements were recorded. The distribution of changes in the hip, knee and ankle joint angles in response to ISMS in various locations of the gray and white matter is shown in figure 4.9. Movements of the knee and ankle joints were larger than movements of the hip. Changes in the hip joint angle from neutral in all recorded hip extension and 95% of hip flexion movements were  $\leq 20^\circ$ . Most of the knee extension movements (57%) had changes in joint angle  $\geq 40^\circ$ , and 75% of the knee flexion movements had joint angle changes between  $20^\circ$  and  $60^\circ$ . In 79% of the ankle flexion movements, changes in the joint angle were between  $10^\circ$  and  $30^\circ$ , and in 67% of the ankle extension movements, joint angle changes were  $\geq 20^\circ$ . The largest total range of motion (ROM) evoked by ISMS for the hip, knee and ankle joints was  $52^\circ$ ,  $107^\circ$  and  $65^\circ$ , respectively (figure 4.10).

The ROMs of the hip, knee and ankle joints during movements evoked by ISMS were compared to those produced during quadrupedal locomotion on a treadmill (Courtine et al. 2005). Figure 4.10 shows the measured ROMs while stepping on a treadmill belt moving at a speed of 1.79 m/s and the ROMs evoked by ISMS in this study. The hip ROM induced by ISMS was 22% smaller (in extension) than the ROM during treadmill locomotion, while the ISMS induced ROMs were larger at the knee (by 35%) and ankle (by 30%) joints.

**Torque.** Isometric forces were measured while isolating the evoked movement to a single joint. For these measurements, the spinal cord was stimulated at a current amplitude beyond which the

joint ROM did not increase (maximal limit of 300  $\mu$ A). In total, forces were recorded for 31/390 locations in the spinal cord that evoked a movement, 27 of which were in the gray matter and 4 in the white matter. The forces were converted to joint torques based on the moment arm.

Knee extension torques measured for 17 select locations (figure 4.11) ranged from 0.25 to 6.95 Nm with a moment arm of  $15.9 \pm 1.1$  cm. For comparison, in one experiment (animal A), a nerve cuff was placed around the femoral nerve and stimulated supra-maximally. The recorded torque under this condition was 7.6 Nm. Therefore, ISMS through a single electrode produced up to 91% of the maximal possible torque.

Ankle extension torques measured in 3 select locations ranged from 0.23 to 2.02 Nm (moment arm:  $7.6 \pm 1.2$  cm). Ankle extension torques resulting from supra-maximal stimulation of the tibial nerve were also recorded (n=3, animals A, B, and D) and ranged from 5.9 to 8.5 Nm. ISMS through a single electrode therefore produced 23.8 to 34.5% of the maximal possible torque.

Measured hip flexion torques (n=3) ranged from 0.26 to 1.21 Nm (moment arm:  $15.3 \pm 1.1$  cm). Isometric forces were also measured for ISMS-evoked extensor synergies (n=3). These measurements were obtained by placing the force transducer at the midpoint of the foot plantar surface, and ranged from 0.7 to 4.7 kg-force.

**Muscle activity.** EMG activity resulting from microstimulation in the spinal cord was recorded through pairs of intramuscular wire electrodes placed in 8 muscles: vastus lateralis, vastus medialis, tibialis anterior, medial gastrocnemius, lateral gastrocnemius, sartorius, semimembranosus anterior, and biceps femoris posterior (example shown in figure 4.12). EMG

recordings were used in conjunction with kinematic recordings to identify the types of evoked movement and distinguish passive (driven by gravity) and active movements.

A cluster analysis was performed on the EMG recordings to assess their possible synergistic activation during ISMS (Moritz et al. 2007; Poliakov and Schieber 1999). In this analysis, a binary activity matrix (7 by 60) was defined with columns representing different muscles (the medial gastrocnemius muscle was not used because it was not recorded in all animals) and rows representing the different locations of stimulation within the gray matter of the spinal cord. Included in the analysis were all recorded trials across animals A, C and D where ISMS was delivered in the gray matter and evoked a movement with a stimulation amplitude of 100  $\mu$ A. A value of 0 or 1 was assigned to matrix elements where EMG activity was absent or present in response to ISMS, respectively. Figure 4.13a shows the clustergram for this matrix. The Euclidian distances between the EMG channels were then calculated in the 7-dimensional space defined by the activity matrix. Distribution of the Euclidian distances between each pair of muscles is shown in figure 4.13b. Pairs with smaller Euclidian distances had a more similar activation pattern. Groups of lateral gastrocnemius-biceps femoris-tibialis anterior, and sartorius-vastus lateralis had the smallest distances suggesting similar activation patterns. The calculated distances were also used to plot a hierarchical cluster tree using the unweighted pair group method with the arithmetic mean algorithm (figure 4.13c).

## 4.4 Discussion

**Functional map of the lumbar enlargement of the spinal cord.** Functional studies of ISMS for restoring standing and walking have been mainly conducted in medium to small animal models (cats (Holinski et al. 2016; Saigal, Renzi, and Mushahwar 2004; Mushahwar, Collins,

and Prochazka 2000; Lau, Guevremont, and Mushahwar 2007; Mushahwar and Horch 2000b; Mushahwar et al. 2002) and rats (Bamford, Putman, and Mushahwar 2005; Bamford, Todd, and Mushahwar 2010)). Although anecdotal testing has been conducted in large animal models (pigs (Hachmann et al. 2013)), cross species comparisons of the functional networks targeted by ISMS has not been performed. The maps obtained in this study are the first functional maps of the lumbosacral spinal cord in primates. These maps demonstrate that an organized, compact motor network exists in the lumbosacral spinal cord of rhesus monkeys which may be targeted to restore lower limb mobility. The functional maps also show that the relative organization of the motor networks for various movements in the lumbosacral enlargement are consistent from one animal to another. In all animals, hip flexors were activated in more rostral regions of the lumbar enlargement than knee extensors, followed by ankle flexors, hip extensors, toe flexors, ankle extensors, extensor synergy, knee flexors, and backward synergy. A consistent organization is also observed in the mediolateral and dorsoventral dimension where for instance ankle flexors are evoked at more lateral and more dorsal locations in the gray matter than knee extensors. Hip extensors are also evoked at more dorsal locations than the knee extensors.

To investigate possible trends in the functional organization of the mammalian lumbosacral spinal cord across species and extrapolate to the human spinal cord, comparisons were made between the functional maps obtained in monkeys and existing maps in cats (Saigal, Renzi, and Mushahwar 2004; Mushahwar et al. 2002; Mushahwar and Horch 2000b). As shown in figure 4.14, the rostrocaudal organizations in cats and monkeys are similar. A similar relative organization is also seen for ankle flexors and knee extensors in the mediolateral and dorsoventral dimensions (Mushahwar and Horch 2000b). The spatial distribution of the functional elements of the maps in cats and monkeys is shown in figure 4.4. Despite the similar

organization of the functional maps, knee extension is evoked in a larger portion of the enlargement in monkeys (39%) compared to cats (22%). Knee flexion however, is evoked in a smaller portion of the enlargement in monkeys (10%) compared to cats (24%).

In addition to the functional organization of the lumbosacral motoneuronal pools, the anatomical location of the motoneuronal cell bodies innervating leg muscles (i.e., the anatomical organization of the motoneuronal pools) are also known in cats (Vanderhorst and Holstege 1997; Yakovenko et al. 2002) (figure 4.14). A comparison between the anatomical and functional maps in cats reveals a similar relative rostrocaudal organization in both maps.

While the functional organization of the lumbosacral motoneuronal pools is not known in humans, the anatomical organization of the motoneuronal pools in this region is available from Sharrard's studies in polio patients (Sharrard 1964; Sharrard 1955). As shown in figure 4.14, the anatomical organization of the motoneuronal pools in the human spinal cord is also similar to the functional and anatomical maps in monkeys and cats.

Given the similarity of the relative organization of the motoneuronal networks across species, and the similarity of the organization of the anatomical and functional maps in cats, we hypothesize that the human functional map will also have the same organization.

**Stimulation thresholds:** Figure 4.15 shows the distribution of the stimulation thresholds in cats compared with the thresholds measured in monkeys in this study. In both species, the largest proportion of the stimulation amplitudes were  $\leq 10 \mu\text{A}$ . This similarity in the distributions of the stimulation thresholds between cats and monkeys is critical because it indicates that not only are the motor networks across species equally excitable, but also that functional movements can be evoked in non-human primates with current amplitudes that have been proven to be safe for

ISMS (Bamford, Todd, and Mushahwar 2010; Mushahwar, Collins, and Prochazka 2000). The similarity in the distribution of the stimulation thresholds in cats and monkeys suggests a similar distribution may exist in humans as well. This knowledge is also important for the technological design of clinical ISMS implants, which includes the design of the microelectrodes and stimulators that can safely accommodate large enough current amplitudes for producing functional movements.

**Kinematics and kinetics of the evoked movements.** Movements produced by ISMS through single electrodes in this study were functionally highly relevant. Movement kinematics produced by ISMS were similar to hindlimb kinematics during quadrupedal stepping on a treadmill, suggesting that by capitalizing on the functional connectivity within the lumbosacral cord, ISMS can produce movements with the ROMs needed for locomotion in rhesus monkeys.

ISMS was also able to evoke functional levels of torque, with knee extension torques reaching up to 91% of the levels evoked by supra-maximal nerve stimulation. This suggests that nearly all the motoneurons innervating the knee extensor muscles were recruited by ISMS through one stimulation site. Because the ISMS current does not directly spread throughout the ~16 mm extent of the quadriceps motoneuronal pools, activation of the motoneurons therein was likely accomplished trans-synaptically through the activation of axons in passage around the electrode tip. In addition to amplifying force production, trans-synaptic activation of motoneurons results in the recruitment of motor units in a near normal physiological order (Bamford, Putman, and Mushahwar 2005), produces graded increases in force (Mushahwar and Horch 2000a; Snow, Horch, and Mushahwar 2006) and reduces the rate of muscle fatigue (Lau, Guevremont, and Mushahwar 2007).

In addition to the relatively large torques around a single joint, ISMS at some sites evoked extensor synergies in one leg that produced isometric forces up to 40% of the animal's body weight. The strength of these synergistic movements further indicates the activation of functional networks that not only connect the motoneurons within a pool but also across pools innervating different muscles. Furthermore, the ability of ISMS to generate functional movements and torques in non-human primates suggests that this may also be the case in humans.

**Cluster analysis of muscle activity.** Cluster analyses of the EMG patterns evoked by ISMS suggest that the lateral gastrocnemius and biceps femoris posterior muscles are most commonly activated together by ISMS (figure 4.13c). This is consistent with the evidence of strong heteronymous Ia afferent excitation (Meunier, Pierrot-Deseilligny, and Simonetta 1993) and heteronymous recurrent inhibition (Meunier, Pierrot-Deseilligny, and Simonetta-Moreau 1994) between these muscles in humans. Similarly, coactivation of these muscles is also reported for cats during unrestrained walking and trotting (Rasmussen, Chan, and Goslow 1978). At a higher Euclidian distance, responses in gastrocnemius-biceps femoris pair and tibialis anterior were coupled. This suggests antagonistic coactivation of tibialis anterior and gastrocnemius muscles, which serves to increase the stiffness of the ankle joint. Coactivation of antagonistic muscles may also be the result of current spread since the EMG responses used in this analysis were recorded during moderate to strong contractions (Baratta et al. 1988) (ISMS intensity of 100  $\mu$ A).

Vastus lateralis and sartorius also had a similar activation pattern. At a greater Euclidean distance, a similar activation pattern was found between the sartorius-vastus lateralis pair and the vastus medialis muscle. Synergistic activation of the vastus lateralis, vastus medialis and the

anterior part of the sartorius muscle (knee extensor and hip flexor (Hoffer et al. 1987)) has also been reported during trotting in cats (Pratt and Loeb 1991; Loeb, Hoffer, and Pratt 1985).

These results suggest that similar to cats (Mushahwar and Horch 2000b; Saigal, Renzi, and Mushahwar 2004; Holinski et al. 2016), ISMS in a given motoneuronal site in monkeys not only activates the targeted motoneuronal pool, but also activates the functional networks, and ultimately the synergistic muscles, connecting a motoneuronal pool to other pools (Bizzi and Cheung 2013).

## 4.5 Conclusions

Knowledge of the functional organization of the motoneuronal networks in the lumbosacral spinal cord of humans is essential for the clinical translation of ISMS implants. This includes knowledge about where in the spinal cord to place the implant for successful targeting of the leg movements required for functional standing and walking, and how to design the implant.

Technical design considerations are: *(i)* the layout of the clinical implant (i.e., number of microelectrodes in the array, spacing between the microelectrodes, and targeting depth and length of the microelectrodes), and *(ii)* the specifications of the clinical microelectrode and stimulator that would safely deliver the current intensities required for producing functional movements.

Since functional mapping of the lumbosacral enlargement of the human spinal cord with a high spatial resolution, as in the present study, is not clinically feasible, and mapping with a low spatial resolution would require a large sample size to yield a complete functional map, we chose to study a non-human primate as the first step. The rhesus macaque monkey was chosen for this study as the closest available neurophysiological animal model to humans. The

functional maps obtained for the monkey spinal cord along with the trends in the functional and anatomical organization of the motoneuronal pools in the discussed mammalian spinal cords can help predict the functional maps in humans.

Importantly, the similarity between the relative organization of the functional maps of the lumbar enlargement of the cat and monkey spinal cords suggests a similar relative organization for the functional map of the human lumbosacral spinal cord. However, differences exist between the spinal cord spatial and segmental distributions of the various movements in the functional maps of cats and monkeys. Assuming monkeys to be a closer animal model to humans (vs. cats), we hypothesize that the spatial and segmental distributions of various movements in the lumbar enlargement of the human spinal cord would be more similar to that of the monkeys. In the path for clinical translation of ISMS, our team is planning to test this hypothesis in the upcoming intraoperative testing experiments in humans involving a relatively coarse (low spatial resolution) electrophysiological mapping of the lumbar enlargement.

## 4.6 Figures

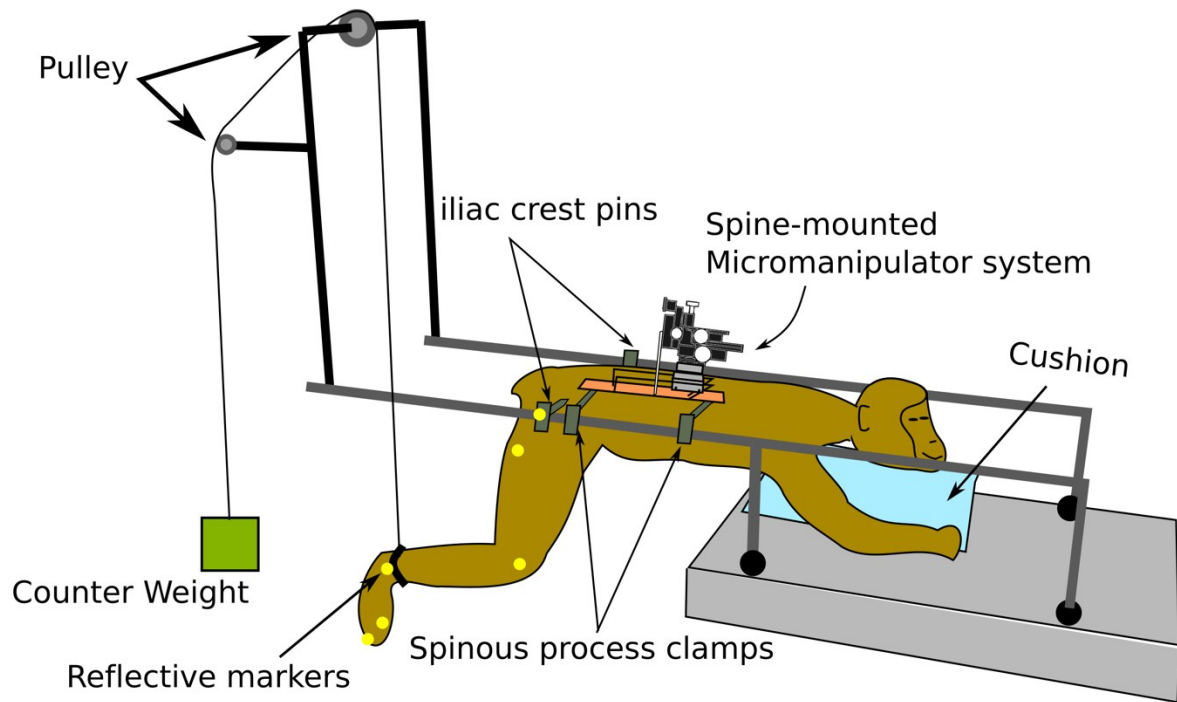


**Figure 4. 1.** Experimental setup for functional mapping of the lumbosacral spinal cord in non-human primates.

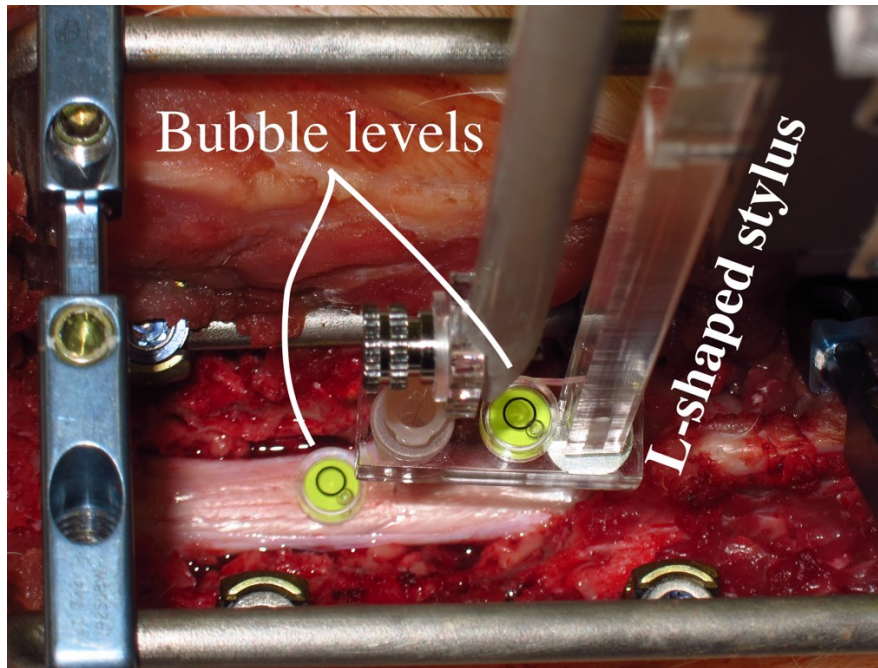


**Figure 4. 2.** Microelectrode alignment using bubble levels.

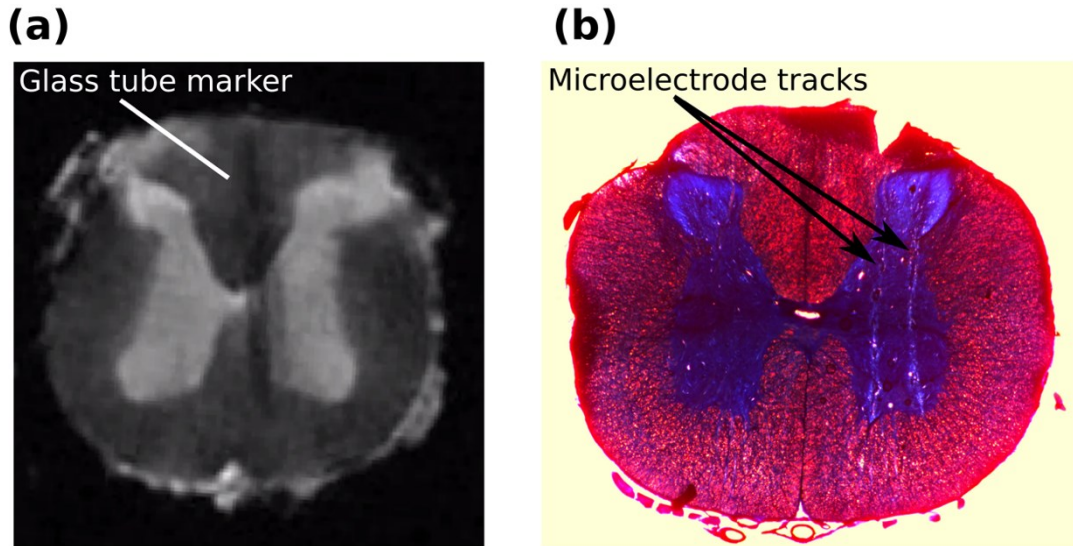


**Figure 4. 3.** MR imaging and histological analyses results. (a) An example of an MR image of the spinal cord (animal B) in the transverse plane. The marked black line is the imaging artifact from a glass tube marker inserted into the spinal cord at the boundary of L4-L5 spinal cord segments. (b) Microscopic image of a 50  $\mu\text{m}$  thick cross-section of the spinal cord (animal C – spinal cord level L3) showing two electrode tracks. Tissue was stained with the Mallory's trichrome stain.

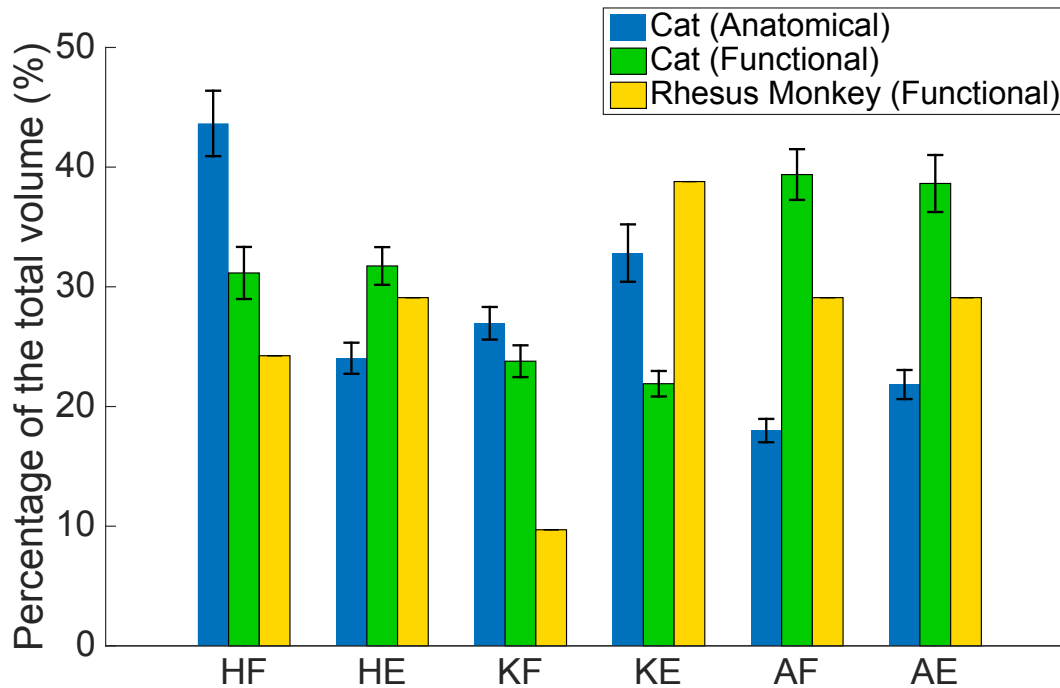


**Figure 4. 4.** Spatial distribution (in the rostrocaudal direction) of the maps of the lumbar enlargement in cats and rhesus monkeys. The total length of the lumbar enlargement in the spinal cords of monkeys, cats and humans are approximately 40 mm, 30 mm (Mushahwar, Collins, and Prochazka 2000; Mushahwar and Horch 2000b; Krieg and Groat 1944) and 50 mm (Lozano, Gildenberg, and Tasker 2009), respectively. Functional map data for cats were obtained from Mushahwar & Horch (Mushahwar and Horch 2000b), Saigal et al (Saigal, Renzi, and Mushahwar 2004), and Mushahwar et al (Mushahwar et al. 2002). Anatomical map data were obtained from Vanderhorst & Holstege (Vanderhorst and Holstege 1997). Functional maps only include responses from ISMS in the gray matter of the spinal cords. The sizes of the spinal cord segments in cats used to convert the maps into spatial distribution were derived from measurements obtained from 4 cat spinal cords. HF: Hip Flexion, HE: Hip Extension, KF: Knee Flexion, KE: Knee Extension, AF: Ankle Flexion, AE: Ankle Extension.

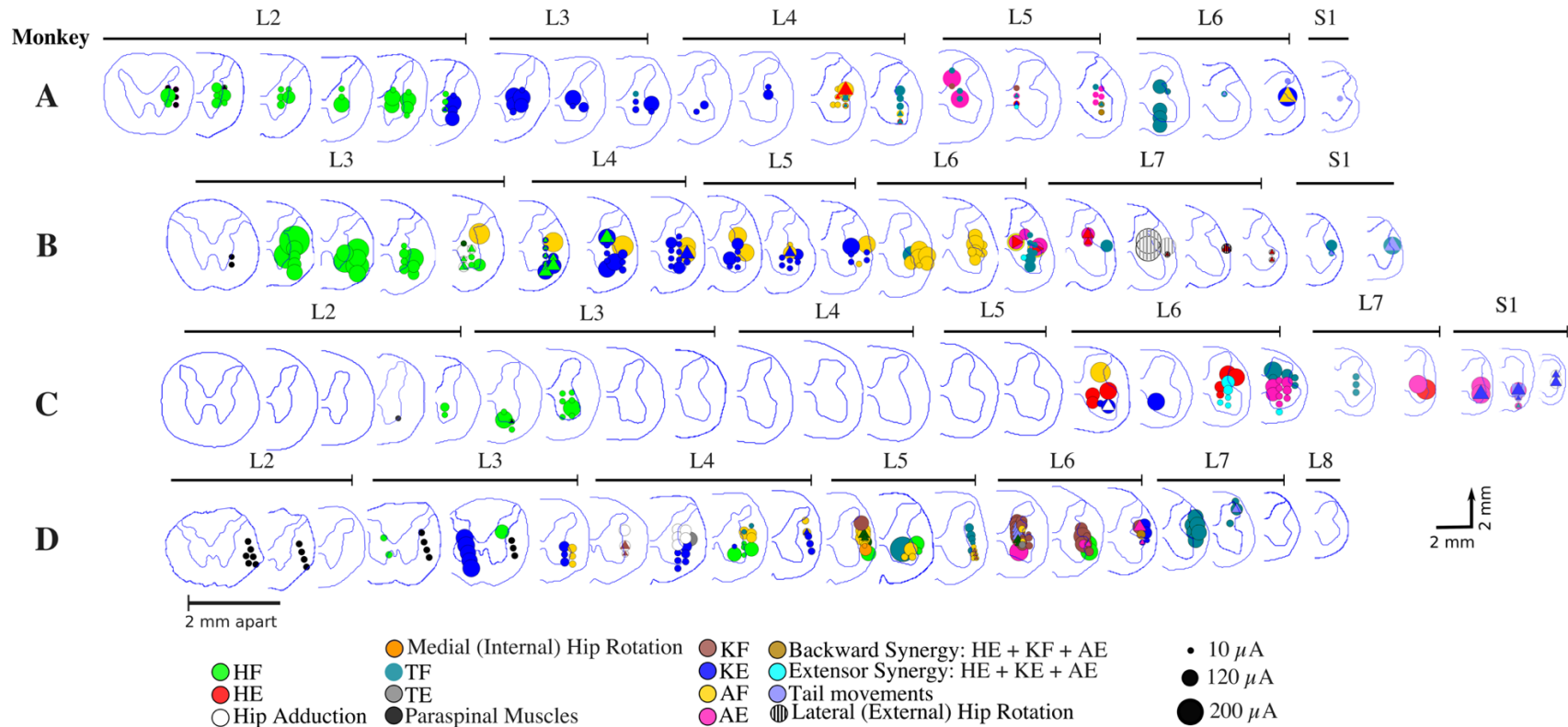


**Figure 4. 5.** Functional map of the lumbosacral enlargement of the spinal cord of 4 rhesus monkeys (A-D). ISMS in the locations shown on the maps resulted in a movement with thresholds  $<120 \mu\text{A}$ . 9 locations with higher stimulation thresholds (up to  $220 \mu\text{A}$ ) are also included in the map where the density of the mapped locations was low (in L3 and L7 segments in animal B, L6 segments in animal C and L5 segment in animal D). Each dot represents a mapped location in the spinal cord that produced a movement. Different colors represent different movements. Sizes of the dots are determined based on the stimulation threshold required for producing a movement according to the spread of electrical current as described by Bagshaw

& Evans (Bagshaw and Evans 1976). Larger dots correspond to larger stimulation thresholds. Spinal cord cross-sections shown in each row are 2 mm apart from their neighboring cross-section irrespective of their spacing on the figure. Total length of the spinal cord covered by the cross sections shown is ~40 mm, ~40 mm, ~46 mm and ~40 mm for animals A, B, C and D, respectively. When multiple movements were evoked as a result of stimulation in one location, different symbols (dot (O), square (□) and triangle (Δ)) were used for each, to set them apart on the map. HF: Hip Flexion, HE: Hip Extension, KF: Knee Flexion, KE: Knee Extension, AF: Ankle Flexion, AE: Ankle Extension, TF: Toe Flexion, TE: Toe Extension. Note that spinal cord segments L4 and L5 were not mapped in monkey C.

## Monkey

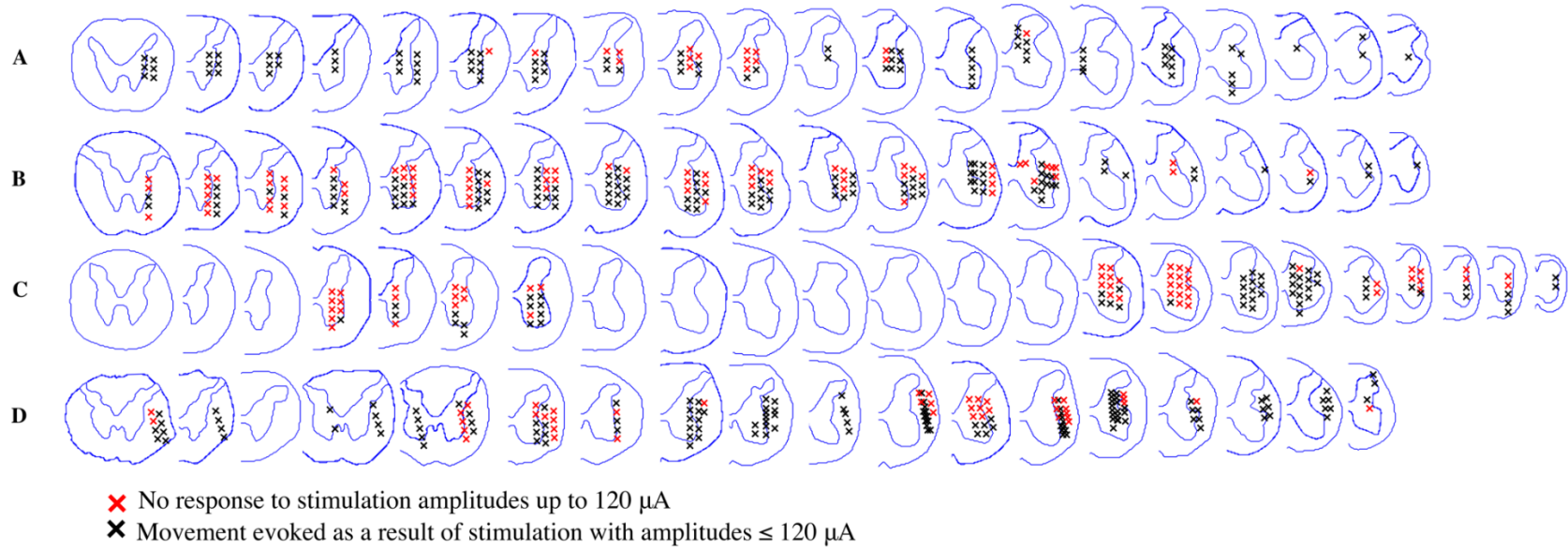


**Figure 4. 6.** All stimulated locations within the spinal cord across all animals. The cross-sections are sequential, separated by 2 mm.

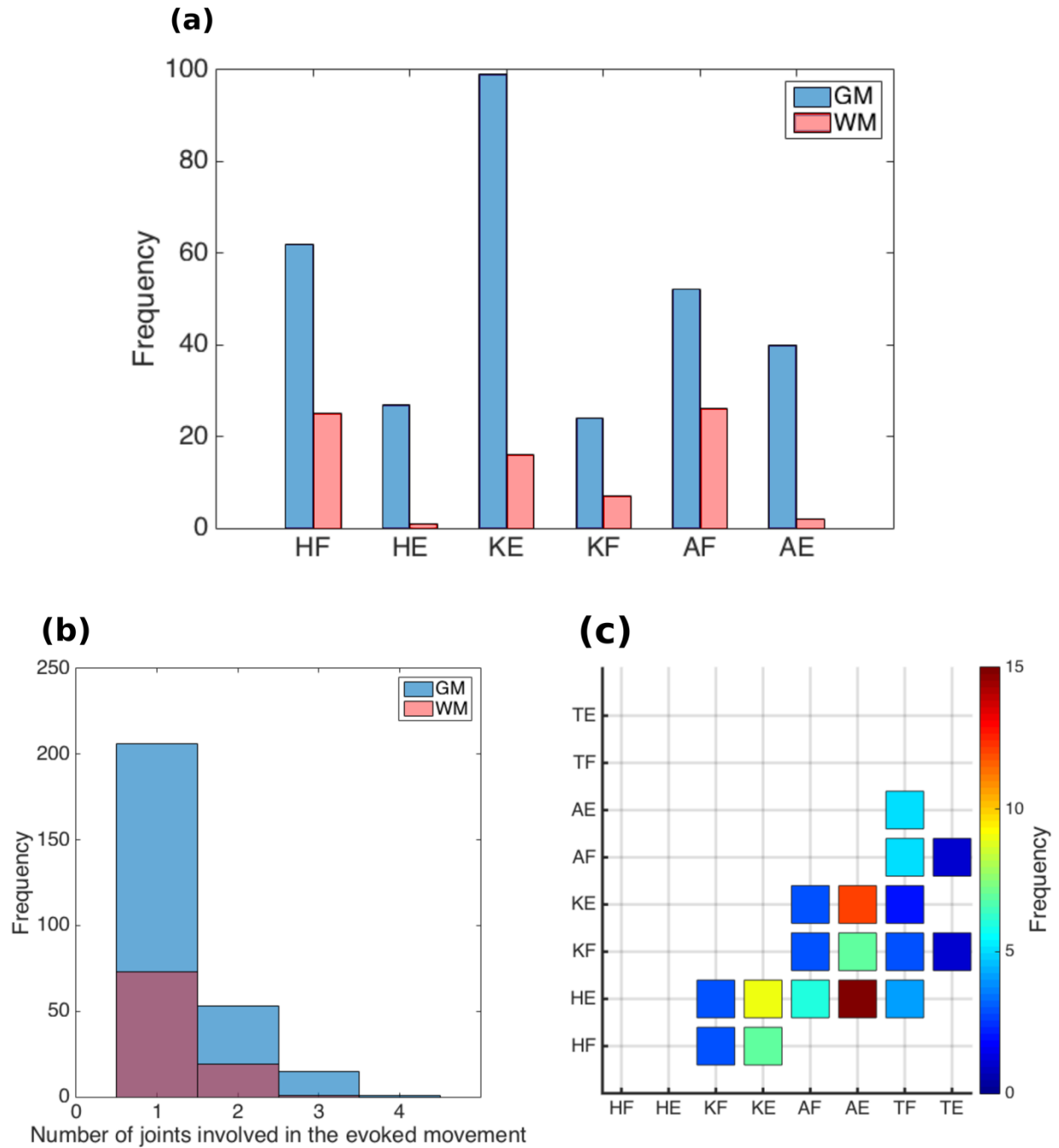


**Figure 4. 7.** Characterization of the movements evoked by ISMS. (a) Overall distribution of the main leg movements resulting from microstimulation in the gray matter (GM) and white matter (WM) of the lumbosacral spinal cord in all animals (n=4). (b) Number of joints (of hip, knee, ankle and, metatarsophalangeal (MTP)) involved in all evoked leg movements. (c) Distribution and frequency of the multi-joint movements evoked by microstimulation only in the GM in all

animals. HF: Hip Flexion, HE: Hip Extension, KF: Knee Flexion, KE: Knee Extension, AF:  
Ankle Flexion, AE: Ankle Extension, TF: Toe Flexion, TE: Toe Extension.

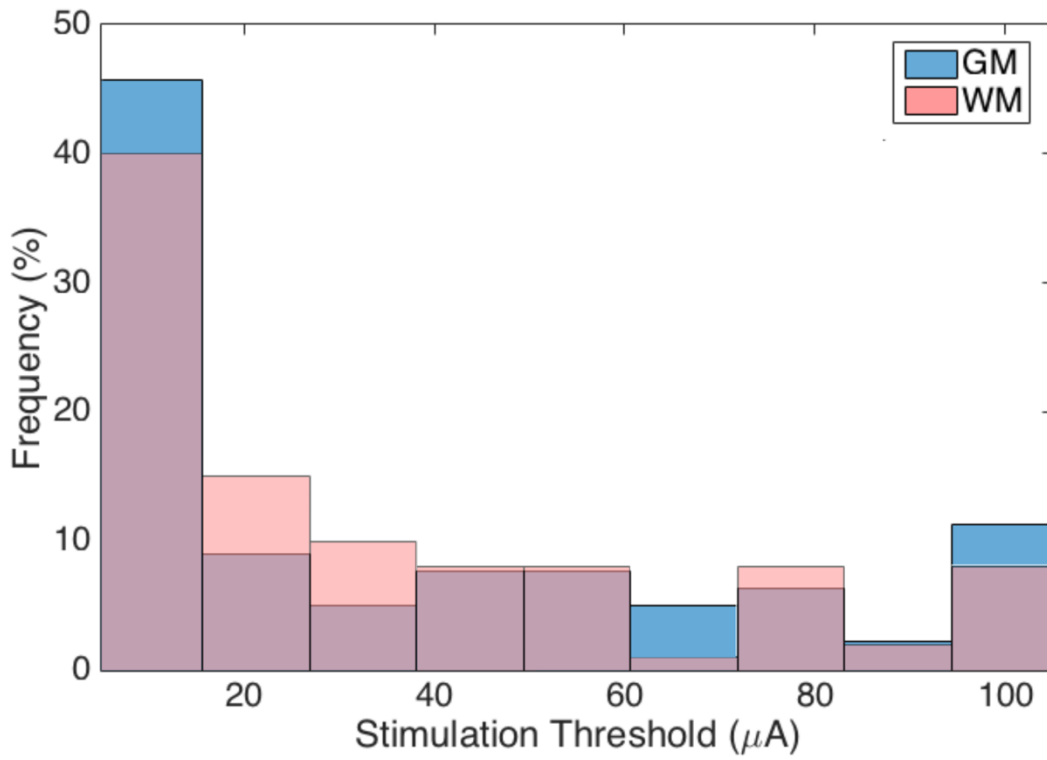


**Figure 4. 8.** Distribution of the stimulation thresholds for producing leg movements in the gray (GM) and white (WM) matters ( $n_{\text{GM}}=221$  and  $n_{\text{WM}}=100$ ) of the spinal cord ( $n=4$  animals).

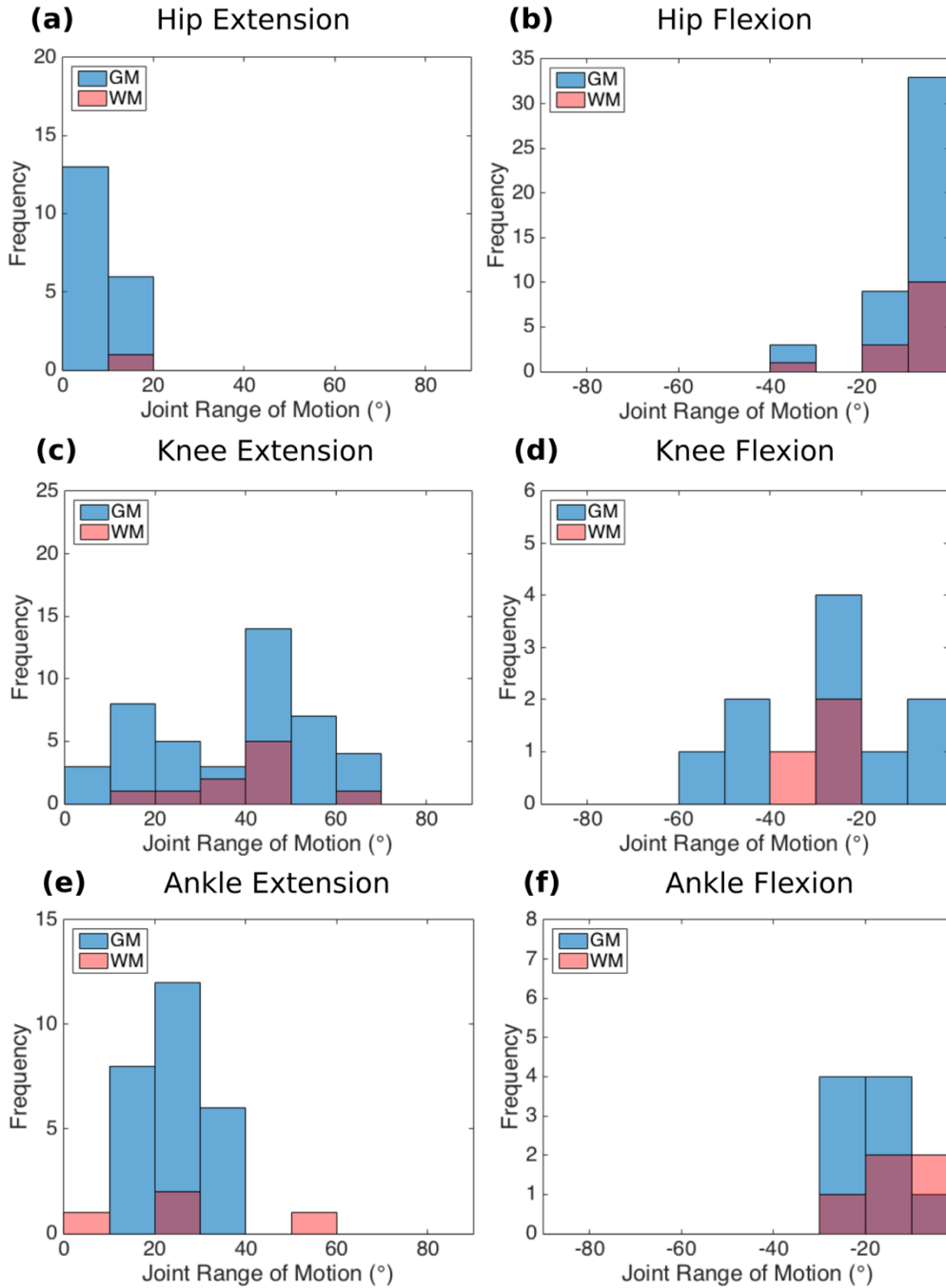


**Figure 4. 9.** Distribution of changes in joint angle (i.e., range of motion) for the movements evoked by microstimulation at sites in the gray and white matter (GM and WM) in all animals. Overall, kinematics were recorded for 40% of all evoked movements. (a) Hip Extension (initial hip angle:  $114.6^{\circ} \pm 3.2^{\circ}$  [mean  $\pm$  standard error]). (b) Hip Flexion (initial hip angle:  $112.6^{\circ} \pm$

3.3° [mean ± standard error]). (c) Knee Extension (initial knee angle:  $84.8^\circ \pm 3.86^\circ$  [mean ± standard error]). (d) Knee Flexion (initial knee angle:  $102.9^\circ \pm 7.9^\circ$  [mean ± standard error]). (e) Ankle Extension (initial ankle angle:  $116.1^\circ \pm 3.9^\circ$  [mean ± standard error]). (f) Ankle Flexion (initial ankle angle:  $114.5^\circ \pm 5.4^\circ$  [mean ± standard error]).

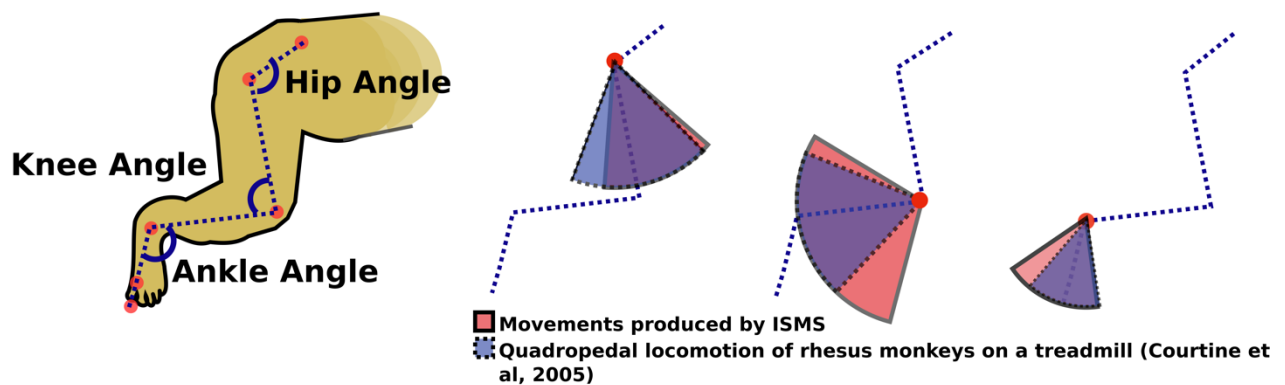


**Figure 4. 10.** Joint range of motion (ROM) of hip, knee and ankle produced by ISMS in the gray matter of the spinal cord (in Red). ROM of hip, knee and ankle joints of rhesus monkeys during quadrupedal locomotion on a treadmill at a speed of 1.79 m/s (in Blue). Treadmill locomotion data were obtained from Courtine et al (Courtine et al. 2005).

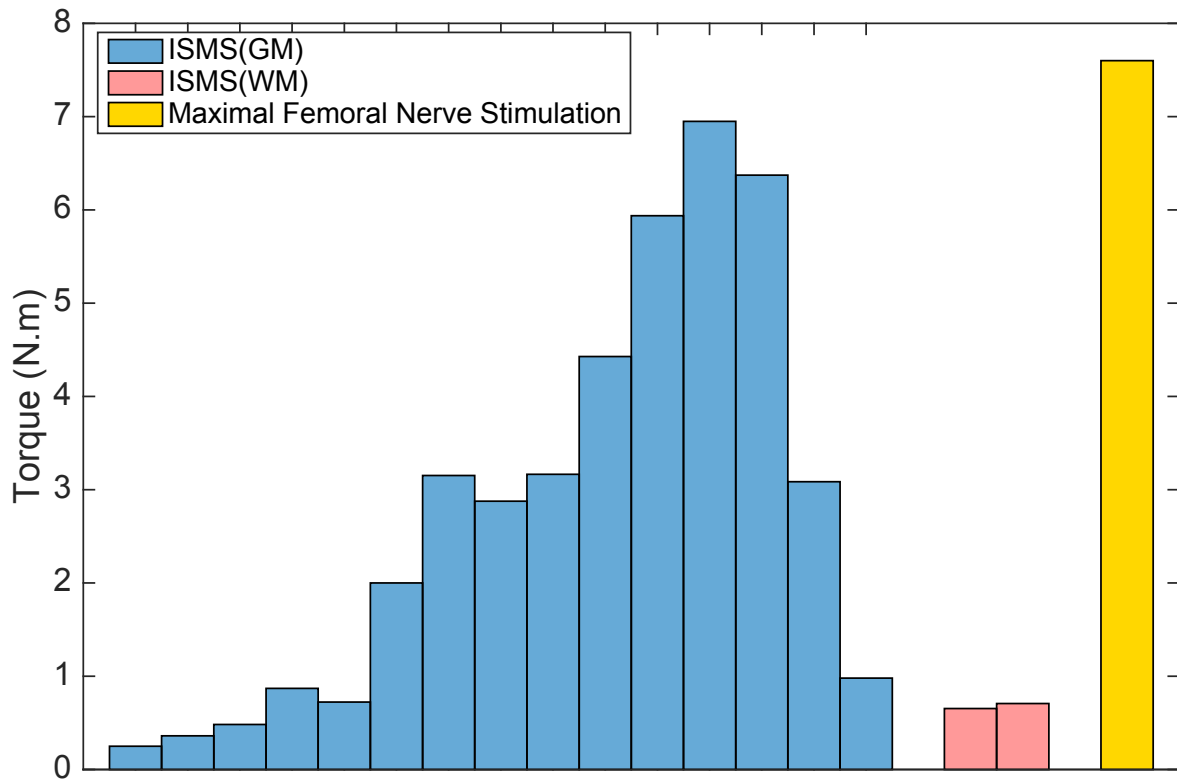


**Figure 4. 11.** Isometric torque measurements for knee extension movements evoked at 17 select locations across 4 animals. Each bar represents a torque measurement. Moment arm was  $15.9 \pm 1.1$  cm (average  $\pm$  standard deviation). Knee extension torques produced with ISMS in the gray (n=15 recordings) and white (n=2 recordings) matter of the spinal cord and with femoral nerve stimulation (n=1 recording) are shown in blue, red and yellow bars, respectively.

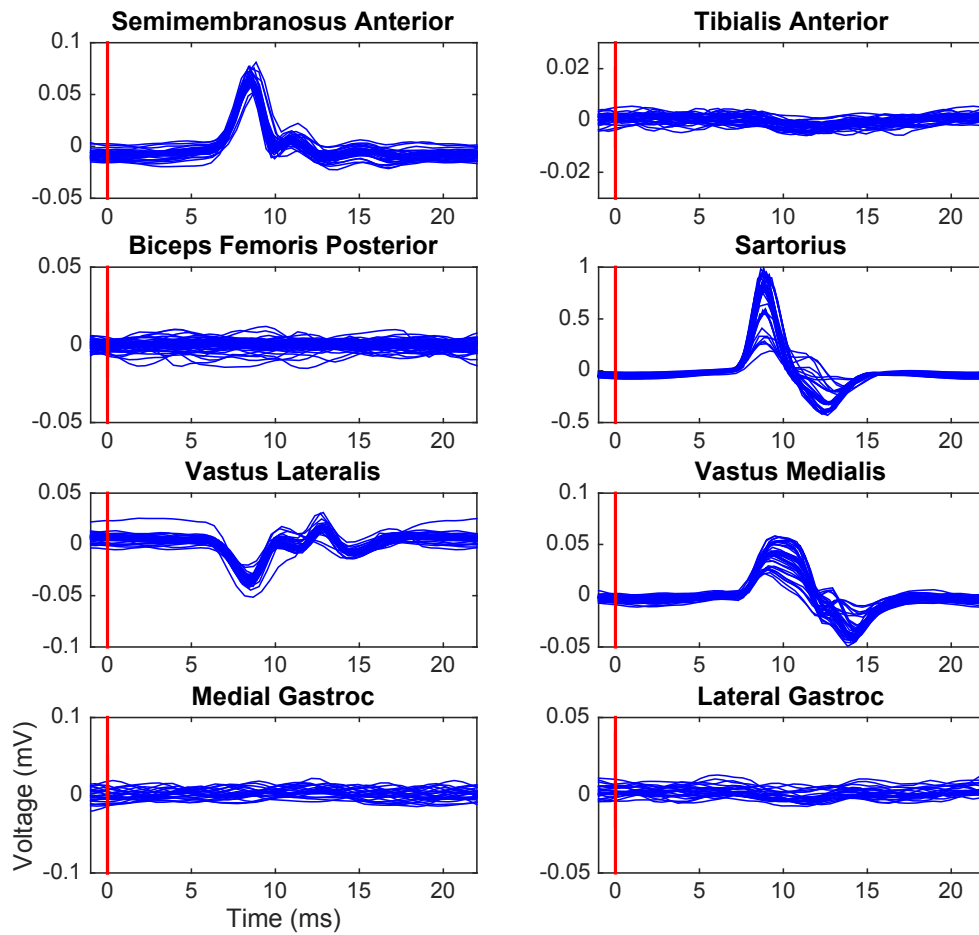


**Figure 4. 12.** Example of evoked electromyographic (EMG) activity during a knee extension movement produced by ISMS in the lumbar enlargement. Red vertical line represents stimulation onset.

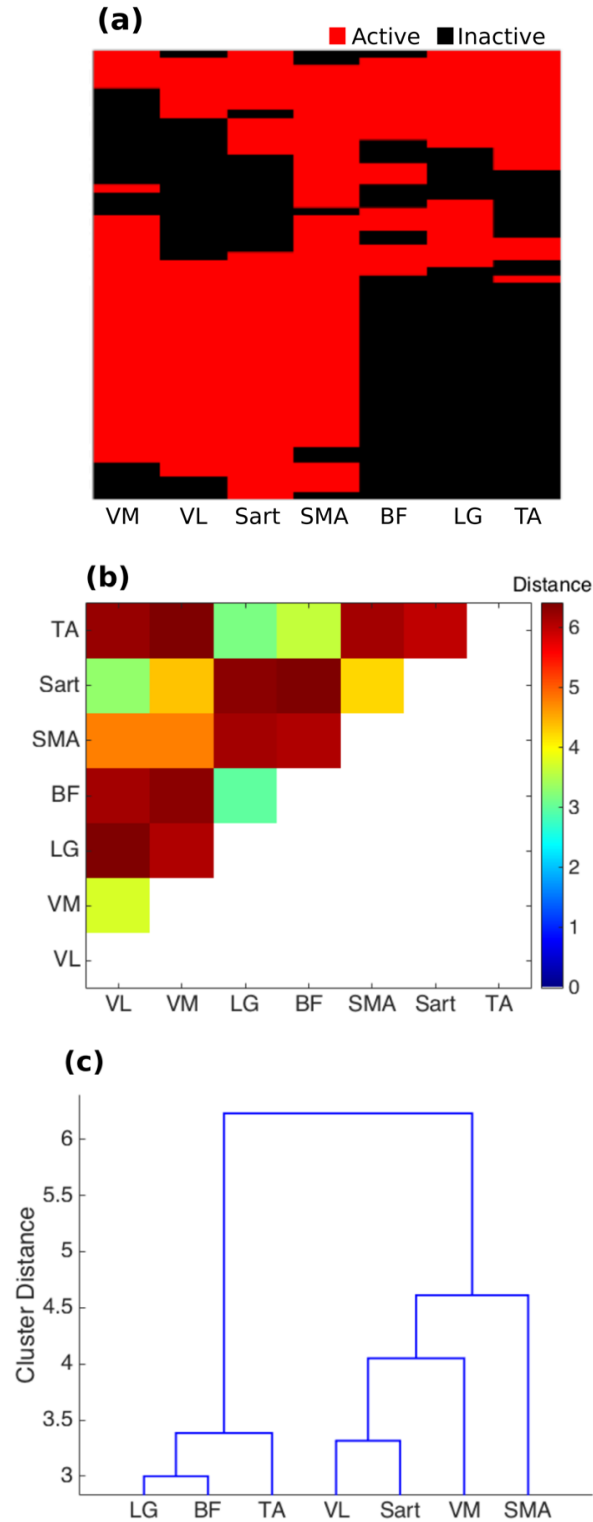


**Figure 4. 13.** Cluster analysis of the EMG responses evoked by stimulation in the gray matter of the spinal cord. (a) Clustergram of the EMG responses collected from 60 locations in the spinal

cord in 3 animals (A, C and, D). Stimulation amplitude was at 100  $\mu$ A for all recordings. (b)

Similarity matrix demonstrating the Euclidian distance between each pair of muscles. (c)

Dendrogram of the EMG responses. SMA: Semimembranous anterior, Sart: Sartorius, VL:

Vastus Lateralis, VM: Vastus Medialis, TA: Tibialis Anterior, BF: Biceps Femoris, LG: Lateral

Gastrocnemius

## Lumbar Enlargement

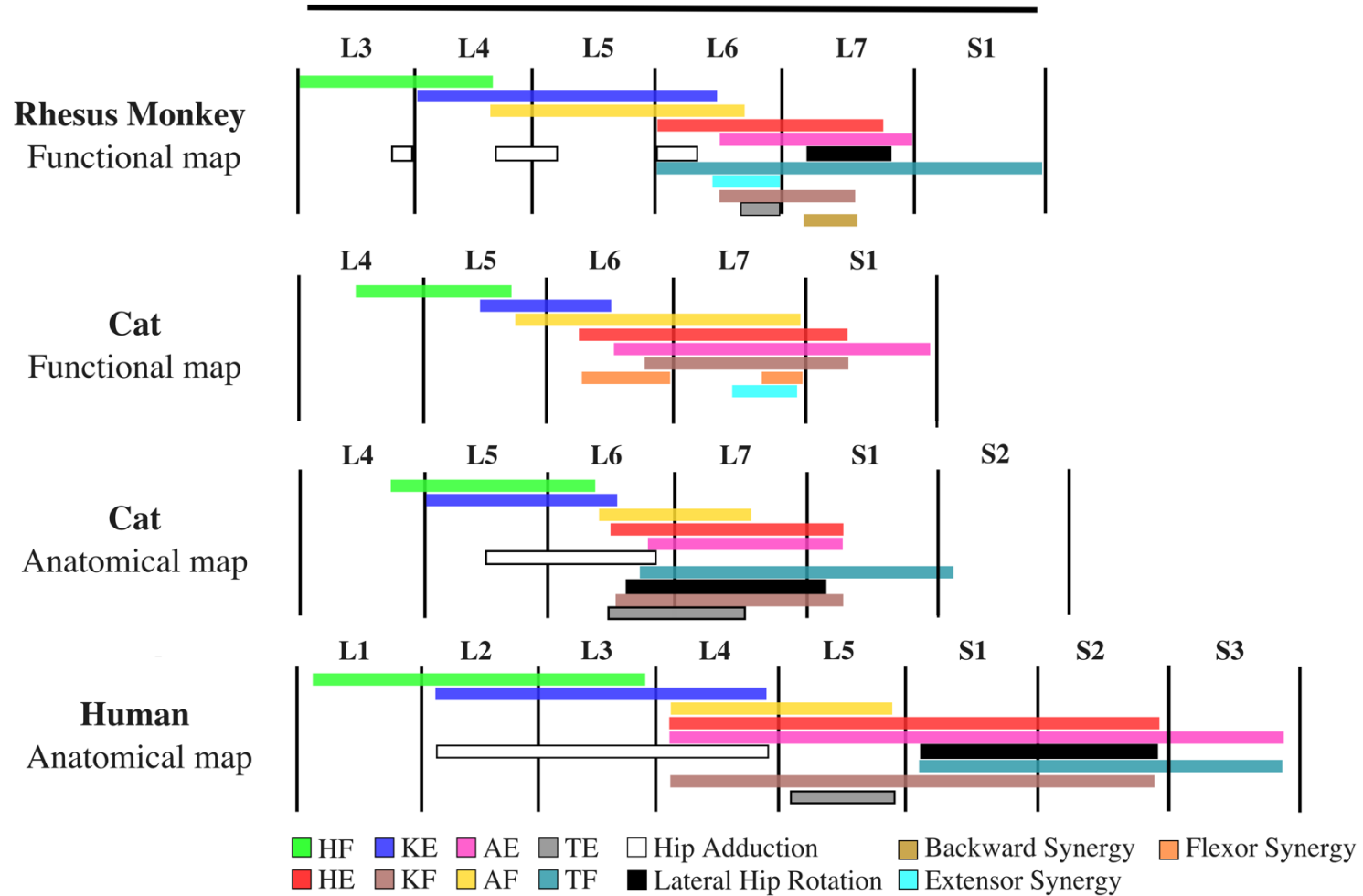


**Figure 4. 14.** Rostrocaudal organization of the lumbar enlargement of the spinal cords of rhesus monkeys, cats and humans. In all species, hip flexors were activated in more rostral regions of the lumbar enlargement than knee extensors, followed by ankle flexors,

hip extensors, ankle extensors and knee flexors. Data for the human anatomical map were obtained from Sharrard (Sharrard 1964; Sharrard 1955). The resolution of the human spinal cord anatomical map is limited to full spinal cord segments. Data for the cat functional map were obtained from Mushahwar et al (Mushahwar et al. 2002; Saigal, Renzi, and Mushahwar 2004; V.K. Mushahwar and Horch 2000b). Data for the cat anatomical map were obtained from Vanderhorst & Holstege (Vanderhorst and Holstege 1997), and Yakovenko et al (Yakovenko et al. 2002) . The total length of the lumbar enlargement in monkeys, cats and humans are approximately 40 mm, 30 mm (Mushahwar, Collins, and Prochazka 2000; Mushahwar and Horch 2000b; Krieg and Groat 1944) and 50 mm (Lozano, Gildenberg, and Tasker 2009), respectively. Extensor synergy is defined as a combination of HE, KE, and AE and backward synergy is defined as HE, KF, and AE. HF: Hip Flexion, HE: Hip Extension, KF: Knee Flexion, KE: Knee Extension, AF: Ankle Flexion, AE: Ankle Extension, TF: Toe Flexion, TE: Toe Extension. Anatomical map of the cat lumbosacral spinal cord was adapted based on the following motoneuronal pools: HF – Psoas, Sartorius, Iliacus, Rectus Femoris, Gracilis; HE – Semimembranosus, Semitendinosus, Biceps Femoris, Gluteus maximus; Hip Adduction – Pectineus, Adductor Femoris Magnus, Gracilis, Adductor brevis, Adductor longus; Lateral Hip Rotation – Gluteus maximus, Internal obturator; KE – Rectus Femoris, Vastus Medialis, Vastus Lateralis, Vastus Intermedius; , KF – Biceps Femoris, Semitendinosus, Semimembranosus; AF – Extensor digitorum longus, Tibialis anterior; AE – Flexor hallucis longus, Tibialis posterior, Plantaris, Soleus, Lateral and Medial Gastrocnemius; TE – Extensor digitorum longus muscle; TF – Intrinsic foot, Flexor hallucis longus, Flexor digitorum longus. Muscles that were used for generating the anatomical map for humans were: Psoas, Hip adductors, Quadriceps, Sartorius, Tibialis anterior,

Extensor digitorum longus, Tibialis posterior, Knee flexors, Gastrocnemius, Soleus, Peroneus, Intrinsic foot, Flexor digitorum longus, Gluteus maximus, and Lateral hip rotators.

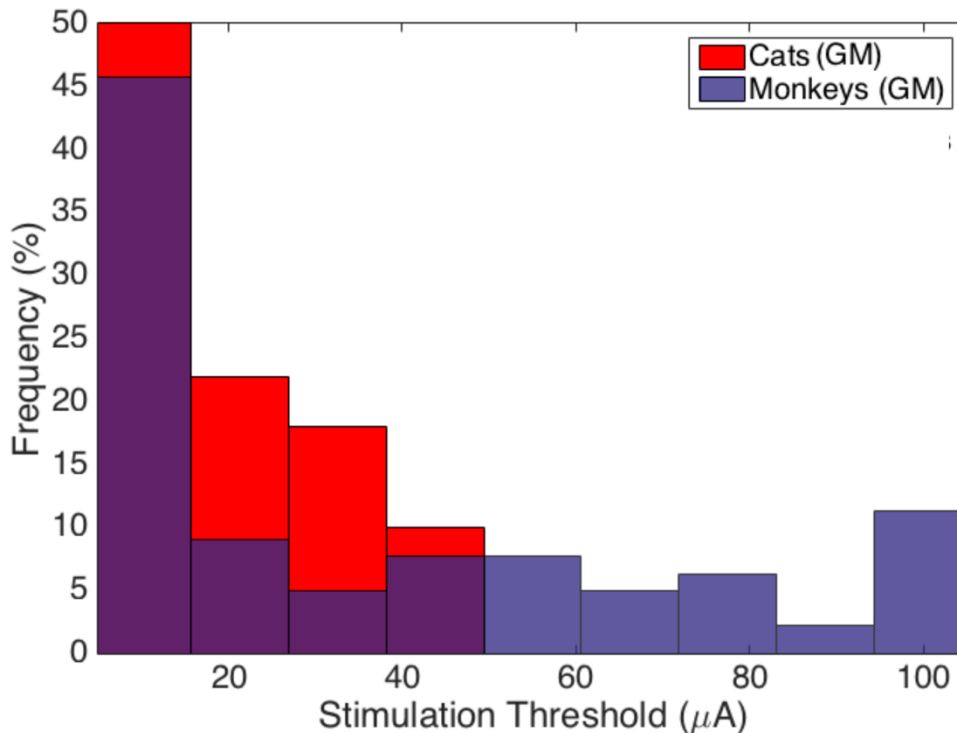


**Figure 4. 15.** The distribution of stimulation thresholds in cats and monkeys. The stimulation thresholds in rhesus monkeys were defined as the minimal amplitude required for producing a visible leg movement or twitch. The stimulation thresholds in cats were based on the minimal stimulation amplitude (up to 40  $\mu A$ ) needed to produce a detectable isometric force or EMG signal in targeted muscles. Stimulation thresholds in cats represent measurements for the quadriceps, triceps surae and tibialis anterior muscles (n=6 animals /muscle) (Mushahwar and Horch 2000b) and stimulation thresholds in monkeys represent measurements from all of the evoked movements by ISMS in the gray matter of the lumbar enlargement (n=4 animals, total of 221 locations). Data from cats were adapted from (Mushahwar and Horch 2000b).

# Chapter 5. Mechanically Stable Intraspinal Microstimulation Implants for Human Translation<sup>2</sup>

Amirali Toossi<sup>1,4</sup>, Dirk G. Everaert<sup>2,4</sup>, Austin Azar<sup>3,4</sup>, Christopher R. Dennison<sup>3,4</sup> and Vivian K. Mushahwar<sup>1,2,4</sup>

<sup>1</sup>Neuroscience and Mental Health Institute, University of Alberta, Edmonton, AB, Canada.

<sup>2</sup>Division of Physical Medicine and Rehabilitation, Department of Medicine, University of Alberta, Edmonton, AB, Canada. <sup>3</sup>Biomedical Instrumentation Lab, Department of Mechanical Engineering, University of Alberta, Edmonton, AB, Canada. <sup>4</sup>Alberta Innovates – Health Solutions Interdisciplinary Team in Smart Neural Prostheses (Project SMART), Edmonton, AB, Canada

---

<sup>2</sup>A version of this chapter has been published.

Toossi et al, 2017. “Mechanically Stable Intraspinal Microstimulation Implants for Human Translation.” *Annals of Biomedical Engineering*, 45(3): 681–694.

## 5.1 Introduction

Spinal cord injury (SCI) affects 250,000-500,000 people around the world each year (“WHO | Spinal Cord Injury” 2013). Depending on the type and level of injury, SCI can result in loss of control over various parts of the body such as the limbs and bladder (“WHO | Spinal Cord Injury” 2013). One of the successful approaches for restoring lost functions after SCI is functional electrical stimulation (FES) (Peckham and Knutson 2005). Intraspinal microstimulation (ISMS) is an FES technique that delivers electrical pulses directly to the ventral horn of the spinal cord. It has the potential to restore standing and walking after SCI by targeting the lumbar enlargement of the spinal cord, which contains neural networks responsible for controlling the movements of the legs.

Movements elicited by ISMS implants in the lumbar enlargement have been extensively studied in animal models (e.g., cats (Lau, Guevremont, and Mushahwar 2007; Mushahwar, Collins, and Prochazka 2000; Mushahwar and Horch 2000; Saigal, Renzi, and Mushahwar 2004) and rats ( Bamford, Todd, and Mushahwar 2010; Bamford, Putman, and Mushahwar 2005)) and show positive outcomes such as the production of functional weight-bearing fatigue-resistant movements in the legs after complete SCI (Saigal, Renzi, and Mushahwar 2004), and production of long durations of standing (Lau, Guevremont, and Mushahwar 2007) and long distances of propulsive over-ground walking in anesthetized animals (Holinski 2013). These results suggest that ISMS is a promising approach for restoring functional leg movements after SCI in humans.

Implants for ISMS in the lumbar cord comprise an array of penetrating electrodes with tips reaching the ventral horn, an electrical stimulator that generates the electrical pulses, and lead wires that connect the electrodes to the stimulator (figure 5.1). The mechanical stability of the implant in chronic studies conducted in cats (Mushahwar, Collins, and Prochazka 2000) and rats

(Bamford, Todd, and Mushahwar 2010) has been a critical factor in the long-term functional success of this approach (Bamford et al. 2016). In those studies, small amounts of slack in the lead wires accommodated for the small movements of the implant region of the spinal cord relative to the spine. Mushahwar et al (Mushahwar, Collins, and Prochazka 2000) demonstrated that at least two thirds of chronically implanted ISMS electrodes remain functional in intact, awake cats for periods up to 6 months (longest tested). Similarly, Bamford et al (Bamford, Todd, and Mushahwar 2010) demonstrated that more than 90% of chronically implanted ISMS electrodes stay functional up to 30 days in rats (longest tested).

Sacral ISMS implants have been implemented in humans after SCI. In 1972, Nashold et al (Nashold et al. 1972, 1977) reported the first clinical implementation of an ISMS implant in 11 patients for restoring bladder function. Two electrodes were implanted subdurally, one in each side of the spinal cord. The electrodes were embedded in a silastic base, and connected to flexible multi-strand stainless steel lead-wires. The lead wires laid on the dorsal surface of the cord and in turn connected to an implanted stimulator. To stabilize the electrodes, a silastic-coated strap fixed to the electrode base was wrapped around the spinal cord. In the five-year follow up (Nashold et al. 1977), implants in 10 patients had remained functional without displacement or dislodgment from their initial position. In one patient, the connection between the implanted electrodes and the stimulator had broken, and one of the electrodes had dislodged from the spinal cord.

Translating ISMS to a lumbar implant for restoring standing and walking is more challenging. This is partly due to the number of electrodes in a lumbar ISMS implant (16-24 vs. only 2) and the size of the implant region (5 cm for lumbar vs. ~1 cm for sacral). To ensure that the implanted electrodes remain stable in the spinal cord, an appropriately designed strain relief

mechanism in the lead wires connecting the electrodes to the stimulator is necessary to prevent the transmission of forces to the electrodes during natural movements of the spine.

In addition to maintaining electrode stability, the strain relief mechanism should mechanically disengage the electrodes that are floating within the soft tissue of the spinal cord from the surrounding hard bones. The mechanical interaction of electrodes with surrounding tissue is an important consideration in neural implants (Bamford et al. 2016). Biran et al (Biran, Martin, and Tresco 2007) demonstrated that microelectrodes implanted in the brain and tethered to the skull result in significantly larger reactivity in the nervous tissue than untethered microelectrodes. This increased reactivity may be due to the relative motion of the tethered electrode with respect to its surrounding tissue, and could be the cause of local neurodegeneration (McConnell et al. 2009; Biran, Martin, and Tresco 2007). Motion of the implanted electrodes relative to surrounding tissue may be caused by rhythmic physiological movements of the tissue such as breathing and blood flow pulsations, or from movements of body parts activated by the implant itself. Lead-wire designs that resemble untethered conditions as closely as possible are needed to minimize these deleterious relative motions.

This study focused on the design of lead wires for ISMS implants with a coil for strain relief that not only guarantees stability of the implants, but also in effect mechanically dissociates the floating implanted electrodes from the fixed implanted stimulator (figure 5.1). The coil required a high degree of flexibility and extensibility to minimize the relative motion between the electrode and surrounding tissue, and maintain the electrode stably in place. The design constraints were systematically identified in an animal model with spine mechanics that closely resembled those of humans. These constraints were: 1) the elongation and displacement of the spinal cord relative to the surrounding spinal vertebrae during physiological motions in

order to determine the required range of coil movement; and 2) the forces that lead to electrode dislodgement which should not be reached within the range of coil movement. Domestic pigs, commonly used in spine research (Busscher et al. 2010; Smit 2002), were chosen as the animal model because of the similarity of their spinal column anatomy (Busscher et al. 2010; Sheng et al. 2010) and range of motion (Wilke, Geppert, and Kienle 2011) to that of humans. To the best of our knowledge, this study not only provides the first design specifications for a strain relief mechanism for a neural implant in the spinal cord, but also provides detailed analysis of the biomechanics of the spine and spinal column of pigs during physiological movements.

## **5.2 Methods**

Studies were conducted in a total of six fresh domestic pig cadavers (48-54 kg). Three cadavers were used to establish the techniques and collect pilot data for the design of different coil types. After finalizing the methods, the remaining three pig cadavers were used to collect the results presented in this manuscript. In all of these experiments, the in-situ dislodgment trials (section 5.2) were conducted first, followed by trials for the assessing the biomechanics (Section 5.1). Cadavers were kept at room temperature for the duration of each experiment. The biomechanical assessment trials started approximately 15 hours post-mortem, the time at which the intensity of rigor mortis was expected to be minimized (Krompecher 1981). The electrode dislodgment trials did not require the full range of motion and therefore were not sensitive to rigor mortis.

### **5.2.1. Biomechanics of the Implant Region**

During movements within the physiological range of motion, the spine and spinal cord move

relative to each other (Harrison et al. 1999). The spinal cord also experiences length changes (elongation or compression) depending on the type of movement. These details are important for the design of a successful strain relief mechanism.

The lumbar enlargement in pigs, the region of interest for the ISMS implant, is located under the L4-L5 vertebrae (Hachmann et al. 2013; Szentkuti and Bruns 1983) (vs. T11-T12 in humans (Purves et al. 2001)). This region is similar to the T11-T12 region in humans in two critical aspects: 1) the range of flexion and extension motion – this is 25° in pigs (L3-L6) (Wilke, Geppert, and Kienle 2011) and 21° to 32° in humans (T10-L1) (Oxland, Lin, and Panjabi 1992; White and Panjabi 1990); and 2) the dimensions of the spinal canal – the average width is 20 mm in pigs and 21 mm in humans, and the average depth is 12.5 mm in pigs and 17.5 mm in humans (Sheng et al. 2010). Furthermore, our gross morphological comparisons of the lumbar enlargement of the spinal cord itself in humans and pigs, suggest that they are similar in size.

A laminectomy was performed between vertebral levels L1-L6 to expose the spinal cord, and the dura mater was opened. Reflective markers were then attached, using a drop of cyanoacrylate, to the inner walls of the facet joints of each vertebra and to the surface of the spinal cord in the middle of every other facet joint (figure 5.2a). In order to quantify the flexion and extension angles of the spinal column, reflective markers were secured on the sacrum and on the spinous processes of vertebrae T4 and T15 (figure 5.2b). Markers were also placed on the hip, knee, shoulder and elbow joints.

A 3D motion capture system (Vicon Motion Systems Ltd., Oxford, UK) was used to quantify the movements of the spinal cord relative to the spinal column. Six to eight cameras were used to cover a volume of about 1.5 m x 0.8 m x 0.8 m (width x height x depth) (figure 5.2c). Before each experiment, the motion capture system was calibrated for both static and dynamic motions and the

measurement error was  $<0.1$  mm. In all of the reported trials, the animal was positioned on its right side on the surgical table. The thoracolumbar spine was moved between neutral, hyperflexion and hyperextension states by bilateral movements of the limbs as shown in figure 5.3. For each trial, the 3D coordinates of the reflective markers were recorded continuously at a rate of 120 frames/s. Therefore, by tracking the kinematics of the animal's spine between hyperflexion and hyperextension, a series of biomechanical data became available for all thoracolumbar angles in this range. The spine neutral position was defined by thoracolumbar angle of  $140^\circ$  consistently across animals (figure 5.3a and figure 5.2b). The acquired data were then filtered with a 2<sup>nd</sup> order low-pass Butterworth filter (cut-off frequency of 12 Hz) before analysis. Data analysis was performed using a custom written Matlab (version R2015a, MathWorks co., Natick, USA) program.

All measurements were associated with the dorsal side of the spinal canal and spinal cord, which are most directly relevant for the lead-wires of the ISMS implants. Also, in all calculations involving the facet joint markers, the coordinates of the markers on the right and left sides of the canal were averaged to find a representative location in the middle (mediolateral direction) of the canal. This is also relevant to the ISMS implants, where the stimulator and bundle of emerging lead wires are attached to the middle of the spinous process, rostral to the implant region (figure 5.1).

### **5.2.2. Measurement of Dislodgement Forces**

Displacements and length changes of the implant region of the spinal cord, collectively referred to as “range of spinal cord movement,” expose the lead wires, and thereby the electrodes, to forces that could cause their dislodgment. Successful lead wire design requires knowledge about

the force levels that could dislodge the electrodes from their initial position.

In-Fiber Bragg Grating (FBG) strain sensors (Dennison et al. 2008, 2010) were placed in line with stiff lead wires connected to ISMS electrodes (figure 5.4a). These sensors are light and relatively small (optical fiber diameter = 125 $\mu$ m); therefore, they could readily be incorporated as part of the lead wires in these experiments. Because FBG sensors are also sensitive to temperature changes (Dennison et al. 2010), a second FBG sensor was placed in close proximity to the force sensor as a reference at all times. Temperature related artefacts were removed from the force measurement recordings by removing the temperature induced signal changes (from the second FBG) from the signal changes of the first (force sensing) FBG. Prior to the experiments, the FBG sensors were calibrated by measuring the weight of suspended masses ranging from 0.1-200 g and were deemed reliable in the range of interest with a coefficient of determination ( $r^2$ ) of 0.9999. Acquired force data were analyzed to determine dislodgment forces using a custom written Matlab program. Statistical analyses were performed using IBM SPSS Statistics software (version 22, IBM Co., Armonk, USA).

*Bench testing:* Dislodgment forces were first measured in a bench-top setup that simulated the horizontal movement of the lead wire on top of the spinal cord during movements (figure 5.4a). Platinum/iridium (Pt/Ir) microwires (80% Pt), 50  $\mu$ m in diameter were bent to 90° close to the tip, leaving a 4.7 mm length between the bend and the tip. The electrode was implanted in surrogate spinal cord materials (tofu (Snow et al. 2006) and gelatin hydrogel (Cheng et al. 2013)) and its lead portion, along with the FBG sensors laid flush with the cord surface. In order to measure dislodgment forces, a perturbing force was gradually applied in line with the lead wire and the FBG sensor by applying controlled translational movements (figure 5.4a). The forces

were recorded continuously at a sampling frequency of 2.5 kHz for the duration of the trial. The effect of electrode insertion angle on the measured dislodgment forces was also investigated in gelatin hydrogel surrogate spinal cords (Cheng et al. 2013) since they were transparent and allowed confirmation of the insertion angles (figure 5.4b).

*In-situ experiments:* Dislodgment forces were also measured *in-situ*. A laminectomy was performed at the L3-L6 vertebrae and the dura mater was opened. In each trial, the ISMS electrode (same as that used in the bench trials, bent to 90°) was implanted into the spinal cord with the lead wire-FBG sensor lying on the dorsal surface of the cord. The sensor's optical fiber was then fixed to the L2 spinous process on its path towards the data recording unit. The implantation protocol was consistent with published ISMS implantation protocols (Bamford et al. 2016; Bamford, Todd, and Mushahwar 2010; Mushahwar, Collins, and Prochazka 2000) with the exception of not using mechanically stabilizing components (i.e., cyanoacrylate) at the entry point of the electrode into the spinal cord. The pigs were then moved from the neutral to the hyperflexed and hyperextended positions (figure 5.3b) while recording forces continuously in real time at a sampling frequency of 625 Hz.

### **5.2.3. Coil Fabrication and Testing**

Based on the information obtained from the pilot experiments in three pig cadavers (the spine-spinal cord mechanics and the dislodgment forces), coils of varying dimensions and effective mechanical stiffness were designed to provide appropriate strain relief in the lead wire (table 5.1). The role of the coils was to eliminate the transmission of forces along the lead wires to the electrodes during physiological movements of the spine. These coils were designed for ISMS

implants that were surgically placed with the pig spine in the neutral position (figure 5.3). In this case, coils needed to accommodate approximately 5 mm of range of spinal cord movement without experiencing forces close to the dislodgment threshold. To increase the design safety margin and minimize the forces experienced by the implanted electrodes, the displacement requirement for the coil was doubled to 1 cm. For the scope of this study, coils were made from two of the most common microwires used in the fabrication of the ISMS arrays: 30  $\mu\text{m}$  and 50  $\mu\text{m}$  Pt/Ir (80%/20%). The pitch was kept constant and the coil outer diameter was limited to a maximum of 800  $\mu\text{m}$ . These coils were manually constructed from microwires using a lathe for coiling, and hypodermic needles of varying outer diameters as coiling shafts.

Each coil was characterized (force vs. strain profile) using a linear micro-actuator (M-227.50 – Physik Instrumente, GMBH & Co., Karlsruhe, Germany) and an FBG sensor. The coil was attached to a static bench clamp on one side and to the FBG sensor and micro-actuator on the other. The micro-actuator strained the coil in 20% steps up to 100% (1 cm), and force was statically recorded at each step. Characterized coils were then incorporated in the ISMS lead wires (figure 5.4c) and tested *in-situ* to evaluate their dislodgment outcomes. The testing protocol was the same as in section 5.2.

## **5.3 Results**

### **5.3.1. Biomechanics of the Implant Region**

In a total of 26 hyperflexion and 20 hyperextension trials in three fresh pig cadavers (figure 5.3), the thoracolumbar spine was flexed from its neutral position by  $19.25^\circ \pm 0.57^\circ$  (mean  $\pm$  standard error) and extended from its neutral position by  $23.45^\circ \pm 1.2^\circ$ .

Figures 5.5a and 5.5b show the segmental length changes of the spinal canal in hyperflexion and hyperextension movements. The length of each segment was calculated as the distance between the locations of the segment markers. The overall change in length of the spinal canal (vertebral levels L1-L6, facet joint marker levels T15-L6) for moving the thoracolumbar spine from hyperextension to hyperflexion was  $2.4 \pm 0.16$  cm (mean  $\pm$  standard error), which was  $14.18 \pm 0.88\%$  longer than its length at the hyperextended position.

The segmental changes in the length of the spinal cord itself were also measured as shown in figures 5.5c and 5.5d. The length of the spinal cord segments was calculated by fitting a curve to the markers to represent the curvature of the dorsal surface of the spinal cord, and measuring the corresponding arc length for each segment (figure 5.3). The overall change in length of the spinal cord segments as the thoracolumbar spine moved from hyperextension to hyperflexion was  $1.58 \pm 0.18$  cm (mean  $\pm$  standard error), which was  $10.73 \pm 1.14\%$  longer than its length in the hyperextended position. The resulting relative displacement of the spinal cord and spinal canal was also measured as shown in figures 5.5e and 5f. Figure 5.5f shows the change in the distance between the spinal cord marker and its closest rostral facet joint marker, for each segment. Figure 5.5e shows the two-dimensional change in the distance between these markers, calculated by projecting the coordinates of the facet joint markers onto the fit curve to the surface of the spinal cord and measuring their distance from the spinal cord markers.

The ISMS implant region in pigs is located approximately between facet markers L3-L5 and spinal cord markers M3-M5 (figure 5.2a). In a lumbar ISMS implant in this model, the bundle of lead wires would be fixed to the L2 spinous process, and the electrodes would be implanted in different locations within the M3-M5 region. The worst-case scenario (largest range of coil movement) in terms of stability would be for an electrode implanted most caudally, near

the M5 marker. The overall movement range that the lead wire should be able to accommodate without dislodgment of an electrode in this location can be calculated by summing the maximal change in spinal cord length in this region (M3-M5) and the relative displacement of the lamina L2 (bony fixation point) and its adjacent spinal cord marker (M3). These values were  $5.64 \pm 0.59$  mm and  $5.66 \pm 0.57$  mm, respectively.

In this study, coils were designed and tested for the case when the ISMS implant is surgically placed with the pig's spine in the neutral position (as opposed to hyperextended position). In this case, the maximal length change of the implant region and the relative displacement of the lamina L2 and the spinal cord marker M3 are  $1.46 \pm 0.39$  mm and  $2.13 \pm 0.38$  mm, respectively.

### **5.3.2. Measurement of Dislodgement Forces**

Examples of force recordings while translational movements were applied to electrodes implanted in gelatin surrogate spinal cords are shown in figure 5.6a. The average dislodgment force of electrodes implanted in the gelatin surrogate cord was  $30.9 \pm 13$  mN (mean  $\pm$  standard deviation), obtained across 30 trials in three cord samples (figure 5.6b). In comparison, the average force for dislodging electrodes from the tofu surrogate spinal cord across 10 trials in two samples was  $70.0 \pm 3.6$  mN (mean  $\pm$  standard deviation).

The electrode insertion angle had a significant effect on the dislodgement force of electrodes implanted in gelatin surrogate cords. In these experiments, the electrodes were implanted at  $45^\circ$  (8 trials),  $90^\circ$  (28 trials) and  $135^\circ$  (17 trials) angles, and the mean dislodgment forces were  $103.5 \pm 19.7$ ,  $33.3 \pm 10.9$  and  $17.3 \pm 6.1$  mN (mean  $\pm$  standard deviation), respectively. The dislodgment forces were significantly different for insertion angles  $45^\circ$ ,  $90^\circ$

and 135° ( $p < 0.001$  for all pairs; Brown-Forsythe corrected statistics and Tamhane's T2 post-hoc analysis).

The average dislodgement force across 52 trials of electrodes implanted with an insertion angle of 90° in the lumbosacral region of the spinal cord in three fresh pig cadavers was  $60.9 \pm 35.5$  mN (mean  $\pm$  standard deviation) (figure 5.6b). Electrode location along the region of interest in the spinal cord did not have a significant effect (one-way ANOVA,  $p = 0.998$ ) on the dislodgment forces (figure 5.26c).

### **5.3.3. Coil Fabrication and Testing**

Six coil types were fabricated and characterized prior to testing *in-situ* in three fresh pig cadavers. Force-strain profiles of two typical coils of types #1 and #2 (table 5.1) are shown in figures 5.7a and 5.7b. Based on the force-strain profiles obtained during bench testing for each coil type and assuming that the implant region, and therefore the coils incorporated in the lead wires, have a movement range of 1 cm, the maximal force transferred to the implanted electrodes was calculated. These values were then compared to the dislodgement thresholds (mean  $\pm$  standard deviation) measured *in-situ*.

Based on bench test results, coil types #1 through #5 (table 5.1) were not expected to transmit forces that would dislodge the electrodes during *in-situ* tests in pig cadavers. Coil type #6, however, was predicted to cause electrode dislodgement as its force-strain profile showed forces higher than the minimal dislodgment forces within the tested strain window.

A total of 78 coils (coil #1:  $n=11$ , coil #2:  $n=12$ , coil #3:  $n=21$ , coil #4:  $n=10$ , coil #5:  $n=11$ , coil #6:  $n=13$ ) were tested *in-situ* and the force transmitted to the electrodes were measured. The outcomes were consistent with the predictions made based on bench test results:

all tested coils from types #1 through #5 allowed the ISMS electrodes to remain in place without displacement or dislodgement. However, 30% of the coils from type #6 caused their respective ISMS electrodes to dislodge during hyperflexion movements of the spine. Examples of the force-displacement curves recorded during *in-situ* dislodgment tests are shown in figures 5.7c – 5.7e. A summary of the average maximal force experienced by the ISMS electrodes for all coil types is shown in figure 5.8.

## **5.4 Discussion**

### **5.4.1. Overview**

Successful performance of neural implants in the central nervous system may be affected by the tissue's foreign body response (FBR) as a result of factors such as material, shape and relative motion of the implanted electrodes (Ward et al. 2009). Many studies have focused on minimizing the FBR by addressing one or more of its contributing factors. This has led to the emergence of various electrode/electrode array designs (e.g., Michigan microelectrode system (Kipke et al. 2003), Utah electrode array (Rousche and Normann 1998), Moxon electrode array (Moxon et al. 2004), Giszter braided electrode (Kim et al. 2013)) as well as electrode coatings (Zhong and Bellamkonda 2007). Among the factors contributing to FBR, “tethering” of the implanted electrodes is shown to be the most important (Ersen et al. 2015). The focus of this study was on designing a strain relief mechanism that would mechanically decouple the implanted floating electrodes from the fixed stimulator. For the systematic design of such strain relief mechanism, detailed knowledge of the biomechanics of the spinal column and spinal cord during physiological movements was needed. Moreover, knowledge of the forces that could displace

electrodes and dislodge them from their site of implantation was also needed. This information was obtained in the present study, and coils that accommodated for the movement range experienced by the spinal cord during physiological movements were successfully designed and tested.

#### **5.4.2. Similarity between the biomechanics of the spine in humans and pigs**

A comparison between the results presented here and a meticulous study conducted by Louis (Louis 1981) in fresh human cadavers demonstrates similarities in all of the measured relevant biomechanical variables. For instance, Louis (Louis 1981) reported the overall change in length of the lumbar spinal canal to be 2.8 cm in humans (measured from spine neutral to hyperflexion positions) while this study found it to be  $2.4 \pm 0.16$  cm in the domestic pig model. With regards to the ISMS implant region (vertebral levels L4-L5 in pigs and T11-T12 in humans), the overall length change of the spinal cord in pigs was  $5.64 \pm 0.59$  mm. In Louis's study (Louis 1981), the overall elongation of the spinal cord under vertebral levels T11-T12 in humans was approximately 7.5 mm (hyperflexion with respect to hyperextension positions). In both studies, similar trends were observed in the direction of the relative displacement of the spinal cord and spinal canal. Results in figure 5.5e suggest that during spine flexion, the direction of spinal cord displacement with respect to the spinal canal changes at the L3-L4 intervertebral disc. Louis's results suggest that this change occurs at intervertebral disc L4-L5 in humans (Louis 1981).

Larger length changes are observed in extension movements than flexion in pigs than in humans (figure 5.5). This is partly because of the difference in the neutral positions and inherent differences in the lordosis angles in the human and pig lumbar spines:  $29.2 \pm 7.6^\circ$  in humans and  $7.9 \pm 5.7^\circ$  in pigs (Busscher et al. 2010). Nonetheless, taken collectively, the results obtained in

this study confirm the assumption that domestic pigs are an appropriate large animal model for humans, particularly for the assessment of the mechanical stability of lumbar ISMS implants.

In the present study, we also successfully measured the minimal force levels (thresholds) for dislodging 4.7mm long ISMS electrodes implanted in pig spinal cords. Results shown in figure 5.6c suggest that these values are not location dependent within the lumbar spinal cord. However, the insertion angle of the electrodes had a significant effect on thresholds for electrode dislodgement, suggesting that it is an important design parameter for mechanical stability of ISMS implants.

Based on bench testing in surrogate spinal cord materials, gelatin hydrogel cords (Cheng et al. 2013) had the lowest thresholds for electrode dislodgement. This suggests that these cords may be an excellent test tool for future bench testing since implanted systems that pass the dislodgment requirements in these cords are expected to perform within the design parameters *in-situ*.

Dislodgment forces measured *in-situ* demonstrated a larger variability compared with measurements obtained from surrogate cords in the bench tests (figure 5.6b). This may be because the topography of the dorsal surface of the spinal cord and its overlying vessels is less uniform than that of the surrogate cord materials; thus resulting in larger variabilities in friction and *in-situ* dislodgment forces. Coil types that passed the *in-situ* dislodgment tests provide examples of specifications of suitable coils for a mechanically stable ISMS implant.

### **5.4.3. Design implications for human implants**

Based on the results obtained in this study, domestic pigs are an appropriate animal model for testing the mechanical stability of human lumbar ISMS implants. An important consideration for

the design of ISMS implants is the difference in the spine neutral positions of humans and pigs, which has important implications for the ranges of elongation and compression for coil testing. For instance, coiled lead wires that would be surgically implanted in humans in a prone position can experience larger elongations than those implanted in the pig's neutral position. Since spine surgeries are commonly performed with patients in the prone position, for best compatibility, coiled lead wires should be designed and surgically implanted in pigs while in an extended spine position.

The range of coil movement as a design constraint should be selected to be larger than 12.11 mm for an ISMS implant in pigs. Past studies in humans did not directly characterize all the relevant variables for the ISMS implant region (e.g., 3D displacement of the spinal cord with respect to the neighbouring lamina as shown in figure 5.5f). However, similarities between the implant regions of pigs and humans suggest the possibility of using the same critical value with a correction factor to increase the design safety margin, until direct measurements in humans become available. Another reason for the use of an appropriate correction factor is the limitations associated with the scope of this study. For instance, we have only investigated extreme conditions for the thoracolumbar spine flexion/extension movements and have not considered more complex combinatory movements (e.g., addition of cervical spine movements or axial rotation and lateral bending of the spine) which could potentially produce larger displacements and length changes in the implant region (Harrison et al. 1999).

In the design of an appropriate coil, the critical movement range of the implant region should account for both elongation and compression of the spinal cord relative to the neutral (prone) position. For instance, the coils that were designed in this study for placement with the pig in neutral position should be able to accommodate at least 8.3 mm of compression and 4.1

mm of elongation (overall movement range of 12.1 mm, figure 5.5c, 5.5f). Although compression tests were not conducted in this study, future designs should include these tests as well.

The critical force limit as a coil design constraint should be lower than the minimal dislodgment forces measured in pig spinal cords (mean – 1 \*standard deviation = 25.4 mN) to ensure implant stability. Because the implanted ISMS electrodes go through the pia mater, the coils should be softer than the pia mater to minimize the electrode's micromotion in the spinal cord. The Young's modulus of the spinal cord pia mater is 2.3 MPa and the spinal cord itself has a Young's modulus of 5 kPa (Ozawa et al. 2004).

The equivalent Young's modulus of springs/coils can be calculated from (Smith 2010):

$$\frac{Force}{Coil\ cross\ sectional\ area} = E \frac{\Delta L}{L}$$

where E is the Young's modulus and L is the coil length. For instance, the equivalent Young's modulus of coil type #2 at 100% strain, is ~2 kPa which is 1150 times lower than the pia mater's modulus and 2.5 times lower than the spinal cord's modulus. Based on the results obtained in this study, coiled lead-wires can be designed to ensure mechanical stability and resemble an untethered condition of the implanted ISMS electrodes as closely as possible.

To the best of our knowledge, the dislodgment forces measured in this study are the first for any spinal cord implant in any species. Therefore, although we do not believe that these forces would be different in humans, correction factors should be used to account for potential variations between species, until measured directly. Consistency of the *in-situ* coil test outcomes with the predictions made based on the design constraints demonstrates the reliability of the

utilized methods (biomechanics and dislodgment force measurements) for the systematic design of a mechanically stable ISMS implant. These techniques may also be applied for the design of any mechanically stable neural implant.

Length changes of the spinal cord resulting from extreme movements also result in elastic deformation of the spinal cord cross-section. In order to minimize the potential effect of such disturbances to the implanted electrodes, an ideal ISMS implant should also consist of electrodes with mechanical properties matching those of the spinal cord, in addition to the lead-wire design considerations presented in the present study.

## **5.5 Conclusions**

In this study, we investigated the design constraints for a mechanically stable lumbar ISMS implant driven mainly by the design of the lead wires. In a domestic pig model, we measured the effect of hyperflexion and hyperextension movements of the thoracolumbar spine on the length changes and relative displacements of the ISMS implant region. The results suggested that domestic pigs are a suitable model for humans for testing lumbar ISMS implants. Electrode dislodgement forces were then measured in pig cadavers. These constraints were used to design a strain relief mechanism in the lead wire that can dissociate the implanted electrode from the rest of the implant.

As a proof of concept, six types of coiled lead wires were fabricated, characterized and tested in pig cadavers. These coils substantially reduced the forces transmitted to the electrode, preventing its dislodgment from the tissue. Future studies will focus on testing the long-term mechanical stability of chronically implanted ISMS systems in pigs.

## 5.6 Tables

**Table 5. 1.** Specifications of the fabricated coil types and results of bench characterization and in-situ testing in fresh pig cadavers.

Coil Type	Wire Diameter ( $\mu\text{m}$ )	Coil Diameter ( $\mu\text{m}$ )	Coil length (cm)	Mean force-displacement slope obtained from <i>bench-tests</i> (mN/cm) $\pm$ SD	Electrode status after the <i>in-situ tests</i>
1	50	800	1	$4.41 \pm 0.6$	In-place
2	25	800	1	$1.0 \pm 0.9$	In-place
3	50	500	1	$7.7 \pm 3.3$	In-place
4	25	500	1	$1.1 \pm 0.49$	In-place
5	25	200	1	$1.2 \pm 0.9$	In-place
6	50	200	1	$67.3 \pm 8.9$	Dislodged in 30% of trials

## 5.7 Figures

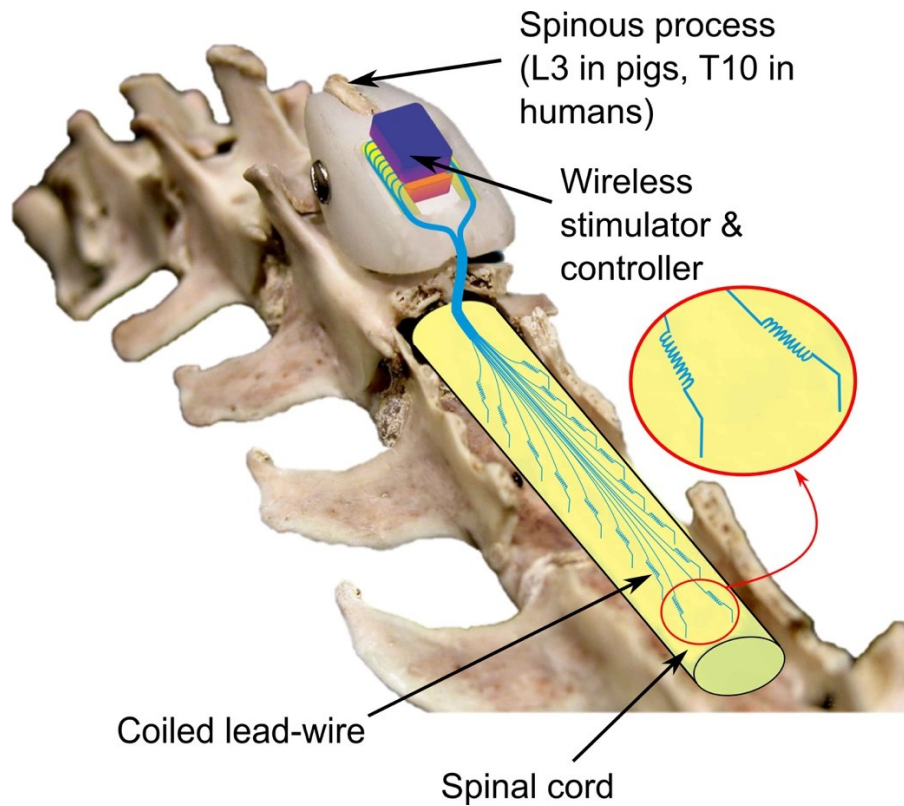
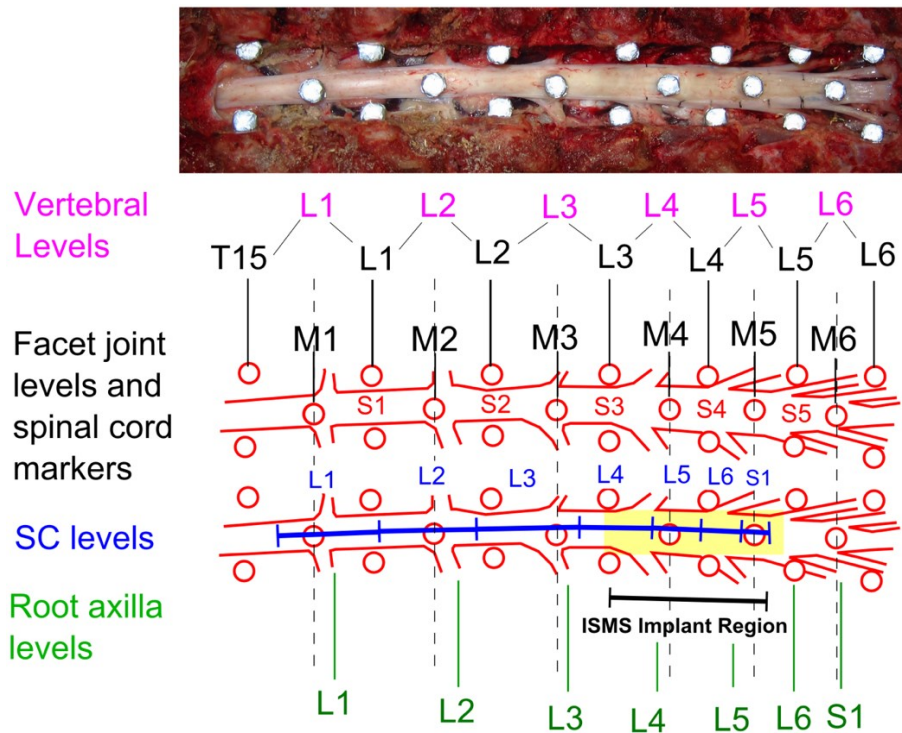
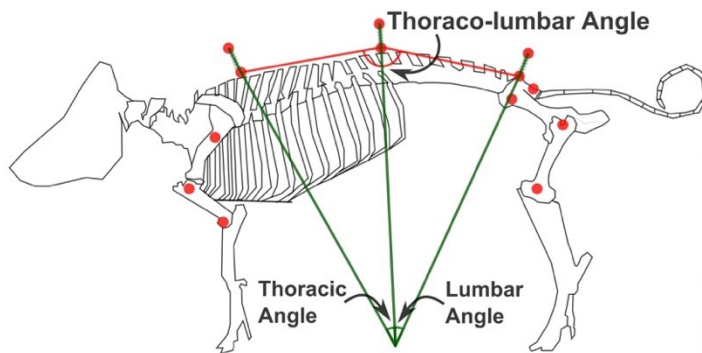


**Figure 5. 1.** Conceptual representation of an ISMS implant. The implant consists of electrodes implanted in the spinal cord with tips reaching the ventral horn, a stimulator, and lead wires connecting the electrodes to the stimulator. This study focused on incorporating a strain relief mechanism (coils) in the lead wires to minimize the effect of relative movement between the spinal column and spinal cord on the implanted electrodes.

(a)



(b)



(c)



**Figure 5. 2.** Reflective markers on the spinal cord and spinal canal. (a) Positions of reflective markers for measurements of the mechanics of the spinal column and spinal cord during physiological movements. The markers on the spinal canal were at the level of the facet joints. The spinal cord markers, placed on the dorsal surface of the spinal cord, were positioned in between the spinal canal markers (rostr-caudally). Spinal cord levels (annotated in blue) were identified by their relationship to the position of the root axilla levels. (b) Positions of the

reflective markers on the pig cadaver and definition of the measured angles. (c) Motion capture camera setup with respect to the surgical table. Six to eight cameras were used to cover a volume of about 1.5 m x 0.8 m x 0.8 m (width x height x depth). In all of the reported trials, the animal was positioned on its right side on the surgical table with the reflective markers on its spine and spinal cord facing the cameras.

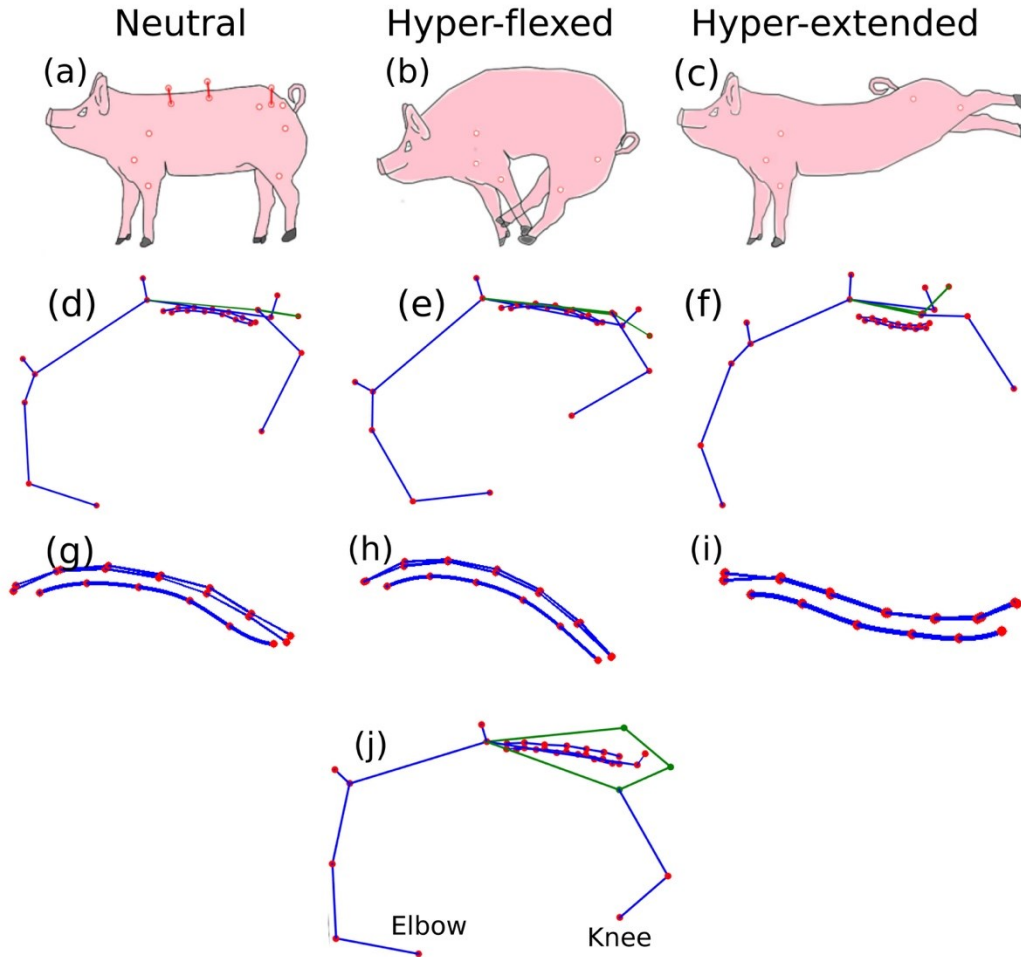


**Figure 5. 3.** Changes in marker position during movements within the physiological range of motion. (a) Spine neutral position. (b) Spine hyperflexed position reached by moving both forelimbs caudally and both hind limbs rostrally. (c) Spine hyperextended position reached by moving both hind limbs caudally and dorsally. Spinal canal reflective markers on the facet joints and spinal cord markers in the sagittal plane with the spine in the neutral (d), hyperflexed (e) and hyperextended (f) state. Close up of the spinal cord markers in the sagittal plane with the spine in the neutral state (g), hyperflexed (h) and hyperextended (i) state. (j) 3D view of the reflective markers in the neutral state. The pigs were placed on their right side on a flat surgical table for all trials.

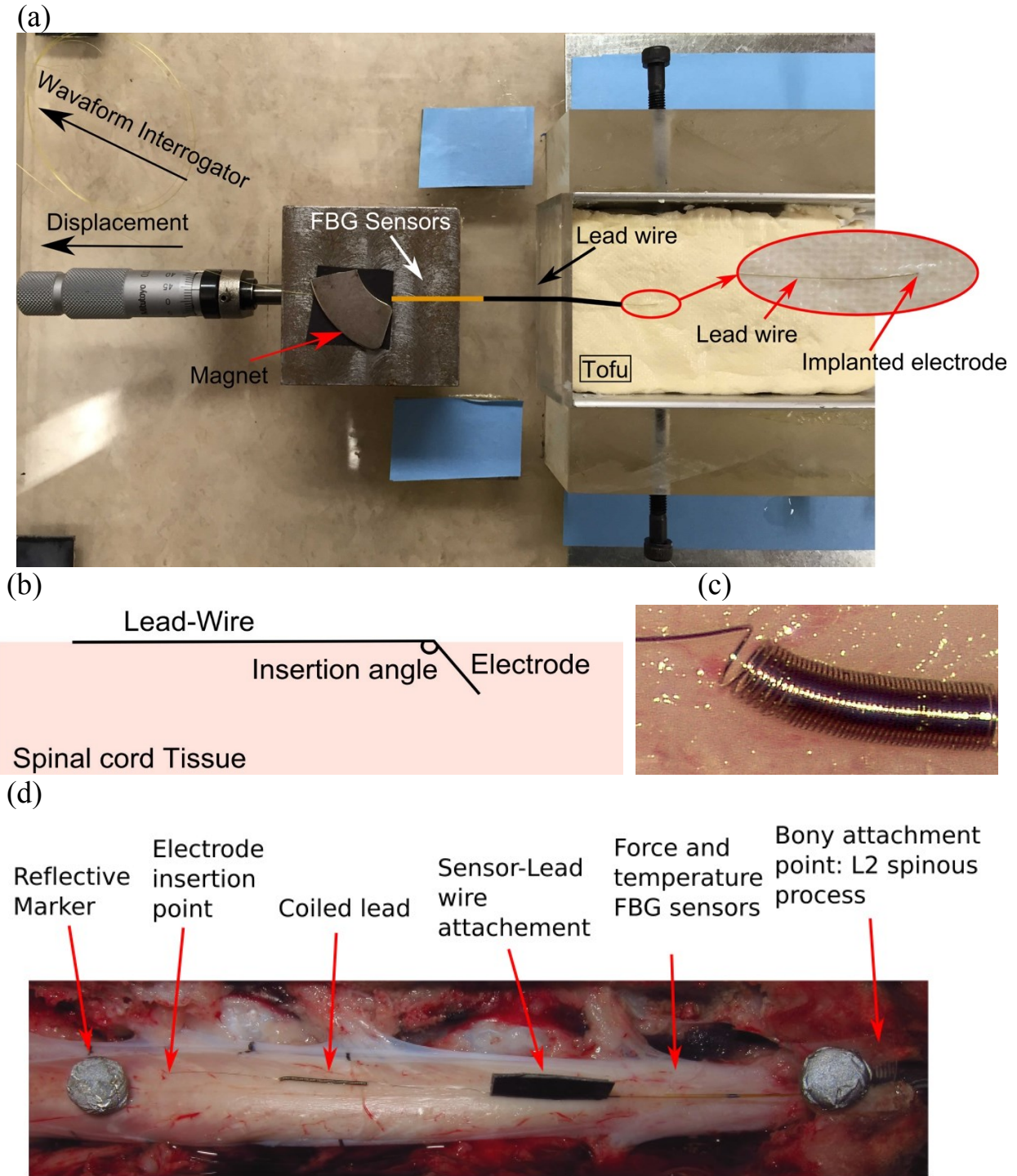


**Figure 5. 4.** Bench and in-situ setups for measurement of electrode dislodgement forces. (a) Bench testing setup shown for a dislodgment trial in Tofu – the thickness of the FBG sensor and the lead wire have been increased to improve their visibility. (b) Electrode insertion angle. (c) A

close-up image of coil type #3 lying on the dorsal surface of the spinal cord. (d) Experimental setup for testing in fresh pig cadavers. One reflective marker is placed on the lead-sensor fixation point on the bone (L2 spinous process) and another close to the insertion point of the electrode. In this example, a coil is attached in-series to an FBG sensor to measure force and another FBG sensor is also used in parallel for temperature compensation.

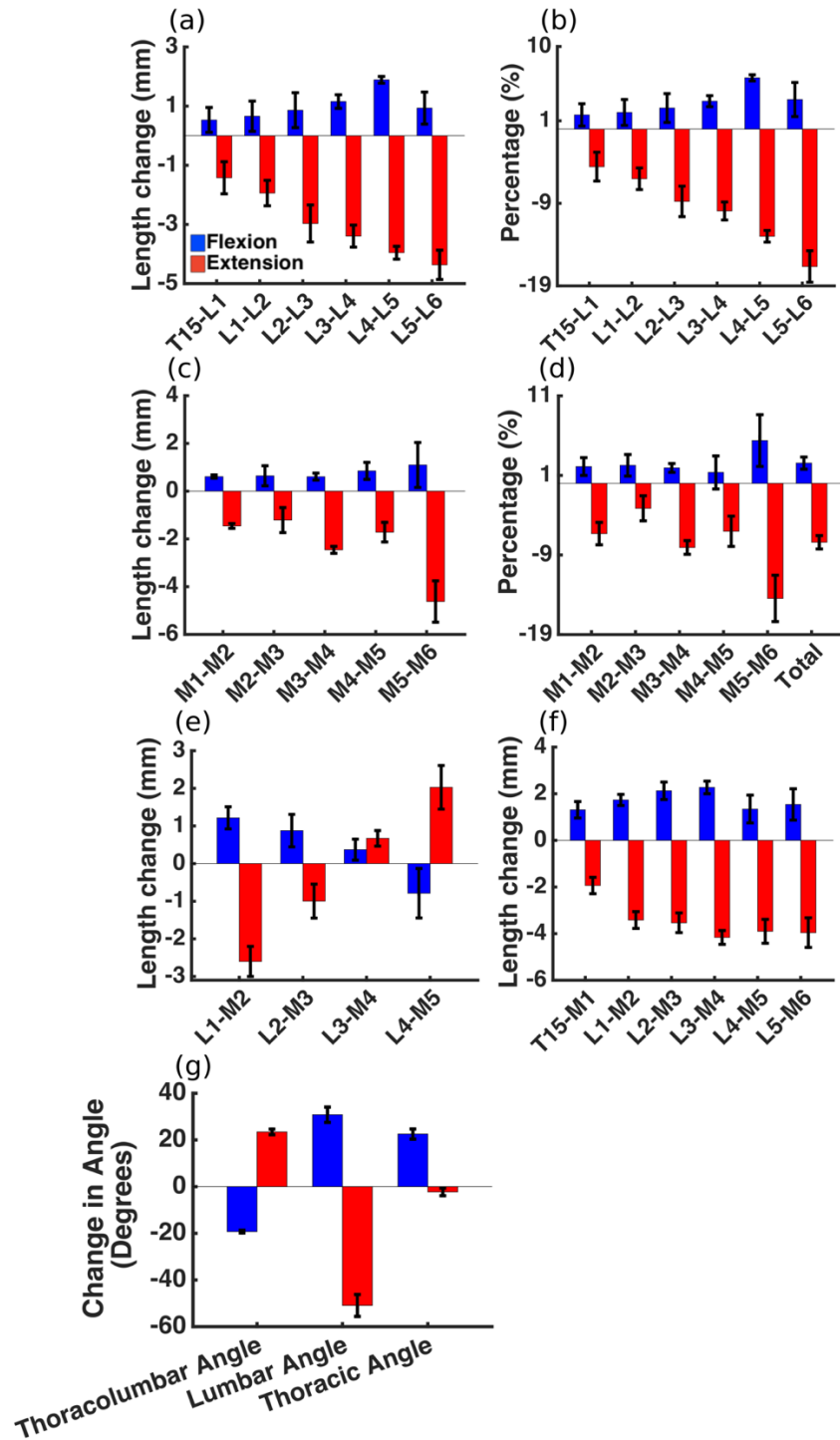


**Figure 5. 5.** Biomechanics of the lumbar spinal cord and canal in fresh pig cadavers. All of the parameters for spine flexion and extension movements were measured with respect to the pig's neutral position, and all measurements were made on the dorsal side of the spinal cord and canal.

(a) Absolute change in the length of spinal canal segments. (b) Change in the length of spinal canal segments relative to their initial length. (c) Absolute measurements of change in length of the spinal cord segments (as defined in figure 4). (d) Segmental strain of the spinal cord. (e) Projected displacement of the spinal cord and the spinal canal. This is measured as the change in the distance between the spinal cord marker and the projected position of the spinal canal marker onto the spinal cord surface. This parameter is independent of canal depth and is compatible with the classical measurement methods in literature (Wilke, Geppert, and Kienle 2011). (f) Displacement of the spinal cord and the spinal canal. This is measured by the change in the 3D distance between the spinal cord and the spinal canal markers. This parameter is more applicable to the definition of the design constraints required for an ISMS implant. (g) Measured changes in angles from neutral to hyperflexion and hyperextension. The thoracolumbar angle for neutral position was 140°.

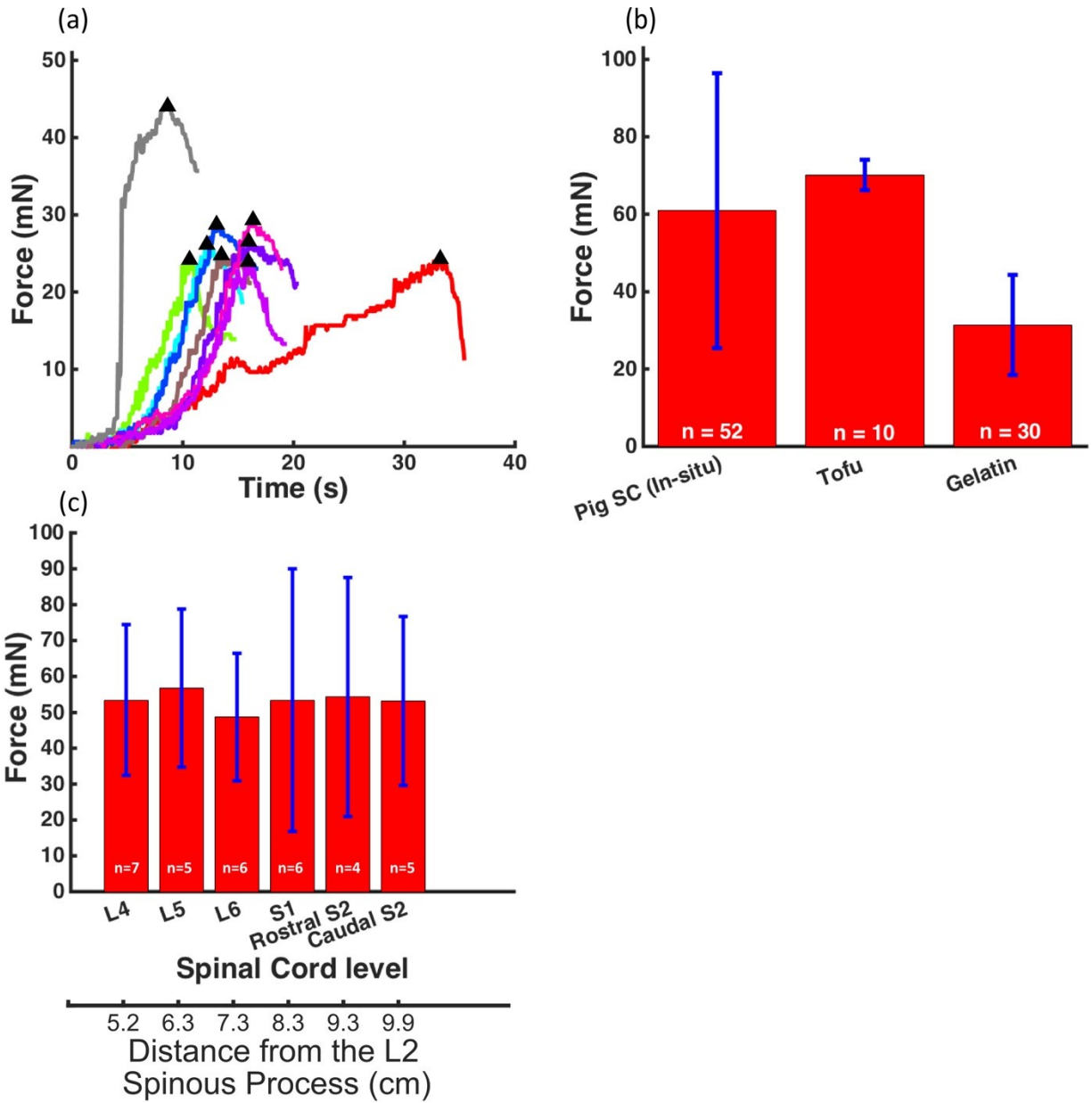


**Figure 5. 6.** Summary of electrode dislodgment forces obtained without coils in the lead wires.

(a) Raw force traces measured in gelatin surrogate spinal cords. As ‘time’ progressed in these trials, more translational movement was applied manually to the lead wires (figure 4a) causing an increase in force transmitted to the electrode, until the electrode dislodged (triangle symbols) from its implanted location. Separations of traces in x-axis represent variations in the speed of the manual displacements. (b) Average dislodgment forces in tofu and gelatin surrogate cord

materials measured in bench-top trials and in-situ in three fresh pig cadavers obtained while moving the pigs from neutral to hyperflexion (mean  $\pm$  standard error). (c) Effect of implantation location on dislodgment forces. In this experiment, electrodes were implanted in a 4.7 cm-long region of the spinal cord (L4 to S2 spinal cord levels). Implantation location did not have a significant impact on the force threshold for electrode dislodgment. 'n' is the number of trials in each experiment.

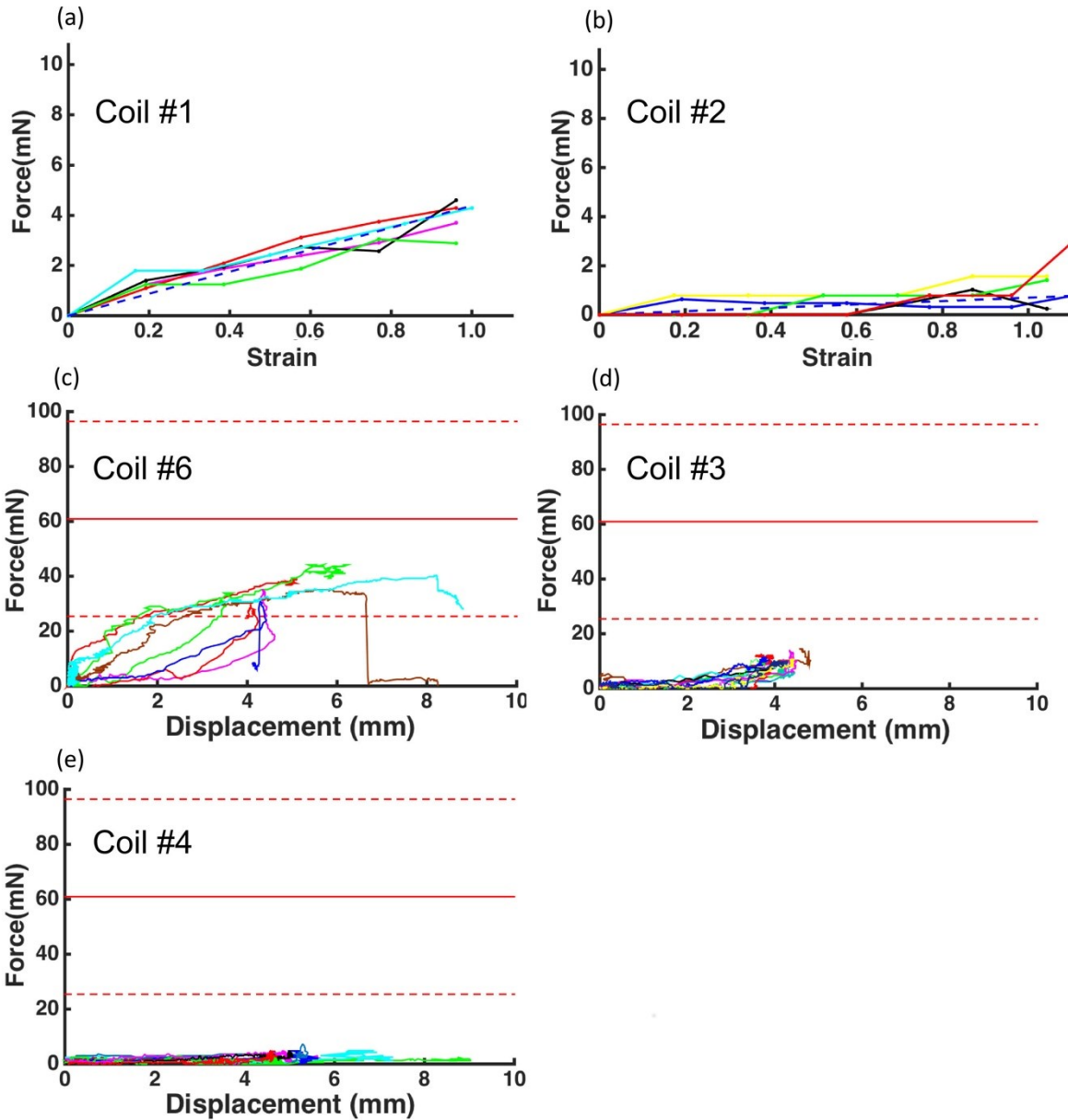


**Figure 5. 7.** Force vs. strain and displacement profiles of different coils obtained from bench and in-situ tests. (a), (b), repeated bench trials (as described in section 5.3) of type #1 (n=5) and type #2 (n=6) coils (table 1), respectively. Dashed blue lines represent the average of the linear fit-curves of each trial for that coil. (c) Example of results obtained from coils type #6 tested in-situ (n=8). Electrodes were dislodged in trials shown in brown, cyan and blue. (d) Example of results obtained from coils type #3 tested in-situ (n=10). (e) Example of results obtained from coils type

#4 tested in-situ (n=13). During in-situ tests, the pig spine was moved from neutral to hyperflexion. The horizontal red lines in (c), (d) and (e) represent the average minimal dislodgment forces measured without coils in-situ in pig cadavers, and the horizontal dashed lines represent  $\pm 1$  standard deviation from the average.

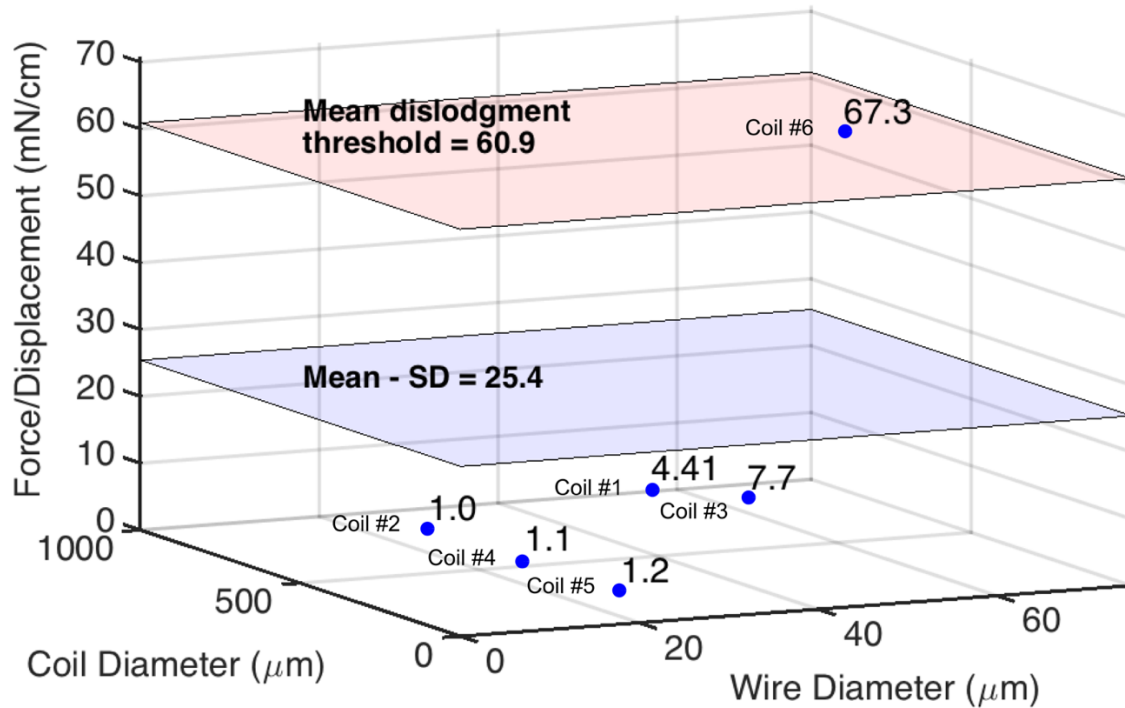


**Figure 5. 8.** Summary of coil design specifications and average *in-situ* test dislodgment outcomes. The force/displacement profiles shown in this figure are obtained from the bench tests. The red plane represents the mean electrode dislodgment forces measured without coils in pig cadavers and the blue plane shows mean - 1 \* standard deviation. All electrodes attached to coil types #1 through #5 (table 1) remained in place, while 30% of the electrodes attached to coil type #6 were dislodged when the spine moved from neutral to hyperflexion.

## **Chapter 6. General Discussions**

## 6.1 Summary and Significance

The overall goal of this thesis was to advance intraspinal microstimulation (ISMS) closer to clinical testing. The described projects addressed the requirements for intraoperative testing of ISMS in humans by developing a stereotactic setup for precise placement of implants in humans, evaluating the influence of a clinical neurosurgical anesthetic protocol on the responses to ISMS, and investigating the organization of implant targets in the spinal cord of primates. It also made contributions to the technological design of a clinical ISMS implant. Considering the aim of clinical translation, all of the studies were conducted in large animals (i.e., domestic pigs) and primates (i.e., rhesus monkeys).

The first project (chapter 2) involved the development of a stereotactic setup for precise placement of ISMS implants into the human spinal cords. The implantation targeting accuracy of microelectrodes is critical for the success of ISMS in activating the intended motor units. For this study, based on an estimation of current spread at the maximal stimulation intensities required for production of standing and walking movements, a maximal acceptable targeting error of 0.5 mm was set. Comparatively, the effective size of the smallest cross-sectional targets in the feline spinal cord is estimated to be  $\sim 0.3 \text{ mm}^2$  (tibialis anterior motoneuronal pool) (Mushahwar and Horch 2000, 1997). Assuming the effective size of motoneuronal pools is proportional to the size of the spinal cord in each species, the smallest targets would be  $\sim 0.4 \text{ mm}^2$  in humans (Sengul et al. 2012). The design goals for the setup also included safety, compatibility with existing surgical instrumentation, modularity, and ease of assembly and disassembly. Therefore, an image-guided, spine-mounted, stereotactic setup was developed that met these goals. This setup is typically mounted on existing surgical pedicle screws and provides fixation over the implant region of the spinal cord, while not allowing for relative motion between the electrode and the subject's spine.

As part of this system, intraoperative ultrasound guidance was used to assist with planning of the implantation trajectory and alignment of the microelectrode for successful targeting.

Intraoperative ultrasound imaging also provided the ability to acquire feedback during and after implantation regarding the location of the electrode tip. Using ultrasound guidance, the targeting error for locations in the ventral horns was significantly reduced and met the targeting error goal. Although this system was primarily developed and tested in domestic pigs, it was also used for experiments in rhesus monkeys (chapter 3). While the primary motivation for the development of this system was for accurate placement ISMS implants, it may also be used for precise delivery of drugs or cells into the spinal cord parenchyma.

In preparation for the first clinical testing of ISMS in the lumbosacral spinal cord, the second project (chapter 3) investigated the effect of a common neurosurgical anesthesia protocol (a total intravenous anesthesia with propofol as the main anesthetic agent) on responses to ISMS in pigs. During the implantation process, feedback from the ISMS responses (e.g., joint torques, movement kinematics, and activity of the muscles) under anesthesia are important for optimization of the locations of the ISMS microelectrodes. They are also critical for intraoperative electrophysiological mapping procedures such as the one described in chapter 3 in rhesus monkeys, where ISMS responses are the primary outcome measures of the experiment. This study demonstrated that under propofol anesthesia, ISMS can produce functional movements in the hindlimbs with large joint torques and ranges of motion. As part of this study, responses to ISMS under propofol were also compared to those produced under common preclinical anesthetic protocols (i.e., pentobarbital and isoflurane). Isoflurane anesthesia significantly suppressed all measured responses to ISMS (joint torques, range of motion, EMG amplitude) and raised the stimulation thresholds for producing movements, compared with

pentobarbital and propofol anesthesia. The responses under the propofol and pentobarbital anesthetic protocols however, were not different from each other. Collectively, these findings suggest that propofol anesthesia is a suitable protocol for clinical testing of ISMS. The substantial suppression of the responses by isoflurane anesthesia indicates that it is not a suitable protocol for procedures involving functional testing of ISMS implants. Importantly, the similarity of the ISMS responses under pentobarbital (most common preclinical anesthetic) and propofol anesthesia suggests that the results of preclinical literature of ISMS using pentobarbital anesthesia, would be comparable with those to be obtained in future clinical intraoperative tests of ISMS.

The third project (chapter 4) characterized the responses to ISMS in rhesus monkeys and obtained the functional organization of the motoneuronal pools in the lumbosacral enlargement. These experiments demonstrated that ISMS in the rhesus monkeys can produce functional single- and multi-joint synergistic movements with large ranges of motion. They also showed that similar to cats, the obtained functional map is consistent from one monkey to another. Most importantly, they showed that the relative organization of the motoneuronal pools of monkeys was similar to cats. The stimulation thresholds for evoking a movement by ISMS was also found to be similar between monkeys and cats. Collectively, these findings led to the hypothesis that not only would ISMS in the human lumbosacral spinal cord produce similar functional motor outputs in the legs, but the motoneuronal pools in humans would have a similar relative functional organization to that in animals. The obtained functional map of the lumbosacral spinal cord in monkeys along with that of the cats will guide the lumbosacral target locations in the first experiments of ISMS in the humans.

The fourth project (chapter 5) quantified the effects of gross movements of the spine on the segmental biomechanics of the lumbosacral spine and spinal cord. This study was conducted in domestic pigs given their similar spinal anatomy to humans. The study also quantified the critical force levels at which implanted electrodes dislodge from the spinal cord. Specifications for strain relief coils to prevent the dislodgment of ISMS electrodes during natural movements of the spine were proposed. Collectively, the information gained from this project informs the design of mechanically stable ISMS implants.

This study also proposed a bench-top setup for testing implant design prototypes. Dislodgment tests using this setup simulate the natural dislodgment thresholds of the spinal cord. The bench-top setup can reduce the need for time-consuming and costly animal experiments in the early design and prototyping stages of spinal cord implants.

The segmental biomechanical measurements of the spine and spinal cord also allow for the design of ISMS implants in regions of the lumbar spine other than the lumbosacral enlargement of the spinal cord. Importantly, the parameters acquired from this study may also be used for the design of neural interfaces with the spine and spinal cord other than ISMS, such as epidural (Minev et al. 2015) and intradural spinal cord stimulation implants (Howard et al. 2011).

In summary, this thesis took critical steps towards preparing for clinical intraoperative testing of ISMS, and proposed specifications and design criteria for mechanically stable ISMS implants in large animals.

## 6.2 Future Directions

One of the remaining questions in the path of clinical translation of ISMS is where should the ISMS implants be placed in the human spinal cord for functional success? In this thesis an intermediate step was taken towards answering this question by obtaining the functional map of the lumbosacral spinal cord of non-human primates and was shown that the functional maps are preserved across species (cats and monkeys). Future studies should investigate this directly in the lumbosacral enlargement of humans. This information not only can confirm the feasibility of ISMS in producing functional movements in the lower limbs of humans, but would guide the final design of human ISMS implants. These design specifications include: the layout of the microelectrode arrays (i.e., inter-electrode spacing), the length of the microelectrodes determined by the locations of ISMS targets for standing and walking in the spinal cord, and the range of stimulation intensities for producing leg movements (to guide the final design of ISMS microelectrodes and ensure long-term stimulation safety).

The clinical experiments investigating the functional organization of the spinal motoneuronal pools, will employ the developed image guided spinal stereotactic system. This system utilized a clinically available intraoperative ultrasound transducer for providing image guidance and demonstrated its effectiveness in improving the targeting accuracy of intraspinal implants. Next steps in the development of this system may include the following for improvements in performance and ease of operation: 1) Improving the resolution of intraoperative ultrasound imaging using micro-ultrasound transducers with higher imaging frequencies (Jakubovic et al. 2018). 2) Adaptation of the available technologies for real-time fusion of pre-operative magnetic resonance images (MRI) with intraoperative ultrasound to surgeries of the spinal cord (Ewertsen et al. 2013). Intraoperative access to both imaging

modalities, may improve reliability of target selection and trajectory planning before implantation of electrodes. 3) Use of computer controlled motorized micromanipulator stages. Incorporating motorized stages into the micromanipulator system design can increase the speed and accuracy of targeting (i.e., reducing possible human error).

In chapter 5, the criteria for the mechanical design of ISMS implants were provided and specifications for a mechanically stable ISMS implant design were presented. Although acute testing of the designed ISMS implants confirmed their stability in the spinal cord of fresh pig cadavers, further studies are required to evaluate the stability of the implants chronically *in-vivo*. It is also important to consider that the design criteria obtained in this study were based on measurements conducted when animals underwent extreme spine flexion and extension movements, but do not account for more complex combinatory movements of the spine. Therefore, appropriate correction factors should be used for the design parameters to incorporate a safety margin for such scenarios. Future studies may also investigate the influence of complex movements on the biomechanics of the implant region and update the criteria presented in this study. Future designs should also consider the effect of physiological mechanical perturbations, such as vibration, on the stability of the implanted electrodes.

In recent years, research into the applications of ISMS in the cervical region of the spinal cord has grown (e.g., for restoration of upper limb mobility (Zimmermann, Seki, and Jackson 2011; Jackson and Zimmermann 2012; Zimmermann and Jackson 2014; Sunshine et al. 2013) and breathing (Sunshine et al. 2018; Mercier et al. 2017)). Therefore, future studies may also employ similar methods as those used in chapter 2, for the design of mechanically stable cervical implants.

Considering that the current implementation of ISMS for restoring walking only targets the lower limb muscles, it is expected that its first clinical trials would require individuals to also use assistive devices for balance. A possible strategy to ease and improve the use of assistive devices with ISMS would be to enhance the users' trunk control and posture. This may be done by combining ISMS with techniques that improve or restore trunk stability. These include the use of implantable peripheral FES systems targeting the axial muscles (Triolo et al. 2009) or rehabilitation paradigms involving epidural stimulation (Angeli et al. 2018).

Finally, given that all preclinical models of ISMS research were quadrupedal animals, the ISMS controller design would also require modifications to enable human bipedal walking. Early clinical trials of chronic ISMS implants are expected to focus on this aim.

# Bibliography

- “First Steps Wellness Centre.” n.d. Accessed August 10, 2018. <http://www.fswcregina.ca/>.
- “Functional Electrical Stimulation Exercise - The Steadward Centre for Personal & Physical Achievement.” n.d. Accessed August 10, 2018. <https://www.ualberta.ca/steadward-centre/programs-and-registration/functional-electrical-stimulation-exercise>.
- “ReWalk™ Personal Exoskeleton System Cleared by FDA for Home Use.” 2014. ReWalk – More Than Walking. May 20, 2014. <http://rewalk.com/rewalk-robotics-announces-expansion-to-india-with-saimed-innovations-2-2-2-2-3-2-3/>.
- “Tuohy Epidural Needle, Pain Management | Smiths Medical.” n.d. Accessed August 27, 2018. <https://www.smiths-medical.com/products/pain-management/epidural-anesthesia/tuohy-epidural-needle>.
- “WHO | Metrics: Disability-Adjusted Life Year (DALY).” n.d. Accessed July 24, 2018. [http://www.who.int/healthinfo/global\\_burden\\_disease/metrics\\_daly/en/](http://www.who.int/healthinfo/global_burden_disease/metrics_daly/en/).
- “WHO | Spinal Cord Injury.” 2013. WHO. November 19, 2013. <http://www.who.int/mediacentre/factsheets/fs384/en/>.
- Adam, H. K., J. B. Glen, and P. A. Hoyle. 1980. “Pharmacokinetics in Laboratory Animals of ICI 35 868, a New i.v. Anaesthetic Agent.” *British Journal of Anaesthesia* 52 (8): 743–46.
- Ahn, Henry, Christopher S. Bailey, Carly S. Rivers, Vanessa K. Noonan, Eve C. Tsai, Daryl R. Fourney, Najmedden Attabib, et al. 2015. “Effect of Older Age on Treatment Decisions and Outcomes among Patients with Traumatic Spinal Cord Injury.” *CMAJ: Canadian Medical Association Journal* 187 (12): 873–80. <https://doi.org/10.1503/cmaj.150085>.
- Alexeeva, Natalia, Carol Sames, Patrick L. Jacobs, Lori Hobday, Marcello M. Distasio, Sarah A. Mitchell, and Blair Calancie. 2011. “Comparison of Training Methods to Improve Walking

- in Persons with Chronic Spinal Cord Injury: A Randomized Clinical Trial.” *The Journal of Spinal Cord Medicine* 34 (4): 362–79. <https://doi.org/10.1179/2045772311Y.0000000018>.
- Ama, Antonio J. del, Juan C. Moreno, Ángel Gil-Agudo, and José L. Pons. 2013. “Hybrid FES-Robot Cooperative Control of Ambulatory Gait Rehabilitation Exoskeleton for Spinal Cord Injured Users.” In *Converging Clinical and Engineering Research on Neurorehabilitation*, 155–59. Biosystems & Biorobotics. Springer, Berlin, Heidelberg. [https://doi.org/10.1007/978-3-642-34546-3\\_25](https://doi.org/10.1007/978-3-642-34546-3_25).
- Anderson, Kim D. 2004. “Targeting Recovery: Priorities of the Spinal Cord-Injured Population.” *Journal of Neurotrauma* 21 (10): 1371–83.
- Angeli, Claudia A., Maxwell Boakye, Rebekah A. Morton, Justin Vogt, Kristin Benton, Yangshen Chen, Christie K. Ferreira, and Susan J. Harkema. 2018. “Recovery of Over-Ground Walking after Chronic Motor Complete Spinal Cord Injury.” *New England Journal of Medicine* 379 (13): 1244–50. <https://doi.org/10.1056/NEJMoa1803588>.
- Angeli, Claudia A., V. Reggie Edgerton, Yury P. Gerasimenko, and Susan J. Harkema. 2014. “Altering Spinal Cord Excitability Enables Voluntary Movements after Chronic Complete Paralysis in Humans.” *Brain*, April, awu038. <https://doi.org/10.1093/brain/awu038>.
- Antognini, J. F., X. W. Wang, M. Piercy, and E. Carstens. 2000. “Propofol Directly Depresses Lumbar Dorsal Horn Neuronal Responses to Noxious Stimulation in Goats.” *Canadian Journal of Anaesthesia = Journal Canadien D’anesthesie* 47 (3): 273–79. <https://doi.org/10.1007/BF03018926>.
- Aoyagi, Y., V. K. Mushahwar, R. B. Stein, and A. Prochazka. 2004. “Movements Elicited by Electrical Stimulation of Muscles, Nerves, Intermediate Spinal Cord, and Spinal Roots in

Anesthetized and Decerebrate Cats.” *IEEE Transactions on Neural Systems and Rehabilitation Engineering* 12 (1): 1–11. <https://doi.org/10.1109/TNSRE.2003.823268>.

Arango-Lasprilla, Juan Carlos, Jessica M. Ketchum, Angela Starkweather, Elizabeth Nicholls, and Amber R. Wilk. 2011. “Factors Predicting Depression among Persons with Spinal Cord Injury 1 to 5 Years Post Injury.” *NeuroRehabilitation* 29 (1): 9–21. <https://doi.org/10.3233/NRE-2011-0672>.

Arango-Lasprilla, Juan Carlos, Silvia Leonor Olivera Plaza, Allison Drew, Jose Libardo Perdomo Romero, Jose Anselmo Arango Pizarro, Kathryn Francis, and Jeffrey Kreutzer. 2010. “Family Needs and Psychosocial Functioning of Caregivers of Individuals with Spinal Cord Injury from Colombia, South America.” *NeuroRehabilitation* 27 (1): 83–93. <https://doi.org/10.3233/NRE-2010-0583>.

Arazpour, M, M A Bani, S W Hutchins, and R K Jones. 2013. “The Physiological Cost Index of Walking with Mechanical and Powered Gait Orthosis in Patients with Spinal Cord Injury.” *Spinal Cord* 51 (5): 356–59. <https://doi.org/10.1038/sc.2012.162>.

Arazpour, Mokhtar, Monireh Ahmadi Bani, and Stephen W. Hutchins. 2013. “Reciprocal Gait Orthoses and Powered Gait Orthoses for Walking by Spinal Cord Injury Patients.” *Prosthetics and Orthotics International* 37 (1): 14–21. <https://doi.org/10.1177/0309364612444665>.

Baars, J. H., S Tas, K. F. Herold, D. A. Hadzidiakos, and B Rehberg. 2006. “The Suppression of Spinal F-Waves by Propofol Does Not Predict Immobility to Painful Stimuli in Humans†.” *British Journal of Anaesthesia* 96 (1): 118–26. <https://doi.org/10.1093/bja/aei283>.

- Baars, Jan H., Falk von Dincklage, Josephine Reiche, and Benno Rehberg. 2006. "Propofol Increases Presynaptic Inhibition of Ia Afferents in the Intact Human Spinal Cord." *Anesthesiology: The Journal of the American Society of Anesthesiologists* 104 (4): 798–804.
- Baars, Jan H., Michael Benzke, Falk von Dincklage, Josephine Reiche, Peter Schlattmann, and Benno Rehberg. 2007. "Presynaptic and Postsynaptic Effects of the Anesthetics Sevoflurane and Nitrous Oxide in the Human Spinal Cord:" *Anesthesiology* 107 (4): 553–62.  
<https://doi.org/10.1097/01.anes.0000282099.30437.46>.
- Baars, Jan H., René Mager, Katharina Dankert, Mark Hackbarth, Falk von Dincklage, and Benno Rehberg. 2009. "Effects of Sevoflurane and Propofol on the Nociceptive Withdrawal Reflex and on the H Reflex." *Anesthesiology: The Journal of the American Society of Anesthesiologists* 111 (1): 72–81. <https://doi.org/10.1097/ALN.0b013e3181a4c706>.
- Badia, Jordi, Tim Boretius, David Andreu, Christine Azevedo-Coste, Thomas Stieglitz, and Xavier Navarro. 2011. "Comparative Analysis of Transverse Intrafascicular Multichannel, Longitudinal Intrafascicular and Multipolar Cuff Electrodes for the Selective Stimulation of Nerve Fascicles." *Journal of Neural Engineering* 8 (3): 036023.  
<https://doi.org/10.1088/1741-2560/8/3/036023>.
- Bagshaw, E. V., and M. H. Evans. 1976. "Measurement of Current Spread from Microelectrodes When Stimulating within the Nervous System." *Experimental Brain Research* 25 (4): 391–400.
- Bailey, J. M. 1997. "Context-Sensitive Half-Times and Other Decrement Times of Inhaled Anesthetics." *Anesthesia and Analgesia* 85 (3): 681–86.

- Baldi, James C., R. D. Jackson, Rich Moraille, and W. Jerry Mysiw. 1998. "Muscle Atrophy Is Prevented in Patients with Acute Spinal Cord Injury Using Functional Electrical Stimulation." *Spinal Cord* 36 (7): 463–69. <https://doi.org/10.1038/sj.sc.3100679>.
- Bamford, J. A., C. T. Putman, and V. K. Mushahwar. 2005. "Intraspinal Microstimulation Preferentially Recruits Fatigue-Resistant Muscle Fibres and Generates Gradual Force in Rat." *The Journal of Physiology* 569 (3): 873–84. <https://doi.org/10.1113/jphysiol.2005.094516>.
- Bamford, Jeremy A., and Vivian K. Mushahwar. 2011. "Intraspinal Microstimulation for the Recovery of Function Following Spinal Cord Injury." *Progress in Brain Research* 194: 227–39. <https://doi.org/10.1016/B978-0-444-53815-4.00004-2>.
- Bamford, Jeremy A., Kathryn G. Todd, and Vivian K. Mushahwar. 2010. "The Effects of Intraspinal Microstimulation on Spinal Cord Tissue in the Rat." *Biomaterials* 31 (21): 5552–63. <https://doi.org/10.1016/j.biomaterials.2010.03.051>.
- Bamford, Jeremy A., R. Marc Lebel, Kian Parseyan, and Vivian K. Mushahwar. 2016. "The Fabrication, Implantation and Stability of Intraspinal Microwire Arrays in the Spinal Cord of Cat and Rat." *Transactions on Neural Systems & Rehabilitation Engineering*.
- Baratta, R., M. Solomonow, B. H. Zhou, D. Letson, R. Chuinard, and R. D'Ambrosia. 1988. "Muscular Coactivation: The Role of the Antagonist Musculature in Maintaining Knee Stability." *The American Journal of Sports Medicine* 16 (2): 113–22. <https://doi.org/10.1177/036354658801600205>.
- Barbeau, H., and S. Rossignol. 1987. "Recovery of Locomotion after Chronic Spinalization in the Adult Cat." *Brain Research* 412 (1): 84–95.

- Barolat, G., J. B. Myklebust, and W. Wenninger. 1988. "Effects of Spinal Cord Stimulation on Spasticity and Spasms Secondary to Myelopathy." *Applied Neurophysiology* 51 (1): 29–44.
- Barolat, Giancarlo, Fulvio Massaro, Jiping He, Sergio Zeme, and Beth Ketcik. 1993. "Mapping of Sensory Responses to Epidural Stimulation of the Intraspinal Neural Structures in Man." *Journal of Neurosurgery* 78 (2): 233–39. <https://doi.org/10.3171/jns.1993.78.2.0233>.
- Barss, Trevor S., Emily N. Ainsley, Francisca C. Claveria-Gonzalez, M. John Luu, Dylan J. Miller, Matheus J. Wiest, and David F. Collins. 2018. "Utilizing Physiological Principles of Motor Unit Recruitment to Reduce Fatigability of Electrically-Evoked Contractions: A Narrative Review." *Archives of Physical Medicine and Rehabilitation* 99 (4): 779–91. <https://doi.org/10.1016/j.apmr.2017.08.478>.
- Baumgart, Joel P., Zhen-Yu Zhou, Masato Hara, Daniel C. Cook, Michael B. Hoppa, Timothy A. Ryan, and Hugh C. Hemmings. 2015. "Isoflurane Inhibits Synaptic Vesicle Exocytosis through Reduced Ca<sup>2+</sup> Influx, Not Ca<sup>2+</sup>-Exocytosis Coupling." *Proceedings of the National Academy of Sciences of the United States of America* 112 (38): 11959–64. <https://doi.org/10.1073/pnas.1500525112>.
- Behrman, Andrea L., and Susan J. Harkema. 2007. "Physical Rehabilitation as an Agent for Recovery after Spinal Cord Injury." *Physical Medicine and Rehabilitation Clinics of North America* 18 (2): 183–202, v. <https://doi.org/10.1016/j.pmr.2007.02.002>.
- Benavides, Francisco D., Andrea J. Santamaria, Nikita Bodoukhin, Luis G. Guada, Juan P. Solano, and James D. Guest. 2016. "Characterization of Motor and Somatosensory Evoked Potentials in the Yucatan Micropig Using Transcranial and Epidural Stimulation." *Journal of Neurotrauma* 34 (18): 2595–2608. <https://doi.org/10.1089/neu.2016.4511>.

- Benevento, Barbara T., and Marca L. Sipski. 2002. "Neurogenic Bladder, Neurogenic Bowel, and Sexual Dysfunction in People With Spinal Cord Injury." *Physical Therapy* 82 (6): 601–12. <https://doi.org/10.1093/ptj/82.6.601>.
- Bergquist, Austin J., Matheus J. Wiest, Yoshino Okuma, and David F. Collins. 2017. "Interleaved Neuromuscular Electrical Stimulation after Spinal Cord Injury." *Muscle & Nerve* 56 (5): 989–93. <https://doi.org/10.1002/mus.25634>.
- Bergquist, Austin J., Matheus J. Wiest, Yoshino Okuma, and David F. Collins. 2014. "H-Reflexes Reduce Fatigue of Evoked Contractions after Spinal Cord Injury." *Muscle & Nerve* 50 (2): 224–34. <https://doi.org/10.1002/mus.24144>.
- Berlowitz, David J., Brooke Wadsworth, and Jack Ross. 2016. "Respiratory Problems and Management in People with Spinal Cord Injury." *Breathe* 12 (4): 328–40. <https://doi.org/10.1183/20734735.012616>.
- Bernardi, M., I. Canale, V. Castellano, L. Di Filippo, F. Felici, and M. Marchetti. 1995. "The Efficiency of Walking of Paraplegic Patients Using a Reciprocating Gait Orthosis." *Spinal Cord* 33 (7): 409–15. <https://doi.org/10.1038/sc.1995.91>.
- Bijak, Manfred, Monika Rakos, Christian Hofer, Winfried Mayr, Maria Strohhofer, Doris Raschka, and Helmut Kern. 2005. "Stimulation Parameter Optimization for FES Supported Standing up and Walking in SCI Patients." *Artificial Organs* 29 (3): 220–23. <https://doi.org/10.1111/j.1525-1594.2005.29039.x>.
- Biran, Roy, Dave C. Martin, and Patrick A. Tresco. 2007. "The Brain Tissue Response to Implanted Silicon Microelectrode Arrays Is Increased When the Device Is Tethered to the Skull." *Journal of Biomedical Materials Research. Part A* 82 (1): 169–78. <https://doi.org/10.1002/jbm.a.31138>.

- Bizzi, Emilio, and Vincent CK Cheung. 2013. "The Neural Origin of Muscle Synergies." *Frontiers in Computational Neuroscience* 7. <https://doi.org/10.3389/fncom.2013.00051>.
- Blanquer, Miguel, Miguel Angel Pérez-Espejo, Juan F. Martínez-Lage, Francisca Iniesta, Salvador Martinez, and Jose M. Moraleda. 2010. "A Surgical Technique of Spinal Cord Cell Transplantation in Amyotrophic Lateral Sclerosis." *Journal of Neuroscience Methods* 191 (2): 255–57. <https://doi.org/10.1016/j.jneumeth.2010.06.014>.
- Boretius, Tim, Jordi Badia, Aran Pascual-Font, Martin Schuettler, Xavier Navarro, Ken Yoshida, and Thomas Stieglitz. 2010. "A Transverse Intrafascicular Multichannel Electrode (TIME) to Interface with the Peripheral Nerve." *Biosensors and Bioelectronics* 26 (1): 62–69. <https://doi.org/10.1016/j.bios.2010.05.010>.
- Borrell, Jordan A., Shawn B. Frost, Jeremy Peterson, and Randolph J. Nudo. 2017. "A 3D Map of the Hindlimb Motor Representation in the Lumbar Spinal Cord in Sprague Dawley Rats." *Journal of Neural Engineering* 14 (1): 016007. <https://doi.org/10.1088/1741-2552/14/1/016007>.
- Bostock, H, and J C Rothwell. 1997. "Latent Addition in Motor and Sensory Fibres of Human Peripheral Nerve." *The Journal of Physiology* 498 (Pt 1): 277–94.
- Braz, G. P., M. Russold, R. M. Smith, and G. M. Davis. 2009. "Efficacy and Stability Performance of Traditional versus Motion Sensor-Assisted Strategies for FES Standing." *Journal of Biomechanics* 42 (9): 1332–38. <https://doi.org/10.1016/j.jbiomech.2009.03.003>.
- Brissot, Régine, Philippe Gallien, Marie-Pierre Le Bot, Anne Beubras, Dominique Laisné, Jocelyne Beillot, and Josette Dassonville. 2000. "Clinical Experience With Functional Electrical Stimulation-Assisted Gait With Parastep in Spinal Cord–Injured Patients." *Spine* 25 (4): 501.

- Burnham, R., T. Martin, R. Stein, G. Bell, I. MacLean, and R. Steadward. 1997. "Skeletal Muscle Fibre Type Transformation Following Spinal Cord Injury." *Spinal Cord* 35 (2): 86–91.
- Busscher, Iris, Joris J. W. Ploegmakers, Gijsbertus J. Verkerke, and Albert G. Veldhuizen. 2010. "Comparative Anatomical Dimensions of the Complete Human and Porcine Spine." *European Spine Journal* 19 (7): 1104–14. <https://doi.org/10.1007/s00586-010-1326-9>.
- Butler, P. B., R. E. Major, and J. H. Patrick. 1984. "The Technique of Reciprocal Walking Using the Hip Guidance Orthosis (Hgo) with Crutches." *Prosthetics and Orthotics International* 8 (1): 33–38. <https://doi.org/10.3109/03093648409145343>.
- Byrne, D. W., and C. A. Salzberg. 1996. "Major Risk Factors for Pressure Ulcers in the Spinal Cord Disabled: A Literature Review." *Spinal Cord* 34 (5): 255–63. <https://doi.org/10.1038/sc.1996.46>.
- Calancie, Blair, K. John Klose, Sylvia Baier, and Barth A. Green. 1991. "Isoflurane-Induced Attenuation of Motor Evoked Potentials Caused by Electrical Motor Cortex Stimulation during Surgery." *Journal of Neurosurgery* 74 (6): 897–904. <https://doi.org/10.3171/jns.1991.74.6.0897>.
- Capogrosso, Marco, Nikolaus Wenger, Stanisa Raspopovic, Pavel Musienko, Janine Beauparlant, Lorenzo Bassi Luciani, Grégoire Courtine, and Silvestro Micera. 2013. "A Computational Model for Epidural Electrical Stimulation of Spinal Sensorimotor Circuits." *The Journal of Neuroscience: The Official Journal of the Society for Neuroscience* 33 (49): 19326–40. <https://doi.org/10.1523/JNEUROSCI.1688-13.2013>.
- Capogrosso, Marco, Tomislav Milekovic, David Borton, Fabien Wagner, Eduardo Martin Moraud, Jean-Baptiste Mignardot, Nicolas Buse, et al. 2016. "A Brain–Spine Interface

- Alleviating Gait Deficits after Spinal Cord Injury in Primates.” *Nature* 539 (7628): 284.  
<https://doi.org/10.1038/nature20118>.
- Chakrabarti, Rajkalyan, Mahmood Ghazanwy, and Anurag Tewari. 2014. “Anesthetic Challenges for Deep Brain Stimulation: A Systematic Approach.” *North American Journal of Medical Sciences* 6 (8): 359–69. <https://doi.org/10.4103/1947-2714.139281>.
- Chan, R. C. K., P. W. H. Lee, and F. Lieh-Mak. 2000. “Coping with Spinal Cord Injury: Personal and Marital Adjustment in the Hong Kong Chinese Setting.” *Spinal Cord* 38 (11): 687–96. <https://doi.org/10.1038/sj.sc.3101085>.
- Charlifue, Susan W., and Kenneth A. Gerhart. 1991. “Behavioral and Demographic Predictors of Suicide after Traumatic Spinal Cord Injury.” *Archives of Physical Medicine and Rehabilitation* 72 (7): 488–92. <https://doi.org/10.5555/uri:pii:000399939190193M>.
- Cheng, Cheng, Jonn Kmech, Vivian K. Mushahwar, and Anastasia L. Elias. 2013. “Development of Surrogate Spinal Cords for the Evaluation of Electrode Arrays Used in Intraspinal Implants.” *IEEE Transactions on Bio-Medical Engineering* 60 (6): 1667–76.  
<https://doi.org/10.1109/TBME.2013.2241061>.
- Clair, Joanna M., Jamie M. Anderson-Reid, Caitlin M. Graham, and David F. Collins. 2011. “Postactivation Depression and Recovery of Reflex Transmission during Repetitive Electrical Stimulation of the Human Tibial Nerve.” *Journal of Neurophysiology* 106 (1): 184–92. <https://doi.org/10.1152/jn.00932.2010>.
- Coburn, B. 1980. “Electrical Stimulation of the Spinal Cord: Two-Dimensional Finite Element Analysis with Particular Reference to Epidural Electrodes.” *Medical and Biological Engineering and Computing* 18 (5): 573–84. <https://doi.org/10.1007/BF02443129>.

- Coburn, Barry, and Wing Kee Sin. 1985. "A Theoretical Study of Epidural Electrical Stimulation of the Spinal Cord Part I: Finite Element Analysis of Stimulus Fields." *IEEE Transactions on Biomedical Engineering* BME-32 (11): 971–77.  
<https://doi.org/10.1109/TBME.1985.325648>.
- Coburn, Barry. 1985. "A Theoretical Study of Epidural Electrical Stimulation of the Spinal Cord - Part II: Effects on Long Myelinated Fibers." *IEEE Transactions on Biomedical Engineering* BME-32 (11): 978–86. <https://doi.org/10.1109/TBME.1985.325649>.
- Cogan, Stuart F. 2008. "Neural Stimulation and Recording Electrodes." *Annual Review of Biomedical Engineering* 10: 275–309.  
<https://doi.org/10.1146/annurev.bioeng.10.061807.160518>.
- Collinger, Jennifer L., Michael L. Boninger, Tim M. Bruns, Kenneth Curley, Wei Wang, and Douglas J. Weber. 2013. "Functional Priorities, Assistive Technology, and Brain-Computer Interfaces after Spinal Cord Injury." *Journal of Rehabilitation Research and Development* 50 (2): 145–60.
- Contreras-Vidal, Jose L., Nikunj A Bhagat, Justin Brantley, Jesus G. Cruz-Garza, Yongtian He, Quinn Manley, Sho Nakagome, et al. 2016. "Powered Exoskeletons for Bipedal Locomotion after Spinal Cord Injury." *Journal of Neural Engineering* 13 (3): 031001.  
<https://doi.org/10.1088/1741-2560/13/3/031001>.
- Courtine, Grégoire, Roland R. Roy, John Hodgson, Heather McKay, Joseph Raven, Hui Zhong, Hong Yang, Mark H. Tuszynski, and V. Reggie Edgerton. 2005. "Kinematic and EMG Determinants in Quadrupedal Locomotion of a Non-Human Primate (Rhesus)." *Journal of Neurophysiology* 93 (6): 3127–45. <https://doi.org/10.1152/jn.01073.2004>.

- Crone, C., and J. Nielsen. 1989. "Methodological Implications of the Post Activation Depression of the Soleus H-Reflex in Man." *Experimental Brain Research* 78 (1): 28–32.  
<https://doi.org/10.1007/BF00230683>.
- Davis, R., J. Patrick, and A. Barriskill. 2001. "Development of Functional Electrical Stimulators Utilizing Cochlear Implant Technology." *Medical Engineering & Physics* 23 (1): 61–68.
- Dennison, Christopher R., Peter M. Wild, David R. Wilson, and Michael K. Gilbart. 2010. "An In-Fiber Bragg Grating Sensor for Contact Force and Stress Measurements in Articular Joints." *Measurement Science and Technology* 21 (11): 115803.  
<https://doi.org/10.1088/0957-0233/21/11/115803>.
- Dennison, Christopher R., Peter M. Wild, David R. Wilson, and Peter A. Crompton. 2008. "A Minimally Invasive In-Fiber Bragg Grating Sensor for Intervertebral Disc Pressure Measurements." *Measurement Science and Technology* 19 (8): 085201.  
<https://doi.org/10.1088/0957-0233/19/8/085201>.
- DeVivo, M. J., P. L. Kartus, R. D. Rutt, S. L. Stover, and P. R. Fine. 1990. "The Influence of Age at Time of Spinal Cord Injury on Rehabilitation Outcome." *Archives of Neurology* 47 (6): 687–91.
- DeVivo, Michael J., La Verne N. Hawkins, J. Scott Richards, and Bette K. Go. 1995. "Outcomes of Post-Spinal Cord Injury Marriages." *Archives of Physical Medicine and Rehabilitation* 76 (2): 130–38. [https://doi.org/10.1016/S0003-9993\(95\)80022-0](https://doi.org/10.1016/S0003-9993(95)80022-0).
- DeWald, Christopher J., and Thomas Stanley. 2006. "Instrumentation-Related Complications of Multilevel Fusions for Adult Spinal Deformity Patients over Age 65: Surgical Considerations and Treatment Options in Patients with Poor Bone Quality." *Spine* 31 (19 Suppl): S144-151. <https://doi.org/10.1097/01.brs.0000236893.65878.39>.

- Dietz, Volker, and Roland Müller. 2004. "Degradation of Neuronal Function Following a Spinal Cord Injury: Mechanisms and Countermeasures." *Brain: A Journal of Neurology* 127 (Pt 10): 2221–31. <https://doi.org/10.1093/brain/awh255>.
- Dimitrijevic, Milan R., Yuri Gerasimenko, and Michaela M. Pinter. 1998. "Evidence for a Spinal Central Pattern Generator in Humans." *Annals of the New York Academy of Sciences* 860 (1): 360–76. <https://doi.org/10.1111/j.1749-6632.1998.tb09062.x>.
- Ditor, D. S., M. J. Macdonald, M. V. Kamath, J. Bugaresti, M. Adams, N. McCartney, and A. L. Hicks. 2005. "The Effects of Body-Weight Supported Treadmill Training on Cardiovascular Regulation in Individuals with Motor-Complete SCI." *Spinal Cord* 43 (11): 664–73. <https://doi.org/10.1038/sj.sc.3101785>.
- Dobkin, B, D. Apple, H. Barbeau, M. Basso, A. Behrman, D. Deforge, J. Ditunno, et al. 2006. "Weight-Supported Treadmill vs over-Ground Training for Walking after Acute Incomplete SCI." *Neurology* 66 (4): 484–93. <https://doi.org/10.1212/01.wnl.0000202600.72018.39>.
- Donaldson, N., T. A. Perkins, R. Fitzwater, D. E. Wood, and F. Middleton. 2000. "FES Cycling May Promote Recovery of Leg Function after Incomplete Spinal Cord Injury." *Spinal Cord* 38 (11): 680–82. <https://doi.org/10.1038/sj.sc.3101072>.
- Doty, F. D., G. Entzminger, and C. D. Hauck. 1999. "Error-Tolerant RF Litz Coils for NMR/MRI." *Journal of Magnetic Resonance (San Diego, Calif.: 1997)* 140 (1): 17–31. <https://doi.org/10.1006/jmre.1999.1828>.
- Douglas, R., P. F. Larson, R. D'Ambrosia, and R. E. McCall. 1983. "The LSU Reciprocation-Gait Orthosis." *Orthopedics* 6 (7): 834–39. <https://doi.org/10.3928/0147-7447-19830701-05>.

- Dueck, Michael H., Aloys Oberthuer, Christoph Wedekind, Matthias Paul, and Ulf Boerner. 2003. "Propofol Impairs the Central but Not the Peripheral Part of the Motor System." *Anesthesia & Analgesia* 96 (2): 449. <https://doi.org/10.1213/00000539-200302000-00029>.
- Dwyer, R., H. L. Bennett, E. I. Eger, and D. Heilbron. 1992. "Effects of Isoflurane and Nitrous Oxide in Subanesthetic Concentrations on Memory and Responsiveness in Volunteers." *Anesthesiology: The Journal of the American Society of Anesthesiologists* 77 (5): 888–98.
- Edgerton, Victor Reggie, and Susan Harkema. 2011. "Epidural Stimulation of the Spinal Cord in Spinal Cord Injury: Current Status and Future Challenges." *Expert Review of Neurotherapeutics* 11 (10): 1351–53. <https://doi.org/10.1586/ern.11.129>.
- Eger, Edmond I., and Steven L. Shafer. 2005. "Tutorial: Context-Sensitive Decrement Times for Inhaled Anesthetics." *Anesthesia and Analgesia* 101 (3): 688–96, table of contents. <https://doi.org/10.1213/01.ANE.0000158611.15820.3D>.
- Eipe, N., S. Gupta, and J. Penning. 2016. "Intravenous Lidocaine for Acute Pain: An Evidence-Based Clinical Update." *BJA Education* 16 (9): 292–98. <https://doi.org/10.1093/bjaed/mkw008>.
- Erickson, Kirstin M., and Daniel J. Cole. 2012. "Anesthetic Considerations for Awake Craniotomy for Epilepsy and Functional Neurosurgery." *Anesthesiology Clinics* 30 (2): 241–68. <https://doi.org/10.1016/j.anclin.2012.05.002>.
- Ersen, Ali, Stella Elkabes, David S. Freedman, and Mesut Sahin. 2015. "Chronic Tissue Response to Untethered Microelectrode Implants in the Rat Brain and Spinal Cord." *Journal of Neural Engineering* 12 (1): 016019. <https://doi.org/10.1088/1741-2560/12/1/016019>.
- Esquenazi, Alberto, Mukul Talaty, Andrew Packel, and Michael Saulino. 2012. "The ReWalk Powered Exoskeleton to Restore Ambulatory Function to Individuals with Thoracic-Level

- Motor-Complete Spinal Cord Injury.” *American Journal of Physical Medicine & Rehabilitation* 91 (11): 911–21. <https://doi.org/10.1097/PHM.0b013e318269d9a3>.
- Ewertzen, Caroline, Adrian Săftoiu, Lucian G. Gruionu, Steen Karstrup, and Michael B. Nielsen. 2013. “Real-Time Image Fusion Involving Diagnostic Ultrasound.” *American Journal of Roentgenology* 200 (3): W249–55. <https://doi.org/10.2214/AJR.12.8904>.
- Fan, S. Z., H. Y. Yu, Y. L. Chen, and C. C. Liu. 1995. “Propofol Concentration Monitoring in Plasma or Whole Blood by Gas Chromatography and High-Performance Liquid Chromatography.” *Anesthesia and Analgesia* 81 (1): 175–78.
- Fann, Jesse R., Charles H. Bombardier, J. Scott Richards, Denise G. Tate, Catherine S. Wilson, and Nancy Temkin. 2011. “Depression After Spinal Cord Injury: Comorbidities, Mental Health Service Use, and Adequacy of Treatment.” *Archives of Physical Medicine and Rehabilitation* 92 (3): 352–60. <https://doi.org/10.1016/j.apmr.2010.05.016>.
- Federici, Thais, Carl V. Hurtig, Kentrell L. Burks, Jonathan P. Riley, Vibhor Krishna, Brandon A. Miller, Eric A. Sribnick, et al. 2012. “Surgical Technique for Spinal Cord Delivery of Therapies: Demonstration of Procedure in Gottingen Minipigs.” *Journal of Visualized Experiments : JoVE*, no. 70 (December). <https://doi.org/10.3791/4371>.
- Féron, F., C. Perry, J. Cochrane, P. Licina, A. Nowitzke, S. Urquhart, T. Geraghty, and A. Mackay-Sim. 2005. “Autologous Olfactory Ensheathing Cell Transplantation in Human Spinal Cord Injury.” *Brain: A Journal of Neurology* 128 (Pt 12): 2951–60. <https://doi.org/10.1093/brain/awh657>.
- Field-Fote, Edelle C., and Kathryn E. Roach. 2011. “Influence of a Locomotor Training Approach on Walking Speed and Distance in People With Chronic Spinal Cord Injury: A

- Randomized Clinical Trial.” *Physical Therapy* 91 (1): 48–60.  
<https://doi.org/10.2522/ptj.20090359>.
- Food and Drug Administration, HHS. 2015. “Medical Devices; Physical Medicine Devices; Classification of the Powered Lower Extremity Exoskeleton; Republication. Final Order; Republication.” *Federal Register* 80 (85): 25226–30.
- Frederiksen, M. C., T. K. Henthorn, T. I. Ruo, and A. J. Atkinson. 1983. “Pharmacokinetics of Pentobarbital in the Dog.” *The Journal of Pharmacology and Experimental Therapeutics* 225 (2): 355–60.
- Friedman, H., B. S. Nashold, and P. Senechal. 1972. “Spinal Cord Stimulation and Bladder Function in Normal and Paraplegic Animals.” *Journal of Neurosurgery* 36 (4): 430–37.  
<https://doi.org/10.3171/jns.1972.36.4.0430>.
- Gaunt, R. A., A. Prochazka, V. K. Mushahwar, L. Guevremont, and P. H. Ellaway. 2006. “Intraspinal Microstimulation Excites Multisegmental Sensory Afferents at Lower Stimulus Levels Than Local  $\alpha$ -Motoneuron Responses.” *Journal of Neurophysiology* 96 (6): 2995–3005. <https://doi.org/10.1152/jn.00061.2006>.
- Gerasimenko, Yu P., V. D. Avelev, O. A. Nikitin, and I. A. Lavrov. 2003. “Initiation of Locomotor Activity in Spinal Cats by Epidural Stimulation of the Spinal Cord.” *Neuroscience and Behavioral Physiology* 33 (3): 247–54.  
<https://doi.org/10.1023/A:1022199214515>.
- Gertler, Ralph, H. Cleighton Brown, Donald H. Mitchell, and Erin N. Silvius. 2001. “Dexmedetomidine: A Novel Sedative-Analgesic Agent.” *Proceedings (Baylor University Medical Center)* 14 (1): 13–21.

- Giovanelli Barilari, M., and H. G. Kuypers. 1969. "Propriospinal Fibers Interconnecting the Spinal Enlargements in the Cat." *Brain Research* 14 (2): 321–30.
- Glickman, S, and M. A Kamm. 1996. "Bowel Dysfunction in Spinal-Cord-Injury Patients." *The Lancet* 347 (9016): 1651–53. [https://doi.org/10.1016/S0140-6736\(96\)91487-7](https://doi.org/10.1016/S0140-6736(96)91487-7).
- Goodall, E. V., J. F. de Breij, and J. Holsheimer. 1996. "Position-Selective Activation of Peripheral Nerve Fibers with a Cuff Electrode." *IEEE Transactions on Bio-Medical Engineering* 43 (8): 851–56. <https://doi.org/10.1109/10.508548>.
- Gorgey, A. S., and G. A. Dudley. 2007. "Skeletal Muscle Atrophy and Increased Intramuscular Fat after Incomplete Spinal Cord Injury." *Spinal Cord* 45 (4): 304–9. <https://doi.org/10.1038/sj.sc.3101968>.
- Grahn, Peter J., Stephan J. Goerss, J. Luis Lujan, Grant W. Mallory, Bruce A. Kall, Aldo A. Mendez, James K. Trevathan, Joel P. Felmlee, Kevin E. Bennet, and Kendall H. Lee. 2016. "MRI-Guided Stereotactic System for Delivery of Intraspinal Microstimulation." *Spine* 41 (13): E806-813. <https://doi.org/10.1097/BRS.0000000000001397>.
- Granat, M. H., A. C. Ferguson, B. J. Andrews, and M. Delargy. 1993. "The Role of Functional Electrical Stimulation in the Rehabilitation of Patients with Incomplete Spinal Cord Injury-- Observed Benefits during Gait Studies." *Paraplegia* 31 (4): 207–15. <https://doi.org/10.1038/sc.1993.39>.
- Grasshoff, C., and B. Antkowiak. 2006. "Effects of Isoflurane and Enflurane on GABAA and Glycine Receptors Contribute Equally to Depressant Actions on Spinal Ventral Horn Neurones in Rats." *BJA: British Journal of Anaesthesia* 97 (5): 687–94. <https://doi.org/10.1093/bja/ael239>.

- Gregory, Chris M, and C Scott Bickel. 2005. "Recruitment Patterns in Human Skeletal Muscle During Electrical Stimulation." *Physical Therapy* 85 (4): 358–64.  
<https://doi.org/10.1093/ptj/85.4.358>.
- Grill, W. M., and J. T. Mortimer. 1996. "Quantification of Recruitment Properties of Multiple Contact Cuff Electrodes." *IEEE Transactions on Rehabilitation Engineering* 4 (2): 49–62.  
<https://doi.org/10.1109/86.506402>.
- Grimnes, Sverre, and Ørjan G Martinsen. 2015. "Chapter 5 - Excitable Tissue and Bioelectric Signals." In *Bioimpedance and Bioelectricity Basics (Third Edition)*, edited by Sverre Grimnes and Ørjan G Martinsen, 119–39. Oxford: Academic Press.  
<https://doi.org/10.1016/B978-0-12-411470-8.00005-2>.
- Guevremont, Lisa, Jonathan A. Norton, and Vivian K. Mushahwar. 2007. "Physiologically Based Controller for Generating Overground Locomotion Using Functional Electrical Stimulation." *Journal of Neurophysiology* 97 (3): 2499–2510.  
<https://doi.org/10.1152/jn.01177.2006>.
- Gustafsson, B., and E. Jankowska. 1976. "Direct and Indirect Activation of Nerve Cells by Electrical Pulses Applied Extracellularly." *The Journal of Physiology* 258 (1): 33–61.
- Gwak, Young Seob, Bryan C. Hains, Kathia M. Johnson, and Claire E. Hulsebosch. 2004. "Effect of Age at Time of Spinal Cord Injury on Behavioral Outcomes in Rat." *Journal of Neurotrauma* 21 (8): 983–93. <https://doi.org/10.1089/0897715041650999>.
- Ha, Kevin H., Hugo A. Quintero, Ryan J. Farris, and Michael Goldfarb. 2012. "Enhancing Stance Phase Propulsion during Level Walking by Combining FES with a Powered Exoskeleton for Persons with Paraplegia." *Conference Proceedings: ... Annual International Conference of the IEEE Engineering in Medicine and Biology Society. IEEE Engineering in*

*Medicine and Biology Society. Annual Conference* 2012: 344–47.

<https://doi.org/10.1109/EMBC.2012.6345939>.

Hachmann, Jan T., Ju Ho Jeong, Peter J. Grahn, Grant W. Mallory, Loribeth Q. Evertz, Allan J.

Bieber, Darlene A. Lobel, Kevin E. Bennet, Kendall H. Lee, and J. Luis Lujan. 2013. “Large Animal Model for Development of Functional Restoration Paradigms Using Epidural and Intraspinal Stimulation.” *PLoS ONE* 8 (12): e81443.

<https://doi.org/10.1371/journal.pone.0081443>.

Hall, Adam C., Kathleen C. Rowan, Renna J. N. Stevens, Jill C. Kelley, and Neil L. Harrison.

2004. “The Effects of Isoflurane on Desensitized Wild-Type and Alpha 1(S270H) Gamma-Aminobutyric Acid Type A Receptors.” *Anesthesia and Analgesia* 98 (5): 1297–1304, table of contents.

Handa, Y., N. Hoshimiya, Y. Iguchi, and T. Oda. 1989. “Development of Percutaneous

Intramuscular Electrode for Multichannel FES System.” *IEEE Transactions on Biomedical Engineering* 36 (7): 705–10. <https://doi.org/10.1109/10.32102>.

Harkema, Susan, Yury Gerasimenko, Jonathan Hodes, Joel Burdick, Claudia Angeli, Yangsheng

Chen, Christie Ferreira, et al. 2011. “Effect of Epidural Stimulation of the Lumbosacral Spinal Cord on Voluntary Movement, Standing, and Assisted Stepping after Motor Complete Paraplegia: A Case Study.” *Lancet* 377 (9781): 1938–47. [https://doi.org/10.1016/S0140-6736\(11\)60547-3](https://doi.org/10.1016/S0140-6736(11)60547-3).

Harrison, D. E., R. Cailliet, D. D. Harrison, S. J. Troyanovich, and S. O. Harrison. 1999. “A

Review of Biomechanics of the Central Nervous System--Part II: Spinal Cord Strains from Postural Loads.” *Journal of Manipulative and Physiological Therapeutics* 22 (5): 322–32.

- Harrison, N. L., J. L. Kugler, M. V. Jones, E. P. Greenblatt, and D. B. Pritchett. 1993. "Positive Modulation of Human Gamma-Aminobutyric Acid Type A and Glycine Receptors by the Inhalation Anesthetic Isoflurane." *Molecular Pharmacology* 44 (3): 628–32.
- Hemmings, Hugh C., Myles H. Akabas, Peter A. Goldstein, James R. Trudell, Beverley A. Orser, and Neil L. Harrison. 2005. "Emerging Molecular Mechanisms of General Anesthetic Action." *Trends in Pharmacological Sciences* 26 (10): 503–10.  
<https://doi.org/10.1016/j.tips.2005.08.006>.
- Henneman, E., and C. B. Olson. 1965. "RELATIONS BETWEEN STRUCTURE AND FUNCTION IN THE DESIGN OF SKELETAL MUSCLES." *Journal of Neurophysiology* 28 (May): 581–98. <https://doi.org/10.1152/jn.1965.28.3.581>.
- Herman, R., J. He, S. D'Luzansky, W. Willis, and S. Dilli. 2002. "Spinal Cord Stimulation Facilitates Functional Walking in a Chronic, Incomplete Spinal Cord Injured." *Spinal Cord* 40 (2): 65–68. <https://doi.org/10.1038/sj.sc.3101263>.
- Herr, Hugh. 2009. "Exoskeletons and Orthoses: Classification, Design Challenges and Future Directions." *Journal of NeuroEngineering and Rehabilitation* 6 (1): 21.  
<https://doi.org/10.1186/1743-0003-6-21>.
- Hesse, Stefan, Henning Schmidt, Cordula Werner, and Anita Bardeleben. 2003. "Upper and Lower Extremity Robotic Devices for Rehabilitation and for Studying Motor Control." *Current Opinion in Neurology* 16 (6): 705–10.  
<https://doi.org/10.1097/01.wco.0000102630.16692.38>.
- Hicken, Bret L., John D. Putzke, and J. Scott Richards. 2001. "Bladder Management and Quality of Life After Spinal Cord Injury." *American Journal of Physical Medicine & Rehabilitation* 80 (12): 916.

- Hicks, A. L., M. M. Adams, K. Martin Ginis, L. Giangregorio, A. Latimer, S. M. Phillips, and N. McCartney. 2005. "Long-Term Body-Weight-Supported Treadmill Training and Subsequent Follow-up in Persons with Chronic SCI: Effects on Functional Walking Ability and Measures of Subjective Well-Being." *Spinal Cord* 43 (5): 291–98.  
<https://doi.org/10.1038/sj.sc.3101710>.
- Hicks, Audrey L., and Kathleen A. Martin Ginis. 2008. "Treadmill Training after Spinal Cord Injury: It's Not Just about the Walking." *Journal of Rehabilitation Research and Development* 45 (2): 241–48.
- Hikasa, Y, K Okuyama, T Kakuta, K Takase, and S Ogasawara. 1998. "Anesthetic Potency and Cardiopulmonary Effects of Sevoflurane in Goats: Comparison with Isoflurane and Halothane." *Canadian Journal of Veterinary Research* 62 (4): 299–306.
- Hill, S. A. 2004. "Pharmacokinetics of Drug Infusions." *Continuing Education in Anaesthesia Critical Care & Pain* 4 (3): 76–80. <https://doi.org/10.1093/bjaceaccp/mkh021>.
- Ho, I. K., and R. A. Harris. 1981. "Mechanism of Action of Barbiturates." *Annual Review of Pharmacology and Toxicology* 21: 83–111.  
<https://doi.org/10.1146/annurev.pa.21.040181.000503>.
- Hoffer, J. A., G. E. Loeb, N. Sugano, W. B. Marks, M. J. O'Donovan, and C. A. Pratt. 1987. "Cat Hindlimb Motoneurons during Locomotion. III. Functional Segregation in Sartorius." *Journal of Neurophysiology* 57 (2): 554–62. <https://doi.org/10.1152/jn.1987.57.2.554>.
- Holinski, B. J., D. G. Everaert, V. K. Mushahwar, and R. B. Stein. 2013. "Real-Time Control of Walking Using Recordings from Dorsal Root Ganglia." *Journal of Neural Engineering* 10 (5): 056008. <https://doi.org/10.1088/1741-2560/10/5/056008>.

- Holinski, B. J., K. A. Mazurek, D. G. Everaert, A. Toossi, A. M. Lucas-Osma, P. Troyk, R. Etienne-Cummings, R. B. Stein, and V. K. Mushahwar. 2016. "Intraspinal Microstimulation Produces Over-Ground Walking in Anesthetized Cats." *Journal of Neural Engineering* 13 (5): 056016. <https://doi.org/10.1088/1741-2560/13/5/056016>.
- Holinski, Bradley J. 2013. "Restoring Walking after Spinal Cord Injury." Edmonton, AB: University of Alberta. <https://era.library.ualberta.ca/public/view/item/uuid:0e698e79-b16a-4519-baf7-552a49dda767/>.
- Holsheimer, J. 1998. "Computer Modelling of Spinal Cord Stimulation and Its Contribution to Therapeutic Efficacy." *Spinal Cord* 36 (8): 531–40.
- Holsheimer, J., J. J. Struijk, and N. J. Rijkhoff. 1991. "Contact Combinations in Epidural Spinal Cord Stimulation. A Comparison by Computer Modeling." *Stereotactic and Functional Neurosurgery* 56 (4): 220–33.
- Horch K. W., and Daryl R. Kipke. 2017. *Neuroprosthetics: Theory And Practice (Second Edition)*. World Scientific.
- Howard, M. A., M. Utz, T. J. Brennan, B. D. Dalm, S. Viljoen, N. D. Jeffery, and G. T. Gillies. 2011. "Intradural Approach to Selective Stimulation in the Spinal Cord for Treatment of Intractable Pain: Design Principles and Wireless Protocol." *Journal of Applied Physics* 110 (4): 044702. <https://doi.org/10.1063/1.3626469>.
- Hubscher, Charles H., April N. Herrity, Carolyn S. Williams, Lynnette R. Montgomery, Andrea M. Willhite, Claudia A. Angeli, and Susan J. Harkema. 2018. "Improvements in Bladder, Bowel and Sexual Outcomes Following Task-Specific Locomotor Training in Human Spinal Cord Injury." *PLOS ONE* 13 (1): e0190998. <https://doi.org/10.1371/journal.pone.0190998>.

- Hughes, M. A., P. S. Glass, and J. R. Jacobs. 1992. "Context-Sensitive Half-Time in Multicompartment Pharmacokinetic Models for Intravenous Anesthetic Drugs." *Anesthesiology* 76 (3): 334–41.
- Hunter, J P, and P Ashby. 1994. "Segmental Effects of Epidural Spinal Cord Stimulation in Humans." *The Journal of Physiology* 474 (3): 407–19.
- Ichiyama, R. M., Yu. P. Gerasimenko, H. Zhong, R. R. Roy, and V. R. Edgerton. 2005. "Hindlimb Stepping Movements in Complete Spinal Rats Induced by Epidural Spinal Cord Stimulation." *Neuroscience Letters* 383 (3): 339–44.  
<https://doi.org/10.1016/j.neulet.2005.04.049>.
- Ihnatsenka, Barys, and André Pierre Boezaart. 2010. "Ultrasound: Basic Understanding and Learning the Language." *International Journal of Shoulder Surgery* 4 (3): 55–62.  
<https://doi.org/10.4103/0973-6042.76960>.
- Israel, Jeffrey F., Donielle D. Campbell, Jennifer H. Kahn, and T. George Hornby. 2006. "Metabolic Costs and Muscle Activity Patterns during Robotic- and Therapist-Assisted Treadmill Walking in Individuals with Incomplete Spinal Cord Injury." *Physical Therapy* 86 (11): 1466–78. <https://doi.org/10.2522/ptj.20050266>.
- Jackson, Andrew, and Jonas B. Zimmermann. 2012. "Neural Interfaces for the Brain and Spinal Cord—Restoring Motor Function." *Nature Reviews Neurology* 8 (12): 690.  
<https://doi.org/10.1038/nrneurol.2012.219>.
- Jaeger, Lukas, Laura Marchal-Crespo, Peter Wolf, Robert Riener, Lars Michels, and Spyros Kollias. 2014. "Brain Activation Associated with Active and Passive Lower Limb Stepping." *Frontiers in Human Neuroscience* 8 (October). <https://doi.org/10.3389/fnhum.2014.00828>.

- Jaeger, R. J. 1992. "Lower Extremity Applications of Functional Neuromuscular Stimulation." *Assistive Technology: The Official Journal of RESNA* 4 (1): 19–30.  
<https://doi.org/10.1080/10400435.1992.10132189>.
- Jakubovic, Raphael, Joel Ramjist, Shaurya Gupta, Daipayan Guha, Arjun Sahgal, F. Stuart Foster, and Victor X. D. Yang. 2018. "High-Frequency Micro-Ultrasound Imaging and Optical Topographic Imaging for Spinal Surgery: Initial Experiences." *Ultrasound in Medicine & Biology*, July. <https://doi.org/10.1016/j.ultrasmedbio.2018.05.003>.
- Jankowska, E. 1992. "Interneuronal Relay in Spinal Pathways from Proprioceptors." *Progress in Neurobiology* 38 (4): 335–78. [https://doi.org/10.1016/0301-0082\(92\)90024-9](https://doi.org/10.1016/0301-0082(92)90024-9).
- Jankowska, E., A. Lundberg, W. J. Roberts, and D. Stuart. 1974. "A Long Propriospinal System with Direct Effect on Motoneurons and on Interneurons in the Cat Lumbosacral Cord." *Experimental Brain Research* 21 (2): 169–94.
- Jankowska, E., and W. J. Roberts. 1972. "An Electrophysiological Demonstration of the Axonal Projections of Single Spinal Interneurons in the Cat." *The Journal of Physiology* 222 (3): 597–622.
- Jefferson, R. J., and M. W. Whittle. 1990. "Performance of Three Walking Orthoses for the Paralyzed: A Case Study Using Gait Analysis." *Prosthetics and Orthotics International* 14 (3): 103–10. <https://doi.org/10.3109/03093649009080335>.
- Jenkins, Andrew, Eric P. Greenblatt, Howard J. Faulkner, Edward Bertaccini, Adam Light, Audrey Lin, Alyson Andreasen, Anna Viner, James R. Trudell, and Neil L. Harrison. 2001. "Evidence for a Common Binding Cavity for Three General Anesthetics within the GABAA Receptor." *Journal of Neuroscience* 21 (6): RC136–RC136.  
<https://doi.org/10.1523/JNEUROSCI.21-06-j0002.2001>.

- Jeon, Young Hoon. 2012. "Spinal Cord Stimulation in Pain Management: A Review." *The Korean Journal of Pain* 25 (3): 143–50. <https://doi.org/10.3344/kjp.2012.25.3.143>.
- Jeong, Se Hoon, Sang Beom Jun, Jong Keun Song, and Sung June Kim. 2009. "Activity-Dependent Neuronal Cell Migration Induced by Electrical Stimulation." *Medical & Biological Engineering & Computing* 47 (1): 93–99. <https://doi.org/10.1007/s11517-008-0426-8>.
- Jia, Fan, Minerva Yue, Dev Chandra, Gregg E. Homanics, Peter A. Goldstein, and Neil L. Harrison. 2008. "Isoflurane Is a Potent Modulator of Extrasynaptic GABAA Receptors in the Thalamus." *Journal of Pharmacology and Experimental Therapeutics* 324 (3): 1127–35. <https://doi.org/10.1124/jpet.107.134569>.
- Jinks, S., J. F. Antognini, E. Carstens, V. Buzin, and C. Simons. 1999. "Isoflurane Can Indirectly Depress Lumbar Dorsal Horn Activity in the Goat via Action within the Brain." *British Journal of Anaesthesia* 82 (2): 244–49.
- Johnston, T. E., R. R. Betz, B. T. Smith, B. J. Benda, M. J. Mulcahey, R. Davis, T. P. Houdayer, M. A. Pontari, A. Barriskill, and G. H. Creasey. 2005. "Implantable FES System for Upright Mobility and Bladder and Bowel Function for Individuals with Spinal Cord Injury." *Spinal Cord* 43 (12): 713–23. <https://doi.org/10.1038/sj.sc.3101797>.
- Jovic, Jovana, Christine Azevedo Coste, Philippe Fraisse, Sonia Henkous, and Charles Fattal. 2015. "Coordinating Upper and Lower Body During FES-Assisted Transfers in Persons With Spinal Cord Injury in Order to Reduce Arm Support." *Neuromodulation: Technology at the Neural Interface* 18 (8): 736–43. <https://doi.org/10.1111/ner.12286>.
- Jurd, Rachel, Margarete Arras, Sachar Lambert, Berthold Drexler, Roberta Siegart, Florence Crestani, Michael Zaugg, et al. 2002. "General Anesthetic Actions in Vivo Strongly

Attenuated by a Point Mutation in the GABAA Receptor B3 Subunit.” *The FASEB Journal* 17 (2): 250–52. <https://doi.org/10.1096/fj.02-0611fje>.

Kalkman, C. J., J. C. Drummond, P. M. Patel, T. Sano, and R. M. Chestnut. 1995. “Effects of Droperidol, Pentobarbital, and Ketamine on Myogenic Transcranial Magnetic Motor-Evoked Responses in Humans.” *Journal of Neurosurgical Anesthesiology* 7 (3): 200.

Kapadia, Naaz, Kei Masani, B. Catharine Craven, Lora M. Giangregorio, Sander L. Hitzig, Kieva Richards, and Milos R. Popovic. 2014. “A Randomized Trial of Functional Electrical Stimulation for Walking in Incomplete Spinal Cord Injury: Effects on Walking Competency.” *The Journal of Spinal Cord Medicine* 37 (5): 511–24. <https://doi.org/10.1179/2045772314Y.0000000263>.

Kapila, A., P. S. Glass, J. R. Jacobs, K. T. Muir, D. J. Hermann, M. Shiraishi, S. Howell, and R. L. Smith. 1995. “Measured Context-Sensitive Half-Times of Remifentanyl and Alfentanil.” *Anesthesiology* 83 (5): 968–75.

Karlsson, Ann-Katrin. 2006. “Autonomic Dysfunction in Spinal Cord Injury: Clinical Presentation of Symptoms and Signs.” *Progress in Brain Research* 152: 1–8. [https://doi.org/10.1016/S0079-6123\(05\)52034-X](https://doi.org/10.1016/S0079-6123(05)52034-X).

Kasten, M. R., M. D. Sunshine, E. S. Secrist, P. J. Horner, and C. T. Moritz. 2013. “Therapeutic Intraspinal Microstimulation Improves Forelimb Function after Cervical Contusion Injury.” *Journal of Neural Engineering* 10 (4): 044001. <https://doi.org/10.1088/1741-2560/10/4/044001>.

Kawashima, Noritaka, Daichi Nozaki, Masaki O. Abe, and Kimitaka Nakazawa. 2008. “Shaping Appropriate Locomotive Motor Output Through Interlimb Neural Pathway Within Spinal

Cord in Humans.” *Journal of Neurophysiology* 99 (6): 2946–55.

<https://doi.org/10.1152/jn.00020.2008>.

Kazama, Tomiei, Kazuyuki Ikeda, Koji Morita, and Yoshimitsu Sanjo. 1998. “Awakening Propofol Concentration with and without Blood-Effect Site Equilibration after Short-Term and Long-Term Administration of Propofol and Fentanyl Anesthesia.” *Anesthesiology: The Journal of the American Society of Anesthesiologists* 88 (4): 928–34.

Kerz, Thomas, Hans-Jürgen Hennes, Annaïk Fève, Philippe Decq, Paul Filipetti, and Philippe Duvaldestin. 2001. “Effects of Propofol on H-Reflex in Humans.” *Anesthesiology: The Journal of the American Society of Anesthesiologists* 94 (1): 32–37.

Kiernan, Matthew C., Cindy S.-Y. Lin, and David Burke. 2004. “Differences in Activity-Dependent Hyperpolarization in Human Sensory and Motor Axons.” *The Journal of Physiology* 558 (Pt 1): 341–49. <https://doi.org/10.1113/jphysiol.2004.063966>.

Kim, JongBun, Aubrey Yao, Richard Atherley, Earl Carstens, Steven L. Jinks, and Joseph F. Antognini. 2007. “Neurons in the Ventral Spinal Cord Are More Depressed by Isoflurane, Halothane, and Propofol Than Are Neurons in the Dorsal Spinal Cord.” *Anesthesia and Analgesia* 105 (4): 1020-contents. <https://doi.org/10.1213/01.ane.0000280483.17854.56>.

Kim, Taegyo, Almut Branner, Tanuj Gulati, and Simon F. Giszter. 2013. “Braided Multi-Electrode Probes: Mechanical Compliance Characteristics and Recordings from Spinal Cords.” *Journal of Neural Engineering* 10 (4): 045001. <https://doi.org/10.1088/1741-2560/10/4/045001>.

King, Bryan S., and Ira J. Rampil. 1994. “Anesthetic Depression of Spinal Motor Neurons May Contribute to Lack of Movement in Response to Noxious Stimuli.” *Anesthesiology: The Journal of the American Society of Anesthesiologists* 81 (6): 1484–1482.

- Kipke, Daryl R., Rio J. Vetter, Justin C. Williams, and Jamille F. Hetke. 2003. "Silicon-Substrate Intracortical Microelectrode Arrays for Long-Term Recording of Neuronal Spike Activity in Cerebral Cortex." *IEEE Transactions on Neural Systems and Rehabilitation Engineering: A Publication of the IEEE Engineering in Medicine and Biology Society* 11 (2): 151–55. <https://doi.org/10.1109/TNSRE.2003.814443>.
- Kirshblum, Steven C., Stephen P. Burns, Fin Biering-Sorensen, William Donovan, Daniel E. Graves, Amitabh Jha, Mark Johansen, et al. 2011. "International Standards for Neurological Classification of Spinal Cord Injury (Revised 2011)." *The Journal of Spinal Cord Medicine* 34 (6): 535–46. <https://doi.org/10.1179/204577211X13207446293695>.
- Klyce, Daniel W., Charles H. Bombardier, Trevor J. Davis, Narineh Hartoonian, Jeanne M. Hoffman, Jesse R. Fann, and Claire Z. Kalpakjian. 2015. "Distinguishing Grief From Depression During Acute Recovery From Spinal Cord Injury." *Archives of Physical Medicine and Rehabilitation* 96 (8): 1419–25. <https://doi.org/10.1016/j.apmr.2015.02.018>.
- Krasowski, Matthew D., Vladimir V. Koltchine, Caroline E. Rick, Qing Ye, Suzanne E. Finn, and Neil L. Harrison. 1998. "Propofol and Other Intravenous Anesthetics Have Sites of Action on the  $\gamma$ -Aminobutyric Acid Type A Receptor Distinct from That for Isoflurane." *Molecular Pharmacology* 53 (3): 530. <https://doi.org/10.1124/mol.53.3.530>.
- Krause, J. Stuart, and Carol A. Anson. 1996. "Self-Perceived Reasons for Unemployment Cited by Persons with Spinal Cord Injury: Relationship to Gender, Race, Age and Level of Injury." *Rehabilitation Counseling Bulletin* 39 (3): 217–27.
- Krause, S.J., Anson, C. A., 1997. "Adjustment after Spinal Cord Injury: Relationship to Participation in Employment or Educational Activities." *Rehabilitation Counseling Bulletin* 40 (3): 202–14.

- Kressler, Jochen, Christine K. Thomas, Edelle C. Field-Fote, Justin Sanchez, Eva Widerström-Noga, Deena C. Cilien, Katie Gant, et al. 2014. "Understanding Therapeutic Benefits of Overground Bionic Ambulation: Exploratory Case Series in Persons With Chronic, Complete Spinal Cord Injury." *Archives of Physical Medicine and Rehabilitation* 95 (10): 1878-1887.e4. <https://doi.org/10.1016/j.apmr.2014.04.026>.
- Kreuter, M. 2000. "Spinal Cord Injury and Partner Relationships." *Spinal Cord* 38 (1): 2–6. <https://doi.org/10.1038/sj.sc.3100933>.
- Krieg, Wendell J.S., and Richard A. Groat. 1944. "Topography of the Spinal Cord and Vertebral Column of the Cat." *Quarterly Bulletin of the Northwestern University Medical School* 18 (4): 265–68.
- Kriz, J., M. Kulakovska, H. Davidova, M. Silova, and A. Kobesova. 2017. "Incidence of Acute Spinal Cord Injury in the Czech Republic: A Prospective Epidemiological Study 2006–2015." *Spinal Cord* 55 (9): 870–74. <https://doi.org/10.1038/sc.2017.20>.
- Krompecher, T. 1981. "Experimental Evaluation of Rigor Mortis V. Effect of Various Temperatures on the Evolution of Rigor Mortis." *Forensic Science International* 17 (1): 19–26. [https://doi.org/10.1016/0379-0738\(81\)90184-5](https://doi.org/10.1016/0379-0738(81)90184-5).
- Krueger, H., V. K. Noonan, L. M. Trenaman, P. Joshi, and C. S. Rivers. 2013. "The Economic Burden of Traumatic Spinal Cord Injury in Canada." *Chronic Diseases and Injuries in Canada* 33 (3): 113–22.
- Kungys, Gudrun, JongBun Kim, Steven L. Jinks, Richard J. Atherley, and Joseph F. Antognini. 2009. "Propofol Produces Immobility via Action in the Ventral Horn of the Spinal Cord by a GABAergic Mechanism." *Anesthesia & Analgesia* 108 (5): 1531. <https://doi.org/10.1213/ane.0b013e31819d9308>.

- Kunj, Vasant. 2016. "Spinal Cord Injury and Its Impact on the Patient, Family, and the Society." *Int J Recent Surg Med Sci* 2 (1): 1–4.
- Kurabe, Miyuki, Hidemasa Furue, and Tatsuro Kohno. 2016. "Intravenous Administration of Lidocaine Directly Acts on Spinal Dorsal Horn and Produces Analgesic Effect: An in Vivo Patch-Clamp Analysis." *Scientific Reports* 6 (May). <https://doi.org/10.1038/srep26253>.
- Kuwabara, Satoshi, Sonoko Misawa, Noriko Tamura, Miho Nakata, Kazuaki Kanai, Setsu Sawai, Kazue Ogawara, and Takamichi Hattori. 2006. "Latent Addition in Human Motor and Sensory Axons: Different Site-Dependent Changes across the Carpal Tunnel Related to Persistent Na<sup>+</sup> Currents." *Clinical Neurophysiology* 117 (4): 810–14. <https://doi.org/10.1016/j.clinph.2005.11.018>.
- Kwon, Brian K., Femke Streijger, Caitlin E. Hill, Aileen J. Anderson, Mark Bacon, Michael S. Beattie, Armin Blesch, et al. 2015. "Large Animal and Primate Models of Spinal Cord Injury for the Testing of Novel Therapies." *Experimental Neurology* 269 (July): 154–68. <https://doi.org/10.1016/j.expneurol.2015.04.008>.
- Lam, Tania, Janice J Eng, Dalton L Wolfe, Jane T Hsieh, and Maura Whittaker. 2007. "A Systematic Review of the Efficacy of Gait Rehabilitation Strategies for Spinal Cord Injury." *Topics in Spinal Cord Injury Rehabilitation* 13 (1): 32–57. <https://doi.org/10.1310/sci1301-32>.
- Lamanna, Jason J., Lindsey N. Urquia, Carl V. Hurtig, Juanmarco Gutierrez, Cody Anderson, Pete Piferi, Thais Federici, John N. Oshinski, and Nicholas M. Boulis. 2017. "Magnetic Resonance Imaging-Guided Transplantation of Neural Stem Cells into the Porcine Spinal Cord." *Stereotactic and Functional Neurosurgery* 95 (1): 60–68. <https://doi.org/10.1159/000448765>.

- Lau, Bernice, Lisa Guevremont, and Vivian K. Mushahwar. 2007. "Strategies for Generating Prolonged Functional Standing Using Intramuscular Stimulation or Intraspinal Microstimulation." *IEEE Transactions on Neural Systems and Rehabilitation Engineering: A Publication of the IEEE Engineering in Medicine and Biology Society* 15 (2): 273–85. <https://doi.org/10.1109/TNSRE.2007.897030>.
- Lee, Jae H. T., Claire F. Jones, Elena B. Okon, Lisa Anderson, Seth Tigchelaar, Paul Kooner, Tamara Godbey, et al. 2013. "A Novel Porcine Model of Traumatic Thoracic Spinal Cord Injury." *Journal of Neurotrauma* 30 (3): 142–59. <https://doi.org/10.1089/neu.2012.2386>.
- Lee, Min Woo. 2014. "Fusion Imaging of Real-Time Ultrasonography with CT or MRI for Hepatic Intervention." *Ultrasonography, Ultrasonography* 33 (4): 227–39. <https://doi.org/2014.33.4.227>.
- Leon, R. D. De, J. A. Hodgson, R. R. Roy, and V. R. Edgerton. 1998. "Locomotor Capacity Attributable to Step Training versus Spontaneous Recovery Following Spinalization in Adult Cats." *J. Neurophysiol*, 1329–1340.
- Li, Yan, Lingzhong Meng, Yuming Peng, Hui Qiao, Lanjun Guo, Ruquan Han, and Adrian W. Gelb. 2016. "Effects of Dexmedetomidine on Motor- and Somatosensory-Evoked Potentials in Patients with Thoracic Spinal Cord Tumor: A Randomized Controlled Trial." *BMC Anesthesiology* 16 (August). <https://doi.org/10.1186/s12871-016-0217-y>.
- Lidal, Ingeborg Beate, Tuan Khai Huynh, and Fin Biering-Sørensen. 2007. "Return to Work Following Spinal Cord Injury: A Review." *Disability and Rehabilitation* 29 (17): 1341–75. <https://doi.org/10.1080/09638280701320839>.
- Lima, Carlos, Pedro Escada, José Pratas-Vital, Catarina Branco, Carlo Alberto Arcangeli, Giovanna Lazzeri, Carlos Alberto Santana Maia, Clara Capucho, Armando Hasse-Ferreira,

- and Jean D. Peduzzi. 2010. "Olfactory Mucosal Autografts and Rehabilitation for Chronic Traumatic Spinal Cord Injury." *Neurorehabilitation and Neural Repair* 24 (1): 10–22. <https://doi.org/10.1177/1545968309347685>.
- Loeb, G. E., J. A. Hoffer, and C. A. Pratt. 1985. "Activity of Spindle Afferents from Cat Anterior Thigh Muscles. I. Identification and Patterns during Normal Locomotion." *Journal of Neurophysiology* 54 (3): 549–64. <https://doi.org/10.1152/jn.1985.54.3.549>.
- Logan, Jennifer K, Soroush Rais-Bahrami, Baris Turkbey, Andrew Gomella, Hayet Amalou, Peter L Choyke, Bradford J Wood, and Peter A Pinto. 2014. "Current Status of MRI and Ultrasound Fusion Software Platforms for Guidance of Prostate Biopsies." *BJU International* 114 (5): 641–52. <https://doi.org/10.1111/bju.12593>.
- López-Larraz, Eduardo, Fernando Trincado-Alonso, Vijaykumar Rajasekaran, Soraya Pérez-Nombela, Antonio J. del-Ama, Joan Aranda, Javier Minguez, Angel Gil-Agudo, and Luis Montesano. 2016. "Control of an Ambulatory Exoskeleton with a Brain–Machine Interface for Spinal Cord Injury Gait Rehabilitation." *Frontiers in Neuroscience* 10. <https://doi.org/10.3389/fnins.2016.00359>.
- Löscher, Wolfgang, and Michael A. Rogawski. 2012. "How Theories Evolved Concerning the Mechanism of Action of Barbiturates." *Epilepsia* 53 Suppl 8 (December): 12–25. <https://doi.org/10.1111/epi.12025>.
- Lotze, Martin, Christoph Braun, Niels Birbaumer, Silke Anders, and Leonardo G. Cohen. n.d. "Motor Learning Elicited by Voluntary Drive." *Brain*, 4–866.
- Lou, Jenny W. H., Austin J. Bergquist, Abdulaziz Aldayel, Jennifer Czitron, and David F. Collins. 2017. "Interleaved Neuromuscular Electrical Stimulation Reduces Muscle Fatigue." *Muscle & Nerve* 55 (2): 179–89. <https://doi.org/10.1002/mus.25224>.

- Louis, R. 1981. "Vertebroradicular and Vertebromedullar Dynamics." *Anatomia Clinica* 3 (1): 1–11.
- Lovely, R. G., R. J. Gregor, R. R. Roy, and V. R. Edgerton. 1986. "Effects of Training on the Recovery of Full-Weight-Bearing Stepping in the Adult Spinal Cat." *Experimental Neurology* 92 (2): 421–35. [https://doi.org/10.1016/0014-4886\(86\)90094-4](https://doi.org/10.1016/0014-4886(86)90094-4).
- Lozano, Andres M., Philip L. Gildenberg, and Ronald R. Tasker. 2009. *Textbook of Stereotactic and Functional Neurosurgery*. Springer Science & Business Media.
- Lucareli, P. R., M. O. Lima, F. P. S. Lima, J. G. de Almeida, G. C. Brech, and J. M. D'Andréa Greve. 2011. "Gait Analysis Following Treadmill Training with Body Weight Support versus Conventional Physical Therapy: A Prospective Randomized Controlled Single Blind Study." *Spinal Cord* 49 (9): 1001–7. <https://doi.org/10.1038/sc.2011.37>.
- MacDonald, D.B., S. Skinner, J. Shils, and C. Yingling. 2013. "Intraoperative Motor Evoked Potential Monitoring – A Position Statement by the American Society of Neurophysiological Monitoring." *Clinical Neurophysiology* 124 (12): 2291–2316. <https://doi.org/10.1016/j.clinph.2013.07.025>.
- Mackiewicz-Milewska, Magdalena, Stanisław Jung, Andrzej C. Kroszczyński, Hanna Mackiewicz-Nartowicz, Zbigniew Serafin, Małgorzata Cisowska-Adamiak, Jerzy Pyskir, Iwona Szymkuć-Bukowska, Wojciech Hagner, and Danuta Rość. 2016. "Deep Venous Thrombosis in Patients with Chronic Spinal Cord Injury." *The Journal of Spinal Cord Medicine* 39 (4): 400–404. <https://doi.org/10.1179/2045772315Y.0000000032>.
- Mahoney, Edward T., C. Scott Bickel, Christopher Elder, Christopher Black, Jill M. Slade, David Apple, and Gary A. Dudley. 2005. "Changes in Skeletal Muscle Size and Glucose Tolerance With Electrically Stimulated Resistance Training in Subjects With Chronic Spinal

- Cord Injury.” *Archives of Physical Medicine and Rehabilitation* 86 (7): 1502–4.  
<https://doi.org/10.1016/j.apmr.2004.12.021>.
- Major, R. E., J. Stallard, and G. K. Rose. 1981. “The Dynamics of Walking Using the Hip Guidance Orthosis (Hgo) with Crutches.” *Prosthetics and Orthotics International* 5 (1): 19–22. <https://doi.org/10.3109/03093648109146224>.
- Maldifassi, Maria C., Roland Baur, and Erwin Sigel. 2016. “Functional Sites Involved in Modulation of the GABAA Receptor Channel by the Intravenous Anesthetics Propofol, Etomidate and Pentobarbital.” *Neuropharmacology* 105 (June): 207–14.  
<https://doi.org/10.1016/j.neuropharm.2016.01.003>.
- Malešević, Nebojsa M., Lana Z. Popović, Laszlo Schwirtlich, and Dejan B. Popović. 2010. “Distributed Low-Frequency Functional Electrical Stimulation Delays Muscle Fatigue Compared to Conventional Stimulation.” *Muscle & Nerve* 42 (4): 556–62.  
<https://doi.org/10.1002/mus.21736>.
- Marks, Leonard, Shelena Young, and Shyam Natarajan. 2013. “MRI–Ultrasound Fusion for Guidance of Targeted Prostate Biopsy.” *Current Opinion in Urology* 23 (1): 43–50.  
<https://doi.org/10.1097/MOU.0b013e32835ad3ee>.
- Mathers, Colin D., and Dejan Loncar. 2006. “Projections of Global Mortality and Burden of Disease from 2002 to 2030.” *PLOS Medicine* 3 (11): e442.  
<https://doi.org/10.1371/journal.pmed.0030442>.
- Mattu, Shazia. 2017. “Priorities of Spinal Cord Injured Population-a Survey.” *American Journal of Applied Psychology* 6 (6): 183–183.

- Matute, E., I. Rivera-Arconada, and J. A. López-García. 2004. "Effects of Propofol and Sevoflurane on the Excitability of Rat Spinal Motoneurons and Nociceptive Reflexes in Vitro." *British Journal of Anaesthesia* 93 (3): 422–27. <https://doi.org/10.1093/bja/ae217>.
- Mazurek, K. A., B. J. Holinski, D. G. Everaert, R. B. Stein, R. Etienne-Cummings, and V. K. Mushahwar. 2012. "Feed Forward and Feedback Control for Over-Ground Locomotion in Anaesthetized Cats." *Journal of Neural Engineering* 9 (2): 026003. <https://doi.org/10.1088/1741-2560/9/2/026003>.
- Mazurek, K. A., B. J. Holinski, D. G. Everaert, V. K. Mushahwar, and R. Etienne-Cummings. 2016. "A Mixed-Signal VLSI System for Producing Temporally Adapting Intraspinal Microstimulation Patterns for Locomotion." *IEEE Transactions on Biomedical Circuits and Systems* 10 (4): 902–11. <https://doi.org/10.1109/TBCAS.2015.2501419>.
- Mazzini, L., I. Ferrero, V. Luparello, D. Rustichelli, M. Gunetti, K. Mareschi, L. Testa, et al. 2010. "Mesenchymal Stem Cell Transplantation in Amyotrophic Lateral Sclerosis: A Phase I Clinical Trial." *Experimental Neurology, Regeneration in the Peripheral Nervous System*, 223 (1): 229–37. <https://doi.org/10.1016/j.expneurol.2009.08.007>.
- McCaughey, E J, M Purcell, A N McLean, M H Fraser, A Bewick, R J Borotkanics, and D B Allan. 2015. "Changing Demographics of Spinal Cord Injury over a 20-Year Period: A Longitudinal Population-Based Study in Scotland." *Spinal Cord* 54 (October): 270.
- McConnell, George C., Howard D. Rees, Allan I. Levey, Claire-Anne Gutekunst, Robert E. Gross, and Ravi V. Bellamkonda. 2009. "Implanted Neural Electrodes Cause Chronic, Local Inflammation That Is Correlated with Local Neurodegeneration." *Journal of Neural Engineering* 6 (5): 056003. <https://doi.org/10.1088/1741-2560/6/5/056003>.

- McDonnell, Michelle N., Susan L. Hillier, George M. Opie, Matthew Nowosilskyj, Miranda Haberfield, and Gabrielle Todd. 2015. "Continuous Passive Movement Does Not Influence Motor Maps in Healthy Adults." *Frontiers in Human Neuroscience* 9. <https://doi.org/10.3389/fnhum.2015.00230>.
- McKenna, John E., and Ian Q. Whishaw. 1999. "Complete Compensation in Skilled Reaching Success with Associated Impairments in Limb Synergies, after Dorsal Column Lesion in the Rat." *Journal of Neuroscience* 19 (5): 1885–94. <https://doi.org/10.1523/JNEUROSCI.19-05-01885.1999>.
- McKinley, W. O., R. T. Seel, and J. T. Hardman. 1999. "Nontraumatic Spinal Cord Injury: Incidence, Epidemiology, and Functional Outcome." *Archives of Physical Medicine and Rehabilitation* 80 (6): 619–23.
- McPherson, Jacob G., Robert R. Miller, and Steve I. Perlmutter. 2015. "Targeted, Activity-Dependent Spinal Stimulation Produces Long-Lasting Motor Recovery in Chronic Cervical Spinal Cord Injury." *Proceedings of the National Academy of Sciences of the United States of America* 112 (39): 12193–98. <https://doi.org/10.1073/pnas.1505383112>.
- Medani, Khalid, Jonathan Riley, Jason Lamanna, and Nicholas Boulis. 2016. "Spinal Cord Cellular Therapeutics Delivery: Device Design Considerations." In *Regenerative Medicine for Degenerative Muscle Diseases*, edited by Martin K. Childers, 109–27. Stem Cell Biology and Regenerative Medicine. Springer New York. [https://doi.org/10.1007/978-1-4939-3228-3\\_5](https://doi.org/10.1007/978-1-4939-3228-3_5).
- Merati, G., P. Sarchi, M. Ferrarin, A. Pedotti, and A. Veicsteinas. 2000. "Paraplegic Adaptation to Assisted-Walking: Energy Expenditure during Wheelchair versus Orthosis Use." *Spinal Cord* 38 (1): 37–44.

- Mercier, L. M., E. J. Gonzalez-Rothi, K. A. Streeter, S. S. Posgai, A. S. Poirier, D. D. Fuller, P. J. Reier, and D. M. Baekey. 2017. "Intraspinal Microstimulation and Diaphragm Activation after Cervical Spinal Cord Injury." *Journal of Neurophysiology* 117 (2): 767–76. <https://doi.org/10.1152/jn.00721.2016>.
- Meunier, S., E. Pierrot-Deseilligny, and M. Simonetta-Moreau. 1994. "Pattern of Heteronymous Recurrent Inhibition in the Human Lower Limb." *Experimental Brain Research* 102 (1): 149–59.
- Meunier, S., E. Pierrot-Deseilligny, and M. Simonetta. 1993. "Pattern of Monosynaptic Heteronymous Ia Connections in the Human Lower Limb." *Experimental Brain Research* 96 (3): 534–44. <https://doi.org/10.1007/BF00234121>.
- Migliorini, Christine, Bruce Tonge, and George Taleporos. 2008. "Spinal Cord Injury and Mental Health." *Australian and New Zealand Journal of Psychiatry* 42 (4): 309–14. <https://doi.org/10.1080/00048670801886080>.
- Mihic, S. John, Qing Ye, Marilee J. Wick, Vladimir V. Koltchine, Matthew D. Krasowski, Suzanne E. Finn, Maria Paola Mascia, et al. 1997. "Sites of Alcohol and Volatile Anaesthetic Action on GABAA and Glycine Receptors." *Nature* 389 (September): 385.
- Minev, Ivan R., Pavel Musienko, Arthur Hirsch, Quentin Barraud, Nikolaus Wenger, Eduardo Martin Moraud, Jérôme Gandar, et al. 2015. "Electronic Dura Mater for Long-Term Multimodal Neural Interfaces." *Science* 347 (6218): 159–63. <https://doi.org/10.1126/science.1260318>.
- Mogyoros, Ilona, Matthew C. Kiernan, and David Burke. 1996. "Strength-Duration Properties of Human Peripheral Nerve." *Brain* 119 (2): 439–47. <https://doi.org/10.1093/brain/119.2.439>.

- Montoto-Marqués, A, M E Ferreiro-Velasco, S Salvador-de la Barrera, V Balboa-Barreiro, A Rodriguez-Sotillo, and R Meijide-Failde. 2017. "Epidemiology of Traumatic Spinal Cord Injury in Galicia, Spain: Trends over a 20-Year Period." *Spinal Cord* 55 (February): 588.
- Moritz, Chet T., Timothy H. Lucas, Steve I. Perlmutter, and Eberhard E. Fetz. 2007. "Forelimb Movements and Muscle Responses Evoked by Microstimulation of Cervical Spinal Cord in Sedated Monkeys." *Journal of Neurophysiology* 97 (1): 110–20.  
<https://doi.org/10.1152/jn.00414.2006>.
- Moxon, Karen A., Steve C. Leiser, Greg A. Gerhardt, Kenneth A. Barbee, and John K. Chapin. 2004. "Ceramic-Based Multisite Electrode Arrays for Chronic Single-Neuron Recording." *IEEE Transactions on Bio-Medical Engineering* 51 (4): 647–56.  
<https://doi.org/10.1109/TBME.2003.821037>.
- Murakami, Hideki, Kai-Jow Tsai, Emad S. Attallah-Wasif, Ken Yamazaki, Tadashi Shimamura, and William C. Hutton. 2006. "A Biomechanical Assessment of Infra-Laminar Hooks as an Alternative to Supra-Laminar Hooks in Thoracolumbar Fixation." *Spine* 31 (9): 967–71.  
<https://doi.org/10.1097/01.brs.0000214932.49027.6a>.
- Mushahwar, V. K., and K. W. Horch. 1997. "Proposed Specifications for a Lumbar Spinal Cord Electrode Array for Control of Lower Extremities in Paraplegia." *IEEE Transactions on Rehabilitation Engineering: A Publication of the IEEE Engineering in Medicine and Biology Society* 5 (3): 237–43.
- Mushahwar, V. K., and K. W. Horch. 1998. "Selective Activation and Graded Recruitment of Functional Muscle Groups through Spinal Cord Stimulation." *Annals of the New York Academy of Sciences* 860 (1): 531–35. <https://doi.org/10.1111/j.1749-6632.1998.tb09096.x>.

- Mushahwar, V. K., D. F. Collins, and A. Prochazka. 2000. "Spinal Cord Microstimulation Generates Functional Limb Movements in Chronically Implanted Cats." *Experimental Neurology* 163 (2): 422–29. <https://doi.org/10.1006/exnr.2000.7381>.
- Mushahwar, V. K., K. W. Horch, 1998. "Selective Activation and Graded Recruitment of Functional Muscle Groups through Spinal Cord Stimulation." *Annals of the New York Academy of Sciences* 860 (1): 531–35. <https://doi.org/10.1111/j.1749-6632.1998.tb09096.x>.
- Mushahwar, V. K., K. W. Horch. 2000b. "Selective Activation of Muscle Groups in the Feline Hindlimb through Electrical Microstimulation of the Ventral Lumbo-Sacral Spinal Cord." *IEEE Transactions on Rehabilitation Engineering* 8 (1): 11–21. <https://doi.org/10.1109/86.830944>.
- Mushahwar, V.K., and K.W. Horch. 2000a. "Muscle Recruitment through Electrical Stimulation of the Lumbo-Sacral Spinal Cord." *IEEE Transactions on Rehabilitation Engineering* 8 (1): 22–29. <https://doi.org/10.1109/86.830945>.
- Mushahwar, Vivian K., Deborah M. Gillard, Michel J. A. Gauthier, and Arthur Prochazka. 2002. "Intraspinal Micro Stimulation Generates Locomotor-like and Feedback-Controlled Movements." *IEEE Transactions on Neural Systems and Rehabilitation Engineering: A Publication of the IEEE Engineering in Medicine and Biology Society* 10 (1): 68–81. <https://doi.org/10.1109/TNSRE.2002.1021588>.
- Mushahwar, Vivian K., Patrick L. Jacobs, Richard A. Normann, Ronald J. Triolo, and Naomi Kleitman. 2007. "New Functional Electrical Stimulation Approaches to Standing and Walking." *Journal of Neural Engineering* 4 (3): S181-197. <https://doi.org/10.1088/1741-2560/4/3/S05>.

- Nagase, Masaki, Kazuo Hanaoka, Megumi Tagami, Yasuo Ide, Toshinobu Sumida, and Hideo Yamamura. 1994. "The Effect of Pentobarbital Sodium on the Dorsal Horn of the Spinal Cord." *Journal of Anesthesia* 8 (3): 321–25. <https://doi.org/10.1007/BF02514659>.
- Nas, Kemal, Levent Yazmalar, Volkan Şah, Abdulkadir Aydın, and Kadriye Öneş. 2015. "Rehabilitation of Spinal Cord Injuries." *World Journal of Orthopedics* 6 (1): 8–16. <https://doi.org/10.5312/wjo.v6.i1.8>.
- Nashold, B. S., H. Friedman, and J. Grimes. 1982. "Electrical Stimulation of the Conus Medullaris to Control Bladder Emptying in Paraplegia: A Ten-Year Review." *Applied Neurophysiology* 45 (1–2): 40–43.
- Nashold, B. S., H. Friedman, J. F. Glenn, J. H. Grimes, W. F. Barry, and R. Avery. 1972. "Electromicturition in Paraplegia. Implantation of a Spinal Neuroprosthesis." *Archives of Surgery (Chicago, Ill.: 1960)* 104 (2): 195–202.
- Nashold, B. S., J. Grimes, H. Friedman, J. Semans, and R. Avery. 1977. "Electrical Stimulation of the Conus Medullaris in the Paraplegic. A 5-Year Review." *Applied Neurophysiology* 40 (2–4): 192–207.
- Nashold, Blaine S., Harry Friedman, and Saul Boyarsky. 1971. "Electrical Activation of Micturition by Spinal Cord Stimulation." *Journal of Surgical Research* 11 (3): 144–47. [https://doi.org/10.1016/0022-4804\(71\)90039-4](https://doi.org/10.1016/0022-4804(71)90039-4).
- Nataraj, Raviraj, Musa L. Audu, and Ronald J. Triolo. 2017. "Restoring Standing Capabilities with Feedback Control of Functional Neuromuscular Stimulation Following Spinal Cord Injury." *Medical Engineering & Physics* 42 (April): 13–25. <https://doi.org/10.1016/j.medengphy.2017.01.023>.

- Nathan, N., F. Tabaraud, F. Lacroix, D. Mouliès, X. Viviand, A. Lansade, G. Terrier, and P. Feiss. 2003. "Influence of Propofol Concentrations on Multipulse Transcranial Motor Evoked Potentials." *BJA: British Journal of Anaesthesia* 91 (4): 493–97. <https://doi.org/10.1093/bja/aeg211>.
- Nicoll, R.A., and J.M. Wojtowicz. 1980. "The Effects of Pentobarbital and Related Compounds on Frog Motoneurons." *Brain Research* 191 (1): 225–37. [https://doi.org/10.1016/0006-8993\(80\)90325-X](https://doi.org/10.1016/0006-8993(80)90325-X).
- Nishikawa, K, A Jenkins, I Paraskevakis, and N.L Harrison. 2002. "Volatile Anesthetic Actions on the GABAA Receptors: Contrasting Effects of A1(S270) and B2(N265) Point Mutations." *Neuropharmacology* 42 (3): 337–45. [https://doi.org/10.1016/S0028-3908\(01\)00189-7](https://doi.org/10.1016/S0028-3908(01)00189-7).
- Nishimura, Yukio, Steve I. Perlmutter, and Eberhard E. Fetz. 2013. "Restoration of Upper Limb Movement via Artificial Corticospinal and Musculoskeletal Connections in a Monkey with Spinal Cord Injury." *Frontiers in Neural Circuits* 7 (April). <https://doi.org/10.3389/fncir.2013.00057>.
- Nooijen, Carla F. J., Nienke Ter Hoeve, and Edelle C. Field-Fote. 2009. "Gait Quality Is Improved by Locomotor Training in Individuals with SCI Regardless of Training Approach." *Journal of Neuroengineering and Rehabilitation* 6 (October): 36. <https://doi.org/10.1186/1743-0003-6-36>.
- Noonan, Vanessa K., Matthew Fingas, Angela Farry, David Baxter, Anoushka Singh, Michael G. Fehlings, and Marcel F. Dvorak. 2012. "Incidence and Prevalence of Spinal Cord Injury in Canada: A National Perspective." *Neuroepidemiology* 38 (4): 219–26. <https://doi.org/10.1159/000336014>.

- NSCISC National Spinal Cord Injury Statistical Center, 2018b. “Spinal Cord Injury Facts and Figures at a Glance.” Birmingham, Alabama: National Spinal Cord Injury Statistical Center. [https://www.nscisc.uab.edu/PublicDocuments/fact\\_figures\\_docs/Facts%202013.pdf](https://www.nscisc.uab.edu/PublicDocuments/fact_figures_docs/Facts%202013.pdf).
- NSCISC National Spinal Cord Injury Statistical Center. 2017. “Annual Statistical Reports.” Birmingham, AL: University of Alabama at Birmingham.
- NSCISC National Spinal Cord Injury Statistical Center. 2018a. “Definition of Spinal Cord Injury.” Birmingham, Alabama: National Spinal Cord Injury Statistical Center. [https://www.nscisc.uab.edu/PublicDocuments/fact\\_figures\\_docs/Facts%202013.pdf](https://www.nscisc.uab.edu/PublicDocuments/fact_figures_docs/Facts%202013.pdf).
- Oakley, John C., and Joshua P. Prager. 2002. “Spinal Cord Stimulation: Mechanisms of Action.” *Spine* 27 (22): 2574–83. <https://doi.org/10.1097/01.BRS.0000032131.08916.24>.
- Ostrý, Svatopluk, Tomáš Belšan, Jakub Otáhal, Vladimír Beneš, and David Netuka. 2013. “Is Intraoperative Diffusion Tensor Imaging at 3.0T Comparable to Subcortical Corticospinal Tract Mapping?” *Neurosurgery* 73 (5): 797–807. <https://doi.org/10.1227/NEU.0000000000000087>.
- Oxland, T. R., R. M. Lin, and M. M. Panjabi. 1992. “Three-Dimensional Mechanical Properties of the Thoracolumbar Junction.” *Journal of Orthopaedic Research: Official Publication of the Orthopaedic Research Society* 10 (4): 573–80. <https://doi.org/10.1002/jor.1100100412>.
- Ozawa, Hiroshi, Takeo Matsumoto, Toshiro Ohashi, Masaaki Sato, and Shoichi Kokubun. 2004. “Mechanical Properties and Function of the Spinal Pia Mater.” *Journal of Neurosurgery: Spine* 1 (1): 122–27. <https://doi.org/10.3171/spi.2004.1.1.0122>.
- Pajewski, Thomas N., Vincent Arlet, and Lawrence H. Phillips. 2007. “Current Approach on Spinal Cord Monitoring: The Point of View of the Neurologist, the Anesthesiologist and the

Spine Surgeon.” *European Spine Journal* 16 (Suppl 2): 115–29.

<https://doi.org/10.1007/s00586-007-0419-6>.

Peckham, P. Hunter, and Jayme S. Knutson. 2005. “Functional Electrical Stimulation for Neuromuscular Applications.” *Annual Review of Biomedical Engineering* 7: 327–60.

<https://doi.org/10.1146/annurev.bioeng.6.040803.140103>.

Phillips, Aaron A., Jordan W. Squair, Dimitry G. Sayenko, V. Reggie Edgerton, Yury Gerasimenko, and Andrei V. Krassioukov. 2018. “An Autonomic Neuroprosthesis: Noninvasive Electrical Spinal Cord Stimulation Restores Autonomic Cardiovascular Function in Individuals with Spinal Cord Injury.” *Journal of Neurotrauma* 35 (3): 446–51.

<https://doi.org/10.1089/neu.2017.5082>.

Phillips, Stuart M., Brian G. Stewart, Douglas J. Mahoney, Audrey L. Hicks, Neil McCartney, Jason E. Tang, Sarah B. Wilkinson, David Armstrong, and Mark A. Tarnopolsky. 2004. “Body-Weight-Support Treadmill Training Improves Blood Glucose Regulation in Persons with Incomplete Spinal Cord Injury.” *Journal of Applied Physiology (Bethesda, Md.: 1985)*

97 (2): 716–24. <https://doi.org/10.1152/jappphysiol.00167.2004>.

Pinter, M. M., F. Gerstenbrand, and M. R. Dimitrijevic. 2000. “Epidural Electrical Stimulation of Posterior Structures of the Human Lumbosacral Cord: 3. Control Of Spasticity.” *Spinal Cord*

38 (9): 524–31.

Poliakov, A. V., and M. H. Schieber. 1999. “Limited Functional Grouping of Neurons in the Motor Cortex Hand Area during Individuated Finger Movements: A Cluster Analysis.”

*Journal of Neurophysiology* 82 (6): 3488–3505. <https://doi.org/10.1152/jn.1999.82.6.3488>.

Pournezam, M., B. J. Andrews, R. H. Baxendale, G. F. Phillips, and J. P. Paul. 1988. “Reduction of Muscle Fatigue in Man by Cyclical Stimulation.” *Journal of Biomedical Engineering*,

- Papers Presented at the 27th Annual Scientific Meeting of the Biological Engineering Society, 10 (2): 196–200. [https://doi.org/10.1016/0141-5425\(88\)90100-8](https://doi.org/10.1016/0141-5425(88)90100-8).
- Pratt, C. A., and G. E. Loeb. 1991. “Functionally Complex Muscles of the Cat Hindlimb. I. Patterns of Activation across Sartorius.” *Experimental Brain Research* 85 (2): 243–56.
- Purves, Dale, George J. Augustine, David Fitzpatrick, Lawrence C. Katz, Anthony-Samuel LaMantia, James O. McNamara, and S. Mark Williams. 2001. “The External Anatomy of the Spinal Cord.” In *Neuroscience*, 2nd ed. Sinauer Associates.  
<http://www.ncbi.nlm.nih.gov/books/NBK11160/>.
- Rasmussen, S., A. K. Chan, and G. E. Goslow. 1978. “The Cat Step Cycle: Electromyographic Patterns for Hindlimb Muscles during Posture and Unrestrained Locomotion.” *Journal of Morphology* 155 (3): 253–69. <https://doi.org/10.1002/jmor.1051550302>.
- Regan, Mary Ann, Robert W. Teasell, Dalton L. Wolfe, David Keast, William B. Mortenson, and Jo-Anne L. Aubut. 2009. “A Systematic Review of Therapeutic Interventions for Pressure Ulcers After Spinal Cord Injury.” *Archives of Physical Medicine and Rehabilitation* 90 (2): 213–31. <https://doi.org/10.1016/j.apmr.2008.08.212>.
- Rejc, Enrico, Claudia Angeli, and Susan Harkema. 2015. “Effects of Lumbosacral Spinal Cord Epidural Stimulation for Standing after Chronic Complete Paralysis in Humans.” *PLoS ONE* 10 (7): e0133998. <https://doi.org/10.1371/journal.pone.0133998>.
- Renshaw, Birdsey. 1940. “Activity in the Simplest Spinal Reflex Pathways.” *Journal of Neurophysiology* 3 (5): 373–87. <https://doi.org/10.1152/jn.1940.3.5.373>.
- Rexed, Bror. 1952. “The Cytoarchitectonic Organization of the Spinal Cord in the Cat.” *Journal of Comparative Neurology* 96 (3): 415–95. <https://doi.org/10.1002/cne.900960303>.

- Rhoades, Rodney, and David R. Bell. 2009. *Medical Physiology: Principles for Clinical Medicine*. Lippincott Williams & Wilkins.
- Richter, Judith A., and Joseph R. Holtman. 1982. “Barbiturates: Their in Vivo Effects and Potential Biochemical Mechanisms.” *Progress in Neurobiology* 18 (4): 275–319.  
[https://doi.org/10.1016/0301-0082\(82\)90013-2](https://doi.org/10.1016/0301-0082(82)90013-2).
- Riley, Jonathan P., Bethwel Raore, Jason S. Taub, Thais Federici, and Nicholas M. Boulis. 2011. “Platform and Cannula Design Improvements for Spinal Cord Therapeutics Delivery.” *Neurosurgery* 69 (2 Suppl Operative): ons147-154; discussion ons155.  
<https://doi.org/10.1227/NEU.0b013e3182195680>.
- Riley, Jonathan, Jonathan Glass, Eva L. Feldman, Meraida Polak, Jane Bordeau, Thais Federici, Karl Johe, and Nicholas M. Boulis. 2014. “Intraspinal Stem Cell Transplantation in Amyotrophic Lateral Sclerosis: A Phase I Trial, Cervical Microinjection, and Final Surgical Safety Outcomes.” *Neurosurgery* 74 (1): 77–87.  
<https://doi.org/10.1227/NEU.0000000000000156>.
- Riley, Jonathan, Thais Federici, Meraida Polak, Crystal Kelly, Jonathan Glass, Bethwel Raore, Jason Taub, Vita Kesner, Eva L. Feldman, and Nicholas M. Boulis. 2012. “Intraspinal Stem Cell Transplantation in Amyotrophic Lateral Sclerosis: A Phase I Safety Trial, Technical Note, and Lumbar Safety Outcomes.” *Neurosurgery* 71 (2): 405–16; discussion 416.  
<https://doi.org/10.1227/NEU.0b013e31825ca05f>.
- Rocha, Raphael Grossi, Eduardo Giarola Almeida, Lara Moreira Mendes Carneiro, Natália Farias de Almeida, Walkíria Wingester Vilas Boas, and Renato Santiago Gomez. 2017. “Anesthesia Recovery Comparison between Remifentanil-Propofol and Remifentanil-

- Desflurane Guided by Bispectral Index® Monitoring.” *Brazilian Journal of Anesthesiology (English Edition)* 67 (5): 500–507. <https://doi.org/10.1016/j.bjane.2016.10.001>.
- Rouhani, Ehsan, and Abbas Erfanian. 2018. “Block-Based Robust Control of Stepping Using Intraspinal Microstimulation.” *Journal of Neural Engineering* 15 (4): 046026. <https://doi.org/10.1088/1741-2552/aac4b8>.
- Rouhani, Hossein, Michael Same, Kei Masani, Ya Qi Li, and Milos R. Popovic. 2017. “PID Controller Design for FES Applied to Ankle Muscles in Neuroprosthesis for Standing Balance.” *Frontiers in Neuroscience* 11. <https://doi.org/10.3389/fnins.2017.00347>.
- Rousche, Patrick J, and Richard A Normann. 1998. “Chronic Recording Capability of the Utah Intracortical Electrode Array in Cat Sensory Cortex.” *Journal of Neuroscience Methods* 82 (1): 1–15. [https://doi.org/10.1016/S0165-0270\(98\)00031-4](https://doi.org/10.1016/S0165-0270(98)00031-4).
- Ruder, Ludwig, Aya Takeoka, and Silvia Arber. 2016. “Long-Distance Descending Spinal Neurons Ensure Quadrupedal Locomotor Stability.” *Neuron* 92 (5): 1063–78. <https://doi.org/10.1016/j.neuron.2016.10.032>.
- Rudomin, P., and Robert F. Schmidt. 1999. “Presynaptic Inhibition in the Vertebrate Spinal Cord Revisited.” *Experimental Brain Research* 129 (1): 1–37. <https://doi.org/10.1007/s002210050933>.
- Rutten, Wim L. C. 2002. “Selective Electrical Interfaces with the Nervous System.” *Annual Review of Biomedical Engineering* 4: 407–52. <https://doi.org/10.1146/annurev.bioeng.4.020702.153427>.
- Saberi, Hooshang, Pouria Moshayedi, Hamid-Reza Aghayan, Babak Arjmand, Seyed-Kazem Hosseini, Seyed-Hassan Emami-Razavi, Vafa Rahimi-Movaghar, Mohsin Raza, and Masoumeh Firouzi. 2008. “Treatment of Chronic Thoracic Spinal Cord Injury Patients with

Autologous Schwann Cell Transplantation: An Interim Report on Safety Considerations and Possible Outcomes.” *Neuroscience Letters* 443 (1): 46–50.

<https://doi.org/10.1016/j.neulet.2008.07.041>.

Saigal, R., C. Renzi, and V.K. Mushahwar. 2004. “Intraspinal Microstimulation Generates Functional Movements after Spinal-Cord Injury.” *IEEE Transactions on Neural Systems and Rehabilitation Engineering* 12 (4): 430–40. <https://doi.org/10.1109/TNSRE.2004.837754>.

Sala, Francesco, Giorgio Palandri, Elisabetta Basso, Paola Lanteri, Vedran Deletis, Franco Faccioli, and Albino Bricolo. 2006. “Motor Evoked Potential Monitoring Improves Outcome after Surgery for Intramedullary Spinal Cord Tumors: A Historical Control Study.” *Neurosurgery* 58 (6): 1129–43; discussion 1129–1143. <https://doi.org/10.1227/01.NEU.0000215948.97195.58>.

Sala, Francesco, Vincenzo Tramontano, Giovanna Squintani, Chiara Arcaro, Ema Tot, Giampietro Pinna, and Mario Meglio. 2014. “Neurophysiology of Complex Spinal Cord Untethering.” *Journal of Clinical Neurophysiology: Official Publication of the American Electroencephalographic Society* 31 (4): 326–36. <https://doi.org/10.1097/WNP.000000000000115>.

Savic, G., M. J. DeVivo, H. L. Frankel, M. A. Jamous, B. M. Soni, and S. Charlifue. 2017. “Long-Term Survival after Traumatic Spinal Cord Injury: A 70-Year British Study.” *Spinal Cord* 55 (7): 651–58. <https://doi.org/10.1038/sc.2017.23>.

Scelza, William M., Steven C. Kirshblum, Lisa-Ann Wuermsler, Chester H. Ho, Michael M. Priebe, and Anthony E. Chiodo. 2007. “Spinal Cord Injury Medicine. 4. Community Reintegration After Spinal Cord Injury.” *Archives of Physical Medicine and Rehabilitation*,

2007 Study Guide, 88 (3, Supplement 1): S71–75.

<https://doi.org/10.1016/j.apmr.2006.12.004>.

Schieppati, Marco. 1987. “The Hoffmann Reflex: A Means of Assessing Spinal Reflex Excitability and Its Descending Control in Man.” *Progress in Neurobiology* 28 (4): 345–76.

[https://doi.org/10.1016/0301-0082\(87\)90007-4](https://doi.org/10.1016/0301-0082(87)90007-4).

Schofield, C. M., and N. L. Harrison. 2005. “Transmembrane Residues Define the Action of Isoflurane at the GABAA Receptor Alpha-3 Subunit.” *Brain Research* 1032 (1–2): 30–35.

<https://doi.org/10.1016/j.brainres.2004.11.002>.

Schrimsher, G. W., and P. J. Reier. 1992. “Forelimb Motor Performance Following Cervical Spinal Cord Contusion Injury in the Rat.” *Experimental Neurology* 117 (3): 287–98.

Schulz, Richard, Sara J. Czaja, Amy Lustig, Bozena Zdaniuk, Lynn M. Martire, and Dolores Perdomo. 2009. “Improving the Quality of Life of Caregivers of Persons with Spinal Cord Injury: A Randomized Controlled Trial.” *Rehabilitation Psychology* 54 (1): 1–15.

<https://doi.org/10.1037/a0014932>.

Schüttler, J., S. Kloos, H. Schwilden, and H. Stoeckel. 1988. “Total Intravenous Anaesthesia with Propofol and Alfentanil by Computer-Assisted Infusion.” *Anaesthesia* 43 Suppl (March): 2–7.

Schwartz, I., A. Sajina, M. Neeb, I. Fisher, M. Katz-Luerer, and Z. Meiner. 2011. “Locomotor Training Using a Robotic Device in Patients with Subacute Spinal Cord Injury.” *Spinal Cord* 49 (10): 1062–67. <https://doi.org/10.1038/sc.2011.59>.

Semerjian, Tamar, Suzanne Montague, Jesus Dominguez, Artin Davidian, and Ray de Leon.

2005. “Enhancement of Quality of Life and Body Satisfaction Through the Use of Adapted

- Exercise Devices for Individuals with Spinal Cord Injuries.” *Topics in Spinal Cord Injury Rehabilitation* 11 (2): 95–108. <https://doi.org/10.1310/BXE2-MTKU-YL15-429A>.
- Sengul, Gulgun, Charles Watson, Ikuko Tanaka, and George Paxinos. 2012. *Atlas of the Spinal Cord: Mouse, Rat, Rhesus, Marmoset, and Human*. 1 edition. London ; Boston: Academic Press.
- Shapiro, Scott, Richard Borgens, Robert Pascuzzi, Karen Roos, Michael Groff, Scott Purvines, Richard Ben Rodgers, Shannon Hagy, and Paul Nelson. 2005. “Oscillating Field Stimulation for Complete Spinal Cord Injury in Humans: A Phase 1 Trial.” *Journal of Neurosurgery. Spine* 2 (1): 3–10. <https://doi.org/10.3171/spi.2005.2.1.0003>.
- Shapiro, Scott. 2014. “A Review of Oscillating Field Stimulation to Treat Human Spinal Cord Injury.” *World Neurosurgery* 81 (5–6): 830–35. <https://doi.org/10.1016/j.wneu.2012.11.039>.
- Sharpe, Abigail N., and Andrew Jackson. 2014. “Upper-Limb Muscle Responses to Epidural, Subdural and Intraspinal Stimulation of the Cervical Spinal Cord.” *Journal of Neural Engineering* 11 (1): 016005. <https://doi.org/10.1088/1741-2560/11/1/016005>.
- Sharrard, W. J. 1955. “The Distribution of the Permanent Paralysis in the Lower Limb in Poliomyelitis; a Clinical and Pathological Study.” *The Journal of Bone and Joint Surgery. British Volume* 37-B (4): 540–58.
- Sharrard, W. J. W. 1964. “The Segmental Innervation of the Lower Limb Muscles in Man.” *Annals of The Royal College of Surgeons of England* 35 (2): 106–22.
- Shavelle, Robert M., Michael J. DeVivo, Jordan C. Brooks, David J. Strauss, and David R. Paculdo. 2015. “Improvements in Long-Term Survival after Spinal Cord Injury?” *Archives of Physical Medicine and Rehabilitation* 96 (4): 645–51. <https://doi.org/10.1016/j.apmr.2014.11.003>.

- Shealy, C. N., J. T. Mortimer, and J. B. Reswick. 1967. "Electrical Inhibition of Pain by Stimulation of the Dorsal Columns: Preliminary Clinical Report." *Anesthesia and Analgesia* 46 (4): 489–91.
- Shen, Xiao-yan, Wei Du, Wei Huang, and Yi Chen. 2016. "Rebuilding Motor Function of the Spinal Cord Based on Functional Electrical Stimulation." *Neural Regeneration Research* 11 (8): 1327. <https://doi.org/10.4103/1673-5374.189199>.
- Sheng, Sun-Ren, Xiang-Yang Wang, Hua-Zi Xu, Guo-Qing Zhu, and Yi-Fei Zhou. 2010. "Anatomy of Large Animal Spines and Its Comparison to the Human Spine: A Systematic Review." *European Spine Journal* 19 (1): 46–56. <https://doi.org/10.1007/s00586-009-1192-5>.
- Sherrington, Charles S. 1892. "Notes on the Arrangement of Some Motor Fibres in the Lumbo-Sacral Plexus." *The Journal of Physiology* 13 (6): 621-772.17.
- Shils, Jay L., and Jeffery E. Arle. 2012. "Intraoperative Neurophysiologic Methods for Spinal Cord Stimulator Placement under General Anesthesia." *Neuromodulation: Journal of the International Neuromodulation Society* 15 (6): 560–71; discussion 571-572. <https://doi.org/10.1111/j.1525-1403.2012.00460.x>.
- Shimada, Yoichi, Kozo Sato, Eiji Abe, Hitoshi Kagaya, Kunio Ebata, Masashi Oba, and Mineyoshi Sato. 1996. "Clinical Experience of Functional Electrical Stimulation in Complete Paraplegia." *Spinal Cord* 34 (10): 615–19. <https://doi.org/10.1038/sc.1996.110>.
- Simpson, Lisa A., Janice J. Eng, Jane T.C. Hsieh, and Dalton L. Wolfe and the Spinal Cord Injury Rehabilitation Evidence (SCIRE) Research Team. 2012. "The Health and Life Priorities of Individuals with Spinal Cord Injury: A Systematic Review." *Journal of Neurotrauma* 29 (8): 1548–55. <https://doi.org/10.1089/neu.2011.2226>.

- Sin, W. K., and B. Coburn. 1983. "Electrical Stimulation of the Spinal Cord: A Further Analysis Relating to Anatomical Factors and Tissue Properties." *Medical and Biological Engineering and Computing* 21 (3): 264–69. <https://doi.org/10.1007/BF02478492>.
- Sloan, Tod B. 2002. "Chapter 49 Anesthesia Effects and Evoked Potentials." In *Supplements to Clinical Neurophysiology*, 54:325–28. Elsevier. [https://doi.org/10.1016/S1567-424X\(09\)70469-6](https://doi.org/10.1016/S1567-424X(09)70469-6).
- Sloan, Tod B., Paul Mongan, Clark Lyda, and Antoun Koht. 2014. "Lidocaine Infusion Adjunct to Total Intravenous Anesthesia Reduces the Total Dose of Propofol during Intraoperative Neurophysiological Monitoring." *Journal of Clinical Monitoring and Computing* 28 (2): 139–47. <https://doi.org/10.1007/s10877-013-9506-x>.
- Smit, Theo H. 2002. "The Use of a Quadruped as an in Vivo Model for the Study of the Spine - Biomechanical Considerations." *European Spine Journal: Official Publication of the European Spine Society, the European Spinal Deformity Society, and the European Section of the Cervical Spine Research Society* 11 (2): 137–44. <https://doi.org/10.1007/s005860100346>.
- Smith, Andrew C., and Maria Knikou. 2016. "A Review on Locomotor Training after Spinal Cord Injury: Reorganization of Spinal Neuronal Circuits and Recovery of Motor Function." *Neural Plasticity* 2016. <https://doi.org/10.1155/2016/1216258>.
- Smith, Julius O. 2010. *Physical Audio Signal Processing*. W3K Publishing. <http://ccrma.stanford.edu/~jos/pasp/>.
- Snow, S., K. W. Horch, and V. K. Mushahwar. 2006. "Intraspinal Microstimulation Using Cylindrical Multielectrodes." *IEEE Transactions on Biomedical Engineering* 53 (2): 311–19. <https://doi.org/10.1109/TBME.2005.857638>.

Snow, Sean, Stephen C. Jacobsen, David L. Wells, and Kenneth W. Horch. 2006.

“Microfabricated Cylindrical Multielectrodes for Neural Stimulation.” *IEEE Transactions on Bio-Medical Engineering* 53 (2): 320–26. <https://doi.org/10.1109/TBME.2005.862552>.

Sonner, James M., Yi Zhang, Caroline Stabernack, Wella Abaigar, Yilei Xing, and Michael J.

Laster. 2003. “GABA(A) Receptor Blockade Antagonizes the Immobilizing Action of Propofol but Not Ketamine or Isoflurane in a Dose-Related Manner.” *Anesthesia and Analgesia* 96 (3): 706–12, table of contents.

Steffey, E. P., J. D. Baggot, J. H. Eisele, N. Willits, M. J. Woliner, K. A. Jarvis, A. R. Elliott, and

M. Tagawa. 1994. “Morphine-Isoflurane Interaction in Dogs, Swine and Rhesus Monkeys.” *Journal of Veterinary Pharmacology and Therapeutics* 17 (3): 202–10.

<https://doi.org/10.1111/j.1365-2885.1994.tb00234.x>.

Stein, Richard B., and Vivian Mushahwar. 2005. “Reanimating Limbs after Injury or Disease.”

*Trends in Neurosciences* 28 (10): 518–24. <https://doi.org/10.1016/j.tins.2005.07.007>.

Stewart, Brian G., Mark A. Tarnopolsky, Audrey L. Hicks, Neil McCartney, Douglas J.

Mahoney, Robert S. Staron, and Stuart M. Phillips. 2004. “Treadmill Training–Induced Adaptations in Muscle Phenotype in Persons with Incomplete Spinal Cord Injury.” *Muscle & Nerve* 30 (1): 61–68. <https://doi.org/10.1002/mus.20048>.

Struijk, J. J., J. Holsheimer, and H. B. Boom. 1993. “Excitation of Dorsal Root Fibers in Spinal

Cord Stimulation: A Theoretical Study.” *IEEE Transactions on Bio-Medical Engineering* 40 (7): 632–39. <https://doi.org/10.1109/10.237693>.

Struijk, J. J., J. Holsheimer, B. K. van Veen, and H. B. Boom. 1991. “Epidural Spinal Cord

Stimulation: Calculation of Field Potentials with Special Reference to Dorsal Column Nerve

Fibers.” *IEEE Transactions on Bio-Medical Engineering* 38 (1): 104–10.

<https://doi.org/10.1109/10.68217>.

Struijk, J.J., J. Holsheimer, G. Barolat, Jiping He, and H.B.K. Boom. 1993. “Paresthesia Thresholds in Spinal Cord Stimulation: A Comparison of Theoretical Results with Clinical Data.” *IEEE Transactions on Rehabilitation Engineering* 1 (2): 101–8.

<https://doi.org/10.1109/86.242424>.

Sunshine, Michael D., Comron N. Ganji, Paul J. Reier, David D. Fuller, and Chet T. Moritz. 2018. “Intraspinal Microstimulation for Respiratory Muscle Activation.” *Experimental Neurology* 302 (April): 93–103. <https://doi.org/10.1016/j.expneurol.2017.12.014>.

Sunshine, Michael D., Frances S. Cho, Danielle R. Lockwood, Amber S. Fechko, Michael R. Kasten, and Chet T. Moritz. 2013. “Cervical Intraspinal Microstimulation Evokes Robust Forelimb Movements before and after Injury.” *Journal of Neural Engineering* 10 (3): 036001. <https://doi.org/10.1088/1741-2560/10/3/036001>.

Swindle, M. M., A. Makin, A. J. Herron, F. J. Clubb, and K. S. Frazier. 2012. “Swine as Models in Biomedical Research and Toxicology Testing.” *Veterinary Pathology* 49 (2): 344–56. <https://doi.org/10.1177/0300985811402846>.

Szentkuti, L., and J. Bruns. 1983. “Motoneurons of M. Semitendinosus in Domestic and Wild Pigs. A Horseradish Peroxidase and Cord-Survey Study.” *Anatomy and Embryology* 167 (2): 213–28.

Talke, Pekka, Charles A. Richardson, Mika Scheinin, and Dennis M. Fisher. 1997.

“Postoperative Pharmacokinetics and Sympatholytic Effects of Dexmedetomidine.”

*Anesthesia & Analgesia* 85 (5): 1136.

- Tan, John F., Kei Masani, Albert H. Vette, José Zariffa, Mark Robinson, Cheryl Lynch, and Milos R. Popovic. 2014. "Inverted Pendulum Standing Apparatus for Investigating Closed-Loop Control of Ankle Joint Muscle Contractions during Functional Electrical Stimulation." Research article. *International Scholarly Research Notices*. 2014. <https://doi.org/10.1155/2014/192097>.
- Tarler, Matthew D., and J. Thomas Mortimer. 2004. "Selective and Independent Activation of Four Motor Fascicles Using a Four Contact Nerve-Cuff Electrode." *IEEE Transactions on Neural Systems and Rehabilitation Engineering: A Publication of the IEEE Engineering in Medicine and Biology Society* 12 (2): 251–57. [https://doi.org/10.1109/TNSRE.2004.828415\(410\) 1](https://doi.org/10.1109/TNSRE.2004.828415(410) 1).
- Tator, Charles H., Karen Minassian, and Vivian K. Mushahwar. 2012. "Spinal Cord Stimulation: Therapeutic Benefits and Movement Generation after Spinal Cord Injury." *Handbook of Clinical Neurology* 109: 283–96. <https://doi.org/10.1016/B978-0-444-52137-8.00018-8>.
- Thrasher, T. A., H. M. Flett, and M. R. Popovic. 2006. "Gait Training Regimen for Incomplete Spinal Cord Injury Using Functional Electrical Stimulation." *Spinal Cord* 44 (6): 357–61. <https://doi.org/10.1038/sj.sc.3101864>.
- Toossi, Amirali, Dirk G. Everaert, Austin Azar, Christopher R. Dennison, and Vivian K. Mushahwar. 2016. "Mechanically Stable Intraspinal Microstimulation Implants for Human Translation." *Annals of Biomedical Engineering*, 1–14. <https://doi.org/10.1007/s10439-016-1709-0>.
- Toossi, Amirali, Dirk G. Everaert, Peter Seres, Jacob L. Jaremko, Kevin Robinson, C. Chris Kao, Peter E. Konrad, and Vivian K. Mushahwar. 2018. "Ultrasound-Guided Spinal Stereotactic

System for Intraspinal Implants.” *Journal of Neurosurgery: Spine*, June, 1–14.

<https://doi.org/10.3171/2018.1.SPINE17903>.

Toossi, Amirali, Dirk G. Everaert, Steve I. Perlmutter, and Vivian K. Mushahwar. 2016.

“Functional Organization of Motoneuronal Pools in the Lumbar Spinal Cord of Monkeys: Intraspinal Microstimulation Targets.” In *2016 Neural Interfaces Conference and North American Neuromodulation Society Meeting*. Baltimore, MD.

Topf, Norbert, Andrew Jenkins, Nicole Baron, and Neil L. Harrison. 2003. “Effects of Isoflurane on  $\gamma$ -Aminobutyric Acid Type A Receptors Activated by Full and Partial Agonists.”

*Anesthesiology: The Journal of the American Society of Anesthesiologists* 98 (2): 306–11.

<https://doi.org/0000542-200302000-00007>.

Triolo, Ronald J., Lisa Boggs, Michael E. Miller, Gregory Nemunaitis, Jennifer Nagy, and

Stephanie Nogan Bailey. 2009. “Implanted Electrical Stimulation of the Trunk for Seated Postural Stability and Function after Cervical SCI: A Single Case Study.” *Archives of Physical Medicine and Rehabilitation* 90 (2): 340–47.

<https://doi.org/10.1016/j.apmr.2008.07.029>.

Triolo, Ronald J., Stephanie Nogan Bailey, Michael E. Miller, Loretta M. Rohde, James S.

Anderson, John A. Davis, James J. Abbas, et al. 2012. “Longitudinal Performance of a Surgically Implanted Neuroprosthesis for Lower-Extremity Exercise, Standing, and Transfers after Spinal Cord Injury.” *Archives of Physical Medicine and Rehabilitation* 93

(5): 896–904. <https://doi.org/10.1016/j.apmr.2012.01.001>.

Tu, Xikai, Jiixin Li, Jian Li, Chen Su, Shali Zhang, Haoran Li, Jingyan Cao, and Jiping He.

2017. “Model-Based Hybrid Cooperative Control of Hip-Knee Exoskeleton and FES Induced Ankle Muscles for Gait Rehabilitation.” *International Journal of Pattern*

*Recognition and Artificial Intelligence* 31 (09): 1759019.

<https://doi.org/10.1142/S0218001417590194>.

Turner, Judith A, Mark P Jensen, Catherine A Warms, and Diana D Cardenas. 2002.

“Catastrophizing Is Associated with Pain Intensity, Psychological Distress, and Pain-Related Disability among Individuals with Chronic Pain after Spinal Cord Injury.” *Pain* 98 (1): 127–34. [https://doi.org/10.1016/S0304-3959\(02\)00045-3](https://doi.org/10.1016/S0304-3959(02)00045-3).

Uhlir, James P., Ronald J. Triolo, John A. Davis, and Carol Bieri. 2004. “Performance of

Epimysial Stimulating Electrodes in the Lower Extremities of Individuals with Spinal Cord Injury.” *IEEE Transactions on Neural Systems and Rehabilitation Engineering: A Publication of the IEEE Engineering in Medicine and Biology Society* 12 (2): 279–87. <https://doi.org/10.1109/TNSRE.2004.827224>.

Ünalın, H., B. Gençosmanođlu, K. Akgün, Ş Karamehmetođlu, H. Tuna, K. Önes, A.

Rahimpenah, E. Uzun, and F. Tüzün. 2001. “Quality of Life of Primary Caregivers of Spinal Cord Injury Survivors Living in the Community: Controlled Study with Short Form-36 Questionnaire.” *Spinal Cord* 39 (6): 318–22. <https://doi.org/10.1038/sj.sc.3101163>.

Urban, Michael K., Kara Fields, Sean W. Donegan, Jonathan C. Beathe, David W. Pinter,

Oheneba Boachie-Adjei, and Ronald G. Emerson. 2017. “A Randomized Crossover Study of the Effects of Lidocaine on Motor- and Sensory-Evoked Potentials during Spinal Surgery.” *The Spine Journal* 17 (12): 1889–96. <https://doi.org/10.1016/j.spinee.2017.06.024>.

Vanderhorst, V. G., and G. Holstege. 1997. “Organization of Lumbosacral Motoneuronal Cell

Groups Innervating Hindlimb, Pelvic Floor, and Axial Muscles in the Cat.” *The Journal of Comparative Neurology* 382 (1): 46–76.

- Veale, J. L., R. F. Mark, and Sandra Rees. 1973. "Differential Sensitivity of Motor and Sensory Fibres in Human Ulnar Nerve." *Journal of Neurology, Neurosurgery & Psychiatry* 36 (1): 75–86. <https://doi.org/10.1136/jnnp.36.1.75>.
- Venkatraghavan, Lakshmi, Pirjo Manninen, Peter Mak, Karolinah Lukitto, Mojgan Hodaie, and Andres Lozano. 2006. "Anesthesia for Functional Neurosurgery: Review of Complications." *Journal of Neurosurgical Anesthesiology* 18 (1): 64. <https://doi.org/10.1097/01.ana.0000181285.71597.e8>.
- Vette A. H., Kim, Joon-young, Masani, K., and Popovic, M. R., 2005. "Closed-Loop Control of FES-Assisted Arm-Free Paraplegic Standing: A Feasibility Study." In *EUROCON 2005 - The International Conference on "Computer as a Tool,"* 1:37–40. <https://doi.org/10.1109/EURCON.2005.1629852>.
- Vette, Albert H., Kei Masani, Joon-Young Kim, and Milos R. Popovic. 2009. "Closed-Loop Control of Functional Electrical Stimulation-Assisted Arm-Free Standing in Individuals With Spinal Cord Injury: A Feasibility Study." *Neuromodulation: Technology at the Neural Interface* 12 (1): 22–32. <https://doi.org/10.1111/j.1525-1403.2009.00184.x>.
- Ward, Matthew P., Pooja Rajdev, Casey Ellison, and Pedro P. Irazoqui. 2009. "Toward a Comparison of Microelectrodes for Acute and Chronic Recordings." *Brain Research* 1282 (July): 183–200. <https://doi.org/10.1016/j.brainres.2009.05.052>.
- Weitzenkamp, David A., Kenneth A. Gerhart, Susan W. Charlifue, Gale G. Whiteneck, and Gordana Savic. 1997. "Spouses of Spinal Cord Injury Survivors: The Added Impact of Caregiving." *Archives of Physical Medicine and Rehabilitation* 78 (8): 822–27. [https://doi.org/10.1016/S0003-9993\(97\)90194-5](https://doi.org/10.1016/S0003-9993(97)90194-5).

- Wessén, A., P. M. Persson, A. Nilsson, and P. Hartvig. 1993. “Concentration-Effect Relationships of Propofol after Total Intravenous Anesthesia.” *Anesthesia and Analgesia* 77 (5): 1000–1007.
- Westgren, N., and R. Levi. 1994. “Motherhood after Traumatic Spinal Cord Injury.” *Spinal Cord* 32 (8): 517–23. <https://doi.org/10.1038/sc.1994.83>.
- White, Augustus A., and Manohar Panjabi. 1990. *Clinical Biomechanics of the Spine*. 2 edition. Philadelphia: Wolters Kluwer.
- Wieler, Marguerite, Richard B. Stein, Michel Ladouceur, Maura Whittaker, Andrew W. Smith, Saad Naaman, Hugues Barbeau, Joanne Bugaresti, and Elaine Aimone. 1999. “Multicenter Evaluation of Electrical Stimulation Systems for Walking.” *Archives of Physical Medicine and Rehabilitation* 80 (5): 495–500. [https://doi.org/10.1016/S0003-9993\(99\)90188-0](https://doi.org/10.1016/S0003-9993(99)90188-0).
- Wiest, Matheus J., Austin J. Bergquist, Helen L. Schmidt, Kelvin E. Jones, and David F. Collins. 2017. “Interleaved Neuromuscular Electrical Stimulation: Motor Unit Recruitment Overlap.” *Muscle & Nerve* 55 (4): 490–99. <https://doi.org/10.1002/mus.25249>.
- Wilke, Hans-Joachim, Jürgen Geppert, and Annette Kienle. 2011. “Biomechanical in Vitro Evaluation of the Complete Porcine Spine in Comparison with Data of the Human Spine.” *European Spine Journal* 20 (11): 1859–68. <https://doi.org/10.1007/s00586-011-1822-6>.
- World Health Organization. 2004. “Global Burden of Disease - Part 4: DALYs.” [http://www.who.int/healthinfo/global\\_burden\\_disease/GBD\\_report\\_2004update\\_part4.pdf](http://www.who.int/healthinfo/global_burden_disease/GBD_report_2004update_part4.pdf).
- Xu, SQ, YH Li, SH Hu, X Ju, and JB Xiao. 2017. “Effects of Intravenous Lidocaine, Dexmedetomidine and Their Combination on Postoperative Pain and Bowel Function Recovery after Abdominal Hysterectomy” 83 (7): 685–94. <https://doi.org/10.23736/S0375-9393.16.11472-5>.

- Yakovenko, Sergiy, Jan Kowalczewski, and Arthur Prochazka. 2007. "Intraspinal Stimulation Caudal to Spinal Cord Transections in Rats. Testing the Propriospinal Hypothesis." *Journal of Neurophysiology* 97 (3): 2570–74. <https://doi.org/10.1152/jn.00814.2006>.
- Yakovenko, Sergiy, Vivian Mushahwar, Veronique VanderHorst, Gert Holstege, and Arthur Prochazka. 2002. "Spatiotemporal Activation of Lumbosacral Motoneurons in the Locomotor Step Cycle." *Journal of Neurophysiology* 87 (3): 1542–53. <https://doi.org/10.1152/jn.00479.2001>.
- Yang, Jaynie F., and Kristin E. Musselman. 2012. "Training to Achieve over Ground Walking after Spinal Cord Injury: A Review of Who, What, When, and How." *The Journal of Spinal Cord Medicine* 35 (5): 293–304. <https://doi.org/10.1179/2045772312Y.0000000036>.
- Yeganeh, M. H., and I. Ramzan. 1997. "Determination of Propofol in Rat Whole Blood and Plasma by High-Performance Liquid Chromatography." *Journal of Chromatography. B, Biomedical Sciences and Applications* 691 (2): 478–82.
- Yoshida, Ken, and Ken Horch. 1993. "Reduced Fatigue in Electrically Stimulated Muscle Using Dual Channel Intrafascicular Electrodes with Interleaved Stimulation." *Annals of Biomedical Engineering* 21 (6): 709–14. <https://doi.org/10.1007/BF02368649>.
- Young, A. J., and D. P. Ferris. 2017. "State of the Art and Future Directions for Lower Limb Robotic Exoskeletons." *IEEE Transactions on Neural Systems and Rehabilitation Engineering* 25 (2): 171–82. <https://doi.org/10.1109/TNSRE.2016.2521160>.
- Zeilig, Gabi, Harold Weingarden, Manuel Zweckner, Israel Dudkiewicz, Ayala Bloch, and Alberto Esquenazi. 2012. "Safety and Tolerance of the ReWalk™ Exoskeleton Suit for Ambulation by People with Complete Spinal Cord Injury: A Pilot Study." *The Journal of Spinal Cord Medicine* 35 (2): 96–101. <https://doi.org/10.1179/2045772312Y.0000000003>.

- Zeller, Anja, Margarete Arras, Rachel Jurd, and Uwe Rudolph. 2007. "Identification of a Molecular Target Mediating the General Anesthetic Actions of Pentobarbital." *Molecular Pharmacology* 71 (3): 852–59. <https://doi.org/10.1124/mol.106.030049>.
- Zhang, Dingguo, Yong Ren, Kai Gui, Jie Jia, and Wendong Xu. 2017. "Cooperative Control for A Hybrid Rehabilitation System Combining Functional Electrical Stimulation and Robotic Exoskeleton." *Frontiers in Neuroscience* 11. <https://doi.org/10.3389/fnins.2017.00725>.
- Zhang, Yi, James M. Sonner, Edmond I. Eger, Caroline R. Stabernack, Michael J. Laster, Douglas E. Raines, and R. Adron Harris. 2004. "Gamma-Aminobutyric Acid A Receptors Do Not Mediate the Immobility Produced by Isoflurane." *Anesthesia and Analgesia* 99 (1): 85–90.
- Zhong, Yinghui, and Ravi V. Bellamkonda. 2007. "Dexamethasone-Coated Neural Probes Elicit Attenuated Inflammatory Response and Neuronal Loss Compared to Uncoated Neural Probes." *Brain Research* 1148 (May): 15–27. <https://doi.org/10.1016/j.brainres.2007.02.024>.
- Zhou, Henry H., Mahesh Mehta, and Arturo A. Leis. 1997. "Spinal Cord Motoneuron Excitability during Isoflurane and Nitrous Oxide Anesthesia." *Anesthesiology: The Journal of the American Society of Anesthesiologists* 86 (2): 302–7.
- Zhou, Hui, Yi Lu, Wanzhen Chen, Zhen Wu, Haiqing Zou, Ludovic Krundel, and Guanglin Li. 2015. "Stimulating the Comfort of Textile Electrodes in Wearable Neuromuscular Electrical Stimulation." *Sensors (Basel, Switzerland)* 15 (7): 17241–57. <https://doi.org/10.3390/s150717241>.
- Zhou, R., L. Alvarado, S. Kim, S. L. Chong, and V. K. Mushahwar. 2017. "Modulation of Corticospinal Input to the Legs by Arm and Leg Cycling in People with Incomplete Spinal

Cord Injury.” *Journal of Neurophysiology* 118 (4): 2507–19.

<https://doi.org/10.1152/jn.00663.2016>.

Zhou, Rui, Laura Alvarado, Robert Ogilvie, Su Ling Chong, Oriana Shaw, and Vivian K.

Mushahwar. 2018. “Non-Gait-Specific Intervention for the Rehabilitation of Walking after SCI: Role of the Arms.” *Journal of Neurophysiology* 119 (6): 2194–2211.

<https://doi.org/10.1152/jn.00569.2017>.

Zimmermann, Jonas B., and Andrew Jackson. 2014. “Closed-Loop Control of Spinal Cord Stimulation to Restore Hand Function after Paralysis.” *Frontiers in Neuroscience* 8.

<https://doi.org/10.3389/fnins.2014.00087>.

Zimmermann, Jonas B., Kazuhiko Seki, and Andrew Jackson. 2011. “Reanimating the Arm and Hand with Intraspinal Microstimulation.” *Journal of Neural Engineering* 8 (5): 054001.

<https://doi.org/10.1088/1741-2560/8/5/054001>.